ULTRAFAST AND NONLINEAR SPECTROSCOPY UTILIZED AS A SENSITIVE PROBE FOR AMYLOID PEPTIDE AGGREGATION

by

Travis B. Clark

A dissertation submitted in partial fulfillment
of the requirements for the degree of
Doctor of Philosophy
(Chemistry)
in The University of Michigan
2012

Doctoral Committee:

Professor Theodore G. Goodson III, Chair
Professor John Montgomery
Associate Professor A. Oveta Fuller
Assistant Professor Anne J. McNeil

"One never notices what has been done; one can only see what remains to be done…"

--Marie Curie, 1894

DEDICATION

To my family, for always believing in me, especially when I didn't believe in myself.

ACKNOWLEDGEMENTS

There is not enough room on the page to personally thank all those that have had a material impact on an accomplishment such as this one. My life's education has built to this point and I owe a huge debt to all those teachers I have had over the years that never stopped encouraging me to reach for the stars. From my days at Fairbrook Elementary to Ankeney Middle School and then Beavercreek High School, each teacher has taught me a lesson that I still carry with me to this day. A special thanks to all my science teachers, whose enthusiasm for the subject made studying science seem like something that wasn't half-bad. Post-secondary school, some of my most formidable years were spent at Wright State University in the Department of Chemistry. During my time there I could not ask for better support and encouragement than I received from my advisor William Feld. He set me on the right track as chemist and always pushed me to achieve all that I could. Finally, the following document is testament to all that I have learned over the years from my time at the University of Michigan in the Department of Chemistry. I am grateful for the constant support that the faculty and staff have provided. Particularly I would like to recognize my dissertation committee: Professors Anne McNeil, John Montgomery, and Oveta Fuller. I appreciate all the suggestions and feedback over the years that have elevated the level of my research and my abilities as a scientist. I owe a great debt to my advisor Ted Goodson III for pushing me toward scientific excellence at every turn. I would not be the scientific thinker I am with the guidance and support all these years.

Lastly, my colleagues in the group especially my diligent undergrads Meghan Orr and Alan McLean who helped me immensely with data collection and stimulating discussion, Meng Guo, a close confidant, and Oleg Varnavski who taught me more about aligning optics that I thought I would ever learn. I am forever indebted to you all.

TABLE OF CONTENTS

List of Figures

List of Schemes

List of Tables

ABSTRACT

The development of new sensitive methods for the detailed collection of structural and conformational information about amyloid peptides is critical to elucidating the fundamental aggregation processes that lead to neurodegenerative disease. This research project demonstrates the development of a combined methodology utilizing nonlinear and ultrafast time-resolved spectroscopies for the study of aggregating peptides. Synthetic organic chemistry was crucially implemented to design a biologically compatible chromophore similar in structure to that found in green fluorescent protein (GFP) but one possessing superior two-photon absorption (TPA) characteristics. The photophysical advantages of tailoring a chromophore to address the challenges of studying a dynamic system like Aβ were clearly evident in the strong environmental sensitivity of the chromophore for the changing conformations of Aβ.

The overall impact in the work lies with the significant two-photon absorption enhancement observed with labeled Aβ1-42 that was found to correspond directly to structural features of the aggregating peptides. This sensitivity demonstrates some of the advantages of a two-photon methodology over a traditionally used method like circular dichroism. A two-photon technique has superior low-concentration sensitivity and no limitations due to background sources of absorption. The complete two-photon absorption and time-resolved fluorescence methodology permits detailed conformational and peptide aggregate characterization of the evolution from early oligomer to fibril formation, something that could have a huge impact toward therapeutic intervention or

fundamental understanding of Alzheimer's disease. As a result of this work, a firm foundation for the continued development of nonlinear and time-resolved ultrafast spectroscopies in the investigation of aggregating peptide systems has been established with the known capability to perform fundamental investigations of amyloid systems that are difficult with other biochemical techniques. Many direct applications for *in vivo* imaging may be envisioned using two-photon-based methodologies including cancer targeted monitoring as well as peptide aggregation associated with Alzheimer's and Parkinson's disease. Two-photon imaging has the capability to permit detailed tracking of the evolution of disease beginning with some initial misfolded monomer to the formation of toxic oligomers and later fibril structure. This could have a profound impact on the ability to detect and prevent the development of neurodegenerative disease.

Chapter 1

Introduction and Background

1.1 Scope

Neurodegenerative disease is one of the most researched fields of biomedical study, as many diseases including: Alzheimer's,[1] Parkinson's,[2] and Huntington's diseases,[3] amyotrophic lateral sclerosis,[4] among many others, are believed to occur via related mechanisms pertaining to peptide misfolding or aggregation within the brain. Alzheimer's disease inflicts more than 5.4 million Americans and 15 million people globally[5] including more than 1 in 8 seniors over the age of sixty-five.[6] Parkinson's disease is estimated to affect more than one million Americans and 5 million people worldwide.[7] Indeed, it is quite clear from these statistics the importance of understanding the fundamental processes that lead to the development of neurodegenerative diseases. Such an understanding permits therapeutic intervention so as to lessen or prevent the negative effects the diseases cause. However, to this date, there are no treatments that provide more than symptomatic relief for any of the abovementioned afflictions.

The problem of neurodegenerative disease is obviously large and multi-faceted with some of the details beyond the scope of interest for a chemical researcher and consequently this dissertation. The primary focus of this document will be directed toward the development of new techniques involving ultrafast nonlinear optical and time-

resolved fluorescence-based laser spectroscopies as the tools for study of soluble amyloid-type peptide structures: the species central to development of neurodegenerative disease. Specific interest is given to the early aggregation of the amyloid-β peptide as it self-assembles, progressing from monomer units into larger soluble units, and the variety of conformational and aggregation states it adopts along the way. The more typical hallmarks observed from a clinical standpoint, that of large insoluble fibrillose plaques visible through brain imaging, are beyond what is relevant for our studies. Further extending these considerations, the mechanisms by which these plaques (or even potentially smaller structures) disrupt the neural-processing in the brain, while significant and important to the overall disease process, are not something approached in our studies.

The following introduction serves to familiarize the reader with the relevant details about what is known about the fibrillization of amyloid-β as it proceeds from monomer size to larger fibril structures and the characteristic conformations that may be associated with each stage. A detailed look at the big questions in the field that have yet to be answered follows and provides the fundamental basis for our studies. Along with this discussion, a selection of techniques presently utilized for characterization and study of amyloid peptides will be highlighted with respect to their strengths and limitations. Previous work in our group and a discussion as to our approach taken in applying two-photon materials to the study of the these problems will conclude the introduction, leading into a detailed look in Chapter 2 at the specific spectroscopic techniques that were utilized for our studies.

1.2 General Introduction to Amyloid Peptides

Before delving deeply into the fibrillization characteristics of amyloid-β, it is instructive to broadly examine what it means to be classified as an amyloid peptide. Amyloid peptides are remarkable for their propensity to avoid the mechanisms in place to prevent misfolded peptides from progressing to the point of aggregation and fibril formation that often lead to disease and cell death. Amyloidosis is the process by which these extracellular fibril deposits are formed due to the misfolding of peptides.[8] There are believed to be only approximately 20 peptides (or proteins) that are involved in such processes, and thusly together are classified as amyloid peptides. Though each peptide varies in size and function, they ultimately adopt similar aggregate morphologies during the course of their fibrillization.[9] While familial point mutations often are believed to be prominent factors in increasing misfolding in amyloid proteins, aggregation events may occur with non-mutated versions as well. The aggregation prone regions of amyloid peptides are generally buried in hydrophobic or main chain regions of the normally folded protein, essentially segregated from the surface and interactions with the solvent and other molecules. Physical and chemical changes to the cellular environment such as variations in pH, however, may instigate peptide conformational changes that expose these buried regions. Other events like proteolysis that change the protein composition could trigger the aggregation process and amyloidosis.[9]

The peptide central to Alzheimer's disease, amyloid-β is one of variable length between 38 and 42 amino acid units long. As shown in Figure 1.1, it is derived from the β-amyloid precursor peptide (APP) following proteolysis by two different secretase enzymes that cleave APP from the transmembrane of the cell; first, into a 99 amino acid

peptide before ultimately being cleaved again into a 38, 40, or 42 amino acid amyloid-β peptide by the final secretase.[10] Of the various sizes formed, Aβ1-42 is most aggregation-prone version[11] and is believed to be a prominent species leading to the development of Alzheimer's disease if generated in large quantities beyond the small amount found in typical individuals.[12] The unusual long-term stability of the amyloid fibrils is a result of the strength of the series of hydrogen bonds formed in the aggregate amyloid-β structures. The highly ordered cross-β sheet structures in amyloids are much favored thermodynamically as compared to the unstructured monomer units with there being no equilibrium returning the peptides to an unfolded state.

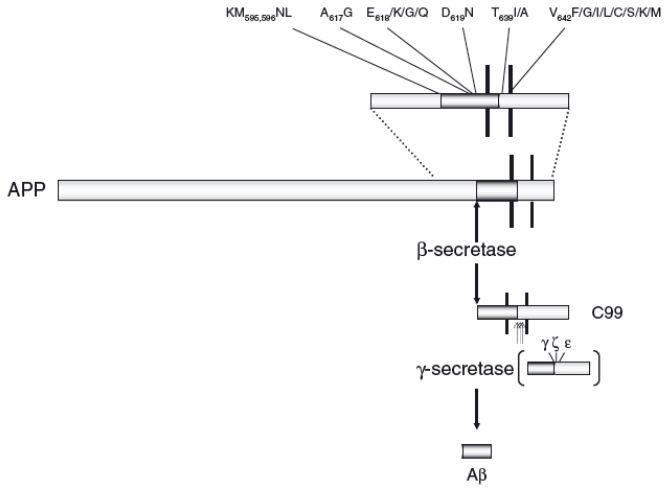

Figure 1.1 Generation of Aβ peptide from amyloid precursor peptide (APP). Figure adapted with permission from Walsh, D. M.; Selkoe, D. J. *J. Neurochem.* **2007**, *101*, 1172. Copyright 2007 John Wiley and Sons.

An aspect central to the study of the aggregation of amyloid peptides and Aβ in particular is an understanding of the development of toxicity and how it relates to the aggregation state of the peptides. It is clear that the simple presence of Aβ in the brain does not alone cause disease as Aβ is found in plenty of normal human subjects,[13] but pinpointing the toxicity-originating conformational or oligomeric structure among the

myriad of structural intermediates is a challenging task. However, over the past several decades extensive scientific contributions from synthetic Aβ studies performed *in vitro* have evidenced that toxicity likely develops somewhere in the oligomeric stage of fibrillization, well before the formation of fibrils.

In vitro studies have become common for observing amyloid aggregation as they give researchers the ability to control environmental conditions in a way not possible *in vivo* while also affording the possibility of easy isolation or modification of the peptides. Using *in vitro* studies, researchers have been able to outline the key stages of fibrillization (Figure 1.2) from random coil monomers to large fibril plaques. Between these two extremes, there have been identified several other distinct intermediate conformational stages with transient paranuclei, soluble oligomer, and protofibril structures among those most widely described. Each peptide assembly is classified according to a combination of particular distinguishing aspects like secondary peptide structure, morphology, and the overall size of the aggregate. Given the various challenges of study presented by each regime, a wide range of techniques has been exploited to structurally characterize the aggregation of amyloid-β. Throughout the next several sections the stages of Aβ aggregation will be introduced in detail, establishing what is known about the conformational or oligomeric morphology of the peptide and some of the common technique methodologies for determining this information.

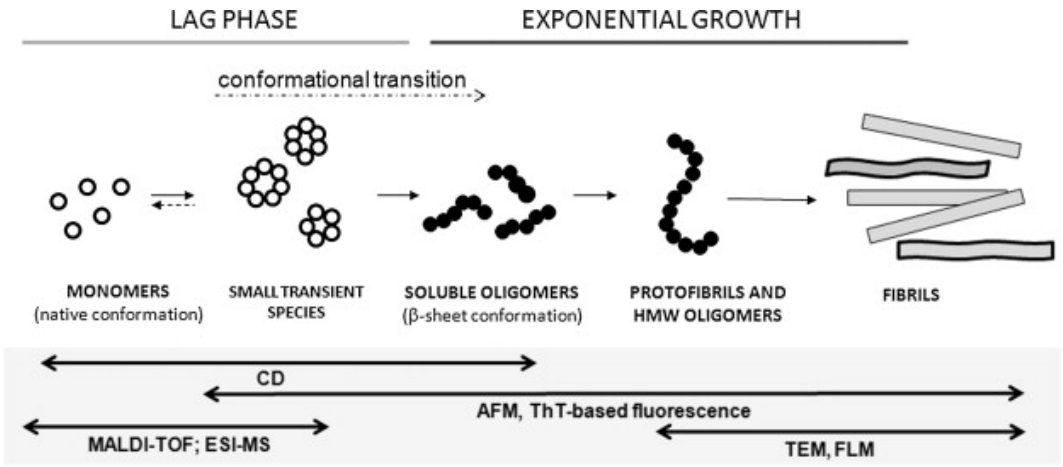

Figure 1.2 Amyloid fibrillization scheme with associated analytical techniques. Figure adapted with permission from Bartolini, M. et al. *Anal. Biochem.* **2011**, *414*, 215. Copyright 2011, with permission from Elsevier.

1.3 Monomers

An understanding of the unfolded initial monomer and the conformational changes it undergoes as it oligomerizes is important as it provides the basis for the entire aggregation process that follows thereafter. Differences in starting conformation may determine whether a peptide ultimately generates toxic amyloid fibrils.[14] However, amyloid-β monomers present a great difficulty in characterization. The very nature of amyloid peptides makes isolating species that are monomeric challenging as most Aβ solutions have peptide assemblies at various stages of aggregation with some fraction of monomers in equilibrium with oligomer structures having numerous conformational and aggregation states. Typical separation methods for amyloid purification like centrifugation and size-exclusion chromatography (SEC) are limited due to the propensity for the peptides to continue aggregating following any such separation. Experimental efforts have been made to try to hinder the rate and extent of aggregation by placing amyloid-β into fluorinated solvents, but this more nonpolar environment promotes additional secondary structure as compared to water-based solutions and

therefore must be removed prior to aggregation study. Even a technique such as the one developed by the Teplow lab[15] that uses a Ru-catalyst to photochemically induce cross-links in the peptide (PICUP), halting aggregation as a snapshot in time has not been very effective at generating significant amounts of isolated monomer. Additionally, common techniques for the structural characterization of proteins like x-ray crystallography or solid-state NMR have found limited success due to the amorphous nature of amyloid peptides. The dearth of highly successful experimental methodologies for monomeric amyloid-β studies has essentially left computational modeling as the best source for detailed information about their conformation features. This void however offers the possibility for development of new techniques to address the challenges.

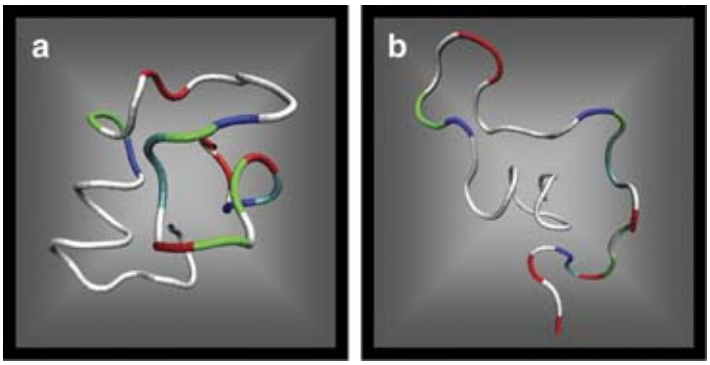

Figure 1.3 Amyloid-β monomer structures obtained from molecular simulations (a) with implicit water and (b) in solvent free environment. Figure adapted with permission from Baumketner, A., et. al *Protein Sci.* **2006**, *15*, 420. Copyright 2006 John Wiley and Sons.

According to a number of published results, monomer structure has various potential conformational forms depending upon the amyloid alloforms (Aβ40 vs. Aβ42), the solvent environment, and general methodology differences. A fundamental difference between the conformational origins of Aβ40 and Aβ42 is an important one as toxicity studies of the oligomers and fibrils have indicated that it is Aβ42 that is the primary form found in amyloid plaques; this despite Aβ40 having a ten times greater presence *in vivo*.[16]

It seems clear that the inherent structural and conformational differences adopted by the alloforms along the fibrillization pathway lead to a significant discrepancy in aggregation and toxicity.[17] A variety of conformational characteristics have been observed from experiments studying Aβ-monomers with the overall body of work indicating that monomers of either alloform (Aβ40 or Aβ42) are generally unstructured in buffer-type solutions (Figure 1.3) and predominately α-helical in fluorinated solutions.`

With a difference in natural propensity for generating conformations that lead to toxicity, a secondary factor that can change the behavior of these monomeric species is the solvent conditions. Often for the study of amyloid aggregation the solvent is simply a buffer solution that serves to broadly mimic the cellular environment, but modified conditions may be created by adjusting pH[18] or using alternative solvents like fluorinated alcohols. These are thought to better represent the type of apolar microenvironments that are found at the lipid cellular membrane. These environmental changes are often significant enough to change the initial conformations that are adopted natively by the amyloid peptide. Fluorinated alcohols tend to promote α-helical secondary structure[19] in amyloid-β and hinder the formation of larger aggregates, while water solutions promote less initially structured monomers but faster rates of aggregation to more structured oligomer units. α-Helical peptide conformation is believed to create membrane channels that may allow for the inclusion of metals ions into the cell and potentially lead to cell death,[20] so the promotion of such structures is beneficial for detailed study of their effects.

The challenges associated with simply isolating monomer units away from all of the other oligomeric species has been discussed, but from a technical standpoint the

problems of working with a small, relatively unstructured peptide are just as great. The reliance on experimental techniques such as ion-mass spectrometry[21] and (to an extent) circular dichroism[22] is limited for obtaining full conformational and structural details without the additional information provided by computational modeling run in parallel to experimental studies. Such combined approaches as the one used by Baumketner et al. utilizing CHARMM[23] and an all-atom force field method developed for protein investigations have yielded structural findings that Aβ42 monomers may adopt either extended chain or collapsed conformation with mostly random coil-like conformations.[24] These results were found to be good in agreement with other studies using CD and NMR that had estimated the unordered structure to be roughly 60-80% of the overall peptide.[18,25] A different modeling package[26] and set of force field modeling parameters (AMBER) were utilized by Sgourakis et al.[14] to model the conformational dynamics of Aβ40 and Aβ42 in accordance with *J*-coupling constants of various amide protons measured experimentally using NMR spectroscopy. These researchers concluded that Aβ42 forms a greater number of conformational variants in the monomeric stage than is present for Aβ40. Structurally, Aβ42 is more constrained at the C-terminus due to a β-hairpin motif versus Aβ40 that has greater flexibility in this region and an N-terminal α-helix.

These studies represent some of the limited work that has been published on elucidating the monomer structure of amyloid-β. The preponderance of work on early peptide aggregation has focused on the more easily observed oligomeric structures found in the transient paranuclei and soluble oligomer stages to come, but it is still guided toward a fundamental understanding of the underlying mechanisms beginning with

monomers and continuing to the point of toxicity. The subsequent sections will continue to delve more deeply into these stages of aggregation.

1.4 Transient Paranuclei

The transition from monomer to oligomer and the structural changes associated with the various amyloid-β alloforms are critical for understanding the specific features that account for the origins of relative toxicity differences. The early phase of this transition to larger aggregates along the fibrillization pathway is widely regarded to generate species called transient paranuclei. Three characteristic features may describe these early aggregates: secondary structure, morphology, and quaternary structure. While more structured than monomers, paranuclei have limited secondary structure with ~20% β-sheet/turn content and ~5% α-helix. They have a distinguishing morphology that is quasispherical as evidenced by microscopy[27] and are often described as having "beaded" structure. The quaternary structure consists of five to six monomer units with the aggregates in equilibrium with their monomer, dimer, trimer precursors. Through efforts to understand the fundamental units responsible for amyloid fibrils, it has become clear that paranuclei oligomers constitute a basic building block for the formation of larger oligomers and protofibrils, essentially superseding monomers as the prominent nuclear species in solution.

The driving force for the generation of these oligomers is understood to be a hydrophobic collapse of peptide due to water interactions with the hydrophilic side-chains that solvate the charged-residues preventing further electrostatic interactions.[27] Also important is the relief of internal conformational stress associated with the hydrophobic regions that encourage the formation of lower-energy fibril formations.[28] As

they are lower energy than other less-ordered states, hydrophobic collapse often results in the generation of α-helix conformations, and eventually β-strand conformations to maximize favorable hydrophobic interactions.[29] Molecular simulations have predicted that initial dimer formation from a predominately α-helical monomer occurs via a transition to a β-rich monomer conformation regardless of alloform, Aβ40 or Aβ42.[30] This result is in line with earlier discussions of the monomer structure adopting β-hairpin characteristics.[24] A significant discovery with respect to the formation of paranuclei was the different conformational behavior between Aβ42 and Aβ40. While both may proceed through dimer formation, Aβ40 does not form the same spherical pentamer/hexamer structures that are observed for Aβ42. The overall rates of formation for larger fibril-type structures are consequently very different with Aβ40 progressing through smaller additions of monomer, dimer, and trimer units (Figure 1.4). It is hypothesized that these divergent mechanisms for fibril formation may hold details as to the heightened toxicity for Aβ42 oligomers.

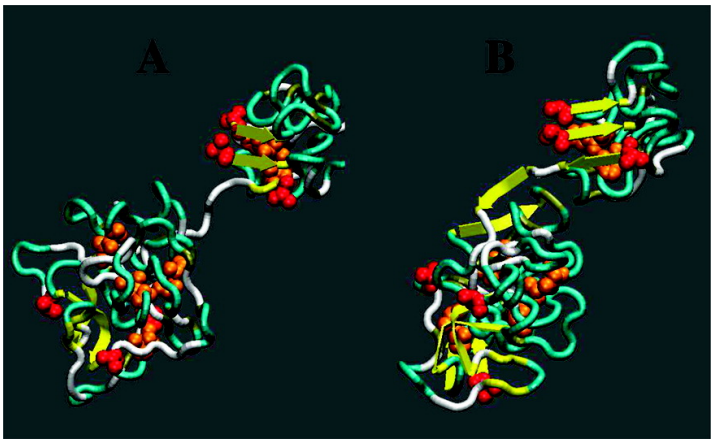

Figure 1.4 Molecular simulation of the formation of Aβ40 hexamer structure from a tetramer and dimer. N-termini represented by red spheres and C-termini by orange spheres. Figure adapted with permission from Urbanc, B. et al. *J. Am. Chem. Soc.* **2010**, *132*, 4266. Copyright 2010 American Chemical Society.

Various experimental methodologies have been developed to characterize paranuclei and the species in equilibrium with the monomeric peptides. According to computational modeling using discrete molecular dynamics performed by Urbanc et al., dimer formation is a critical first step to the formation of oligomers as they were the predominate structure generated in Aβ oligomer simulations.[27] Further analysis indicated that nominal increases in α-helical structure for the oligomer aggregates were generated prior to assembly into protofibrils, as had been previously observed in the literature. Experimentally, the critical evidence for the existence of these small paranuclei comes from the observation of the build up of large quantities of pentamer and hexamer structures when studies were performed on Aβ42 using photo-induced cross-linking of unmodified proteins (PICUP).[31] Using SDS/PAGE to characterize the distribution of assembly sizes, Bitan et al. observed a Gaussian distribution of oligomers centered around 5-6 units in size for Aβ42, however no such behavior for Aβ40. Further characterization of the pre-cross-linked mixture using size exclusion chromatography (SEC) indicated that these oligomer structures were in dynamic equilibrium with the monomer species and could not be isolated. Additional studies[32] using ion mobility mass spectrometry confirmed these initial results and detected a long-lived dodecamer (12-mer) species generated from the assembly of two hexamer units. Conformationally, the N-termini region of Aβ42 was primarily found at the surface of the paranuclear structure with significant freedom of motion. Urbanc, et al. suggests that the additional hydrophobicity provided by the additional two amino acids (Ile-41, Ala-42) at the C-terminus of Aβ42 form the core of the structure and are critical for making the generation of paranuclei favorable only in Aβ42.[33] Bitan et al. expands on this hypothesis

emphasizing that the self-association of paranuclei is facilitated specifically by the *sec*-butyl side-chain of isoleucine and may not be replaced with a smaller alkyl chain or another amino acid. The size of the 5-6 unit aggregate (~55.2 kDa) corresponds to a soluble Aβ peptide assembly that was observed to be toxic via *in vivo* studies in Tg2576 mice that indicated accelerated memory loss.[34] Ono et al. observed in neurotoxicity studies on a range of low molecular weight (LMW) oligomeric structures that dimers were threefold times more toxic than monomers, and tetramers were 13-times more toxic.[35] This is another indication of the importance of studying the early aggregation to find appropriate therapeutic targets for disease prevention.

1.5 Soluble Oligomers

Amyloid peptide formation proceeds through a nucleation method[9] which is comprised of two periods; a lag phase, where overall fibril growth is slow as oligomerization events occur to form the small oligomer nuclei; and an exponential growth phase, where rapid addition of oligomers to generate well-structured fibrils. The rate at which amyloid-β transitions through these phases is dependent on the specific conditions for the system under consideration including peptide concentration, solvent composition, and presence of nucleation "seeds". This being said, the clear instigator of exponential growth is the generation of β-sheet structure that pushes the equilibrium toward larger structures.[36] Plots of β-sheet structure versus time show a prototypical sigmoidal curve with the lag phase having near constant β-sheet content followed by a period of exponential growth before leveling out at some maximum value. For amyloid-β, the paranuclei species are the building blocks and the direct driving force for formation

of larger soluble oligomers and protofibril structures that start to have better defined structural features.

As paranuclei self-associate, they form beaded superstructures that are characteristic of the majority of soluble oligomer species.[31] These high molecular weight (HMW) oligomers are the last of the relatively unstructured intermediates lacking predominate β-sheet/β-turn characteristics. The structural distribution of HMW oligomers is much more diverse than the low-molecular weight (LMW) paranuclei as these assemblies are very much transitory, gradually transforming into protofibrils with significant changes in the secondary structure and increasing fibril-like characteristics. The broader classification of soluble oligomers is often omitted or combined with either the transient paranuclei as a larger class of soluble oligomers or grouped together with the next pathway intermediate, protofibrils. The overarching objectives remain to characterize the transition from LMW oligomers into fibril structure and determine the fundamental details of structural changes that are taking place. For instance, the differences between alloforms Aβ40 and Aβ42 become less pronounced as structurally both eventually generate similar oligomeric forms.[31] Research by Deshpande et al. using neuronal cultures and a variety of Aβ oligomers observed rapid cell death even at very low concentration (~5 μM),[37] highlighting the potential toxicity of oligomer structures.

Experimentally, the techniques associated with the detection and characterization of the aggregate conformations or morphology begin to change with the progression to HMW assemblies, becoming more morphology-based and less atomistic. Fluorescence-based techniques, to an extent however, bridge the gap between aggregate morphology and molecular level interactions. With larger assemblies, understanding what is occurring

on the amino acid residue size-scale becomes increasingly challenging. Fluorescence probes can target specific regions for study based on the method of implementation and type of fluorophore. Mass spectrometry techniques such as MALDI-TOF are ineffective to study these aggregates as the ionization ability is low for HMW structures.[38] Circular dichroism may still be widely implemented for bulk characterization as long as the species remain soluble, however the increasingly diverse structural environment of Aβ-oligomers leads to concerns about how specific of structural contributions may be extracted from such highly averaged data.[25] Aggregate-size determination using confocal microscopy and fluorescence correlation spectroscopy[39] is especially prevalent for the study of larger aggregates as these other techniques become less sensitive due to the high molecular weights (>100 kDa).[40] Other imaging techniques like atomic force microscopy (AFM) become useful starting in this fibrillization regime for studying the morphological aspects of these larger soluble oligomers. As shown by Mastrangelo et al.,[41] the simplest oligomer identified in their studies was found to have a disk shape, approximately 15-25 nm in diameter with a height of ~2 nm. From their research they were also able to identify significant segments of ordered structure, indicative of the transition occurring to protofibrils.

There remains a great opportunity to develop sensitive techniques to more completely probe this regime of the fibrillization pathway given the overwhelming nature of the diversity of structures. Such an array of structures have meant that full-length HMW soluble oligomers are infrequently modeled theoretically as the complexity of the sampling for these larger structures becomes prohibitively difficult beyond a handful of interacting peptides. The structural heterogeneity and general lack of well defined

secondary structure information onto which to original calculations can be based has led the multitude of HMW oligomer *in silico* studies to be geared toward protofibril and fibril characterizations.

1.6 Protofibrils

The progression of amyloid aggregation from HMW soluble oligomers to protofibril stage is marked by a dramatic increase in β-sheet structural characteristics. The transition to protofibril structure is last intermediate before progression irreversibly to amyloid fibrils. With the increased secondary structure and β-sheet formation, a wider array of techniques becomes available for performing detailed studies. Fluorescence-binding dyes that selectively interact with the β-sheet structure of the amyloid aggregates have shown great ability[42] to identify the origination of protofibrils through the use of such dyes as Congo Red (CR) and Thioflavin T (ThT). The principle behind this technique is that in the absence of the amyloid β-sheet with which to interact there is sufficient rotational freedom about the central carbon-carbon bond of the molecule[43] so that upon the molecule's excitation the majority of the emission is lost nonradiatively due to twisting and rotational motions about this bond. However, when these dyes interact with specific sites of β-sheet in amyloid peptides, the rotational freedom is effectively lost, and the molecule now emits a greater fraction of emission as fluorescence and becomes a good signaling process for the presence of amyloid fibril structure. These classically used dyes are limited by a lack of selectivity for the multitude of peptide aggregates that are generated in solution and thus cannot elucidate the conformational characteristics of the smaller, predominately unstructured intermediates that precede protofibrils. Efforts by Gestwicki and others have been geared toward developing new

molecules for more discriminating interactions with Aβ that can be targeted to specific aggregate features.[42]

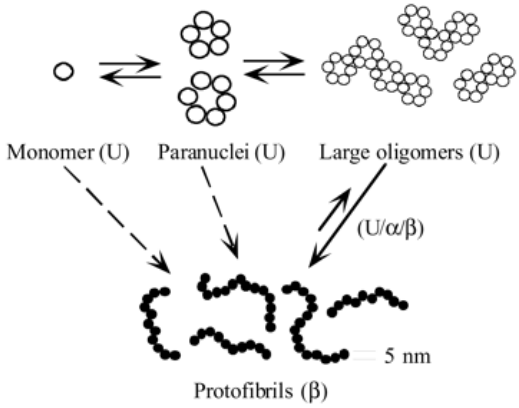

Figure 1.5 Representation of the formation of protofibril structures from the combination of paranuclei and other small oligomers. Figure adapted with permission Bitan, G., et al. *Proc. Natl. Acad. Sci. USA* **2003**, *100*, 330. Copyright 2003 National Academy of Sciences, USA.

Structural details revealed by AFM and other imaging methods have indicated that protofibrils are generally around 5 nm in diameter and assembled from the paranuclei and oligomeric structures previously discussed (Figure 1.5). The longitudinal length is variable depending upon the conditions, but protofibrils themselves are short with lengths approaching ~150 nm as compared to the eventual fibrils whose lengths may be measured in microns.[44] Upon their initial discovery, Walsh et al. described the electron microscopy images of protofibrils and their morphology as "short, curly fibrils".[45] Characterization of their secondary structure using circular dichroism to estimate the relative percentages of the structural components has indicated that consistently between 45-50% of the overall structure is β-sheet with the remainder being predominately random coil (40%) and only 13% α-helical.[25] Comparing these values to those previously described for the paranuclei (~20% β-sheet/turn, ~5% α-helix),[27] there is clearly a substantial increase in the overall secondary structure mostly in the form of β-sheet

character, signaling the larger transition to fibril structures. Kheterpal et al. implemented a technique for characterizing the extent of hydrogen-bonding in protofibril structure using hydrogen-deuterium exchange,[46] finding that nearly 40% of the amide protons were involved in hydrogen bonding. This is significantly less than that found in fibril structures, however the same hydrophobic patches (16-21, 31-36) were found in both protofibrils and fibrils.[47] The authors cite the overall incremental nature of the increase in hydrogen bonding progressing from monomers through fibrils as reasonable evidence for their observed structural forms being on-pathway to fibrils.[48] Toxicity studies performed by Kayed et al.[49] examining lipid bilayer conductance associated with interactions involving amyloid peptides found that HMW oligomers and protofibril structures were predominately responsible for increased membrane conductance response, a sign of pathogenesis. Particularly interesting in their findings was that only spherical oligomer structures caused the noted membrane effect, LMW oligomers and amyloid fibrils had no impact.

1.7 Fibrils

The last structural transition that occurs to form amyloid fibrils is the conversion of the protofibrils into these larger morphologies. Fibril structures are generally insoluble species with very specific structural characteristics involving the formation of protofilaments as generated from the elongation of protofibril intermediates.[50] The protofilaments constitute the fundamental units of the amyloid fibril structure[8] and tend to twist around one another to form the final morphology.[51] With the generation of very well ordered structures, experimental techniques such as solid-state NMR and diffraction studies that were ineffective for the unstructured intermediates and low-molecular weight oligomers become critical to understanding the morphology and conformation of these

species. Amyloid plaques have been analyzed using fiber diffraction to indicate that prominent β-structure runs perpendicular to the fibril axis[52] and are associated with one another via side chain interactions.[53] These β-strands then hydrogen bond with one another to form β-sheets that run parallel to the axis of the fibril (Figure 1.6).[54] The eventual fibrils are composed of 5-6 protofilaments with diameters reaching ~10 nm.[55] The generation of insoluble species drastically shifts the equilibrium in amyloid formation strongly toward fibrils as they precipitate out of solution. Lomakin et al. developed a kinetic theory utilizing quasielastic light scattering (QLS) to model the *in vitro* fibrillization of amyloid-β. They conclude that fibrillogenesis requires nucleation from smaller seeds and that fibril growth occurs via irreversible addition of monomers.[56] Similar studies were performed by Inouye and Kirschner using Congo Red binding dyes to examine the seeding rate of amyloid fibrillization, potentially important for study of pharmacological agents directed toward therapeutic intervention.[57]

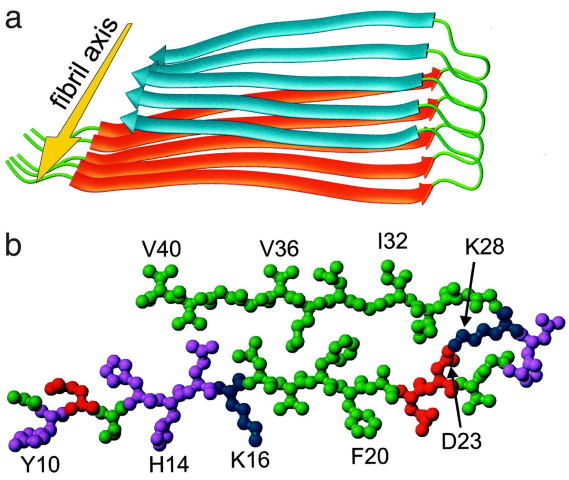

Figure 1.6 Fibril structural model showing beta-sheet interaction of Aβ40. Figure used with permission Petkova, A. T., et al. *Proc. Natl. Acad. Sci. USA* **2002**, *99*, 16742. Copyright 2002 National Academy of Sciences, USA.

Given the ability to perform additional structure-based characterization techniques, a very ordered picture of the orientation of the peptide units in the fibril structure may be obtained. These constraints derived from experimental results provide a good starting point for a diverse set of computational modeling to better probe the molecular-level structural features that are found in the amyloid fibrils. Röhrig et al.[58] looked at all-atom, explicit solvent modeling of a fragment of amyloid-β ranging from 16-22 to understand the characteristics of the fibril β-sheet. They examined the stability of the formed structures as a function of number of units involved, then using calculated x-ray diffraction patterns, compared their results to experimental findings. From a variety of different theoretical and experimental characterizations, a set of molecular distances associated with the sheet spacing of the fibril has consistently been found with ~4.5-4.9 Å interpeptide distance between neighboring anti-parallel strands and a ~10 Å intersheet distance. However, the resolution of the experimental data is not sufficiently high to provide detailed molecular information. Consequently, a number of research groups have implemented refined modeling techniques to provide detailed theoretical calculations as an extension of their studies. Petkova et al.[55] demonstrated with a combined approach of solid-state NMR and computational modeling using CHARMM the detailed fibril structure of Aβ40. They found that the N-terminus region of the peptide, even those in the fibril form, was largely unstructured with the β-sheet structure being generated only with residues 12-24 and 30-40. A kink at residues 25-29 generates the anti-parallel β-structure in Aβ fibrils, permitting intermolecular hydrogen bonding between the aforementioned β-strand segments. With studies like these, the pursuit of detailed structural studies remains driven toward the identification of the important structural

elements that could be therapeutic targets for intervention, and the development of approaches for elucidating fibril assembly.

As has been described throughout, the progression from a monomer-state to a complex fibril formation is a complicated process proceeding through a variety of pathway structures each with different conformational and aggregation states that require characterization. From the earliest aggregation stages, transitions of secondary structure from random coil to β-sheet, random coil to α-helix, and α-helix to β-sheet have been observed using a myriad of biophysical techniques. Extensive study has indicated that non-fibrillar oligomeric Aβ forms are likely significant toxic contributors to Alzheimer's disease (AD).[59] However, there remains a number of prevailing questions regarding the pathways of fibrillogenesis and identifying specific steps along the way that present opportunities for targeted therapeutic intervention.[44] Recent studies have shown that soluble oligomers anywhere from 2 to 24 peptides in size[40] and protofibril structures[8] that contain substantial fractions of β-sheet secondary structure may be critical originators of the cytotoxicity for neurodegenerative peptides such as amyloid-β, but as with formation mechanism, the conformational characteristics at the pre-fibrillar stage remain to be definitively established.[40]

1.8 Previous Work in the Laboratory

Based on the discussion over the course of the previous sections, it is clear there remains a great deal to be understood about the overall aggregation process of amyloid–β peptides especially at the earliest aggregation stages. The development of new techniques to better target these areas and draw new insight may be critical to fully understanding the structure-function relationship of oligomeric species and toxicity, thereby allowing

for targeted intervention of therapeutics. Looking beyond just the study of Alzheimer's disease, many of the same technological advances applied to amyloid-β may aid in the generalized study of conformational changes associated with other aggregating proteins, and prove vital to understanding the fundamental events involved in the development of many neurodegenerative diseases.[9,35]

A number of years ago, our group began investigating ways to implement established ultrafast techniques often directed toward materials characterizations to biological systems, especially toward questions about peptide structural characteristics. A feature of particular importance for investigation of detailed peptide conformational changes is the acknowledged potential for some materials to have additional two-photon absorption characteristics due to cooperative enhancement resulting from inter-chromophore coupling interactions among neighboring molecules.[60-62] Our group and others in recent years have utilized non-linear optical spectroscopy in conjunction with fluorescence-based techniques to observe molecular interactions in such enhanced systems. Extensive investigations into conjugated dendrimer systems including branched thiophenes[63] and a variety of triarylamine systems[61,64-66] have led to an understanding that due to strong interactions amongst chromophore structural elements in the ground state, two-photon enhancement is noted from delocalized excitations hopping between these chromophores.[64] These concepts will be addressed in more detail later. However, the overall sensitivity of our techniques for molecular interactions coupled with the potential of two-photon excitation in imaging and other biological applications are compelling motivations for the exploration of a two-photon methodology as a tool for understanding complex interactions taking place in biological systems.

Our initial studies in this arena demonstrated that a two-photon methodology could probe the structural dynamics of a Cascade Yellow-labeled B5 protein associated with herpes simplex virus (HSV).[67] These studies led to evidence indicating that a pH-insensitive dissociation of the coiled coils was taking place. Further studies expanding our methodology, again using Cascade Yellow (CY) as a fluorescent tag, examined the self-assembly of a CY-bound prion peptide ($PrP_{106-126}$) using two-photon excitations[68] in tandem with femtosecond time-resolved fluorescence spectroscopy to reveal distinct correlations of each spectroscopy with the level of β-sheet formation. Finally, as will be fully described in Chapter 3, the approach was then extended using site-specific labeling of the N-terminus of amyloid-β with a TAMRA dye to interrogate the early conformational dynamics, and demonstrating a distinct sensitivity for aggregate structures when two-photon excitation is utilized.[69] Based on these studies, applied two-photon absorption techniques utilizing fluorescent markers have shown clear promise for the examination of conformation changes and aggregation of peptides. The continued development of better environmentally sensitive two-photon absorbing chromophores remains important for obtaining fundamental details that can be put toward answering critical questions about amyloids. The combined approach of two-photon absorption spectroscopy with ultrafast fluorescence lifetime and depolarization studies should provide a strong avenue for continued exploration of these systems.

1.9 Utilizing Two-Photon Materials for Biological Applications

As discussed in the previous section, methodology development has occurred using a number of peptide systems that were labeled with commercially available dyes having reasonable two-photon absorption properties. Limitations of these systems,

however, include the inability to control the photophysical properties of chromophore and select the means of attachment to the biomolecules being studied. As such, a central component of the research project presented in this dissertation was the design and synthesis of chromophores having photophysical characteristics that lend to better implementation of the two-photon techniques and are specifically tailored for the study of aggregating peptides. The remaining introductory material serves to discuss some of the fundamental principles of nonlinear optical spectroscopy and begins to establish the basis for the design of two-photon absorbing materials both generally and for our specific application.

Nonlinear optical spectroscopy, of which two-photon spectroscopy is a subset, is governed by the intensity dependence on the strength of the electric field that arises from incident radiation. The interaction of an organic molecule with such a field can be modeled quantum mechanically as polarizability of the molecule governed by the following power series equation:

$$P(t) = \chi^{(1)}E(t) + \chi^{(2)}E^2(t) + \chi^{(3)}E^3(t) + \ldots$$

Where $\chi^{(1)}$, $\chi^{(2)}$, $\chi^{(3)}$, are the first, second, and third nonlinear susceptibilities. Two-photon absorption is a third-order process with a quadratic dependence on the incident radiation. A two-photon absorption process is one in which two photons are simultaneously absorbed to complete an electronic transition. The typical means for describing the extent of this absorption is via the two-photon absorption cross-section of a molecule that is reported in the units of GM, where 1 GM = 10^{-50} $cm^4 \cdot s \cdot photon^{-1}$. Further derivation of two-photon absorption principles may be performed using quantum mechanics and

perturbation theory but is beyond the scope of this dissertation. Further details about the practical implementation of two-photon spectroscopy will be discussed in Chapter 2.

Fundamental to any nonlinear process is the change in transition dipole moment of the studied molecule upon simultaneous absorption of two photons and promotion of an electron from the ground state to an allowed excited state. For organic molecules, the creation of a large dipole transition and two-photon absorption (TPA) cross-section is strongly associated with conjugated asymmetric systems designed to have charge-transfer across the molecule.[70] These systems generally take the structural form of "donor-π-acceptor" involving large conjugated molecules with select electron-withdrawing and electron-donating substituents. A wide variety of such donor-acceptor molecules with distinct charge-transfer characteristics have been examined for their responsiveness to two-photon excitation.[71] Many of these TPA materials[70,72] have found use in a number of applications including optical limiting,[73] microscopy,[74] data storage,[75] photodynamic therapy,[76] among others. For this reason the continued design of two-photon absorbing molecules has been an area of great interest. Researchers have developed a range of structures possessing strong TPA characteristics geared toward these many applications.

From a molecular design perspective, there have been a number of principles established for creating materials with high two-photon absorption cross-sections over the course of several decades of research. Albota et al. published a highly cited paper[71] in *Science* in the late 1990s that summarized the main synthetic accomplishments toward achieving high two-photon absorbing materials. In their studies of bis(styrylbenzene) derivatives they found that, upon excitation, molecules having symmetric charge-transfer across their structure facilitate large changes in transition dipole moment and

consequently TPA cross-sections. The particular structural characteristics that were observed to increase the cross-section were: 1) increasing the conjugation length of the molecules and 2) the incorporation of donor (D) and acceptor (A) functional groups to create D-A-D and A-D-A type motifs. Across numerous papers published in this area since that time, other groups including our own[65] have found that increasing a molecule's polarizability (or dipole moment) through the extension of conjugation and addition of strong donor or acceptor groups on a systematic basis produces higher TPA cross-sections. Typical examples from the literature of groups that act as good donors include various amino groups (e.g. $–NMe_2$) and alkoxy groups (e.g. –OMe), with often-used acceptors commonly being cyano derivatives (e.g. –CN) or nitro substituents (e.g. $–NO_2$).

Theoretical calculations often are used to predict two-photon absorption cross-sections, yielding important principles for the specific design of different structural motifs.[77] The framework for the initial design of our two-photon absorbing chromophore to be used for this research was based upon some theoretical calculations[78] found in the literature that were performed on model chromophores of the type found naturally in fluorescent proteins. The results of this study indicated that for being small molecules a range of fluorescent protein chromophores possessed reasonably high two-photon absorption cross-sections. Figure 1.7 shows the structures of the modeled chromophores and the predicted two-photon absorption cross-sections.

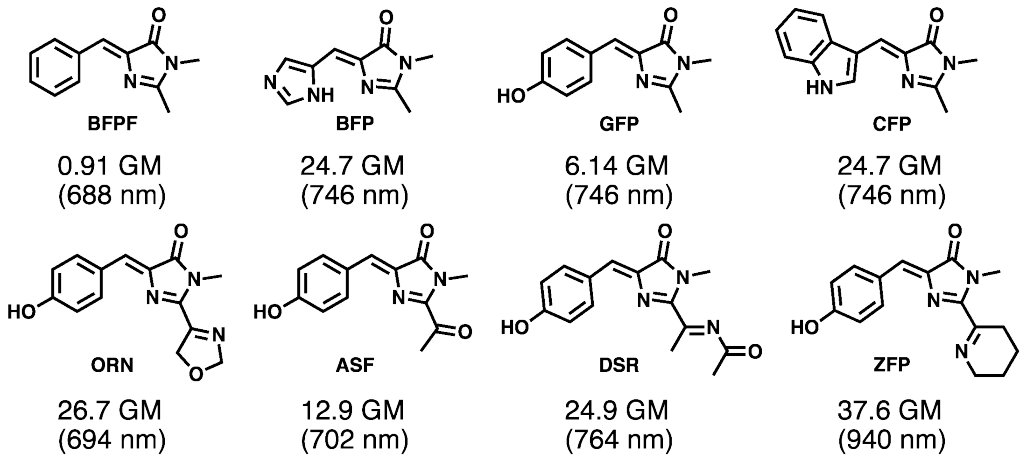

Figure 1.7 Calculated two-photon absorption cross-sections for various fluorescence protein chromophores. Cross-sections above are selected at wavelengths to be relatively near 800 nm.

Similarly, during the course of this dissertation research, the Rebané group performed a series of two-photon absorption studies on fluorescent proteins measuring experimentally their two-photon absorption cross-sections.[79, 80] Figure 1.8 below shows a selection of the chromophores associated with these proteins and their respective cross-sections.

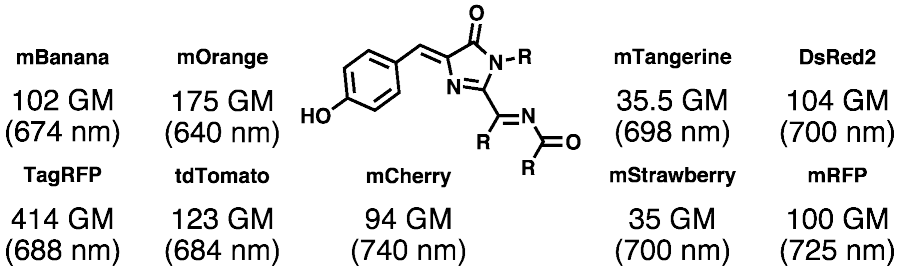

Figure 1.8 Experimentally determined TPA cross-sections for red fluorescent protein derivatives. The basic structure is indicated at the center, different protein mutations account for the different photophysical properties.

With the potential for high two-photon response, these types of chromophores are also attractive for biological labeling as they are derived from a natural source via an autocatalyzed reaction of specific amino acid motifs in proteins[81] and likely would present limited cytotoxic effects if implemented as a fluorescence label in the study of

amyloid-β. Additionally, the photophysical characteristics are well established for the fluorescent proteins series with absorptions ranging widely throughout the visible spectrum, providing a good foundation for our photophysical studies. Another attractive characteristic about this class of compounds is the potential for fluorescence quantum yield switching based on environmental features. The chromophores found in fluorescent proteins are highly fluorescent (quantum yield ~0.8) when held within the β-barrel shaped structure of the surrounding protein; however, when isolated the quantum yield drops by several orders of magnitude to ~10^{-3}. This indicates the kind of environmental sensitivity that is very appealing for a peptide label if it can show varied responses based upon the intramolecular or intermolecular interactions that happen as a peptide changes conformation.

The pioneering work of Nobel Prize laureates Tsien,[82] Chalfie,[83] and Shimomura[84] has led to the development of a wide range fluorescent proteins with varying photophysical characteristics.[85] A number of researchers have worked extensively over the past several decades to isolate,[86] characterize,[87] and synthetically mimic[88] the chromophores of these fluorescent proteins to understand the chemistry behind their unique characteristics. Our work sought to build upon this foundation by applying the principles for creating strong two-photon absorbing materials to generate a chromophore with improved photophysical properties, tailored for study with nonlinear and ultrafast spectroscopy techniques for the specific application of observing amyloid peptide aggregation. Additional details associated with the development of the chromophore design will be discussed in Chapter 2.

The dissertation work that follows describes the development of a combined methodology utilizing nonlinear and ultrafast time-resolved spectroscopies for the study of aggregating peptides through the implementation of novel two-photon absorbing chromophores. The potential impact in this work lies with the ability to observe changes in the two-photon absorption cross-section of labeled peptides as a function of the evolving structural features for aggregating peptides. Such a two-photon methodology has the ability to have great low-concentration sensitivity and no limitations due to background sources of absorption that are presented by other optical techniques. The two-photon absorption-based technique when combined with ultrafast time-resolved fluorescence spectroscopy creates a methodology that will allow for the detailed conformational and aggregate characterization from early peptide oligomerization to fibril formation. This development may have the ability to profoundly impact the fundamental understanding of the detection and prevention of neurodegenerative disease.

1.10 Dissertation Outline

The remaining body of this dissertation will be organized as follows. Chapter 2 will discuss the relevant techniques that were utilized in the implementation of our experimental design. Brief explanations for our synthetic methodology, steady-state spectroscopy, two-photon absorption spectroscopy via the TPEF route, time-resolved fluorescence upconversion spectroscopy, time-correlated single-photon counting (TCSPC), and circular dichroism will be included. These descriptions should familiarize the reader with the fundamental details of the experiments that may be cursorily covered in chapters 3, 4, & 5 where published work forms the basis of the content.

Chapter 3 will discuss work published in the *Journal of Physical Chemistry* detailing our initial body of work on amyloid-β peptide. Within this chapter will be our

studies applying many of the ultrafast techniques described in chapter 2, however most notably TPEF, TCSPC, and CD to characterize the conformational and aggregation of a labeled amyloid peptide as a function of solution concentration. Importantly highlighted in this chapter will be the development of the methodology at this stage of the research that would prove critical to the subsequent study. The experimental work was largely performed by my predecessor in the group Dr. Ying Wang, but significant data analysis, interpretation, and writing were performed on my part.

Chapter 4 will detail the extensive synthetic work that was performed in generating the chromophores to be used in application as fluorescent tags covalently bound to amyloid peptides. A short exploration of our molecular design and initial synthetic attempts introduces this chapter followed by an explanation of its evolution leading to our eventual synthetic outline. The bulk of the subsequent synthetic and spectroscopic characterization is presented as was published in an article in the *Journal of Physical Chemistry*. This chapter also makes relevant connections to the literature of GFP-type chromophores and contains discussion driven toward our established goal of biological applications.

In chapter 5, the focus becomes the biochemical studies of amyloid-β utilizing the best chromophore synthesized and characterized in chapter 4 and an implementation of techniques in a similar fashion as described in chapter 3. This chapter is based upon work submitted to the *Proceedings of the National Academy of Sciences*. Synthetic details as to the preparation and spectroscopic characterization of the label and peptide will be presented along with a variety of preliminary investigations into the folding dynamics of a N-terminus labeled amyloid-β. The steady-state spectroscopy of the labeled and

unlabeled peptide was investigated and a characterization of secondary structure as it relates to concentration. Ultrafast time-resolved fluorescence studies were also performed to monitor changes in both lifetime and depolarization as a function of peptide interactions. An examination of the two-photon absorption cross-sections of the labeled peptide was also extensively performed comparing structural sensitivity to a traditionally used technique of circular dichroism.

Chapter 6 highlights some residual studies related to my research that are corollaries to the overall narrative established in the chapters that precede it. In collaboration with Barbara Imperiali's group at MIT, two-photon absorption studies were performed on a calmodulin peptide system examining the effect of calcium ion binding on the two-photon excited fluorescence enhancement of a custom labeled system. Future development of this project will be discussed and how it ties into the overall themes of the larger dissertation work.

In chapter 7, a short summary is presented on the overall efforts we have made on developing a two-photon based methodology for the study of amyloid aggregation and conformational change throughout the course of this dissertation. Also, further work necessary to advance this research is proposed. Chapter 8 presents a generalized look at my research geared toward a non-expert science audience with descriptions of my dissertation work written at a more broadly relatable level.

References

1. Hardy, J.; Selkoe, D. J. *Science* **2002**, *297*, 353.

2. Spillantini, M. G.; Crowther, R. A.; Jakes, R.; Hasegawa, M.; Goedert, M. *Proc. Natl. Acad. Sci. USA* **1998**, *95*, 6469.

3. DiFiglia, M.; Sapp, E.; Chase, K. O.; Davies, S. W.; Bates, G. P.; Vonsattel, J. P.; Aronin, N. *Science* **1997**, *277*, 1990.

4. Walker, L.; LeVine, H. *Mol. Neurobiol.* **2000**, *21*, 83.

5. Blennow, K.; de Leon, M. J.; Zetterberg, H. *The Lancet* **2006**, *368*, 387.

6. Alzheimer's Assocation: Alzheimer's Facts and Figures, http://www.alz.org/alzheimers_disease_facts_and_figures.asp (accessed July 2012).

7. The Michael J. Fox Foundation: I've Got What?, http://www.michaeljfox.org/living_aboutParkinsons_parkinsons101.cfm (accessed July 2012)

8. Chiti, F.; Dobson, C. M. *Annu. Rev. Biochem.* **2006**, *75*, 333.

9. Dobson, C. M. *Nature* **2003**, *426*, 884.

10. Vassar, R.; Bennett, B. D.; Babu-Khan, S.; Kahn, S.; Mendiaz, E. A.; Denis, P.; Teplow, D. B.; Ross, S.; Amarante, P.; Loeloff, R.; Luo, Y.; Fisher, S.; Fuller, J.; Edenson, S.; Lile, J.; Jarosinski, M. A.; Biere, A. L.; Curran, E.; Burgess, T.; Louis, J.-C.; Collins, F.; Treanor, J.; Rogers, G.; Citron, M. *Science* **1999**, *286*, 735.

11. Burdick, D.; Soreghan, B.; Kwon, M.; Kosmoski, J.; Knauer, M.; Henschen, A.; Yates, J.; Cotman, C.; Glabe, C. *J. Biol. Chem.* **1992**, *267*, 546.

12. Suzuki, N.; Cheung, T.; Cai, X.; Odaka, A.; Otvos, L.; Eckman, C.; Golde, T.; Younkin, S. *Science* **1994**, *264*, 1336.

13. Walsh, D. M.; Tseng, B. P.; Rydel, R. E.; Podlisny, M. B.; Selkoe, D. J. *Biochemistry* **2000**, *39*, 10831.

14. Sgourakis, N. G.; Yan, Y.; McCallum, S. A.; Wang, C.; Garcia, A. E. *J. Mol. Biol.* **2007**, *368*, 1448.

15. Bitan, G.; Lomakin, A.; Teplow, D. B. *J. Biol. Chem.* **2001**, *276*, 35176.

16. Murray, M. M.; Bernstein, S. L.; Nyugen, V.; Condron, M. M.; Teplow, D. B.; Bowers, M. T. *J. Am. Chem. Soc.* **2009**, *131*, 6316.

17. Dahlgren, K. N.; Manelli, A. M.; Stine, W. B.; Baker, L. K.; Krafft, G. A.; LaDu, M. J. *J. Biol. Chem.* **2002**, *277*, 32046.

18. Kirkitadze, M. D.; Condron, M. M.; Teplow, D. B. *J. Mol. Biol.* **2001**, *312*, 1103.

19. Hong, D.-P.; Hoshino, M.; Kuboi, R.; Goto, Y. *J. Am. Chem. Soc.* **1999**, *121*, 8427.

20. Crescenzi, O.; Tomaselli, S.; Guerrini, R.; Salvadori, S.; D'Ursi, A. M.; Temussi, P. A.; Picone, D. *Eur. J. Biochem.* **2002**, *269*, 5642.

21. Bernstein, S. L.; Wyttenbach, T.; Baumketner, A.; Shea, J.-E.; Bitan, G.; Teplow, D. B.; Bowers, M. T. *J. Am. Chem. Soc.* **2005**, *127*, 2075.

22. Barrow, C.; Yasuda, A.; Kenny, P.; Zagorski, M.; Wright, P. *J. Mol. Biol.* **1992**, *225*, 1075.

23. MacKerell, A. D.; Bashford, D.; Bellott; Dunbrack, R. L.; Evanseck, J. D.; Field, M. J.; Fischer, S.; Gao, J.; Guo, H.; Ha, S.; Joseph-McCarthy, D.; Kuchnir, L.; Kuczera, K.; Lau, F. T. K.; Mattos, C.; Michnick, S.; Ngo, T.; Nguyen, D. T.; Prodhom, B.; Reiher, W. E.; Roux, B.; Schlenkrich, M.; Smith, J. C.; Stote, R.; Straub, J.; Watanabe, M.; Wiórkiewicz-Kuczera, J.; Yin, D.; Karplus, M. *J. Phys. Chem. B* **1998**, *102*, 3586.

24. Baumketner, A.; Bernstein, S. L.; Wyttenbach, T.; Bitan, G.; Teplow, D. B.; Bowers, M. T.; Shea, J.-E. *Protein Sci.* **2006**, *15*, 420.

25. Walsh, D. M.; Hartley, D. M.; Kusumoto, Y.; Fezoui, Y.; Condron, M. M.; Lomakin, A.; Benedek, G. B.; Selkoe, D. J.; Teplow, D. B. *J. Biol. Chem.* **1999**, *274*, 25945.

26. Lindahl, E.; Hess, B.; van der Spoel, D. *J. Mol. Mod.* **2001**, *7*, 306.

27. Urbanc, B.; Betnel, M.; Cruz, L.; Bitan, G.; Teplow, D. B. *J. Am. Chem. Soc.* **2010**, *132*, 4266.

28. Zhang, S.; Iwata, K.; Lachenmann, M. J.; Peng, J. W.; Li, S.; Stimson, E. R.; Lu, Y. a.; Felix, A. M.; Maggio, J. E.; Lee, J. P. *J. Struc. Biol.* **2000**, *130*, 130.

29. Klimov, D. K.; Thirumalai, D. *Structure* **2003**, *11*, 295.

30. Urbanc, B.; Cruz, L.; Ding, F.; Sammond, D.; Khare, S.; Buldyrev, S. V.; Stanley, H. E.; Dokholyan, N. V. *Biophys. J.* **2004**, *87*, 2310.

31. Bitan, G.; Kirkitadze, M. D.; Lomakin, A.; Vollers, S. S.; Benedek, G. B.; Teplow, D. B. *Proc. Natl. Acad. Sci. USA* **2003**, *100*, 330.

32. Bernstein, S. L.; Dupuis, N. F.; Lazo, N. D.; Wyttenbach, T.; Condron, M. M.; Bitan, G.; Teplow, D. B.; Shea, J.-E.; Ruotolo, B. T.; Robinson, C. V.; Bowers, M. T. *Nat Chem* **2009**, *1*, 326.

33. Urbanc, B.; Cruz, L.; Yun, S.; Buldyrev, S. V.; Bitan, G.; Teplow, D. B.; Stanley, H. E. *Proc. Natl. Acad. Sci. USA* **2004**, *101*, 17345.

34. Lesné, S.; Koh, M. T.; Kotilinek, L.; Kayed, R.; Glabe, C. G.; Yang, A.; Gallagher, M.; Ashe, K. H. *Nature* **2006**, *440*, 352.

35. Ono, K.; Condron, M. M.; Teplow, D. B. *Proc. Natl. Acad. Sci. USA* **2009**, *106*, 14745.

36. Bartolini, M.; Bertucci, C.; Bolognesi, M. L.; Cavalli, A.; Melchiorre, C.; Andrisano, V. *ChemBioChem* **2007**, *8*, 2152.

37. Deshpande, A.; Mina, E.; Glabe, C.; Busciglio, J. *J. Neurosci.* **2006**, *26*, 6011.

38. Bartolini, M.; Naldi, M.; Fiori, J.; Valle, F.; Biscarini, F.; Nicolau, D. V.; Andrisano, V. *Anal. Biochem.* **2011**, *414*, 215.

39. Garai, K.; Sengupta, P.; Sahoo, B.; Maiti, S. *Biochem. Biophys. Res. Commun.* **2006**, *345*, 210.

40. Sakono, M.; Zako, T. *FEBS J.* **2010**, *277*, 1348.

41. Mastrangelo, I. A.; Ahmed, M.; Sato, T.; Liu, W.; Wang, C.; Hough, P.; Smith, S. O. *J. Mol. Biol.* **2006**, *358*, 106.

42. Reinke, A. A.; Gestwicki, J. E. *Chem. Biol. Drug Des.* **2011**, *77*, 399.

43. Srivastava, A.; Singh, P. K.; Kumbhakar, M.; Mukherjee, T.; Chattopadyay, S.; Pal, H.; Nath, S. *Chem. Eur. J.* **2010**, *16*, 9257.

44. Roychaudhuri, R.; Yang, M.; Hoshi, M. M.; Teplow, D. B. *J. Biol. Chem.* **2009**, *284*, 4749.

45. Walsh, D.; Lomakin, A.; Benedek, G.; Condron, M.; Teplow, D. *J. Biol. Chem.* **1997**, *272*, 22364.

46. Kheterpal, I.; Zhou, S.; Cook, K. D.; Wetzel, R. *Proc. Natl. Acad. Sci. USA* **2000**, *97*, 13597.

47. Williams, A. D.; Sega, M.; Chen, M.; Kheterpal, I.; Geva, M.; Berthelier, V.; Kaleta, D. T.; Cook, K. D.; Wetzel, R. *Proc. Natl. Acad. Sci. USA* **2005**, *102*, 7115.

48. Kheterpal, I.; Lashuel, H. A.; Hartley, D. M.; Walz, T.; Lansbury, P. T.; Wetzel, R. *Biochemistry* **2003**, *42*, 14092.

49. Kayed, R.; Sokolov, Y.; Edmonds, B.; McIntire, T. M.; Milton, S. C.; Hall, J. E.; Glabe, C. G. *J. Biol. Chem.* **2004**, *279*, 46363.

50. Serpell, L. C. *Biochim. Biophys. Acta* **2000**, *1502*, 16.

51. Rambaran, R. N.; Serpell, L. C. *Prion* **2008**, *2*, 112.

52. Kirschner, D. A.; Abraham, C.; Selkoe, D. J. *Proc. Natl. Acad. Sci. USA* **1986**, *83*, 503.

53. Makin, O. S.; Atkins, E.; Sikorski, P.; Johansson, J.; Serpell, L. C. *Proc. Natl. Acad. Sci. USA* **2005**, *102*, 315.

54. Fink, A. L. *Fold. Des.* **1998**, *3*, R9.

55. Petkova, A. T.; Ishii, Y.; Balbach, J. J.; Antzutkin, O. N.; Leapman, R. D.; Delaglio, F.; Tycko, R. *Proc. Natl. Acad. Sci. USA* **2002**, *99*, 16742.

56. Lomakin, A.; Teplow, D. B.; Kirschner, D. A.; Benedek, G. B. *Proc. Natl. Acad. Sci. USA* **1997**, *94*, 7942.

57. Inouye, H.; Kirschner, D. A. *J. Struct. Biol.* **2000**, *130*, 123.

58. Rohrig, U. F.; Laio, A.; Tantalo, N.; Parrinello, M.; Petronzio, R. *Biophys. J.* **2006**, *91*, 3217.

59. Walsh, D. M.; Selkoe, D. J. *J. Neurochem.* **2007**, *101*, 1172.

60. Lahankar, S. A.; West, R.; Varnavski, O.; Xie, X.; Goodson, T.; Sukhomlinova, L.; Twieg, R. *J. Chem. Phys.* **2004**, *120*, 337.

61. Varnavski, O.; Yan, X.; Mongin, O.; Blanchard-Desce, M.; Goodson, T. *J. Phys. Chem. C* **2007**, *111*, 149.

62. Drobizhev, M.; Karotki, A.; Dzenis, Y.; Rebane, A.; Suo, Z.; Spangler, C. W. *J. Phys. Chem. B* **2003**, *107*, 7540.

63. Ramakrishna, G.; Bhaskar, A.; Bauerle, P.; Goodson, T. *J. Phys. Chem. A* **2007**, *112*, 2018.

64. Goodson, T. G. *Acc. Chem. Res.* **2005**, *38*, 99.

65. Bhaskar, A.; Ramakrishna, G.; Lu, Z.; Twieg, R.; Hales, J.; Hagan, D.; Van Stryland, E.; Goodson III, T. *J. Am. Chem. Soc.* **2006**, *281*, 1653.

66. Guo, M.; Varnavski, O.; Narayanan, A.; Mongin, O.; Majoral, J.-P.; Blanchard-Desce, M.; Goodson, T. *J. Phys. Chem. A* **2009**, *113*, 4763.

67. Brown, O.; Lopez, S.; Fuller, A.; Goodson III, T. *Biophys. J.* **2007**, *93*, 1068.

68. Wang, Y.; Goodson III, T. *J. Phys. Chem. B* **2007**, *111*, 327.

69. Wang, Y.; Clark, T. B.; Goodson III, T. *J. Phys. Chem. B* **2010**, *114*, 7112.

70. Marder, S. R. *Chem. Commun.* **2006**, 131

71. Albota, M.; Beljonne, D.; Brédas, J.-L.; Ehrlich, J. E.; Fu, J.-Y.; Heikal, A. A.; Hess, S. E.; Kogej, T.; Levin, M. D.; Marder, S. R.; McCord-Maughon, D.; Perry, J. W.; Röckel, H.; Rumi, M.; Subramaniam, G.; Webb, W. W.; Wu, X.-L.; Xu, C. *Science* **1998**, *281*, 1653.

72. Pawlicki, M.; Collins, H. A.; Denning, R. G.; Anderson, H. L. *Angew. Chem. Intl. Ed.* **2009**, *48*, 3244.

73. W. Spangler, C. *J. Mat. Chem.* **1999**, *9*, 2013

74. Zipfel, W. R.; Williams, R. M.; Webb, W. W. *Nat. Biotechnol.* **2003**, *21*, 1369.

75. Walker, E.; Rentzepis, P. M. *Nat. Photon.* **2008**, *2*, 406.

76. Fisher, W. G.; Partridge, W. P.; Dees, C.; Wachter, E. A. *Photochem. Photobiol.* **1997**, *66*, 141.

77. Rumi, M.; Ehrlich, J. E.; Heikal, A. A.; Perry, J. W.; Barlow, S.; Hu, Z.; McCord-Maughon, D.; Parker, T. C.; Röckel, H.; Thayumanavan, S.; Marder, S. R.; Beljonne, D.; Brédas, J.-L. *J. Am. Chem. Soc.* **2000**, *122*, 9500.

78. Nifosi, R.; Luo, Y. *J. Phys. Chem. B* **2007**, *111*, 14043.

79. Drobizhev, M.; Makarov, N. S.; Hughes, T.; Rebané, A. *J. Phys. Chem. B* **2007**, *111*, 14051.

80. Drobizhev, M.; Tillo, S.; Makarov, N. S.; Hughes, T. E.; Rebané, A. *J. Phys. Chem. B* **2009**, *113*, 855.

81. Zimmer, M. *Chem. Rev.* **2002**, *102*, 759.

82. Tsien, R. Y. *Ann. Rev. Biochem.* **1998**, *67*, 509.

83. Chalfie, M.; Tu, Y.; Euskirchen, G.; Ward, W.; Prasher, D. *Science* **1994**, *263*, 802.

84. Shimomura, O. *FEBS Lett.* **1979**, *104*, 220.

85. Verkhusha, V. V.; Lukyanov, K. A. *Nat. Biotechnol.* **2004**, *22*, 289.

86. Zagranichny, V. E.; Rudenko, N. V.; Gorokhovatsky, A. Y.; Zakharov, M. V.; Shenkarev, Z. O.; Balashova, T. A.; Arseniev, A. S. *Biochemistry* **2004**, *43*, 4764.

87. Tolbert, L. M.; Baldridge, A.; Kowalik, J.; Solntsev, K. M. *Acc. Chem. Res.* **2011**, *45*, 171.

88. Ivashkin, P.; Yampolsky, I.; Lukyanov, K. *Russ. J. Bioorg. Chem.* **2009**, *35*, 652.

Chapter 2

Experimental Techniques

2.1 Explanation

The experimental techniques utilized and/or developed over the course of my dissertation are spread across the several publications that make up the central core of this document, often referencing the literature for larger explanations of the more specific aspects of the specialized experimental techniques utilized to gather the data contained herein. The basic details describing all the major techniques will be described here in a general fashion that should prepare the reader for more fluid entry into the middle chapters without needing to consult a multitude of external sources for explanation.

2.2 Synthetic Methodology

The synthetic approach for the development of all the materials utilized in these studies was one that stressed product purity. The idea was to obtain the desired products without concern to high reaction yield in a form that was pure and suitable for spectroscopy characterization. Given the limitations in our available synthetic facilities, the reactions run needed to be relatively simple, not requiring the use of gloveboxes or sophisticated vacuum systems. Product characterization was primarily performed using thin-layer chromatography to confirm a difference in retention factor as compared to starting materials or against known products. Subsequent structure determination prior to

purification was generally performed with ^{1}H NMR spectroscopy and any additional purification normally involved either recrystallization or column chromatography on silica gel. Additional characterization on the purified product included ^{13}C NMR spectroscopy, mass spectrometry, and UV-Vis absorption and fluorescence emission.

The major synthetic portion of my dissertation will be discussed at length in Chapter 4 wherein chromophores are designed and synthesized. However in brief, our initial chromophore design was based on a modified version of a fluorescent protein chromophore structure known to occur in a specific type of coral (*Zoanthus*).[1] The particular chromophore was chosen due to its favorable photophysical characteristics as parameterized in Chapter 1. The naturally occurring chromophore (ZsYellow) has a predominate absorption[2] at 470 nm that is well suited for two-photon excitation. The two-photon absorption cross-sections that were predicted by Nifosí, et al. were significant, but possibly could be improved upon by incorporating a stronger charge-transfer group like a dimethylamino moiety instead of a hydroxyl. A well-defined synthetic scheme was outlined as shown in Scheme 2.1, attempting to minimize synthetic steps but still generate the relatively complicated structure desired.

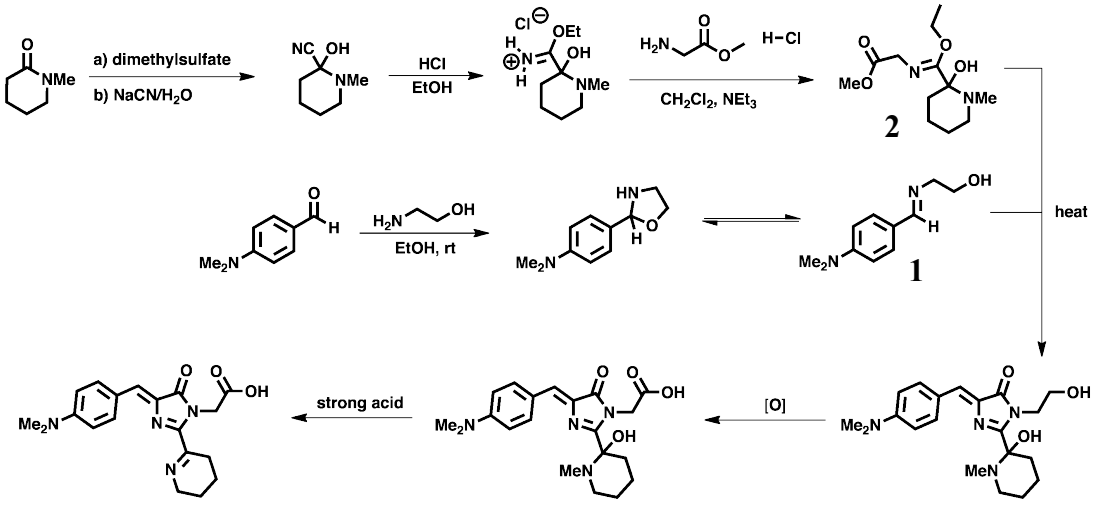

Scheme 2.1 Outline for synthesis of modified ZsYellow chromophore.

The experimental details of our attempts to carry out this synthetic scheme will be fully described in Chapter 4. A great deal of difficulty resulted from our attempts to obtain cyclized product via the [3+2] cycloaddition with the two corresponding precursor molecules. There remained a great deal of questions regarding the viability of this synthetic route after many months of effort and especially great difficulty was found in obtaining workable yields of purified precursor **2**. Ultimately, we revisited the characteristics that we deemed important from a photophysical standpoint and were able to adapt a more generalized synthesis using a variety of functionalized precursor molecules to generate chromophores for further characterization. Shown below in Scheme 2.2 is the developed methodology that utilizes commercially available imidate salts with simpler functionality in place of the complex nitrogen heterocycle from the initial design.

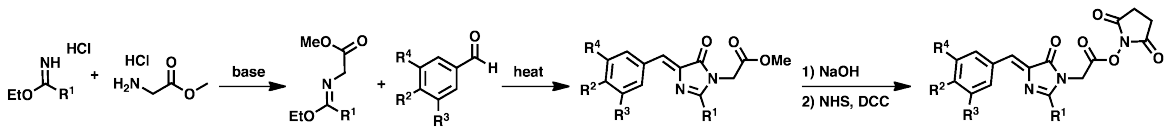

Scheme 2.2 Full general scheme for preparation of chromophore ready for covalent attachment to peptide.

It should be noted however that attempts were made to reimagine the methodology to obtain the initially outlined modified-ZsYellow chromophore. In consultation with Professor Montgomery, we sketched a new pathway to generate the first precursor from different starting materials and utilizing a late stage cyclization to form the nitrogen heterocycle instead of attempting to carry it throughout (Scheme 2.3). While seemingly viable, the number of synthetic steps and careful weighing of the potential for more generalized chromophore synthesis versus the uncertain final characteristics of the modified ZsYellow led us not to invest time into a completely different synthetic route.

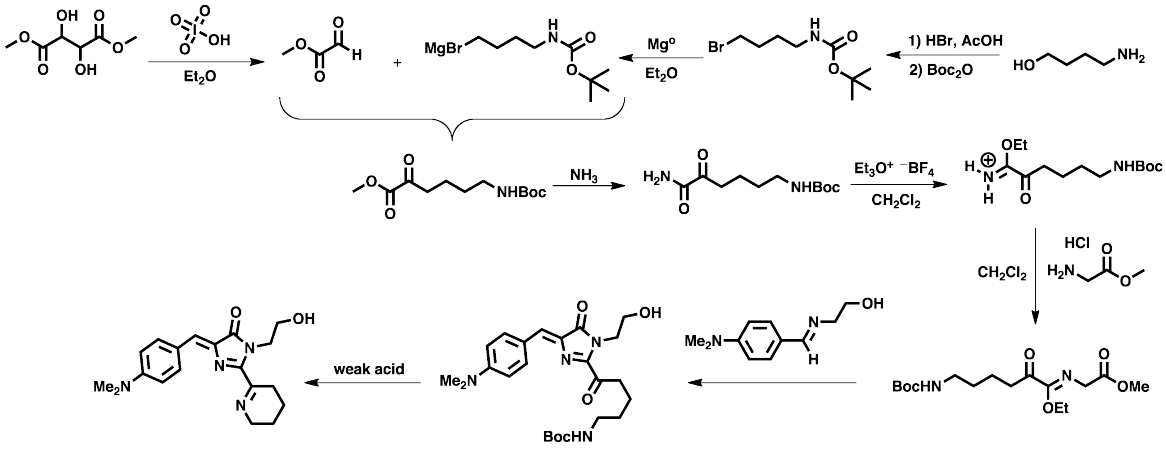

Scheme 2.3 New scheme for modified ZsYellow synthesis outlined in consultation with Professor Montgomery.

Lastly, a few months following the decision not to continue with the synthesis of modified ZsYellow a paper[3] was published in the journal *Biochemistry* that detailed the synthesis of the ZsYellow chromophore (known as zFP538 in the paper) and characterization of some of its basic photophysical properties. The chromophore synthesized by Yampolsky et al. was a model system meant to prove various details about the crystallographic structure of the natural system, and consequently instead of the pendant carboxylic acid as in our design they simply used a functionally mild methyl

group attached to the nitrogen. Using their synthetic scheme as a basis for envisioning another potential route to our initial desired chromophore, a methodology can be derived to incorporate the missing pendant group[4] required for later covalent linkage to biomolecules (Scheme 2.4). The scheme shown below does not incorporate the dimethylamino group on the benzylidiene ring, however substituting 4-dimethylaminobenzaldehyde for 4-acetoxybenzaldehyde at the appropriate step could accomplish this functionality. The protected amino group should be able to be carried throughout the remainder of the synthesis.

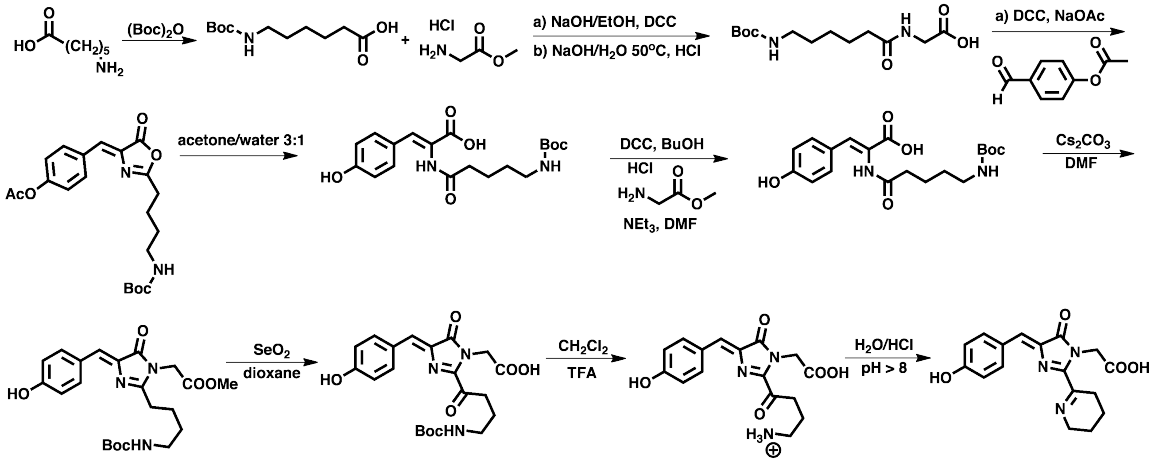

Scheme 2.4 Alternate modified ZsYellow synthetic scheme based upon published synthesis of model system.

2.3 Steady-State Spectroscopy

Steady-state spectroscopy encompasses the two very commonly used optical characterization phenomena called absorption and fluorescence. As will be seen throughout the discussion of my research data, steady-state spectroscopy provides a great deal of the initial investigation into the synthesized chromophores (Chapter 4) or labeled peptides (Chapter 5) prior to utilizing any laser spectroscopy or advanced characterization techniques.

UV-Vis absorption spectroscopy is typically governed for solution-phase study by the Beer-Lambert law[5] that relates the intensity of the light (I) absorbed to concentration ([c], mol/L) and path length (l, cm) of the solution held in the cuvette via a parameter called the molar extinction coefficient (ε, $M^{-1}cm^{-1}$):

$$A = \log \frac{I_0}{I} = \varepsilon \cdot [c] \cdot l \qquad \textbf{(Equation 1)}$$

Experimentally, the absorption will be determined directly by the UV-vis instrumentation as an absorbance measurement that directly translates to the optical density of the sample. The other parameters in **Equation 1** often may be subsequently determined using either a solution of known concentration to calculate the molar extinction coefficient or a literature-found molar extinction coefficient to calculate a solution concentration. If so desired, the one-photon absorption cross-section (σ, cm^2) may be determined having knowledge of the molar extinction coefficient, through the following relation:

$$\sigma = 2.303 \cdot \frac{\varepsilon \cdot [c]}{N} \qquad \textbf{(Equation 2)}$$

Where N is the number of light absorbing molecules in an area of volume (molecules/cm^3). Absorption characteristics of molecules, however, are more typically reported in the literature and compared using molar extinction coefficients. Values for organic molecules are commonly in the range of 10^3-10^6 $M^{-1}cm^{-1}$ depending on how strongly they are able to absorb photons. Many of the materials that were synthesized or used in this dissertation were fairly modest in magnitude and fall on the lower end of this range.

From an experimental perspective, the largest molar extinction coefficient will be found at the wavelength with the highest absorbance. The wavelength of light absorbed

translates into an excitation of the ground state of the molecule to some excited state governed by the energy associated with the photon. Absorption in the UV region results in higher energy $\pi \rightarrow \sigma^*$ transitions, while longer visible to near infrared may often be assigned to $\pi \rightarrow \pi^*$ transition. Often UV-Vis absorption can also give an indication of potential molecular aggregation behavior that can result in a shift in the absorption maximum either to longer or shorter wavelengths depending on the type of aggregate (h- or j-type).[6]

For the collection of our absorption data, an Agilent Model 8341 spectrophotometer having duel lamps of deuterium and tungsten were used allowing for absorption characteristics to be measured over a wide range from 200-1100 nm. Quartz cuvettes manufactured by Starna were used in all experiments with a typical optical path of 0.4 cm (though 1 cm and 0.1 cm may also have been used for very dilute or concentrated solutions respectively). Spectra were background-corrected using a blank taken with the cell containing either solvent or left empty.

The second of the two steady-state processes, emission, is essentially the reverse process of molecular absorption. A special subset of emission processes is fluorescence emission where photons are released, typically lower in energy than those absorbed. For most compounds fluorescence is an inefficient process and as such a quantity referred to as quantum yield is often measured relating the number of photons emitted to the number of photons absorbed. This quantum yield ratio is an important consideration for our studies and any investigation in general where the detection of fluorescence is a critical means for the type of spectroscopy or microscopy being performed. The determination of the quantum yield for a simple solution is difficult without the use of a standard to which

a quantitative comparison can be made. Some fluorimeters may be outfitted with an integrating sphere that can efficiently collect the entirety of the photons emitted from all directions. Without such an apparatus, accurate absolute determination is nearly impossible with the typical instrument setup, but quantitative comparison with literature standards can provide an efficient means for quantum yield determination.[7] By preparing standard and sample solutions to have similar low optical densities at the same absorption wavelength, the following ratio may be set up to determine the quantum yield of the sample, exciting both systems at the matched absorbance wavelength:

$$\Phi_{\text{sample}} = \Phi_{\text{STD}} \cdot \frac{\int J_{\text{sample}}(\bar{\nu})\mathrm{d}\bar{\nu}}{\int J_{\text{STD}}(\bar{\nu})\,\mathrm{d}\bar{\nu}} \cdot \frac{(J_{\text{abs}})_{\text{STD}}}{(J_{\text{abs}})_{\text{sample}}} \cdot \left(\frac{n_{\text{sample}}}{n_{\text{STD}}}\right)^2 \qquad \textbf{(Equation 3)}$$

Where Φ_{STD} is quantum yield of the fluorescence standard at a specified wavelength, $\int J(\bar{\nu})\mathrm{d}\bar{\nu}$ are the respective integrated fluorescence for the standard and sample in units of cm^{-1}, J_{abs} is the corrected absorbance at the wavelength of excitation, and n is the refractive index of the solvent used to prepare each solution. Fluorescence quantum yield studies performed over the course of this dissertation were measured comparing the integrated fluorescence intensity from the samples at low optical densities (<0.1 OD) to that of Coumarin 307 in methanol or fluorescein at pH 11 in water, under the same fluorimeter conditions, and using the same excitation wavelength.

For the collection of fluorescence spectra, a SPEX Fluoromax-2 fluorimeter was used both for general emission and excitation scans as well as for quantum yield. A typical Xenon lamp was the light source and diffraction grating created single wavelength excitations with a photomultiplier tube used to collect the number of fluorescence counts, having good detection sensitivity from 300 nm to near 800 nm. Standard 1 cm quartz

cuvettes were used for data collection allowing for easy 90° detection of the sample emission, though often for peptide samples small volume (45 μL) cell were utilized.

2.4 Two-Photon Absorption Spectroscopy

Two-photon absorption is an intensity-squared dependent process wherein to complete the overall electronic transition from ground state to some excited state there must be near simultaneous absorption of two photons, often of the same energy though this is not required. For example, to achieve nearly the same transition as the one-photon absorption of a 400 nm photon by a molecule, in a two-photon process the absorption of two photons of 800 nm would be required to approximately complete the transition. Figure 2.1 shows this example with OPA of the higher energy blue light, and the same transition occurring via TPA of the lower energy red light. Two-photon excited fluorescence is depicted following relaxation from the initial excited state.

The idea of two-photon absorption spectroscopy was first theoretically predicted[8] in the 1930s by Maria Göppert-Mayer, however was not able to be experimentally verified until the invention of lasers several decades later. The use of a laser light source was required due to the low efficiency with which most molecules nonlinearly absorb photons at several orders of magnitude below that of the linear absorption rate. The capabilities of pulsed laser systems to deliver high peak power, low average power makes the observation of such processes like two-photon excited fluorescence possible. The typical quantity sought when performing two-photon spectroscopy is the two-photon absorption (TPA) cross-section having units of $cm^4 \cdot s \cdot photon^{-1}$, although TPA cross-sections are more typically reported in Göppert-Mayer (GM) with 1 GM = 10^{-50} $cm^4 \cdot s \cdot photon^{-1}$.

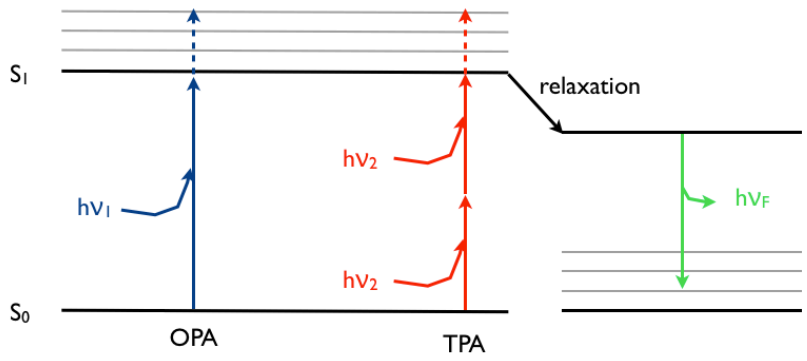

Figure 2.1 Jabolonski diagram representing general two-photon absorption and fluorescence processes.

Of the methods for determining two-photon absorption cross-sections, the methodology utilizing two-photon excited fluorescence is among the more accurate and easily accomplished techniques for observing the two-photon absorption process, and was the means through which we determined all of our two-photon absorption cross-sections. Two-photon excited fluorescence is intrinsically no different than one-photon excited fluorescence though it may be different based upon differences in the relaxation dynamics from the individual excited state reached between the two processes as the ground to excited state selection rules are different for each excitation.

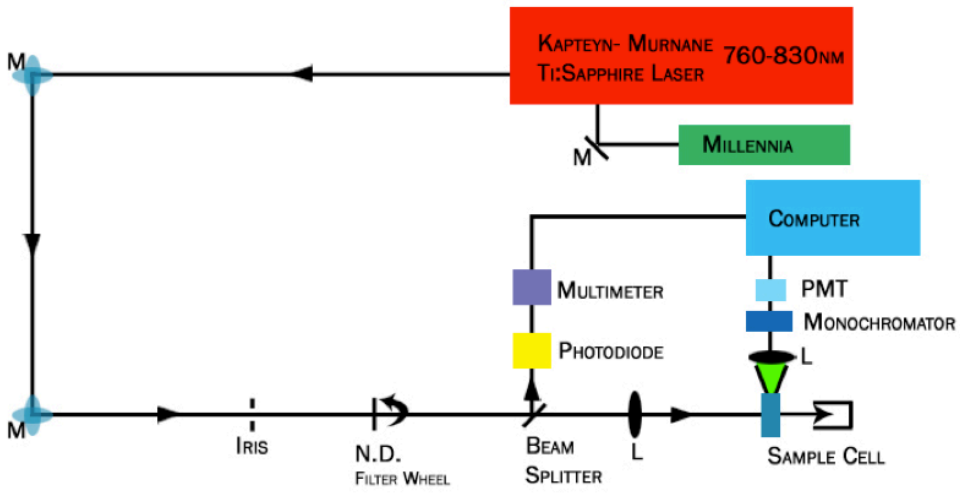

Figure 2.2 Two-photon absorption setup used in the lab.

Two-photon absorption cross-sections throughout my research were measured using the two-photon excited fluorescence (TPEF) method described as following. A Kapteyn Murnane Laboratories diode-pumped mode-locked Ti:sapphire laser was the predominate excitation source for the experiments (Figure 2.2). This system has a limited tunability range allowing output excitation sources from ~770-830 nm, however a wider range of excitation sources from 690-1020 nm where also available on a similar setup elsewhere in the lab using a tunable MaiTai. Typical peak output powers of ~250-320 mW with ~40 nm pulse widths were obtained. A small fraction of the initial laser output was redirected using a piece of optical glass into a fiber optic cable attached to an OceanOptics spectrometer. This detector was used to observe both the wavelength of the laser and assist with establishing a good quality mode-locked beam. Beam quality and mode-locking could be adjusted by changing the laser cavity characteristics though moving prism positions.

The main beam is directed down the table to a periscope beam steerer that redirects the laser perpendicularly across the table while also adjusting the beam-height upward. A second mirror on the near side of the table reflects the beam once again parallel to the original path and through a variable neutral-density filter wheel that permits fine control of the excitation power. Another piece of optical glass directs a small portion of the beam into a high-speed silicon photodiode that is connected to a multimeter feeding an electronic signal proportional to the beam power to the computer interface. The excitation beam enters into the protective box that houses the photomultiplier tube (PMT), monochromator, and sample holder away from direct exposure to background light sources. Within the box, a final focusing lens narrowly focuses the beam onto the

sample placed in a quartz cuvette in the sample holder. The fluorescence is collected at a right angle to the excitation beam using another focusing lens to place the beam through the monochromator and onto the PMT detector. The photomultiplier tube is connected to the computer via a photo-counting unit (Hamamatsu) that interfaces the detected signal. A set of previously developed custom LabView programs provides the front-end graphical user interface for data collection and generates the raw data files of the two-photon excited fluorescence as a function of either wavelength or excitation power depending upon the experiment.

Two-photon absorption cross-sections for unknown samples were calculated using a reference solution having a known TPA cross-section. Most typically Coumarin 307 dissolved in methanol (< 10^{-4} M) was used as the TPA reference for wavelengths studied near 800 nm, as it already has been well characterized previously by Xu et al.[9] From fundamental considerations[10] described in Chapter 1, a relationship may be obtained that relates the observed fluorescence emission from two-photon excitation to various laser and solution parameters,

$$F(t) = \frac{1}{2}\eta\delta[c]n \cdot \frac{g_p}{\pi\lambda f\tau}\phi\left\langle P(t)\right\rangle^2 \qquad \textbf{(Equation 4)}$$

Where, F(t) is the fluorescence photons collected per second; η is the fluorescence quantum yield; δ is the two-photon absorption cross-section of the sample in GM; [c] is the sample concentration in molarity; n is the refractive index of the solvent; g_p is the shape factor for the laser pulse (generally 0.664 for a Gaussian shape); f is the frequency of the pulses from the laser source; τ is the pulse duration; ϕ is the collection efficiency of the system; and <P(t)> is the input intensity.

However, by running a two-photon absorption standard under the same laser conditions along with the sample whose cross-section needs to be determined, the task of calculating the TPA cross-section is simplified enormously. The respective concentrations, refractive indexes, and quantum yields are easily determined. So, if one has knowledge of the TPA cross-section value for the standard, it is not required that quantities associated with the laser beam be known as long as they can be assumed to be the same. The relationship that relates the cross-section of the sample then to the cross-section of the standard may then be derived accordingly.

Using **Equation 4** given above, and taking the logarithm of each side, utilizing a property of logs that the logarithm of a product is equivalent to the sum of the logs, yields a form that can be made to match the equation of a line (y = mx + b),

$$\log\left[F(t)\right] = 2\log\left[\left\langle P(t)\right\rangle\right] + \log\left[\frac{1}{2}\eta\delta[c]n\cdot\frac{g_p}{\pi\lambda f\tau}\phi\right] \qquad \textbf{(Equation 5)}$$

So, if fluorescence counts are collected as a function of input power and the resulting data is manipulated into the form of a line, the plot of the log of fluorescence counts versus the log of excitation power should be a straight line with the slope of 2.

With two data sets, one each for the sample and standard, both having an equivalent slope of 2, the following relation holds true,

$$m_{std}x_{std} = m_{sample}x_{sample}$$

At any point along the x-axis, the product of the slope and the input power should be equivalent. After substituting in quantities from **Equation 5**, then,

$$2\log\left[\langle P(t)\rangle\right]_{std} = 2\log\left[\langle P(t)\rangle\right]_{sample}$$
$$\log\left[F(t)\right]_{sample} - b_{sample} = \log\left[F(t)\right]_{std} - b_{std}$$

$$\left(\text{with } b = \log\left[\frac{1}{2}\eta\delta[c]n\cdot\frac{g_p}{\pi\lambda f\tau}\phi\right]\right)$$

A relationship has now been generated relating the two-photon excited fluorescence of the standard to the sample. (For simplicity, the large collection of variables that make up the y-intercept have been short-handed as b_{sample} and $b_{standard}$.) Further rearranging of the equation to group like quantities yields,

$$\log\left[F(t)_{sample}\right] - b_{sample} = \log\left[F(t)_{std}\right] - b_{std}$$
$$\log\left[F(t)_{sample}\right] - \log\left[F(t)_{std}\right] = b_{sample} - b_{std}$$
$$\log\left(\frac{F(t)_{sample}}{F(t)_{std}}\right) = b_{sample} - b_{std}$$
$$\frac{F(t)_{sample}}{F(t)_{std}} = 10^{b_{sample}-b_{std}}$$

(Equation 6)

When the Log power is equal to zero, **Equation 6** simplifies to the relation, $F(t) = b$ with $F(t) = \frac{1}{2}\eta\delta[c]n\cdot\frac{g_p}{\pi\lambda f\tau}\phi$ which, if then substituted into the expression above and taking into account the parameters that are unique to each sample we get,

$$\frac{\frac{1}{2}\eta_{sample}\delta_{sample}[c]_{sample}n_{sample}\cdot\frac{g_p}{\pi\lambda f\tau}\phi}{\frac{1}{2}\eta_{std}\delta_{std}[c]_{std}n_{std}\cdot\frac{g_p}{\pi\lambda f\tau}\phi} = 10^{b_{sample}-b_{std}}$$

As can be seen, all laser related parameters cancel out and after solving for the cross-section of the sample, we are left with the final expression:

$$\delta_{sample} = \frac{10^{b_{sample}-b_{std}}\cdot\eta_{std}\delta_{std}[c]_{std}n_{std}}{\eta_{sample}[c]_{sample}n_{sample}}$$

(Equation 7)

Solution concentrations are easily determined from either their direct preparation or through molar extinction coefficients. The intercepts may be taken directly from the intensity-power log-log plots provided that the standard and sample slopes are very close to the same value of 2. Quantum yields may be determined using the technique described earlier, or it may sometimes be appropriate to report the "action" cross-section that is simply the product of quantum yield and actual TPA cross-section.

2.5 Time-Resolved Fluorescence Upconversion

For fluorescent molecules, quantifying the fluorescence lifetime is important for understanding the electronic processes occurring in the excited state. A couple different techniques are generally utilized for measuring time-resolved fluorescence: fluorescence upconversion and time-correlated single photon counting (TCSPC). The resolutions of these techniques make them suitable for very different time-scale measurements with TCSPC generally having picosecond instrument response functions, well-suited for nanosecond or longer lifetimes, and upconversion with an IRF of ~100 femtoseconds, best suited for ultrafast processes in the femtosecond or picosecond time-scales.

A great many electronic processes occur on the ultrafast time-scale including those processes associated with molecular interactions and charge-transfer processes thus making time-resolved fluorescence upconversion a very valuable technique. Fundamentally fluorescence upconversion takes advantage of the pulse widths of picosecond and femtosecond pulsed lasers whose times scales substantially beat that of the electronic detectors used in TCSPC. Along with the capability to measure fs and ps fluorescence lifetimes, typical upconversion setups provide for the ability to control the excitation beam polarization, allowing for distinct polarization of the sample emission upon excitation. The dipole transition moments of fluorophores are typically randomly

oriented in solution and through excitation with selective polarization only those molecules oriented parallel along the field of excitation will have a distinct orientation in the excited state. The depolarization of these excited states during emission can be observed through the measuring of fluorescence anisotropy by changing the excitation beam polarization. Such studies have been shown to give detailed information about energy migration and charge-transfer.[11-13]

Polarization settings can be made such that the emission will be oriented parallel (I_{par}) or perpendicular (I_{per}) to the excitation beam. It can be shown[5] that the observed fluorescence anisotropy is related to the relative intensities of these two signals through the following relationship,

$$r = \frac{I_{par} - G \cdot I_{per}}{I_{par} + 2G \cdot I_{per}} \qquad \textbf{(Equation 8)}$$

where r is the fluorescence anisotropy and G is the g factor, a correction factor for the difference in sensitivity of the detection system for the vertically and horizontally polarized light. Anisotropy is a dimensionless quantity relating the ratio of the difference in polarized intensity with that of the overall intensity.[5] For a one photon process, the maximum achievable anisotropy value is 0.4 corresponding to a molecule that undergoes no depolarization from excitation to emission, translating to angle of 0° between the two dipoles. Further examining the generalized equation that relates the anisotropy (r_0) to the angle between the absorption and emission transitions by an angle θ,

$$r_0 = \frac{2}{5} \cdot \left(\frac{3\cos^2 \theta - 1}{2} \right) \qquad \textbf{(Equation 9)}$$

The factor of 2/5 results from the photoselection of the excitation. Anisotropy measurements are wavelength dependent so the initial value will often change as a function of excitation wavelength. Multiphoton excitation may also be performed with the added benefit of having a larger dynamic range with a maximum initial value of 0.57 in the case of two-photon excitation.[14]

Ultrafast processes that have been observed using fluorescence upconversion are manifold and provide crucial information as to the excited state dynamics for many electronic systems. For example, resonance energy-transfer (RET) processes such as Förster energy transfer[15] have been studied using parameters obtained from time-resolved fluorescence. **Equation 10** describes the interaction relationship between two molecules undergoing a Förster-type energy transfer,

$$k_T(r) = \frac{1}{\tau_D}\left(\frac{R_0}{r}\right)^6 \qquad \textbf{(Equation 10)}$$

where k_T is the rate of energy transfer; τ_D is the fluorescence lifetime of the donor molecule (not in the presence of the acceptor molecule); R_0 is the Förster radius, the distance separation between which RET is 50% efficient; and r is the center to center distance between donor and acceptor molecules involved in the interaction. A great deal of research in our group has been performed examining such transfer events in multi-chromophore systems.[16] The ability to perform such measurements will be incredibly useful for examining chromophore-chromophore interactions during the course of my peptide studies in Chapter 5.

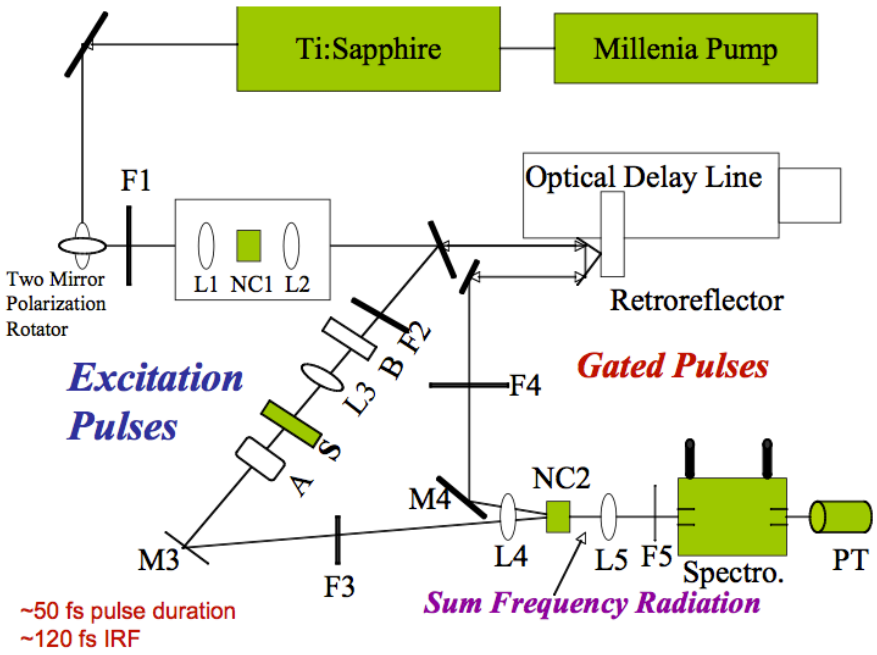

Figure 2.3 Time-resolved fluorescence upconversion setup. Lenses are indicated with 'L'; Nonlinear crystals, 'NC'; Focusing elements, 'F'; Mirrors, 'M'; Sample 'S'; Berek compensator, 'B'; Acromat, 'A'.

As shown in Figure 2.3, at the core of the fluorescence upconversion system used for time-resolved measurements is a Millennia-pumped, Tsunami Mode-Locked Ti:Sapphire (Spectra Physics) laser that operates with 120 fs pulses of 780-820 nm at a repetition rate of 82 MHz with an average output power of ~700 mW. Using a FOG-100 system (CDP Inc.), this 800 nm beam is passed through a β-barium borate (BBO) crystal generating light of ~400 nm from second harmonic generation. The residual 800 nm from this process acts as our gate pulse and is passed through a dichroic mirror into an optical delay line, while the blue 400 nm light is reflected down the excitation pathway toward our sample. A focusing lens directs the beam first through a Berek compensator that controls the polarization of excitation and then through a second lens onto the cell. Samples were prepared in a rotating cell (two quartz glass plates with a plastic spacer between them) and, if possible, to have an optical density near 1. The rotating cell helps

to minimize photo-damage from prolonged exposure of a single spot to the high-energy beam.

The generated fluorescence emission is collected using an acromat and focused onto a second BBO crystal where it is spatially and temporally overlapped with the gate pulse that has passed delayed with time. This generates sum frequency radiation that is the combination of the two beams, typically around 300-400 nm. This signal is gathered using another focusing lens and directed into a monochromator after which it is detected by a photomultiplier tube (PMT). The signal is then passed digitally into a computer where *Lumex* software collects and displays the number of photons counted as a function of delay position. Using our delay stage, one step of the stepper motor corresponds to 6.25 fs of delay time with a range out to ~1 ns. For prolonged runs, the photo-stability of the molecules being studied is a concern given the excitation sources, so steady state measurements prior to excitation and post-excitation were generally used to verify that no photo-damage had occurred. The collected data may be plotted and fit using a graphing program like *Origin*. The Gaussian shape of the IRF is generally overlaid on the data to aid in establishing the proper zero position for the lifetime and anisotropy data. For extremely fast components nearing the timescale of the instrument function, more rigorous deconvolution fits may be determined using a program like *MatLab*. The overall fluorescence lifetime may be determined from generating the isotropic fluorescence curve and fitting with an exponential function.

2.6 Time-Correlated Single Photon Counting (TCSPC)

The other method for investigation of fluorescence dynamics utilized was time-correlated single photon counting (TCSPC). All of the time-resolved fluorescence principles described for fluorescence upconversion are still applicable, however the time-

resolution is limited to the picosecond time-scale and longer. Unlike the optical fluorescence upconversion process, TCSPC is an electronic process based upon the repetitive collection of single photons over the course of many different molecular excitations. A timing reference is used, typically that of the excitation pulse itself, to sort the detected photons into bins according to the time difference between when the emission pulse is detected with respect to the reference pulse. The signal for each reference pulse is converted during the process into a growing voltage by a time-to-amplitude converter (TAC) until the point at which the emission pulse arrives and stops the charging operation. The resulting signal that relates to the difference in these times is directed into a multichannel analyzer via an analog to digital converter (ADC) where a numerical value is assigned and the count is sorted into its appropriate bin. After many cycles have been completed, the distribution of the counted photons in their respective bins creates the fluorescence lifetime of the sample.

Several considerations must be made to ensure that accurate data is collected using a TCSPC setup. Primarily, the electronic components utilized must have sufficiently fast processing so that each photon event may be discretely measured. TCSPC systems are designed to combat any latency of response by measuring only a single photon per excitation cycle allowing for a period of dead time between photon detections. Time-resolution is another significant issue that depends strongly on the quality of the two detectors and the analog-to-digital converter. A scattering medium is generally used to measure the instrument response function and resolution of the system. Appropriate fitting may then occur using multiple exponentials if necessary to determine the fluorescence lifetime of the sample.

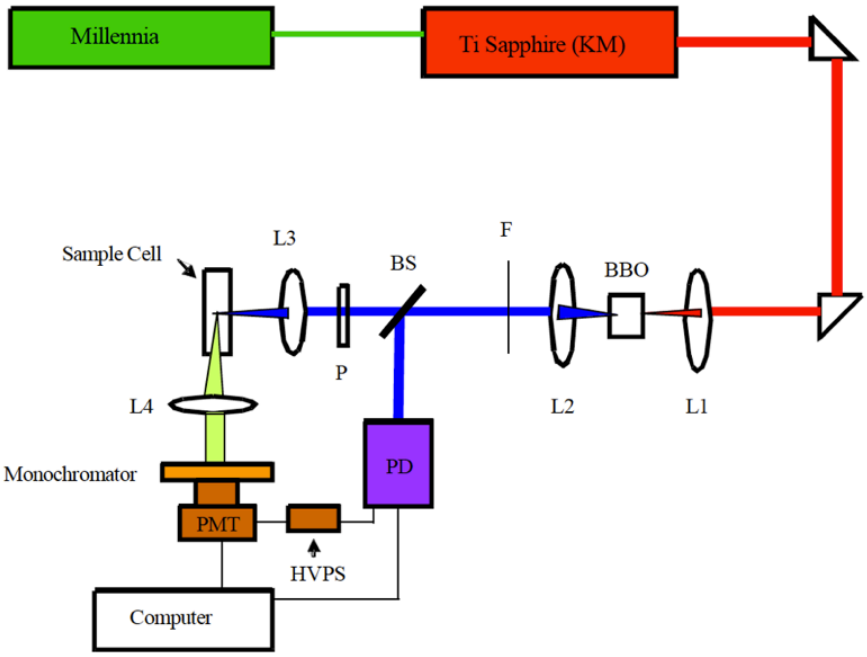

Figure 2.4 Time-correlated single photon-counting instrumental (TCSPC) setup utilized in the lab. Lenses are indicated with 'L'; Nonlinear crystals, 'BBO; Focusing elements, 'F'; Photodiode, 'PD'; Photomultipler tube, 'PMT'.

As shown in Figure 2.4, our TCSPC experimental setup utilizes the same Kapteyn Murnane Laboratories femtosecond laser system pumped by a Millennia 5 W Nd:YYO laser (Spectra Physics) as was used for the two-photon experiments described eariler. The system delivers stable ultrashort light pulse sequences with ~30-fs output pulses at 800 nm having a repetition rate of 90 MHz. The laser can be tuned from 780 to 830 nm and through second harmonic generation with a doubling crystal 390-415 nm light may also be obtained allowing for both two-photon (800 nm) and one-photon (400 nm) excitations respectively. The SYNC (reference) signal is generated from a small portion of the 800 nm excitation beam reflected toward a silicon photodiode. One-photon excitations may be obtained by directing the laser beam through a BBO doubling crystal to generate the requisite 400 nm light while two-photon excitations are made by removing the crystal and subsequently dampening the intensity of the excitation with a neutral density filter. In

either instance, the excitation beam is then directed through a polarizer that allows for control of the polarization of the light prior to hitting the sample contained in a 45 μL quartz cell. For fluorescence measurements, the polarizer is oriented at a magic angle (54.70º) relative to the vertical polarization of the excitation beam allowing for the collection of total fluorescence emission without distinct polarization. Fluorescence anisotropy decay measurements can then also be carried out using the appropriate parallel and perpendicular orientations to obtain data for use with **Equation 8**. An average excitation power near 10 mW was used for 400 nm excitation and higher values for 800 nm.

The fluorescence emission of the sample may be collected perpendicular to the excitation beam and using a focusing lens is directed toward the monochromator (Oriel 77250). After wavelength selection by the monochromator, a photomultiplier tube detects the emission and transmits the signal to the computer via an interface card (Time-Harp) and the histogram is displayed with a specialized software suite (PicoQuant). The obtained fluorescence decay curves can then be fit within the PicoQuant FluoFit software. An instrument response function (IRF) for the system was found to have a full width at half maximum of 330 ps. For two-photon excitations, the instrumental response function (IRF) was recorded using a Rayleigh scattering medium prepared by mixing colloidal gold nanoparticles with a few drops of 6 M NaCl.[17] The absorption spectra and the reproducibility of the fluorescence dynamics were monitored to make sure that the sample was stable under the excitation conditions.

2.7 Circular Dichroism Spectroscopy

One of the typical methods for determining secondary structure in peptides is circular dichroism spectroscopy (CD).[18] As a means to compare the capabilities of our new two-photon methodology for examining peptide aggregation, CD was used in the biochemical studies of the labeled peptides. Generally speaking, CD spectroscopy involves the differential absorption of circularly polarized light, either left or right, commonly by peptides or proteins. The typical excitation is in the UV region from ~190-260 nm and interacts with the amide bonds of peptide molecules. Many of the same considerations can be made for CD as were made for basic absorption spectroscopy.

The overall CD signal is a measure of the difference in absorption between the left and right components of polarized light ($\Delta A = A_L - A_R$). Using Beer's Law, this can be related to the concentration [c] and path length [l] of the solution.

$$\Delta A = (A_L - A_R) \cdot [c] \cdot l$$

More commonly, CD is represented as ellipticity, which is defined as the angle whose tangent is the ratio of the minor to the major axis of the ellipse. This can be simplified through mathematical approximations to the linear absorption of the handed-light by the following relationship:

$$[\theta] = 3298.2 \cdot \Delta\varepsilon$$

Where [θ] is the molar ellipticity in units of deg·cm^2·dmol^{-1} when ε, the molar extinction coefficient, is used with units of M^{-1}cm^{-2}.

Considerations must be made for potential sources of background absorption that may be found in some solutions.[19] Some buffer solutions have various additives that could be could distort the actual CD signal because they absorb light in the same spectral

region as the biomolecules of interest. Along these same lines, the types of cuvettes used for these studies need to be very transparent in the UV region, eliminating optical glass cells that are not transparent below 300 nm. Also, particulate matter makes for problems relating to scattering of the light and must be filtered prior to scanning. Molecular oxygen may also be problematic depending upon the wavelength region of study as it absorbs around 200 nm.

Using CD data, the secondary structure composition of peptides studied may be determined by comparing the sample data collected to a reference set of curves having known percentages of alpha-helical, beta-sheet, and random coil. There are a wide range of statistical methods and programs available to analyze the data. In the case of amyloid peptides, the combination of structural characteristics makes it difficult to achieve definitively accurate results using more generalized methodologies. Constrained least-squares fitting analysis programs provide the best results with reference libraries that are polypeptide-based. The K2D fitting program developed by Andrade et al.[20] was utilized for our secondary structure determinations in Chapter 3.

References

1. Remington, S. J.; Wachter, R. M.; Yarbrough, D. K.; Branchaud, B.; Anderson, D. C.; Kallio, K.; Lukyanov, K. A. *Biochemistry* **2005**, *44*, 202.

2. Ivashkin, P.; Yampolsky, I.; Lukyanov, K. *Russ. J. Bioorg. Chem.* **2009**, *35*, 652.

3. Yampolsky, I. V.; Balashova, T. A.; Lukyanov, K. A. *Biochemistry* **2009**, *48*, 8077.

4. Stafforst, T.; Diederichsen, U. *Eur. J. Org. Chem.* **2007**, 899.

5. Lakowicz, J. R.; SpringerLink *Principles of fluorescence spectroscopy*; Springer: New York, **2006**.

6. Kasha, M. *Radiation Res.* **1963**, *20*, 55.

7. Rurack, K.; Spieles, M. *Anal. Chem.* **2011**, *83*, 1232.

8. Göppert-Mayer, M. *Ann. Phys.* **1931**, *401*, 273.

9. Xu, C.; Williams, R.; Zipfel, W.; Webb, W. *Bioimaging* **1996**, *4*, 198.

10. Xu, C.; Webb, W. *J. Opt. Soc. Am. B* **1996**, *13*, 481.

11. Varnavski, O. P.; Ostrowski, J. C.; Sukhomlinova, L.; Twieg, R. J.; Bazan, G. C.; Goodson, T. *J. Am. Chem. Soc.* **2002**, *124*, 1736.

12. Lahankar, S. A.; West, R.; Varnavski, O.; Xie, X.; Goodson, T.; Sukhomlinova, L.; Twieg, R. *J. Chem. Phys.* **2004**, *120*, 337.

13. Yan, X.; Goodson, T.; Imaoka, T.; Yamamoto, K. *J. Phys. Chem. B* **2005**, *109*, 9321.

14. Volkmer, A.; Subramaniam, V.; Birch, D. J. S.; Jovin, T. M. *Biophys. J.* **2000**, *78*, 1589.

15. Scholes, G. D. *Ann. Rev. Phys. Chem.* **2003**, *54*, 57.

16. Guo, M.; Varnavski, O.; Narayanan, A.; Mongin, O.; Majoral, J.-P.; Blanchard-Desce, M.; Goodson, T. *J. Phys. Chem. A* **2009**, *113*, 4763.

17. Ryderfors, L.; Mukhtar, E.; Johansson, L. *Chem. Phys. Lett.* **2005**, *411*, 51.

18. Kelly, S. M.; Price, N. C. *Curr. Protein Pept. Sci.* **2000**, *1*, 349.

19. Greenfield, N. J. *Nat. Protocols* **2007**, *1*, 2876.

20. Andrade, M. A.; Chacón, P.; Merelo, J. J.; Morán, F. *Protein Eng.* **1993**, *6*, 383.

Chapter 3

Two-Photon and Time-Resolved Fluorescence Conformational Studies of Aggregation in Amyloid Peptides

3.1 Original Publication Information

The bulk of this chapter was originally published as the following document:

> "Two-Photon and Time-Resolved Fluorescence Conformational Studies of Aggregation in Amyloid Peptides" Ying Wang, Travis B. Clark, and Theodore Goodson III. *Journal of Physical Chemistry B* **2010**, *114*, 7112-7120

Modifications to the original document were made solely for adapting the content to this form. References between the original manuscript and supporting information have been unified into a single numbering system. It should be noted that the experimentation for this chapter was largely performed by the lead author with my contributions in data interpretation and the writing of the manuscript.

3.2 Abstract

The conformational changes associated with the aggregation of proteins are critical to the understanding of fundamental molecular events involved in early processes of neurodegenerative diseases. A detailed investigation of these processes requires the development of new approaches that allow for sensitive measurements of protein

interactions. In this report, we applied two-photon spectroscopy coupled with time-resolved fluorescence measurements to analyze amyloid peptide interactions through aggregation-dependent concentration effects. Labeled amyloid-β peptide (TAMRA-Aβ1-42) was used in our investigation and measurements of two-photon-excited fluorescence of the free and covalently conjugated peptide structure were carried out. The peptide secondary structure was correlated with a short fluorescence lifetime component and this was associated with intramolecular interactions. Comparison of the fractional occupancy of the fluorescence lifetime measured at different excitation modes demonstrates the high sensitivity of the two-photon method in comparison to one-photon excitation (OPE). These results give strong justification for the development of fluorescence lifetime-based multiphoton imaging and assays.

3.3 Introduction

Protein misfolding is important to the conformational transition which facilitates the processes of protein aggregation.[1] Amyloid proteins undergo structural transitions leading to the appearance of amyloidogenic intermediates followed by aggregate formation.[1] The formation of soluble and protofibrillar aggregates composed of a small number of monomers constitutes the primary toxic species in several neurodegenerative disorders.[2-5] Oligomer toxicity appears to be related to a common conformational state, as shown by similar reactivity with conformation-dependent antibodies and comparable toxicity with oligomers synthesized from non-disease-related proteins and peptides.[2,6,7] These results suggest that different conformations of the amyloid peptides may contribute to the pathology via various mechanisms.[8] In the event of multiple conformational pathways of amyloid protein folding, the characterization of these conformations and the mechanisms involved in protein misfolding and aggregation are very important for

identifying targets and designing inhibitors that could limit the toxicity of amyloid proteins.

Amyloid β peptide (Aβ1-42) is one of the major constituents of amyloid plaques found in the brains of Alzheimer's disease (AD) patients and is derived from a proteolytic process of the amyloid precursor protein (APP).[9-10] Direct observation of real-time conformational transitions in Aβ is difficult due to its lack of solubility in water. Previous NMR studies on structural and conformational changes during monomer folding and assembly of Aβ were conducted in acidic solutions,[11] organic solvents,[12] and a mixture of organic solvent with water.[13] Among the organic solvents utilized, hexafluoroisopropanol (HFIP) is very promising due to its tunable polarity properties.[14] This feature offers the opportunity to mimic membrane induced conformational changes from monomers to the protofibrillar formation at concentrations suitable for NMR studies.[15] By controlling experimental conditions and utilizing several spectroscopic techniques, such as Circular Dichroism (CD), Fourier Transform Infrared (FTIR), and Nuclear Magnetic Resonance (NMR), assembly-dependent conformational changes of the Aβ have been observed, including random coil→β-sheet,[16-19] α-helix→β-sheet,[19,20-22] and random coil→α-helix→β-sheet.[23] The components of the peptide sequences involved in these transitions are rather diverse,[24-26] however, and it is vital to know how particular subdomains direct conformational transitions and aggregation of the amyloid peptides at the molecular level. For example, the N-terminal domain of the Aβ1-42 contains a sequence that is not only critical for initiating α-β conformational switching,[27,28] but also essential for targeting antibodies[29,30] and compounds that alter Aβ aggregation.[31] A detailed investigation of this domain motion (flexibility) within the Aβ1-42 at the residue level has not been reported.

Therefore, it is urgent to establish a novel fluorescence-based method for measuring intramolecular interactions involved in this particular region. Such information will provide insights into the design of effective and preventative treatments for neurodegenerative diseases.

The conformational transition of the Aβ has been extensively studied by pH changes, alterations of environmental hydrophobicity or through binding with other proteins.[32-34] Spectroscopic techniques such as NMR and CD have been used to gather a wealth of information on the conformational pathways of Alzheimer's peptides in aqueous media.[13,15,34] However, the limitations of these techniques have restricted their use. For example, the low sensitivity of NMR techniques requires high protein concentrations and as such the proteins tend to aggregate in their native states or change the natural structural conformations. Much attention should also be given to the relevance of NMR results (mM concentration) with the structural information obtained from CD spectroscopy (μM concentration). Furthermore, CD spectroscopy is not residue-specific, and hence cannot resolve the environmental effects at the residue level or measure the motional degrees of proteins and peptides. In contrast, the utility of fluorescence emission in studying protein motions and residue recognition has been realized due to its sensitivity, kinetic resolution, and compatibility with both living cells and physiological assays.[35-39] These features offer great opportunities in determining protein aggregates (biomarkers) at physiological conditions,[35,36] in residue-specific studies[37,38] and in optical-imaging.[39] Presently, there have been no reports on the application of TPE coupled with time-resolved fluorescence as a sensitive approach toward the studies of conformation and aggregation processes in amyloid peptides and proteins.

The use of fluorescence methods to probe the conformations and dynamics of proteins often requires the labeling of these biomolecules with an extrinsic fluorescent dye. Preservation of protein function and activity is a prerequisite for covalent attachment of fluorophores to a biomolecule. The vast majority of fluorescence labeled biopolymers (proteins and peptides) are achieved by labeling the common amino acids (lysine, glutamic acid, and arginine) found in proteins with widely available fluorescent probes. To closely interrogate the connection of the fluorescence dynamics of the probe to the conformation and motion dynamics of the proteins, several strategies including the reduction of flexible linkers between probes and proteins,[40] as well as the synthesis of environmentally sensitive near-infrared (NIR) chromophores have been suggested.[41] To eliminate the conjugation effect on aggregation properties and to effectively couple the probe motion from the local and segmental motions[42,43] of the Aβ1-42, we used a system where the TAMRA was conjugated at the N-terminus of the peptide to study fluorescence dynamics and subsequently correlate those properties with conformational changes and aggregation of Aβ1-42.

The significance of this investigation also lies in the recent interest in amyloid polymorphism[44], highlighting the need to measure the conformations facilitating the aggregation processes under various conditions. Different cellular and tissual surroundings provide the environments that are likely to determine the particular amyloid structures,[45,46] so it is very important to develop methods and probes that can eventually be applied to Aβ aggregates in cells and tissue samples. In this regard, nonlinear materials and optical approaches with particular emphasis on multiphoton excited spectroscopy and microscopy enable more widespread and accessible detection platforms for both early

diagnosis of the disease, and evaluation of anti-Aβ therapeutics.[47,48] In this contribution, we show that TPE coupled with time-resolved fluorescence spectroscopy is a promising technique to sensitively characterize conformational changes associated with aggregation of proteins and peptides. Accordingly, we suggest that TAMRA-labeled Aβ1-42 is a probe that may be used for monitoring protein conformational changes, a potential fluorescent marker for lifetime-based multiphoton imaging and assays, and a promising reporter for high-throughput assays.

3.4 Experimental

3.4.1 Chemicals

5-Carboxytetramethylrhodamine (TAMRA) and 1,1,1,3,3,3-hexafluoro-2-propanol (HFIP) were obtained from Molecular Probe and Sigma-Aldrich, respectively. Phosphate Buffered Saline (PBS, Cat. No: P312-500, pH 7.4, without Ca or Mg) was received from Invitrogen Corporation. Sodium azide (NaN_3) was obtained from Fluka. Synthetic TAMRA-labeled Aβ1-42 (lot 39003, HPLC purity >90%) and Aβ1-42 (lot 44103, HPLC purity >95%) were purchased from AnaSpec Inc. (San Jose, CA). All chemicals and peptides were used without further purification as obtained from the manufacturer. Unless specified, a PBS buffer prepared containing 211 ppm NaN_3 was used in the preparations of HFIP/PBS solutions.

3.4.2 Aβ Sample Preparation

To disaggregate the Aβ and generate monomeric α-helical structures, a stock solution of the TAMRA-Aβ1-42 was prepared by dissolving 0.1 mg of this peptide into 100 μL of HFIP and was then stored in the refrigerator (-20 ºC) until use. The concentration of this stock solution was estimated by measuring the optical absorption at 547 nm (extinction $\varepsilon = 7.3\times10^4$ M^{-1} cm^{-1} for 5-TAMRA in neat HFIP). A stock solution

of the Aβ1-42 was also prepared by dissolving 1 mg of this peptide into 445 μL of HFIP and then subsequently stored in the refrigerator (-20 ºC) before use. For concentration-dependent aggregation measurements, peptide samples of various concentrations were prepared by dilution from the stock solution and maintained in a co-solvent of HFIP/PBS (20:80). These solutions were then stored in the dark at room temperature.

3.4.3 Steady-State Measurements

All CD spectra were recorded with an Aviv model 202 circular dichroism spectrometer at 25 ºC using a bandwidth of 1.0 nm, and a wavelength step of 0.5 nm. A quartz cell with an optical path of 0.1 cm was used for far-UV (190-240 nm) measurements. Estimation of the percentage of β-sheet, α-helix, and random coil was made using a K2D program.[49,50] In the case of a negligible contribution of β-sheet, the percentage of α-helical content was estimated using the following equation for ellipticities at 208 nm and 222 nm:[51,52]

$$\alpha - helix(\%)_{208nm} = \frac{\theta_{208} - 4000}{-33000 - 4000} \times 100$$

$$\alpha - helix(\%)_{222nm} = \frac{\theta_{222} - 3000}{-36000 - 3000} \times 100$$

Where θ is mean residue ellipticity in unit of deg cm^2 $dmol^{-1}$.

Unless specified, absorption and fluorescence spectra were recorded on an Agilent (Model # 8341) spectrophotometer and Fluoromax-2 fluorimeter (ISA instruments New Jersey), respectively. Measurements were performed using a 45 μL quartz cell with an optical path of 0.3 cm at room temperature. Emission spectra were collected at increments of 1 nm over the range λ_{em} = 550-700 nm (λ_{ex} = 535 nm) for both the free dye and the dye-labeled peptide. The two-photon absorption cross-sections (δ) of all samples were measured by the two-photon induced fluorescence method.[53] These

measurements have been described in detail elsewhere.[54] Fluorescence quantum yields (φ) were measured using a known procedure.[55] The integrated fluorescence intensity from the sample was compared with that for the standard dye Rhodamine B in methanol.

3.4.4 Two-Photon Excited Fluorescence Lifetime and Polarization Measurements

Two-photon-excited time-resolved fluorescence measurements were carried out by time-correlated single photon counting (TCSPC) with two-photon excitation (TPE). The TCSPC system has been described in detail elsewhere.[56] The excitation source was a Kapteyn Murnane Laboratories (KML) mode-locked Ti-Sapphire laser system delivering ~30-fs output pulses at 800 nm at a repetition rate of 90 MHz. The average excitation power at the sample was near 10 mW. The absorption spectra and the reproducibility of the fluorescence dynamics in the course of the experiment were monitored to make sure that the sample was stable. No photodegradation of the sample has been detected at this power level. For one-photon excitation (OPE) the laser frequency ~800 nm laser output was frequency doubled in a nonlinear crystal to generate excitation pulses at ~400 nm. The excitation beam for either 400 nm or 800 nm excitation routes was focused on the sample in a 45 μL quartz cell using a lens with a focal length of 9 cm. The fluorescence was taken at a right angle to the excitation and detected by a PMT (photomultiplier tube) module mounted at the exit slit of a monochromator (Thermo Oriel 77250). A TimeHarp 200 (PicoQuant) detection card was used for time-correlated single photon counting measurements. For fluorescence decay measurements a prism polarizer was oriented at a magic angle (54.70º) relative to the vertical polarization of the excitation beam. Fluorescence anisotropy decay measurements were carried out by recording the fluorescence with the polarizer oriented either parallel or perpendicular with respect to

the excitation polarization. For TPE, the instrumental response function (IRF) was recorded using a Rayleigh scattering medium prepared by mixing colloidal gold nanoparticles with a few drops of 6 M NaCl.[57] The time profile of the fluorescence was analyzed and fitted to the model decay-function using PicoQuant Fluofit software including deconvolution with the IRF. The goodness of the fitting of time-resolved decay profiles was evaluated by χ^2.

3.5 Results and Discussion

3.5.1 Circular Dichroism

In order to establish an understanding of the initial conformation of the TAMRA-labeled Aβ1-42 peptide and to make correlations with fluorescence lifetimes, circular dichroism spectroscopy was used to analyze the secondary structure of these systems. Previous reports have shown the relative structural heterogeneity in the residues 1-17 of Aβ1-42,[58,59] so determination as to whether labeling the N-terminus of Aβ1-42 significantly alters the structural characteristics of the unlabeled peptide is critical for our studies as the chromophore should not influence the peptide interactions.[58]

The approximate fraction of α-helix secondary structure was determined for the unlabeled peptide and compared to that obtained from the labeled peptide in neat hexafluoroisopropanol (Figure 3.1). The percentage of α-helix for each sample was found to be the same within experimental uncertainties and any residual random coil structure remained similar between systems. This indicates that labeling with TAMRA at the N-terminus does not appreciably change the structural nature of the Aβ1-42 over the concentration ranges of interest. Other recent reports[60-62] using various biochemical techniques including CD spectroscopy seem to corroborate this finding, as Bateman[62] observed that similarly labeled Aβ showed no structural differences compared to that of

the unlabeled peptide. The structural information gathered from the TAMRA-labeled Aβ1-42 would therefore reflect those properties like conformational changes and aggregation of the native peptide.

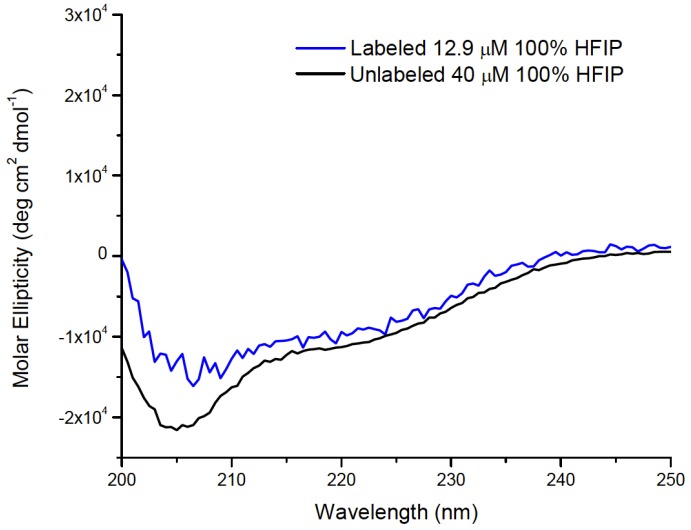

Figure 3.1 Initial CD spectroscopy of labeled and unlabeled Aβ1-42 in neat HFIP.

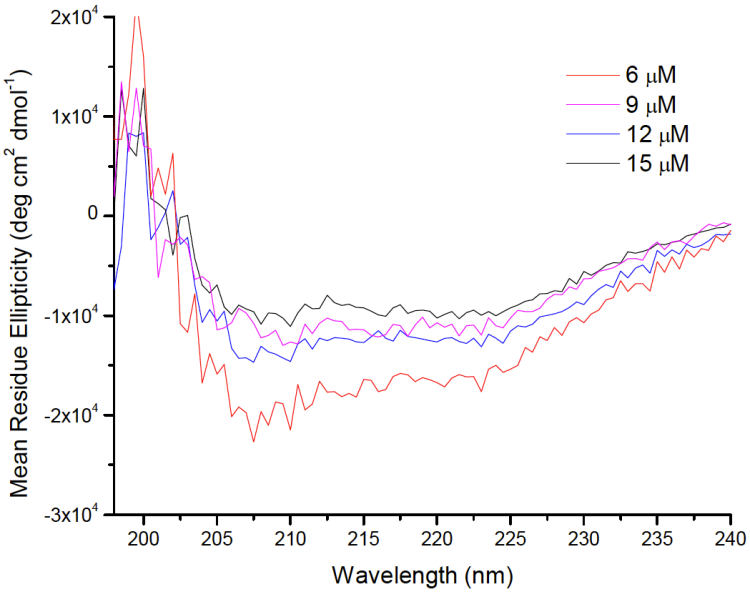

Figure 3.2 Circular dichroism spectra collected as a function of peptide concentration. Incubated with HFIP/PBS (20:80) solvent composites for two weeks prior to the measurements.

3.5.2 Steady-State Spectroscopy

To further analyze whether the attachment of TAMRA to Aβ1-42 significantly altered the behavior of the native peptide, the absorption and emission spectra where obtained for the TAMRA-labeled Aβ1-42, the unattached TAMRA chromophore, and a mixture of unlabeled Aβ1-42 with the unattached chromophore. Figure 3.3 shows the absorption and emission spectra obtained for each system as prepared in neat HFIP. The absorption spectrum of the dye-labeled peptide shows an absorbance maximum at 545 nm which is slightly blue-shifted as compared with TAMRA. Similarly, the emission spectra show a progressive red-shift from the free-TAMRA (λ_{max}= 564 nm), to the TAMRA-labeled Aβ1-42 (λ_{max}= 566 nm), and to the mixture of TAMRA with Aβ1-42 (λ_{max}= 568 nm). The emission spectrum of the labeled peptide does not exhibit a typical mirror-image relationship with the absorption spectrum, notably showing only a small red-shifted emission resulting from the excitation of the 545 nm band. These small shifts can be attributed to either some small aggregates of rhodamine dyes[63] forming ground-state complexes or to interactions between certain amino acid side-groups of Aβ1-42 and TAMRA[64] causing a slight bathochromic shift.

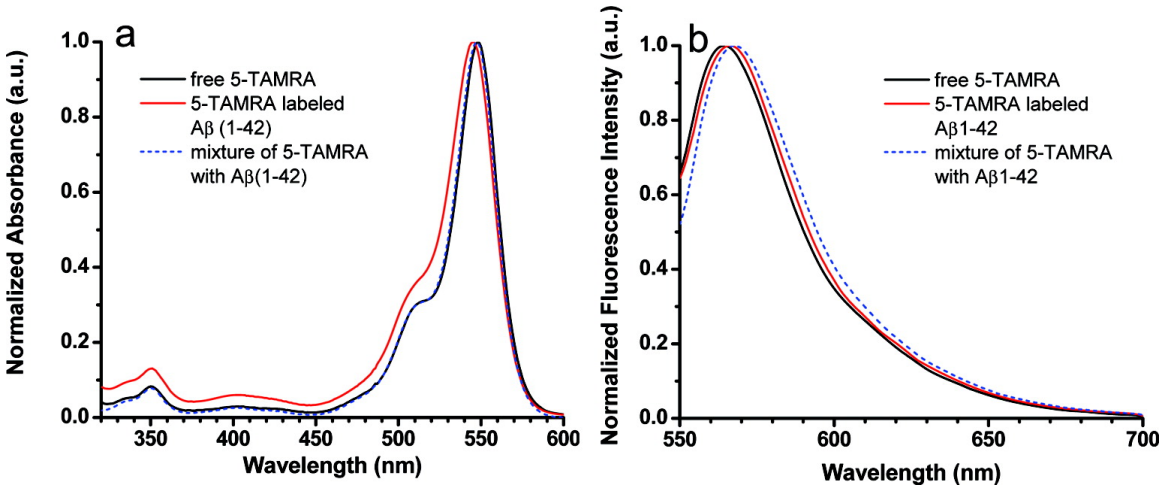

Figure 3.3 Steady-state comparison TAMRA, labeled peptide, and mixture. (a) The absorption spectra normalized at the maximum absorption peak. (b) The normalized emission spectra of the chromophore-Aβ1-42 systems. Samples were prepared to have a concentration of 15 μM in HFIP.

A comparison of the absorption spectra for free-TAMRA and the mixture of free chromophore and unlabeled Aβ1-42 notably demonstrates the absence of ground-state complexes being formed in the mixture where the dye is not covalently conjugated to the peptide. This indicates that any interactions that may be occurring in TAMRA-Aβ1-42 are resulting from the covalently attached chromophore and not from interactions between free dye molecules. With respect to the free-TAMRA system, this feature also suggests that any ground-state interactions that may be occurring are too weak to shift the maximum absorption peak. The noticeably blue-shifted absorption spectrum of the TAMRA-labeled Aβ1-42 could be a consequence of intermolecular complexes formed among the covalently conjugated TAMRA as was observed previously in a polypeptide system labeled with 5',6'-carboxytetramethyl-rhodamine probes that aggregated into H-type dimers.[65]

Figure 3.4 depicts a schematic representation of possible aggregation and peptide-TAMRA interactions for TAMRA-labeled Aβ1-42. These may include the fluorescence

quenching of TAMRA by intramolecular interactions with certain amino acids (as described below) or the formation of a ground-state complex between two TAMRA molecules. It should be noted that the peptide concentration (15 μM) utilized in our steady-state measurements is lower than the concentrations generally required for the formation of ground-state complexes among free rhodamine chromophores.[63] However, since TAMRA is covalently conjugated to the peptide, the dye is constrained to the N-terminus of the Aβ1-42. As a result, the effective local concentration of the covalently conjugated TAMRA in the immediate vicinity of a particular region of the peptide may be high enough to bring the chromophores into close proximity leading to ground-state complex formation. The blue-shifted absorption maximum may suggest the formation of H-type aggregate geometry with a parallel or side-by-side alignment of the two covalently conjugated TAMRA chromophores.[65] However, it is clear that the steady-state spectroscopy does not afford the ability to definitively confirm the types of aggregates being formed in solution and does not provide information as to the peptide secondary structure. Time-resolved fluorescence lifetime and anisotropy measurements should permit more definitive conclusions to be drawn as to the charge interactions taking place and types of aggregates formed.

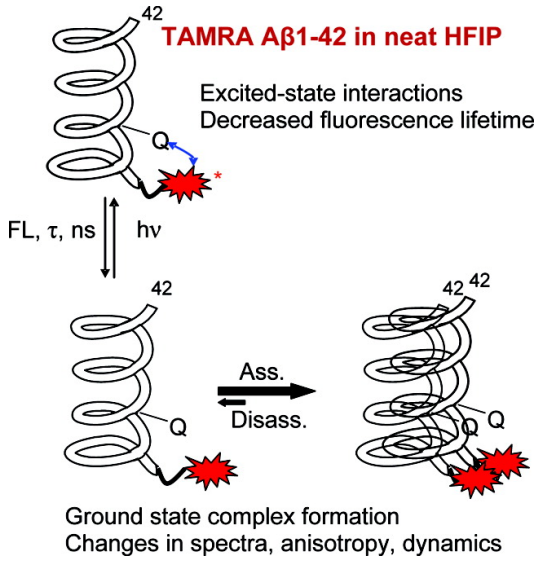

Figure 3.4 Schematic representation of conjugation effects and structural conformation of TAMRA-Aβ 1-42 in neat HFIP.

3.5.3 Two-Photon Absorption (TPA)

Before we measured the two-photon excited fluorescence of the conjugated peptide, the two-photon response of the TAMRA chromophore was investigated. The TPA excitation spectra for rhodamines typically have a substantial peak around 820 nm[66] and initial anisotropy values that are very high, reaching as high as $r_0 = 0.5$ for Rhodamine 6G.[66,67] This makes rhodamine derivatives including TAMRA attractive probes for TPA excitation around 800 nm where robust and flexible Ti:Sapphire laser sources of femtosecond light pulses are available.

The excitation power dependence of the TAMRA fluorescence detected at 565 nm was determined by a log-log plot of the fluorescence signal versus incident peak photon flux at ~800 nm. For photon flux densities $\leq 6.0\times10^{26}$ photons cm^{-2} s^{-1}, the induced fluorescence obeyed a quadratic intensity dependence as indicated by a measured slope of 2.0, thereby confirming the dominance of TPA excitation route at this wavelength. TPA cross-sections at 800 nm were measured for the dye-labeled Aβ1-42

and free dye using the two-photon excited fluorescence method. The cross-sections (δ) for the TAMRA and TAMRA-labeled Aβ1-42 in pure HFIP were found to have relatively large TPA cross-sections similar to those of comparable rhodamine chromophores.[66] The free-TAMRA chromophore was found to have a TPA δ = 185 GM and the peptide-conjugated TAMRA with a larger cross-section of 313 GM (Table 3.1). The increase in cross-section can be rationalized due to differences in dipole moment of the chromophore when it is attached to the peptide versus unattached in solution and due to the possible intermolecular interactions of the labeled peptide molecules in solution as illustrated in Figure 3.4. This enhanced cross-section of the TAMRA-labeled Aβ1-42 is advantageous for our studies using time-resolved fluorescence lifetimes and anisotropy as it permits easier signal detection and increased sensitivity to aggregates.

	λ_{abs} (nm)[d]	λ_{emiss} (nm)[c]	Fl lifetime (short) (ns)[d]	Fl lifetime (long) (ns)[d]	η	δ (GM)[c]	ηδ (GM)[c]
Labeled Aβ1-42[a]	545	566	0.4 ± 0.1	4.5 ± 0.3	0.61	313	191
Free TAMRA[b]	548	564	--	4.07 ± 0.05	0.75	185	139

Table 3.1 Summary of linear and nonlinear optical properties of TAMRA-labeled Aβ1-42 and TAMRA free chromophore. [a]Prepared concentration of 19 μM; [b]Prepared concentration of 20 μM; [c]Solution 100% HFIP; [d]Solution HFIP:PBS (30:70).

Comparing the TPA excitation route with OPA, two-photon absorption at 800 nm excites the molecule well above the lowest energy level (S_1) located at 545 nm (Figure 3.3**a**). Due to the ultrafast (femtosecond) internal conversion of the TPA-state to the relaxed fluorescence state, the fluorescence originates from the same state as for resonant OPA-excitation. At 400 nm, the OPA is essentially non-resonant. The respective initial anisotropies for 400 nm are quite low for rhodamines ($r_0 < 0.1$) as excitation to the higher state (S_2) located at 350 nm also takes place at this wavelength.[68,69] The excitation route via S_2 leads to a negative contribution to the anisotropy while the excitation to the S_1

produces fluorescence with positive anisotropy.[69] The combination of these two contributions produces very low total initial anisotropy, making accurate measurement of orientational dynamics for this excitation regime very difficult.

3.5.4 Fluorescence Lifetime Measurements

Fluorescence emission with two-photon excitation is particularly interesting as it gives a more specific signature regarding conformational changes of proteins and peptides than the emission detected using one-photon excitation. By utilizing the promising TPEF decay time technique, efforts were made to investigate conformational changes and molecular interactions of the amyloid peptides. To apply the unique TPE-TCSPC technique to the structural characterization of Aβ1-42, fluorescence decays of a 15 μM dye-labeled Aβ in a solvent of HFIP/PBS (20:80) were measured. As shown in Figure 3.5, the excited-state population decays of the covalently conjugated TAMRA were fitted with a two-component exponential decay function and the fluorescence lifetimes were found to be 0.4 ± 0.1 ns (36%) and 3.4 ± 0.2 ns (64%), respectively. This differs from the excited-state population decay of the free dye measured under the same conditions which gives only a single fluorescence lifetime (4.08 ± 0.05 ns), in agreement with the first-order dynamics that have been reported in the literature.[70] This discrepancy between the dynamics of the free and covalently conjugated TAMRA has significant implications on the application of its photophysical properties to the study of amyloid peptide structures and their molecular interactions. The labeled N-terminus of the peptide is likely interacting with other amino acids found in the peptide, resulting in fluorescence quenching and the appearance of a shorter lifetime decay component not seen in the free dye system. If we could identify the particular Aβ1-42 conformation that permits this

interaction, then fluorescence lifetimes may provide insight into the larger secondary structure of the peptide.

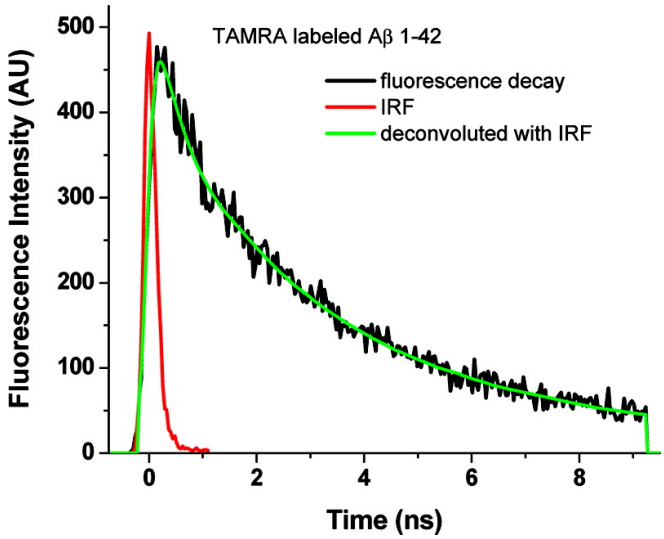

Figure 3.5 Typical TCSPC decay trace of the TAMRA labeled Aβ1-42. TAMRA labeled Aβ1-42 (15 μM) was incubated in HFIP/PBS (20:80) for two weeks prior to measurements.

Previous investigations on the molecular interactions of TAMRA-labeled macromolecules suggest the existence of various conformational states of TAMRA, each with distinct fluorescence lifetimes.[55,71-73] Depending upon the techniques utilized in these investigations, the number of conformational states and fluorescence lifetimes could vary among the different systems.[55,73] However, two major conformational states of the covalently conjugated TAMRA have been observed in all systems.[55,71-73] One (type A) occurs when the dye molecule is close in proximity to a quenching site, and the other (type B) when the chromophore is far removed from quenching sites. The molecules with type A conformations have picosecond ("ps") fluorescence lifetimes with low quantum yields due to photoinduced electron transfer (PET) reactions.[71-76] Molecules with type B conformations have long-decay fluorescence lifetimes (several nanoseconds), high quantum yields (since there is no PET), and are more associated with the solvent

environment.[74,75] Since the two-component fluorescence decays obtained from the TAMRA-labeled Aβ1-42 system are similar to those decays observed in TAMRA-DNA[55,71-73] and TAMRA-peptide[64] conjugated systems, it can be inferred that both type A and B conformations of the conjugated TAMRA may be present in our peptide system. Consequently, the short decay component would reflect the interactions of the covalently conjugated TAMRA with amino acid quenchers constituted in the Aβ1-42, while the long decay component reveals solvent-related environmental changes in relation to the chromophore.

In reviewing the amino acid sequence in the Aβ1-42, the potential fluorescence quenchers are methionine and histidine as well as the aromatic amino acids tyrosine and phenylalanine. Previous investigations on fluorescence quenching of TAMRA by these amino acids have demonstrated that tyrosine is the most pronounced fluorescence quencher.[64] By working at sufficiently low peptide concentrations (μM), a tyrosine residue in Aβ1-42 at sequence position 10 could serve as an efficient electron acceptor for a two-photon induced electron transfer (2PET) reaction. NMR analysis of the structural ensembles of Aβ1-42 in HFIP/water (30:70) has shown that most α-helical structure corresponds to the amino acid sequence in the 10-23 region.[13] This result provides insight into tyrosine behavior when the peptide is dissolved in HFIP/PBS (20:80) to induce the formation of more ordered conformations and aggregates.

As shown in Figure 3.6, the N-terminus of Aβ1-42 is part of a flexible sequence of amino acid residues not prone to forming larger secondary structure like α-helix or β-sheet. Therefore, the labeled N-terminus has the flexibility to adopt conformations in which the chromophore may interact with nearby amino acids such as tyrosine. As

illustrated in Figure 3.6, the tyrosine located at position 10 is accessible for close contact with TAMRA under certain conditions in which the peptide is structured allowing for the possibility of charge-transfer between the two residues. In probing this connection by measuring 2PET-based fluorescence methods, it becomes possible to correlate the fluorescence lifetimes associated with this interaction with the basic conformational state of the peptide.

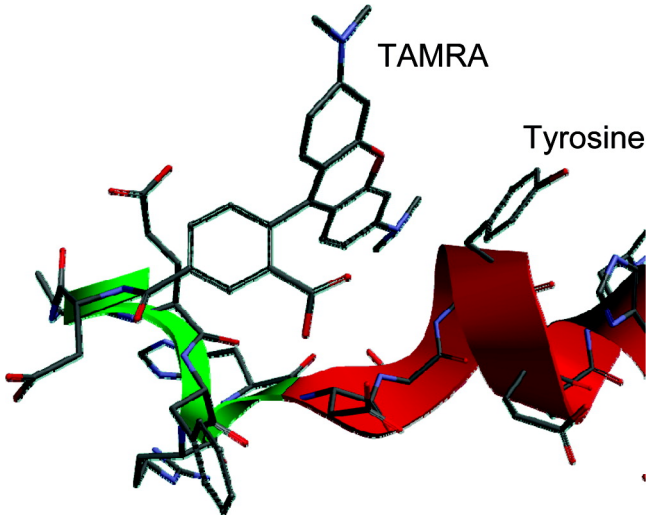

Figure 3.6 Interaction between TAMRA chromophore and tyrosine molecule at position 10. Under certain conditions, labeled Aβ1-42 may be present in conformations conducive for close intramolecular contact between TAMRA and the tyrosine residue at sequence position 10 resulting in fluorescence quenching and the short picosecond fluorescence lifetime.

The connection between the fluorescence lifetimes and molecular interactions associated with the secondary structure was established by characterizing the secondary structures of the dye-labeled peptide at different concentrations using CD measurements and the short-time component fluorescence lifetimes obtained using TCSPC. An estimation of the secondary structural content versus peptide concentration is shown in Figure 3.7. After incubation of the peptides in HFIP/PBS (20:80) for two weeks, all peptides are predominantly in a random coiled structure. However, the relative

proportions of random coil, α-helix, and β-sheet are concentration dependent due to the co-existence of equilibria among these composites. As can be seen from Figure 3.7, the amount of α-helix structure increases with a decrease in random coil, and similar β-sheet content is retained as the peptide concentration increases from 6 to 9 μM. These results indicate that at such low concentrations, peptide interactions are probably important for stabilization and formation of α-helical conformations, but not important for formation of β-sheet conformations. However, at peptide concentrations over 9 μM, there is seen a rapid increase in the percentage of β-sheet structure coincident with a large decrease in random coil content. This result implies that at high peptide concentrations the conformational transition from random coil to β-sheet is due to increased intermolecular hydrophobic interactions and not through intramolecular interactions.[12]

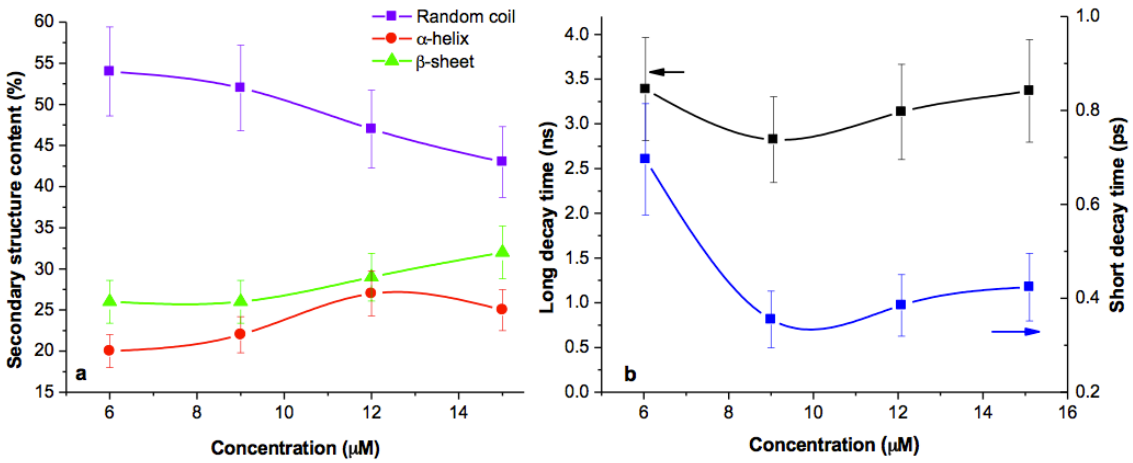

Figure 3.7 Relationship of fluorescence lifetimes to peptide secondary structure. (a) The percentages of random coil, α-helix, and β-sheet as a function of peptide concentration. (b) Concentration-dependent nanosecond fluorescence lifetime and the 2PET-based fluorescence decay time of the covalently conjugated TAMRA. All peptides samples were incubated with HFIP/PBS (20:80) solvent composites for two weeks prior to the measurements. The traces are meant to guide the eye and are not the result of best fits.

3.5.5 2PET-Based Fluorescence Quenching Model

To correlate 2PET-based fluorescence quenching with peptide conformational changes involving intramolecular interactions between the TAMRA–label and tyrosine residue, the absence of intermolecular charge-transfer fluorescence quenching at these low peptide concentrations is assumed. Based on this assumption, the "ps" (short-decay time) fluorescence dynamics relates information about the interaction between a tyrosine residue and the electronically excited TAMRA.[64,77] The correlation of concentration-dependent picosecond fluorescence decay time with secondary structural composites and consequently with conformational flexibility of the N-terminus of the peptides is also shown in Figure 3.7. To better understand this correlation, we present a schematic model for description of conformation in an associated distance-dependent 2PET process (Figure 3.8).

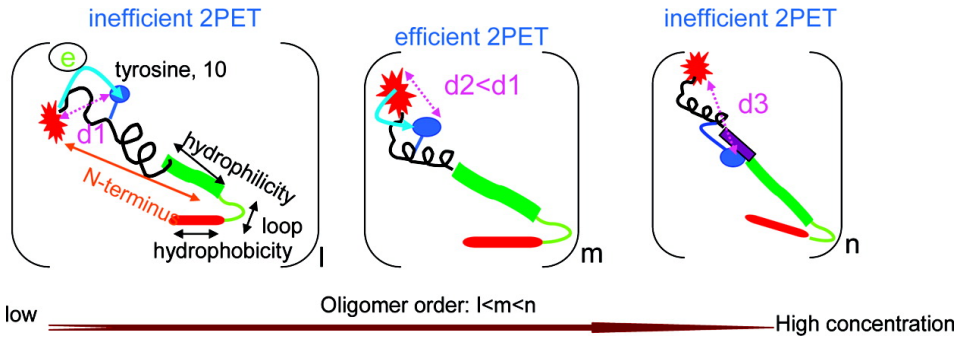

Figure 3.8 Model for description of intramolecular interaction between the covalently conjugated TAMRA and the tyrosine residue within Aβ1-42. Due to the flexibility of the N-terminus, the concentration-dependent conformational changes bring the TAMRA close to tyrosine, yielding efficient 2PET-based fluorescence quenching.

At a low peptide concentration, the peptide is characterized by a high percentage of random coiled structure giving rise to the small degree of fluorescence quenching, i.e. "picosecond" fluorescence lifetimes on the order of 700 ps. This may take place when the tyrosine residue is trapped within a groove of the random coil which keeps the covalently

conjugated TAMRA far away from the tyrosine residue, possibly at a large contact distance (>1 nm).[78] At an intermediate peptide concentration, the peptide is less flexible and is characterized by more ordered structure (increased α-helix content), which reduces the contact distance between TAMRA and tyrosine residue (Figure 3.6), leading to efficient intramolecular charge-transfer fluorescence quenching indicated by faster fluorescence decays. At higher peptide concentrations (for example, over 9 μM), the flexibility of the N-terminus decreases due to a rapid increase in β-sheet content and decrease in random coil. The peptides with such secondary structures may lead the tyrosine to be buried within the "hydrophobic pocket". As a result, the 2PET-based fluorescence quenching is inefficient leading the "ps" decay time to increase as peptide concentrations are increased from 9 to 15 μM.

The long-lived fluorescence component originating from conformational state B of the conjugated TAMRA (away from quencher sites) reveals environmental changes associated with Aβ aggregation also critical to understanding the overall process. A clear assignment of fluorescence lifetimes to specific substances is impossible due to the heterogeneities of Aβ systems as well as the absence of a comprehensive theory relating excited-state lifetime to either local environment or molecular properties for systems which emission bands experience significant inhomogeneous broadening. However, the measurement of excited-state lifetime can aid understanding the impact of environmental factors, such as concentration, on fluorescence lifetime. The "ns" fluorescence decay is predominantly associated with these and reports such factors as solvent accessibility[88] and peptide aggregation-induced chromophoric interactions.[36] Figure 3.7b displays the "ns" fluorescence lifetime as a function of peptide concentration. A monotonic decrease

in the nanosecond (ns) fluorescence lifetime is observed as the peptide concentration increases from 6 to 9 μM. At these concentrations, a decrease in random coil parallel with an increase in α-helix content (Figure 3.7a) suggests ordered structures are formed through peptide-peptide interactions, leading the covalently conjugated TAMRA to be more solvent accessible. As a result, the fluorescence lifetimes decrease with an increase in peptide concentration from 6 to 9 μM. However, when peptide concentration is over 9 μM, a monotonic increase in the long-lived fluorescence lifetime is observed. CD analysis indicates that interactions among the peptides result in an increased aggregation rate and β-sheet. These interactions yield large aggregates making it likely that the covalently conjugated TAMRA becomes trapped inside the aggregates with less solvent accessibility than at lower concentrations. By observing the change in fluorescence decay times measured with respect to solvent accessibility of the TAMRA-label, the suggestion is furthered that the peptide aggregates formed at low concentrations differ from those formed at high concentrations. From these results, we conclude that intra- and intermolecular interactions lend 2PET-based fluorescence to the study of the conformational flexibility of the N-terminus in Aβ with residue-specific assays. This ability to correlate the peptide conformational state with its fluorescence lifetime at low concentrations opens a new avenue toward the measurement of Aβ conformational fluctuation at the signal molecular level unachievable with other predominately used techniques such as CD spectroscopy.

3.5.6 Distribution of Conformational States from Fluorescence Lifetimes

The concentration-dependent peptide interactions (aggregation) not only affect fluorescence lifetimes, but also influence the distribution of conformational states (**A** and

B) of the covalently conjugated TAMRA. Figure 3.9 shows the fractional occupancy (amplitude) **A1** of the "ps" decay lifetime as a function of peptide concentration. As seen from this figure, there is an initial increase in **A1** as the peptide concentration is varied from 6 to 12 μM followed by a decrease as the concentration is further increased to 18 μM. At low peptide concentrations, the structures of the peptides are flexible, an indication of a larger percentage of random coil. In this case, intramolecular contact between tyrosine and TAMRA becomes more feasible, giving rise to a larger distribution of the short decay component **A1**. However, at higher peptide concentrations, the rate of peptide aggregation increases to form large aggregates with increased β-sheet content. The greater structural content of these peptides prevents the covalently conjugated TAMRA from having fluorescence quenching interactions resulting in smaller values for amplitude **A1**. These results when analyzed in conjunction with the concentration-dependent fluorescence lifetimes provide a clear picture as to the conformational flexibility of amyloid peptides over a range of concentrations while also giving an indication as to the types of intra/intermolecular interactions influencing these conformational states.

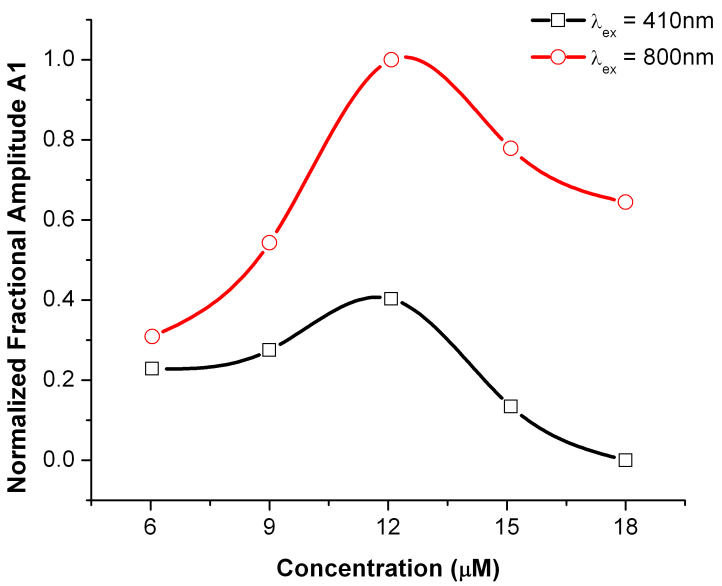

Figure 3.9 The comparison of excitation sensitivity and the effect of peptide concentration on fractional occupancy A1 of the "ps" lifetime.

Figure 3.9 also compares the sensitivity to the mode of excitation of the fractional occupancy **A1** of the covalently conjugated TAMRA. The fractional occupancy **A1** obtained from the two-photon excited fluorescence lifetimes is much larger than that determined from OPE. The heterogeneities of a given peptide may lead to a wide range of excited-states to which the excitation is sensitive and selective. As demonstrated previously, the emitting molecule with type **A** conformation emerges from the case where the covalently conjugated TAMRA is situated in the vicinity of tyrosine (Figure 3.6). This intramolecular contact induces the excited TAMRA-tyrosine to have charge-transfer character that is associated with concentration-dependent peptide conformations. While TAMRA molecules with type **B** conformations are photophysically unaffected by tyrosine due to the large distance separation between them, the fluorescence decay times arising from such conformations may reflect the effects of intermolecular interactions caused by peptide aggregation. Since TPE is a nonlinear process and strongly affected by charge-transfer character of the molecule,[55] the two-photon absorption cross-section is

expected to be large for the molecules with type **A** conformations over type **B**, thus differentiating TPE from OPE which cannot discriminate between the two types. Two-photon excitation could therefore permit the monitoring of larger population decays from molecules with type **A** conformation more easily than that using OPE (Figure 3.9), the primary implication being that TPE predominates the distribution of excited-state molecules relating to the amount of charge-transfer. This additional specificity makes it advantageous over OPE because with inhomogeneous systems such as Aβ1-42 many different conformations and aggregates are co-existing at the same time, so the ability to selectively monitor a particular conformation or aggregate is vitally important to being able to completely understand the system.

3.5.7 Two-Photon Excited Depolarization

Two-photon-excited time-resolved fluorescence anisotropy (TPE-TRFA) takes advantage of the large fluorescence dynamic range permitted which is particularly beneficial to the determination of rotational correlation times greater than the fluorescence lifetimes.[58] While the essential physics of molecular motion is independent of the excitation mechanism, the means by which the initial anisotropic distribution is excited can provide more detailed and complementary information on a molecular motion.[79] In particular, initial fluorescence anisotropy for TPA excitation (0.57) is substantially higher than that for OPE (0.4) which is potentially very useful for resolving complex rotational kinetics with multiple rotational correlation times and restricted rotation.[69,80] Additionally it has been found that the TPE initial anisotropy is nearly independent of the excitation wavelength[81] allowing for use of a larger variety of probes

at a particular excitation wavelength or a broader choice of excitation wavelengths for a specific probe.

The conjugated TAMRA located on the N-terminus of the Aβ1-42 is unable to sense the true dynamics at the C-terminus due to the relatively long separation provided by the hydrophobic core of the Aβ. TPE-TRFA studies on the conjugated TAMRA were used to detect the local motion of the random side-chain to which the probe is covalently attached or the motion of short Aβ1-42 segments. Table 3.2 lists the two-photon excited fluorescence anisotropic decays measured at different peptide concentrations. All decays were successfully deconvoluted into a single rotational correlation time. Systematic decreases in both the rate of motion and initial value of fluorescence anisotropy are observed when the peptide concentration increases from 12 to 18 μM.

Concentration (μM)	**τ (ns)**	**r_0**
6	1.01 ± 0.07	0.36
9	1.18 ± 0.09	0.29
12	0.99 ± 0.07	0.35
15	1.5 ± 0.2	0.33
18	1.8 ± 0.4	0.29

Table 3.2 Rotational anisotropy decay parameters for TAMRA-Aβ1-42 dissolved in HFIP/PBS (20:80).

The anisotropic fluorescence decay of the conjugated TAMRA is complicated due to the heterogeneous nature of our system. It is difficult to attribute our single-exponential anisotropic decay to specific conformational states as was done with the previously measured multi-component fluorescence lifetimes. However, the concentration dependence of the orientational dynamics of the covalently conjugated TAMRA may reveal local motions associated with the packing state of the peptides. This packing is clearly evidenced by the increased rotational correlation times (τ) of the

chromophore as the concentration of the peptide is increased, an indication of the growing size of the aggregates. As shown in Figure 3.10, at peptide concentrations ranging from 6 to 12 μM, the rotational correlation times of the covalently conjugated TAMRA are slightly longer than the local motion of the free dye (700 ± 50 ps) under the same conditions. This implies that there is more restricted movement of the covalently conjugated TAMRA. Closer relative intermolecular packing of the chromophores and weak coupling of the TAMRA to the orientational dynamics of the peptide N-terminus explain the longer correlation times, much the way it has been observed in a TAMRA-labeled DNA system.[82] As the peptide concentrations are increased from 12 to 18 μM, the rate of depolarization of the covalently conjugated TAMRA becomes more than two times slower than that of the free dye. The measured slower decays are evidence of the fact that as more compacted conformations (or aggregates) begin to dominate the system at higher concentrations (Figure 3.7), the motion of the TAMRA probe becomes increasingly hindered.

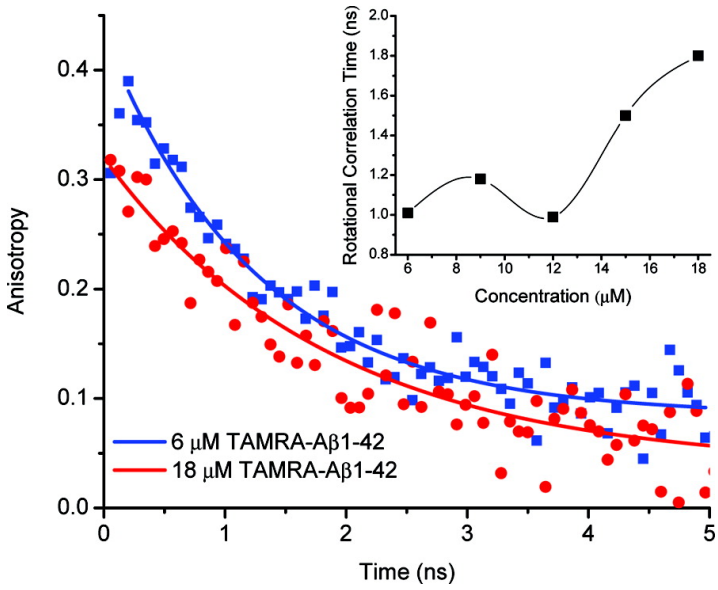

Figure 3.10 Time-resolved fluorescence anisotropy lifetimes of 6 μM and 18 μM TAMRA-labeled Aβ1-42. Inset shows rotational correlation time as a function of concentration.

3.6 Conclusions

The sensitive approach of coupling two-photon emission with time-resolved fluorescence and fluorescence anisotropy was applied to study the conformational changes and early aggregation of amyloid peptides. The characterization of these early aggregates may lead to important discoveries allowing for the prevention or treatment of neurodegenerative diseases, but research into these early stages of aggregation has been hindered by the limitations of other techniques. It remains critical though to understand these early forms as they may be indicative of the pathway leading to the formation of toxic amyloid fibrils. By labeling Aβ1-42 with TAMRA, we were able to probe the conformational flexibility of the peptide by detecting intramolecular, residue-specific interactions involving our chromophore and a tyrosine residue in the peptide (Figure 3.6). Using the short fluorescence lifetime of the labeled peptide and conformational measurements performed using circular dichroism spectroscopy, the secondary structure

of the peptide was able to be correlated to specific fluorescence lifetimes (Figure 3.7), thereby permitting the study of conformational changes in amyloid peptides at the residue level, something not able to be achieved with more commonly used techniques. Fluorescence anisotropy measurements demonstrate that two-photon excitation allows for enhanced selectivity and sensitivity for aggregating peptides especially for those conformations exhibiting short fluorescence lifetimes and strong charge-transfer interactions between chromophore and residue. These depolarization results differ significantly compared with those obtained from typical one-photon excitation (Figure 3.9) which show far lower amplitude for the same systems. The anisotropic decays and fluorescence lifetimes together provide a clear picture as to the conformational flexibility of amyloid peptides over a range of concentrations (6-18 μM) while also giving an indication as to the types of intra/intermolecular interactions influencing these conformational states.

The ability to monitor the fluorescence dynamics (lifetimes and anisotropy) of the covalently conjugated TAMRA as a function of aggregation and secondary structural changes of Aβ provides a valuable tool for the characterization of conformation and molecular interactions of amyloid peptides even at low concentrations. Our findings have implications in the utilization of fluorescence methods to measure and image Aβ conformational fluctuation at the signal molecular level and in the detection of small neurotoxic aggregates formed at low peptide concentrations. The high sensitivity of TPE to peptide structural changes offers the possibility to quantitatively monitor the early aggregation of Aβ at physiological conditions. A promising application of these decay time techniques using the TAMRA-labeled peptide is in the detection of early aggregates

of amyloid proteins via multiphoton fluorescence lifetime imaging and lifetime-based assays.

References

1. Ohnishi, S.; Takano, K. *Cell Mol. Life Sci.* **2004,** *61*, 511-24.

2. Kayed, R.; Head, E.; Thompson, J. L.; McIntire, T. M.; Milton, S. C.; Cotman, C. W.; Glabe, C. G. *Science* **2003**, *300*, 486–489.

3. Lashuel, H. A.; Hartley, D. M.; Balakhaneh, D.; Aggarwal, A.; Teichberg, S.; Callaway, D. J. *J. Biol. Chem.* **2002**, *277*, 42881-42890.

4. Caughey. B.; Lansbury, P. T. *Annu. Rev. Neurosci.* **2003**, *26,* 267–298.

5. Kirkitadze, M. D.; Bitan, G.; Teplow, D. B. *J. Neurosci. Res.* **2002**, *69*, 567-577.

6. Bucciantini, M.; Giannoni, E.; Chiti, F.; Baroni, F.; Formigli, L.; Zurdo, J.; Taddei, N.; Ramponi, G.; Dobson, C. M.; Stefani, M. *Nature* **2002**, *416*, 507-511.

7. Demuro, A.; Mina, E.; Kayed, R.; Milton, S. C.; Parker, I.; Glabe, C. G. *J. Biol. Chem.* **2005**, *280*, 17294 –17300.

8. Deshpande, A.; Mina E.; Glabe, C.; Busciglio, J. *J. Neurosci.* **2006**, *26*, 6011-6018.

9. Masters, C. L.; Simms, G.; Weinman, N. A.; Multhaup, G.; McDonald, B. L.; Beyreuther, K. *Proc. Natl. Acad. Sci. USA*, **1985**, *82*, 4245–4249.

10. Kang, J.; Lemaire, H. G.; Unterbeck, A.; Salbaum, J. M.; Masters, C. L.; Grzeschik, K. H.; Multhaup, G.; Beyreuther, K.; Muller-Hill, B. *Nature* **1987**, *325*, 733–736.

11. Olofsson, A.; Sauer-Eriksson, E.; Öhman, A. *J. Biol. Chem.* **2006**, *281*, 477-483.

12. Barrow, C. J.; Yasuda, A.; Kenny, P. T. M.; Zagorski, M. G. *J. Mol. Biol.* **1992**, *225*, 1075-1093.

13. Tomaselli, S.; Esposito,V.; Vangone, P.; van Nuland, Nico A. J.; Bonvin, A. M. J. J.; Guerrini, R.; Tancredi,T.; Temussi, P. A.; Picone, D. *ChemBioChem* **2006**, *7*, 257-267.

14. Buck, M. *Q. Rev. Biophys.* **1998**, *31*, 297-355.

15. Crescenzi, O.; Tomaselli, S.; Guerrini, R.; Salvadori, S.; D'Ursi, A. M.; Temussi, P. A.; Picone, D. *Eur. J. Biochem.* **2002**, *269*, 5642-5648.

16. Halverson, K.; Fraser, P. E.; Kirschner, D. A.; and Lansbury, P. T., Jr. *Biochemistry* **1990**, *29*, 2639-2644.

17. Lim, K. H.; Collver, H. H.; Le, Y.; Nagchowduri, P.; Kenney, J. M. *Biochem. Biophys. Res. Comm.* **2007**, *2*, 443-449

18. Yang, D. S.; Yip, C. M.; Huang, T. H. J.; Chakrabartty, A.; Fraser, P. E. *J. Biol. Chem.* **1999**, *274*, 32970-32974.

19. Janek, K.; Rothemund, S.; Gast, K.; Beyermann, M.; Zipper, J.; Fabian, H.; Bienert, M.; and Krause, E. *Biochemistry* **2001**, *40*, 5457-5463.

20. Walsh, D. M.; Hartley, D. M.; Kusumoto, Y.; Fezoui, Y.; Condron, M. M.; Lomakin, A.; Benedek, G. B.; Selkoe, D. J.; Teplow, D. B. *J. Biol. Chem.* **1999**, *274*, 25945-25952

21. Shao, H. Y.; Jao, S. C.; Ma, K.; and Zagorski, M. G. *J. Mol. Biol.* **1999**, *285*, 755-773.

22. Zagorski, M. G.; and Barrow, C. J. *Biochemistry* **1992**, *31*, 5621-5631.

23. Kirkitadze, M. D.; Condron, M. M.; and Teplow, D. B. *J. Mol. Biol.* **2001**, *312*, 1103-1119.

24. Serpell, L. C. *Biochim. Biophys. Acta* **2000**, *1502*, 16-30.

25. Soto, C.; Branes, M.; Alvarez, J.; Inestrosa, N. *J. Neurol. Chem.* **1994**, *63***,** 1191-1198.

26. Kirschner, D.; Inouye, H.; Duffy, L.; Sinclair, A.; Lind, M.; Selkoe, D. *Proc. Natl. Acad. Sci. USA* **1987**, *84*, 6953-6957.

27. Barrow, C. J.; Zagorski, M. G. *Science* **1991**, *253*, 179-182.

28. Qahwash, I.; Weiland, K. L.; Lu, Y. F.; Sarver, R. W.; Kletzien, R. F.; Yan, R. Q. *J. Biol. Chem.* **2003**, *278*, 23187-23195.

29. Solomon, B. *DNA Cell Biol.* **2001**, *20*, 697-703.

30. Frenkel, D.; Katz, O.; Solomon, B. *Proc. Natl. Acad. Sci. U.S.A.* **2000**, *97*, 11455-11459.

31. Orner, B. P.; Liu, L.; Murphy, R. M.; Kiessling, L. L. *J. Am. Chem. Soc.* **2006**, *128*, 11882-11889.

32. Soto, C.; Castano, E. M.; Frangione, B.; Inestrosa, N. C. *J. Biol. Chem.* **1995**, *270*, 3063-3067.

33. Kirshenbaum, K.; Daggett, V. *Biochemistry* **1995**, *34*, 7629–7639.

34. Jarvet, J.; Damberg, P.; Bodell, Karl.; Eriksson, L. E. G.; Gralslund, A. *J. Am. Chem. Soc.* **2000**, *122*, 4261-4268.

35. LeVine III, H. *Anal. Biochem.* **2004**, *335*, 81-90.

36. Wang, Y. Goodson, T. *J. Phys. Chem. B.* **2007**, *111*, 327-330.

37. Mukhopadhyay, S; Nayak, P. K.; Udgaonkar, J. B; Krishnamoorthy, G. *J. Mol. Biol.* **2006**, *358*, 935-942.

38. Maji, S. K.; Amsden, J. J.; Rothschild, K. J.; Condron, M. M.; Teplow, D. B. *Biochemistry* **2005**, *44*, 13365-13376.

39. Pelet S.; Previte, M. R.; So, P. T. C. *J. Biomed. Opt.* **2006**, *11*, 034017-1-11.

40. Cohen, B. E.; Pralle, A.; Yao, X.; Swaminath, G.; Gandhi, C. S.; Jan, Y. N.; Kobilka, B. K.; Isacoff, E. Y.; Jan, L. Y. *Proc. Natl. Acad. Sci. U.S.A.* **2005**, *102*, 965-970.

41. Jose, J.; Burgess, K. *Tetrahedron* **2006**, *62*, 11021-11037.

42. Tao, T. *FEBS, Lett.* **1978**, *93*, 146-150

43. Tleugabulova, D.; Czardybon, W.; Brennan, J. D. *J. Phys. Chem. B* **2004**, *108*, 10692-10699.

44. Paravastu, A. K.; Petkova, A. T.; Tycko, R. *Biophy. J.* **2006**, *90*, 4618-4629.

45. Kelly, J. W.; Balch, W. E. *Nat. Chem. Bio.* **2006**, *2*, 224-227.

46. Skoch, J.; Dunn, A.; Hyman, B. T. Bacskai, B. J. *J. Biomed. Opt.* **2005***, 10,* 011007.

47. Bacskai, B. J.; Skoch, J.; Hickey, G. A.; Allen, R.; Hyman, B. T. *J. Biomed. Opt.* **2003***, 8*, 368-375.

48. Schafer-Hales, K. J.; Belfield, K. D.; Yao, S.; Frederiksen, P. K.; Hales, J. M.; Kolattukudy, P. E. *J. Biomed. Opt.* **2005**, *10*, 051402.

49. Andrade, M. A.; Chacón, P.; Merelo, J. J.; Morán, F. *Prot. Eng*. **1993**, **6**, 383-390.

50. Merelo, J. J.; Andrade, M. A.; Prieto, A.; Morán F. *Neurocomputing* **1994**, *6*, 443-454

51. Greenfield, N.; Fasman, G. D. *Biochemistry* **1969**, *8*, 4108-4116.

52. Morrisett, J. D.; David, J. S. K.; Pownall, H. J.; Gotto, A. M. *Biochemistry*, **1973**, *12*, 1290-1299.

53. Xu, C.; Webb, W. W. *J. Opt. Soc. Am. B.* **1996**, *13*, 481-491.

54. Bhaskar, A.; Ramakrishna, G.; Lu, Z.; Twieg, R.; Hales, J. M.; Hagan, D. J.; Stryland, E. V.; Goodson III, T. *J. Am. Chem. Soc.* **2006**, *128*, 11840-11849.

55. Vámosi, G.; Gohlke, C.; Clegg, R. M. *Biophys. J.* **1996**, *71*, 972-994.

56. Lahankar, S. A.; West, R.; Varnavski, O.; Xie, X.; Goodson III, T.; Sukhomlinova, L.; Twieg, R. *J. Chem. Phys.* **2004**, *120*, 337-344.

57. Ryderfors, L.; Mukhtar, E.; Johansson, L. B.-A. *Chem. Phys. Lett.* **2005**, *411,* 51–60.

58. Lührs, T.; Ritter, C.; Adrian, M.; Riek-Loher, D.; Bohrmann, B.; Döbeli, H.; Schubert, D.; Riek, R. *Proc. Natl. Acad. Sci. U.S.A.* **2005**, *102*, 17342–17347.

59. Torok, M.; Milton, S.; Kayed, R.; Wu, P.; McIntire, T.; Glabe, C. G.; Langen, R. *J. Biol. Chem.* **2002**, *277*, 40810–40815.

60. Huang, T.H.; Frazer, P.E.; Chakrabarttty, A. *J. Mol. Biol.* **1997**, *269*, 214-224.

61. Huang, T.H.; Yang, D.S.; Plaskos, N.P.; Go, S.; Yip, C.M.; Frazer, P.E.; Chakrabarttty, A. *J. Mol. Biol.* **2000**, *297*, 73-87.

62. Bateman, D.A.; Mclaurin, J.; Chakrabartty, A. *BMC Neurosci.* **2007**, *8*, 29.

63. Selwyn J. E.; Steinfeld, J. I. *J. Phys. Chem.* **1972**, *76*, 762-774.

64. Marmé, N.; Knemeyer, J-P.; Sauer, M.; Wolfrum, J. *Bioconjugate Chem.* **2003**, *14*, 1133-1139.

65. Packard, B. Z.; Toptygin, D. D.; Komoriya, A.; Brand, L. *Proc. Natl. Acad. Sci. U.S.A.* **1996**, *93*, 11640-11645.

66. Makarov, N.S.; Drobizhev, M.; Rebane, A. *Opt. Express* **2008**, *16*, 4029-4047.

67. Varnavski, O.; Bäuerle, P.; Goodson III, T. *Opt. Lett.* **2007**, *32*, 3083-3085.

68. Volkmer, A.; Hatrick, D. A.; Birch, D. J. S. *Meas. Sci. Technol.* **1997**, *8*, 1339-1349.

69. Lakowicz, J. *Principles of Fluorescence Spectroscopy*, 3rd ed.; Kluwer Academic/Plenum: New York, 2006.

70. Vogel, M.; Rettig, W.; S. R.; Drexhage, K. H. *Chem. Phys. Lett.* **1988**, *147*, 452-460.

71. Edman L.; Mets, U.; Rigler, R. *Proc. Natl. Acad. Sci. USA* **1996**, *93*, 6710-6715.

72. Wennmalm S.; Edman, L.; Rigler, R. *Proc. Natl. Acad. Sci. USA* **1997**, *94*, 10641-10646.

73. Eggeling, C.; Fries, J. R.; Brand, L.; Günther, R.; Seidel, C. A. M. *Proc. Natl. Acad. Sci. USA* **1998**, *95*, 1556-1561.

74. Doose, S.; Neuweiler H.; Sauer, M. *ChemPhysChem* **2005**, *6*, 2277-2285.

75. Wang L.; Gaigalas, A. K.; Blasic J.; Holden, M. J. *Spectrochimica. Acta A* **2004** *60*, 2741-2750.

76. Vaiana, A. C.; Neuweiler, H.; Schulz, A.; Wolfrum, J.; Sauer, M.; Smith, J. C. *J. Am. Chem. Soc.* **2003**, *125*, 14564-14572.

77. Kim, J.; Doose, S.; Neuweiler, H.; Sauer, M. *Nucleic Acids Research* **2006**, *34*, 2516-2527.

78. Adams, D. M.; Brus, L.; Chidsey, C. E. D. etc. *J. Phys. Chem. B* **2003**, *107*, 6668-6697.

79. Greenough, K. P.; Blanchard, G. J. *J. Phys. Chem. B* **2006**, *110*, 6351-6358.

80. Gryczynski, I.; Malak, H.; Lakowicz, J. R. *Chem. Phys. Lett.* **1995**, *245*, 30-35.

81. Fu, J.; Przhonska, O.V.; Padilha, L.A.; Hagan, D.J.; Van Stryland, E.W.; Belfield, K.D.; Bondar, M.V.; Slominsky, Y.L.; Kachkovski, A.D. *Chem. Phys.* **2006,** *321*, 257-268.

82. Unruh, J. R.; Gokulrangan, G.; Lushington, G. H.; Johnson, C. K.; Wilson, G. S. *Biophys. J.* **2005**, *88*, 3455-3465.

83. Brown, O.; Lopez, D.; Fuller, A. O.; Goodson III, T. *Biophys. J.* **2007**, *93*, 1068-1078

Chapter 4

Synthesis and Optical Properties of Two-Photon Absorbing GFP-type Probes

4.1 Original Publication Information

The bulk of this chapter was originally published as the following document:

> "Synthesis and Optical Properties of Two-Photon Absorbing GFP-type Probes" Travis B. Clark, Meghan E. Orr, Daniel C. Flynn, and Theodore Goodson III. *Journal of Physical Chemistry C* **2011**, *115*, 7331-7338

Modifications to the original document were made solely for adapting the content to this form. References between the original manuscript and supporting information have been unified into a single numbering system. Section 4.2 is included to highlight the efforts made in developing the synthetic procedures that resulted in creating the chromophore library ultimately reflected in this chapter, but were not included in the published material relating to this work.

4.2 Unpublished Initial Synthetic Attempts

The development of a chromophore with strong two-photon characteristics was the focus of concentrated research during preliminary investigations, however a great deal of energy was invested into our initial synthetic attempts prior to finding a synthetic strategy that generated the desired chromophore characteristics. Research into the literature suggested that certain GFP-type chromophores had very strong two-photon

emission maxima around 500 nm that would be suitable for use in conjunction with our ultrafast systems.

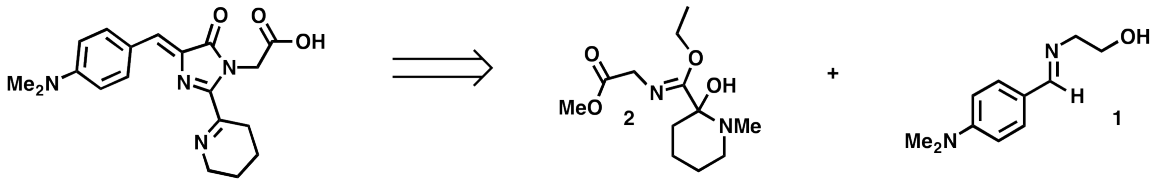

Scheme 4.1 Retrosynthesis of modified ZsYellow chromophore.

The initial target was a modified version of the ZsYellow chromophore (Scheme 4.1**)** that is structurally similar that of the intrinsic chromophore found in GFP however with a fluorescence emission maximum at slightly longer wavelengths due to the incorporation of a dimethylamino group instead of the naturally occurring hydroxyl. This chromophore was expected to possess a high two-photon cross-section suitable implementation as a label into amyloid-β peptide. The core imidazolidinone moiety of the desired chromophore was designed to be synthesized through a 1,3-dipolar cycloaddition reaction between two precursor molecules (Scheme 4.1, **1** & **2**).[1,2] The individual syntheses of which involve a series of established literature reactions. Precursor **1** may be formed through a high-yielding, simple imine-forming reaction between 4-(dimethylamino)benzaldehyde and 2-aminoethanol as reported previously by Fülöp et al.[3] Reactions to make iminoalcohols of this type are known to result in a mixture of tautomers resulting from the additional formation of the closed-ring 1,3-oxazolidine structure. As seen from our results, the open-chain form is the over-whelming favorite in the equilibrium.[4]

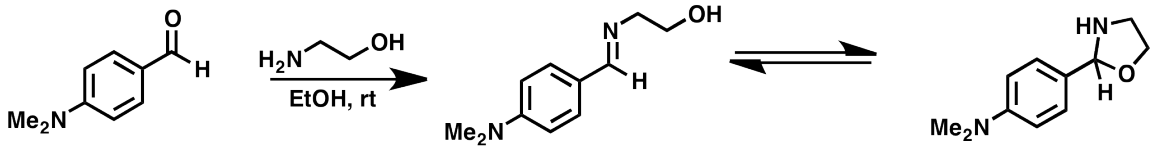

Scheme 4.2 Synthesis of aminoethanol precursor **1**.

The synthesis of the protected aniline precursor proceeded smoothly through the reaction of 4-(dimethylamino)benzaldehyde and ethanolamine stirred in ethanol at room temperature. After performing several times, it was conclusively determined that the protected open-chain alcohol is almost the exclusive product after allowing the reaction to proceed for two days. Isolated yields were achieved at upwards of 90%. A different purification method was developed for this step in order to obtain the highest purity product. Recrystallization from methanol was able to successfully remove any residual impurities to yield white crystals.

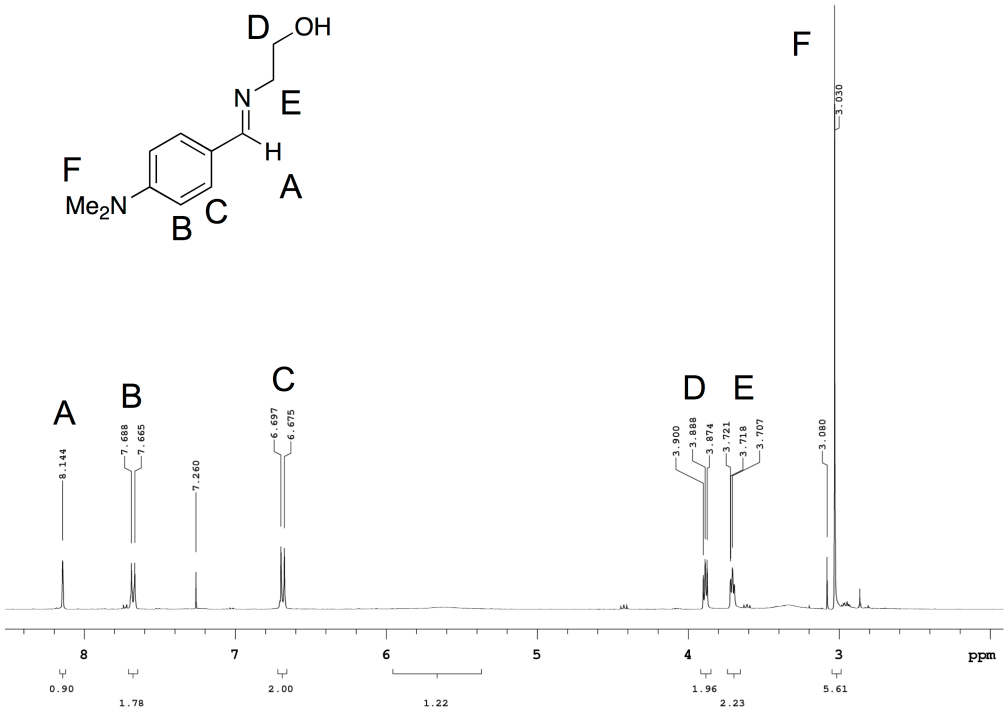

Figure 4.1 Labeled ^{1}H NMR ($CDCl_3$) of aminoethanol precursor **1**. δ ($CDCl_3$): 3.030 (s, 6H) (**F**); 3.718 (t, 2H) (**E**); 3.888 (t, 2H) (**D**); 6.686 (d, J = 8.8 Hz, 2H) (**C**); 7.677 (d, J = 9.2 Hz, 2H) (**B**); 8.144 (s, 1H) (**A**).

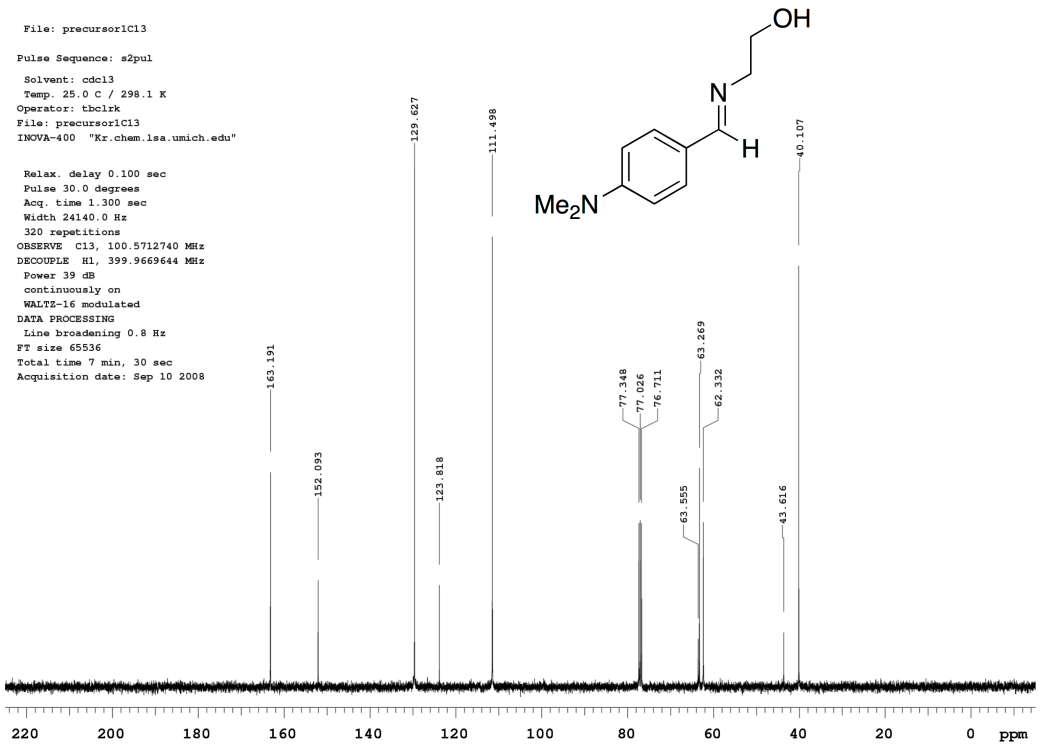

Figure 4.2 Labeled ^{13}C NMR ($CDCl_3$) of aminoethanol precursor **1**. δ ($CDCl_3$): 40.107, 63.332, 63.269, 111.498, 123.818, 129.627, 152.093, 152.093, 163.191

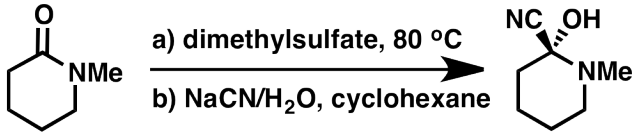

Scheme 4.3 Synthesis of cyanohydrin from corresponding lactam.

The synthesis of precursor **2** was extremely challenging as a result of three synthetic steps. The first step is the formation of a cyanohydrin[5] from *N*-methylpiperidone through stepwise-treatment with dimethyl sulfate and sodium cyanide (Scheme 4.3). The resulting crude oil product was able to be purified using column chromatography to give pure product in only moderate yields. The expected product should contain a methoxy[6] group, but it was not observed either in my experimentation or previous studies by my predecessor. The hydrolyzed product is likely is the result of a quick E1 elimination of the formed ether due to the presence of a strong acid (H_2SO_4) in

the dimethyl sulfate. Thin-layer chromatography analysis of the reaction shows that the reaction goes largely to completion after 48 h reflux and addition of sodium cyanide. Clean cyanohydrin product was relatively easy to isolate using column chromatography with a developing solvent comprised of ethyl acetate and hexanes (75:25). ^{1}H NMR showed clean isolation of the product with no presence of starting material in the combined fractions. Isolated yields were disappointing low (~10%).

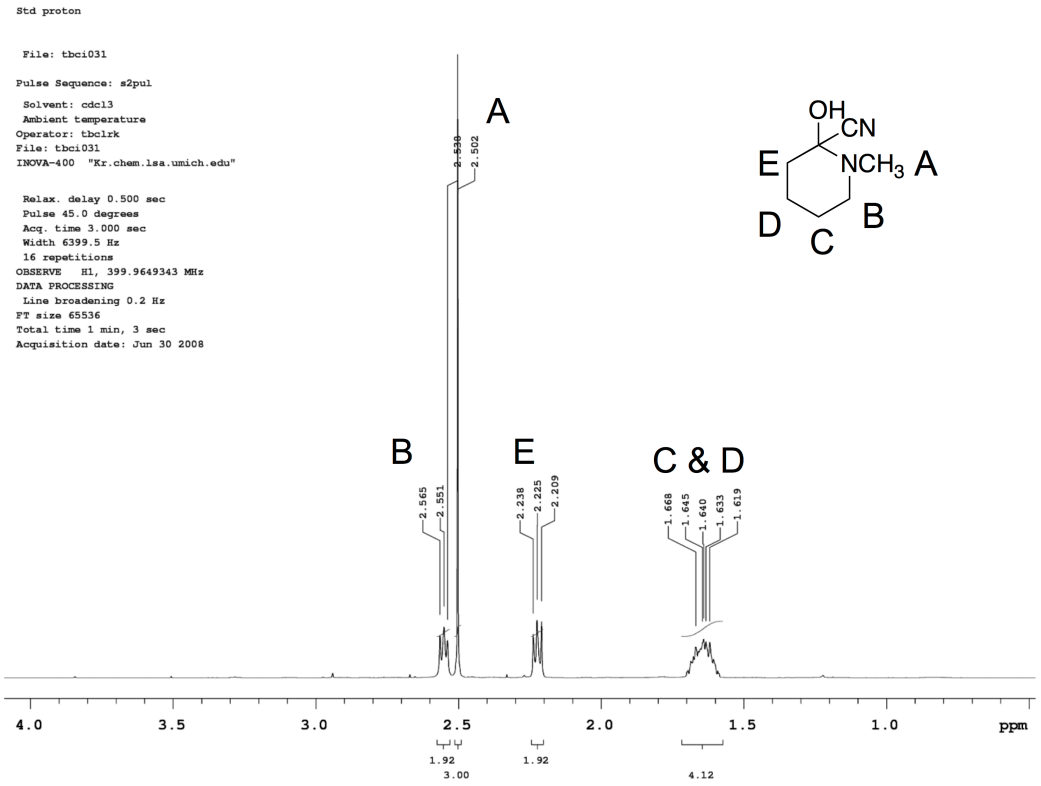

Figure 4.3 Labeled ^{1}H NMR ($CDCl_3$) of cyanohydrin formed. δ ($CDCl_3$): 1.640 (m, 4H) (**C** and **D**); 2.25 (t, J = 5.2 Hz, 2H) (**E**); 2.502 (s, 3H) (**A**); 2.551 (t, J = 5.2 Hz, 2H) (**B**).

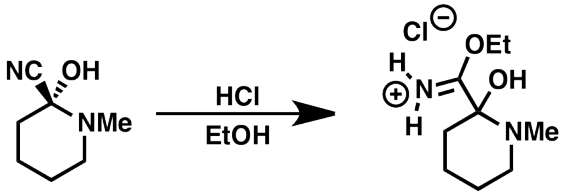

Scheme 4.4 Synthesis of activated imidate salt from corresponding precursor.

Successful isolation and purification of the cyanohydrin allowed for quick access to the imidate salt through a Pinner reaction[7] by bubbling gaseous hydrochloric acid through a solution of the cyanohydrin dissolved in ethanol. The highly reactive solid intermediate was often able to be obtained through filtration and used without further purification to prevent accelerated degradation from exposure to air. TLC qualitative analysis indicated conversion of the cyanohydrin to a far more polar molecule on the plate, which is consistent with a successful synthesis of the imidate salt.

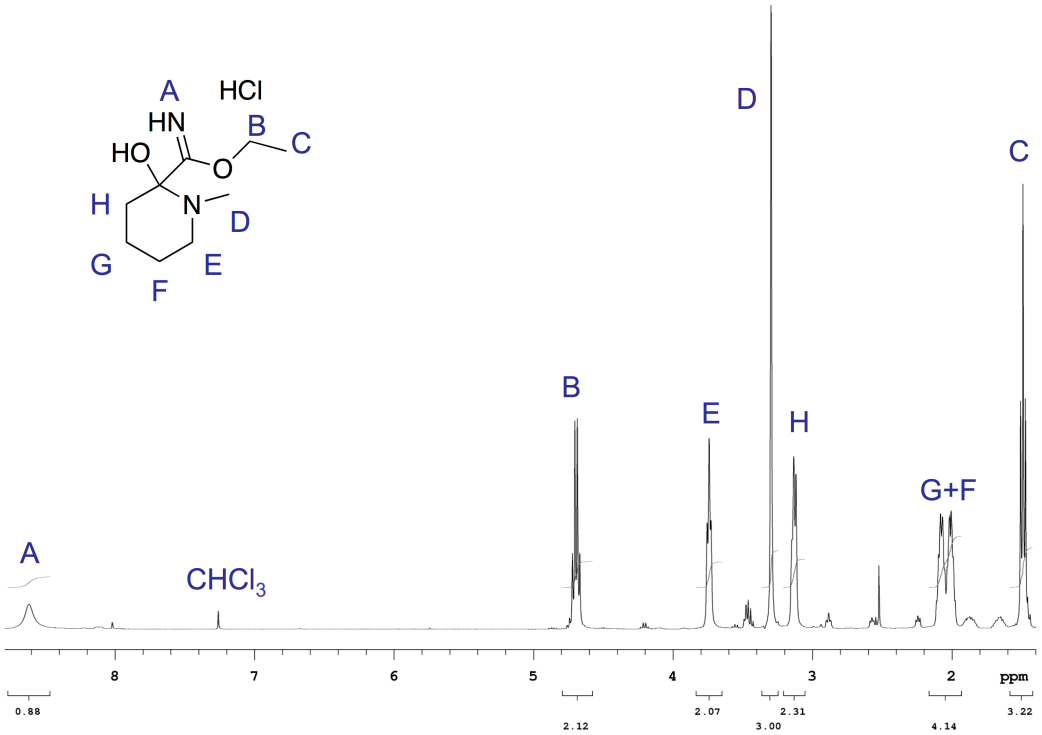

Figure 4.4 Labeled ^{1}H NMR ($CDCl_3$) for synthesized imidate salt. δ ($CDCl_3$): 1.5 (t, 3H) (**C**); 2.1 (m, 4H) (**G** and **F**); 3.1 (d, 2H) (**H**); 3.3 (s, 3H) (**D**); 3.75 (t, 3H) (**E**); 4.7 (q, 2H) (**B**); 8.6 (bs, 1H) (**A**).

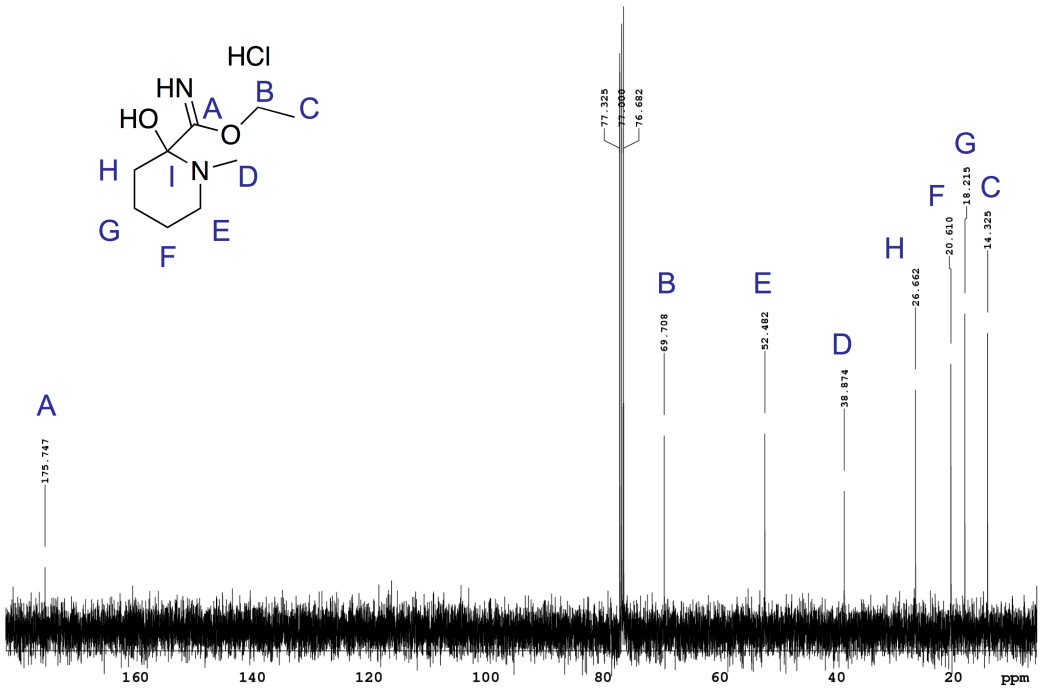

Figure 4.5 Labeled ^{13}C NMR ($CDCl_3$) for synthesized imidate salt. δ ($CDCl_3$): 14.325 (**C**), 18.215 (**G**), 20.610 (**F**), 26.662 (**H**), 38.874 (**D**), 52.482 (**E**), 69.708 (**B**), 175.747 (**A**).

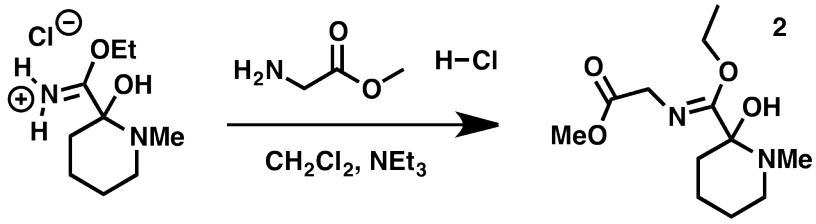

Scheme 4.5 Glycine methyl ester addition to generate imidate intermediate.

To complete the synthesis of the precursor **2** the solid imidate salt was then used in an addition reaction with glycine methyl ester hydrochloride[8] by suspending it in methylene chloride followed by the addition of triethylamine, forming the corresponding functionalized-imide, precursor **2** (Figure 4.6). Anhydrous conditions with the previously investigated synthesis[8] using glycine methyl ester hydrochloride and dry solvent (CH_2Cl_2) from the McNeil Lab solvent system and distilled triethylamine that had been dried over KOH all while under an argon atmosphere. An additional synthetic strategy

was explored in which glycine was used instead of glycine methyl ester hydrochloride to create an analogous imide. The objective here was to observe whether the reactivity of the methyl ester had any effect on the formation of the imide product or contributed in any way to a decomposition pathway. Imidate synthesis using the glycine resulted in equally poor yields of the desired imide, but also the loss of the nitrogen protecting group according to NMR studies. This indicated that the carboxylate group has poor compatibility with the protecting groups used in the synthesis. Purification for the imide was generally limited to extraction of the soluble imidate in ether, and removal of the insoluble starting glycine methyl ester through filtration.

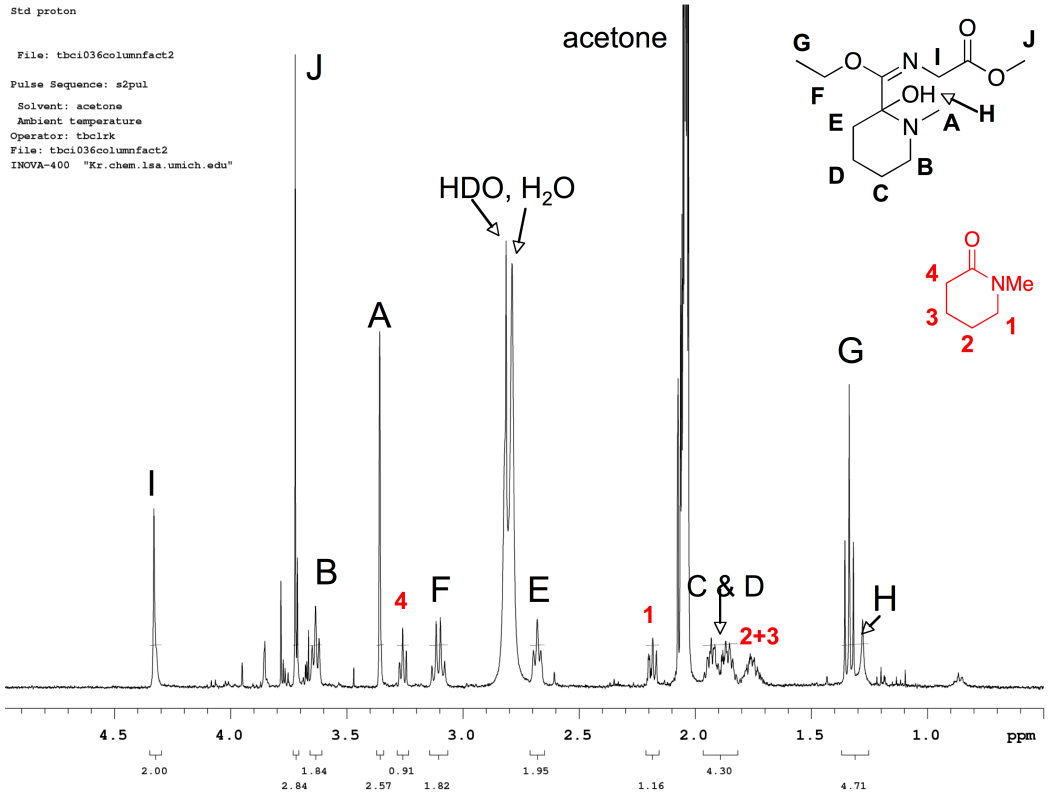

Figure 4.6 ^{1}H NMR (Acetone) depicting possible precursor **2** impure product. Precursor 2, δ (Acetone): 1.29 (bs, 1H) (**H**); 1.32 (t, 3H) (**G**); 1.8 (m, 4H) (**C** and **D**); 2.68 (t, 2H) (**E**); 3.1 (q, 2H) (**F**); 3.35 (s, 1H) (**A**); 3.65 (t, 2H) (**B**); 3.72 (s, 3H) (**J**); 4.31 (s, 2H) (**I**).

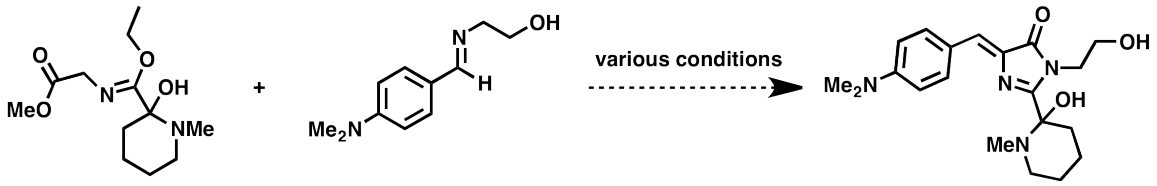

Scheme 4.6 Cycloaddition attempts with precursor **1** & **2**.

With the imide precursor and the protected aniline in hand, the 1,3-dipolar cycloaddition was attempted several times with various conditions meant to achieve full cyclization with elimination of the ethoxy group to create the above illustrated product. Only trace amounts of a product were ever observed using NMR spectroscopy. According to a paper published in *Heterocycles*,[9] the ether group can be made to leave thermodynamically with heating in an appropriate solvent after about 48 h. The procedure was later attempted using a minimum amount of chloroform as a solvent and running the cycloaddition over the course of many hours. ^{1}H NMR and ^{13}C NMR spectroscopy showed that product mixture was predominately the protected aniline imide that was hydrolyzed back into its aldehyde precursor from the very first step in the synthesis. Other signals in the spectra seemed to indicate that the other component may also have reverted to its original form that of 1-methylpiperidin-2-one. This proved to be quite a disappointing result.

Another attempt was made using acetonitrile as the solvent and following the same procedures; a slightly more promising result was achieved. An orange oil/solid was obtained upon isolation of the reaction material, and the ^{1}H NMR showed the presence of small peaks consistent with the expected chemical shift of the protons in the cyclized product. The reaction clearly was not entirely efficient as significant quantities of the undesired aldehyde byproduct show up in the spectrum. TLC analysis of the product mixture however indicated a new spot, possibly corresponding to the cyclized product.

A variety of reaction conditions were investigated to improve the poor yielding glycine addition reaction to generate precursor **2**. Longer reaction times, extra dry solvents, reaction temperatures, and implementation of cool baths were all attempted to increase yields. TLC and NMR analyses were inconclusive in confirming the actual composition of product mixture formed. Once cyclized to form the core structure of the chromophore various oxidation[10] and deprotection[11,12] strategies were envisioned to synthetically transform this intermediate structure to the desired modified-ZsYellow chromophore, but ultimately never implemented due to the struggles to obtain useable amounts of product. There has only been limited precedence[8,13] in the literature for such reactions between two imidate salts as we attempted with reactions of imidate salts much more typically being performed with aldehydes.[14]

In an effort to eliminate some of the synthetic challenges presented by the initial target molecule, a simpler architecture and synthetic design was developed in a compromise with some of the chromophore conjugation, but presuming to maintain most of the photophysical properties we desired. Using readily available starting materials, ethyl acetimidate hydrochloride and glycine methyl ester hydrochloride, and following the procedure[1] outlined by Lerestif et al. a structurally analogous precursor **2** could be synthesized having a methyl group in place of the bulkier nitrogen heterocycle. The cycloaddition reaction could then be performed with previously synthesized precursor **1** to form the basic structure of the chromophore. Simple oxidation of the alcohol to a carboxylic acid completes the synthesis and readies the chromophore for attachment to peptide.

4.3 Abstract

Two-photon active green fluorescent protein type chromophores were

successfully synthesized following investigations directed toward a modified version of zFP538 chromophore, a structural analog to the GFP-chromophore. A generalized approach for the chromophore synthesis via a well-studied cycloaddition reaction combining an iminoglycine methyl ester and a substituted benzaldehyde was developed allowing for flexibility in the incorporation of functional groups such as donor-acceptor substituents and for additional groups to provide extended conjugation. Steady-state spectroscopy, fluorescence quantum yields, and time-resolved fluorescence lifetimes for synthesized chromophores were extensively investigated for the functionalized chromophores. Time-resolved fluorescence lifetimes were found to be bi-exponential generally with sub-picosecond and picosecond components. The individual effects of substitution position of functional groups and relative bulk size were evaluated and found to be rather significant in changing the fluorescence-decay characteristics in the case of positioning, but ambiguous with respect to relative bulk. The GFP-type chromophores were found to possess modest to low two-photon absorption cross-sections with the dimethylamino-substituted analog possessing the largest value at nearly 40 GM. These molecules show promise as biological markers for application in the study of conformation changes and aggregation of amyloid peptides, known to play an important role in many neurodegenerative diseases.

4.4 Introduction

The Green Fluorescent Protein (GFP)[15-17] is one of the most widely used tools in biomedical studies and has long fascinated researchers with its naturally occurring high fluorescence quantum yield. Due to their unique fluorescence characteristics, GFP and structurally analogous proteins[18] have been utilized in many research applications including protein-dynamics studies, real-time molecular & cellular analysis[19], and a

variety of imaging applications.[20] In the past few decades, the chemical structures of the fluorescently active chromophore of GFP[21,22] as well as several of its homologues[23] have been discovered, and researchers have begun to synthetically model the chromophore outside of the protein environment. Niwa, et al.[24] were first to synthesize a model compound of the GFP-chromophore in 1996 and computational studies[25] quickly began to examine the photophysical mechanism of the chromophore when it is isolated in solution.

Ultrafast laser spectroscopy has increasingly been used as a tool to develop better theories to describe the fast electronic processes occurring in this system[26] and to understand how the tertiary protein structure contributes to the overall photophysics of GFP. Much of the significant research in this area has been based on the early discovery of a tremendous discrepancy between the fluorescence quantum yield of the chromophore in solution (~10^{-3}) and that of the intact GFP (~0.8). The reason for such a dramatic difference has long been thought to be the result increased bond-rotation effects such as Z-E isomerization of the chromophore in solution as compared to inside the protein-cage where such motion may be suppressed.[27] Overcoming this limited fluorescence has led to numerous synthetic attempts through either functional-group modifications or changes in environmental conditions[28] to improve the general characteristics of GFP-type chromophores. Many of these changes have led directly to targeted application in materials science[29] and biomedical studies.[30]

By eliminating the protein-cage structure, the determination of the photophysical properties (such as the molar extinction coefficients as well as the elucidation of complex dynamics such as fluorescence decay) for these chromophores has been simplified.

Consequently, a wide variety of synthetic model systems have now been investigated.[31-33] However, the implementation of these types of chromophores in actual applications has been relatively scarce. One fairly clear area of interest for GFP-type chromophores is to further broaden their use as biological probes by covalently attaching them to macromolecules like DNA and proteins. Their implementation as biological probes for labeling of biomolecules such as DNA or peptides has only seen nascent interest in the literature,[30] but presents many encouraging attributes due to its small size and potential for fluorescence enhancement upon aggregation. A great deal is left to be understood about the complicated process by which amyloid peptides misfold to result in neurotoxic diseases such as Alzheimer's and Parkinson's disease. Fluorescence methods utilizing probes to track changes in particular are promising, but there remains a need for improvements in both fluorescence labels and methodology.[34] To best utilize these properties, a sophisticated technique must be implemented to detect the minute changes in the chromophore and its environment.

Two-photon excited fluorescence (TPEF) has been shown to be an effective tool to interrogate the fundamentals of the excited state and identify structure-function relationships in organic molecules.[35,36] As a consequence two-photon excited spectroscopy has been increasingly used as a tool for fluorescence imaging and the monitoring of aggregation[37] and conformational changes[38] in biomolecules to provide additional details inaccessible via linear spectroscopy. In the case of two-photon microscopic imaging, infrared excitations result in more localized, deeper imaging capabilities with reduced likelihood of autofluorescence and photodamage.[39] Based on a survey of the literature, there have been no previous studies performed determining the

two-photon absorption cross-sections or utilizing two-photon excited fluorescence of GFP-type chromophores. Many papers have been published investigating these characteristics for native fluorescent proteins[39-42] and computational studies have been done on model chromophores, but neither affords a detailed, systematic examination for how substituent groups affect the overall two-photon absorption response, something that is permitted through investigation of the chromophores in solution.

Combining chemical modification and two-photon excited fluorescence as a guide for the design of an ideal chromophore for biological applications, efforts have recently been made in our lab toward the synthesis of two-photon active GFP-type chromophores having strong absorption and fluorescence emission in the visible region that are well suited for direct two-photon excitation using typical Ti:Sapphire lasers. Preliminary synthetic investigations were directed toward a yellow-fluorescent protein chromophore (zFP538)[43] that is structurally similar to that of the intrinsic chromophore found in GFP but with absorption/emission maxima at slightly longer wavelengths (376/468 nm) as compared to the more commonly used GFP. This chromophore is predicted to possess among the highest two-photon cross-sections of the GFP-type chromophores due to its strong dipolar[44] character, making it an ideal candidate for future applications as a biological tag[30] in peptide studies.

A diverse library of derivatized structures provides a valuable opportunity to look at a wide range of structural analogs and compare their behavior. The excited state dynamics of GFP-type chromophores is an important area of study geared toward understanding the photophysical properties of the native chromophore and how such unique fluorescence characteristics are achieved. By synthesizing chromophores outside

of the protein, researchers have investigated features isolated to the chromophore allowing for clearer determination of the significance of the protein structure in facilitating fluorescence as well as allowing for the ability to ascertain the role substituent groups play in altering these characteristics. The works of Meech[45-48] and Tolbert[49-51] have looked extensively at the dynamics of synthetic GFP-model systems striving to characterize their excited-states. Making slight modifications to the general chromophore structure of GFP allows for probing both the structural and electronic roles played in the excited state of the protein.

4.5 Experimental Details

4.5.1 Synthesis of Chromophores

All chemicals were used as received from the vendors, without further purification. NMR spectra were obtained on either Varian Inova 400 (399.96 MHz for ^{1}H; 100.57 MHz for ^{13}C) or Varian MR400 spectrometers. ^{1}H and ^{13}C NMR chemical shifts are reported in parts per million (ppm) relative to TMS, with the residual solvent peak used as an internal reference. Multiplicities are reported as follows: singlet (s), doublet (d), doublet of doublets (dd), triplet (t), quartet (q), and multiplet (m). All NMR spectra were recorded at room temperature.

4.5.2 Steady-State Spectroscopy

Unless otherwise specified, absorption and fluorescence emission spectra were recorded on an Agilent (Model 8341) spectrophotometer and Fluoromax-2 fluorimeter (ISA instruments New Jersey), respectively. Measurements were performed using a standard quartz cell with an optical path of 0.4 cm at room temperature. Fluorescence quantum yields (φ) were measured comparing the integrated fluorescence intensity from

the samples at low optical densities to that of the standard Coumarin 307 in methanol under the same conditions.

4.5.3 Two-Photon Absorption

Cross-sections were measured using the two-photon excited fluorescence (TPEF) method as described elsewhere.[52] A solution of Coumarin 307 in methanol ($< 10^{-4}$ M) was used as the TPA reference across all the wavelengths studied. Both MaiTai and Kapteyn Murnane Laboratories diode-pumped mode-locked Ti:sapphire lasers were utilized for sample excitation. The beam was directed onto the sample cell (quartz cuvette, 0.4 cm path length), and the resultant fluorescence was collected perpendicular to the incident beam. A 1-in. focal length plano-convex lens was used to direct the collected fluorescence into a monochromator whose output was coupled to a photomultiplier tube. The photons were converted into counts by a photon-counting unit. A logarithmic plot of collected fluorescence photons versus input intensity was verified to yield a slope of 2 indicating the quadratic power dependence.

4.5.4 Ultrafast Time-Resolved Fluorescence Upconversion

The fluorescence upconversion system used for time-resolved measurements of the chromophores has been described previously.[53,54] In brief, a Tsunami Mode-Locked Ti:Sapphire (Spectra Physics) Laser operated 120 fs pulses of 770-840 nm (gate pulse), with a repetition rate of 82 MHz, to generate light of 370-420 nm (excitation) from second harmonic generation in a β-barium borate crystal. Using a FOG-100 system (CDP Inc.), the gate pulse was channeled through a delay line while the excitation light was up-converted and used to excite the samples. A monochromator detected the second harmonic generation of the gate pulse and emission from the samples, and was enhanced

by a photomultiplier tube. The samples were prepared in a solution of acetonitrile with an optical density of approximately 1. The measurements of the chromophores were observed using a quartz, rotating cell of 1 mm. The photo-stability of the chromophores in this study was confirmed by steady state measurements prior to excitation. The kinetic fitting for the measurements of these chromophores was done after 1 ps of the date to avoid issues with deconvolution with the instrument response function.

4.6 Results and Discussion

4.6.1 Synthesis

The core imidazolone moiety of the GFP-type chromophore was synthesized using a well-studied cycloaddition reaction[1,8,55] combining an iminoglycine methyl ester and a substituted benzaldehyde as depicted in Scheme 4.7. Each of these precursors was readily obtainable from either commercial sources or a few synthetic steps. Two versions of iminoglycine methyl esters were used in our experiment with each obtained in a single step from the base-catalyzed condensation reaction of the corresponding ethyl imidate hydrochloride with glycine methyl ester hydrochloride. These products were prone to decomposition upon prolonged exposure to water/air so minimal purification was performed if NMR analysis showed high conversions rates for the crude product. Reactions with benzaldehyde derivatives were performed to great success under moderate heating in toluene overnight. Products were generally collected as oils that often crystallized upon standing for a few hours. A series of nine different GFP-type chromophores were eventually synthesized with a variety of different functional groups designed to examine different substituent effects (Table 4.1).

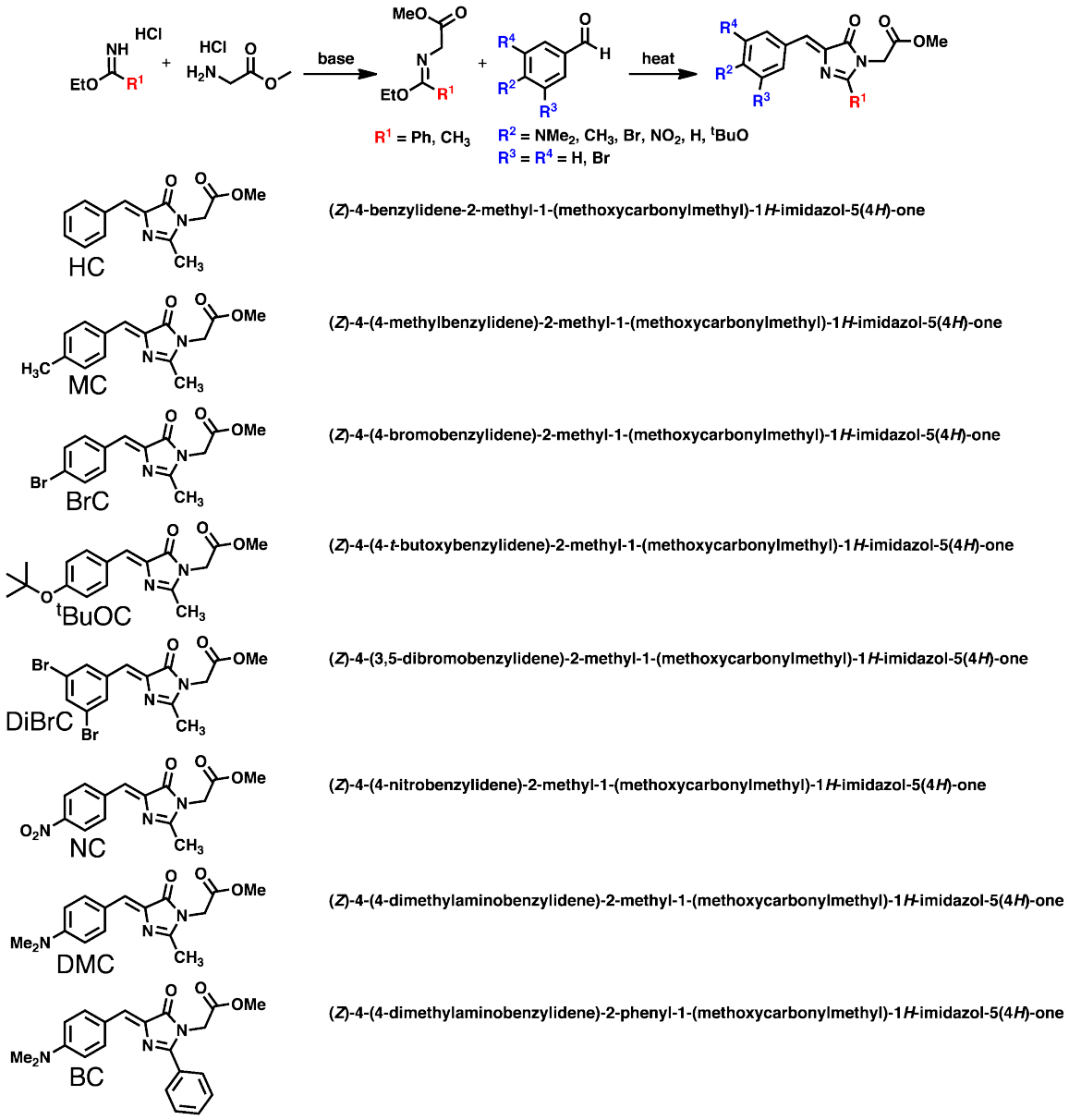

Scheme 4.7 General synthesis of GFP-type chromophores and chromophore library.

The effects of conjugation length were primarily examined through the substitution of a phenyl ring at position R^1 for a methyl group with the expectation of red-shifted steady-state spectra and increased TPA cross-sections (BC, NPC). At positions R^2-R^4 along the benzylidene moiety charge-transfer groups were incorporated (NC, DMC) as a means for improving the overall TPA characteristics. Other derivatives with weaker electronic effects such as MC substituted with a methyl group at R^2 and HC with

a hydrogen at the same position served as systems to judge the how significant the hydroxyl group is in defining the photophysical characteristics of the GFP chromophore. Two different chromophores were synthesized with bromine substituent groups, BrC with substitution at the *para*-position and DiBrC substituted with bromines at both *meta* positions to interrogate whether substitution position would substantially change the fluorescence characteristics of the chromophore. Similarly, a derivative (^{t}BuOC**)** was synthesized to examine the physical size effects of substituent groups as well as to structurally mimic the electronic effects of the hydroxyl group found in the GFP-chromophore. With the broad applicability of this synthesis, more diverse functionality could be incorporated into the chromophore by further varying the R-groups with a wider variety of substituents. Our synthetic strategy has also permitted the incorporation of the critical pendant ester into the basic chromophore structure which may be utilized as a means to attach the molecule to peptide chains or otherwise covalently bond to molecules of interest.

Other typical synthetic strategies have implemented variations of the Erlenmeyer azlactone synthesis[56,57] to incorporate glycine and benzaldehyde to yield upon cyclizing under alkaline conditions in acetic anhydride an azlactone structure.[58] This may be further transformed to the corresponding imidazolinone structure by reacting with an amine (typically methylamine) to give the final model GFP chromophore with a methyl or some other alkyl chain substituted at the amidic nitrogen. Modifications can be made to this synthetic methodology to broaden the resultant chromophore functionality, however a synthetic strategy such as the one implemented in this study offers

substantially more ability for tuning the overall characteristics of the final synthesized chromophore though the incorporation of diverse functionality.

4.6.2 Steady State Absorption and Emission

Initial steady-state properties were investigated for the synthesized chromophores. Figure 4.7 shows the steady-state absorption of the chromophores plotted as molar extinction coefficient versus wavelength. The relative positioning of the absorption bands follow the expected trends pertaining to conjugation effects and charge-transfer groups on photon absorption. The chromophores with the shortest wavelength absorptions are those with shortest conjugation lengths (methyl groups at R^1) and fairly weak electronic groups at R^2 (HC, MC, BrC). Substitution position (DiBrC) and the relative bulk of a group (^{t}BuOC) seem to have no marked influence on relative shape or position of the band. The absorption of dibromo-substituted DiBrC is indistinguishable from BrC, indicative of a small effect from either *meta* or *para* group-substitution on the steady state. The charge-transfer NC chromophore has the broadest absorption centered at 376 nm, but demonstrates a much less pronounced effect from the strongly electron withdrawing nitro group than that caused by the tertiary amine in DMC whose absorption is red-shifted more than 70 nm compared to that of HC. Further interrogating the tunability of the absorption of GFP-type chromophores, NPC and BC provide evidence as to the impact of conjugation on the wavelength of absorption. No noteworthy shift in position is found between NC and NPC, while the same comparison of BC with DMC shows a further 30 nm shift results from the additional conjugation.

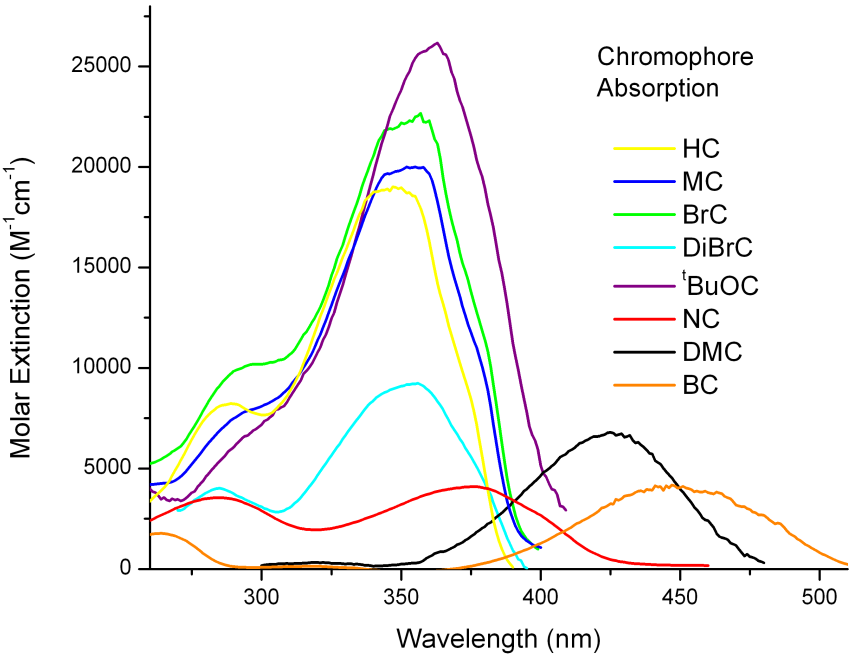

Figure 4.7 Chromophore steady-state absorption. Absorption spectra of synthesized chromophores in acetonitrile, scaled to reflect the molar extinction coefficient for each. HC, yellow; MC, blue; BrC, green; DiBrC, cyan; ^{t}BuOC, purple; NPC, magenta; NC, red; DMC, black; BC, orange.

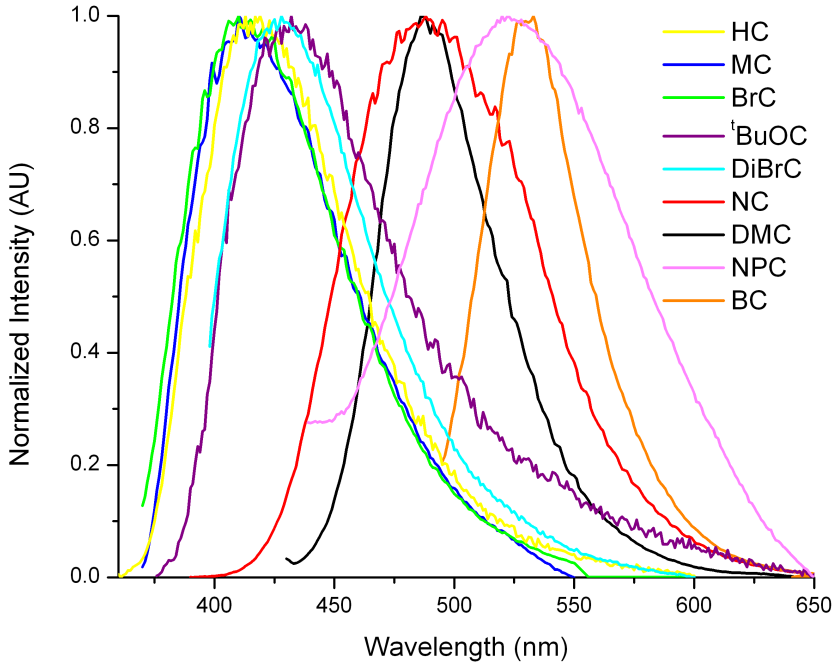

Figure 4.8 Normalized emission spectrum of the synthesized chromophores in acetonitrile. HC, yellow; MC, blue; BrC, green; DiBrC, cyan; ^{t}BuOC, purple; NPC, magenta; NC, red; DMC, black; BC, orange.

Bromo (BrC), methyl (MC), and hydrogen (HC) derivatives have absorption profiles very similar to that of the GFP chromophore (λ = 376 nm) but have fluorescence emission significantly blue-shifted without the donating character of the hydroxyl group present for GFP chromophore (λ = 490 nm). The emission profiles for HC, MC, BrC, and DiBrC exhibit good mirror image symmetry with respect to their respective absorption curves indicative of very similar transitions occurring in both absorption and emission. ^{t}BuOC has a shifted emission compared to those four previously referenced chromophores that is consistent with its red-shifted absorption profile. The Stokes shift for ^{t}BuOC is very similar to those chromophores containing similarly weak electronic functional groups with all having shifts between 4300-4900 cm^{-1}. As observed the absorption studies, with the incorporation of stronger donor (NMe_2) or acceptor (NO_2) substituents into the structure, pronounced red shifts in the emission spectra are induced. The addition of either group onto the core chromophore results in approximately the same fluorescence maximum near 488 nm, but with a large difference in Stokes shift between NC (6100 cm^{-1}) and DMC (3210 cm^{-1}). A significant difference in the emission peak-shape is noted as NC has a broad fluorescence emission pronounced over a wide range of wavelengths, while DMC has a much narrower peak-shape that has a far larger degree of symmetry on both the blue and red edges. Finally, further increases of the effective conjugation length of the molecule through the inclusion of an additional phenyl substituent (NPC, BC) at R^1 also induces a large shift in the fluorescence emission to near that of the initial zFP538 target chromophore (λ = 538 nm).

Fluorescence quantum yields for the synthesized chromophores have values on the order of 10^{-3}-10^{-4} (Table 4.1) consistent with those previously synthesized.[19]

Interestingly when R^1 is changed to dibromo-functionalized at the meta positions, the quantum yield is increased significantly to 10^{-2}. This indicates that the position of the substitution can have a profound effect on the E-Z isomerization and reduce the radiationless loss of fluorescence intensity. As such the GFP-type chromophores where synthesized using the procedure described earlier to incorporate functionality meant to illuminate some the basic photophysical characteristics as well as the effect of attaching different groups at positions within the chromophore. The steady-state measurements provide a baseline for the overall photophysical considerations, but more information may be extracted from time-resolved and ultrafast measurements reported in that follows.

Abb.	R_1	R_2	R_3	R_4	λ_{abs} (nm)	λ_{emiss} (nm)	ε ($M^{-1}cm^{-1}$)	Stokes Shift (cm^{-1})	QY
HC	Me	H	H	H	347	417	1.9×10^4	4840	1.3×10^{-4}
MC	Me	Me	H	H	355	419	2.0×10^4	4300	2.2×10^{-4}
BrC	Me	Br	H	H	354	419	2.2×10^4	4380	6.5×10^{-4}
DiBrC	Me	H	Br	Br	355	426	9.2×10^3	4700	1.5×10^{-2}
^{t}BuOC	Me	^{t}BuO	H	H	361	436	2.6×10^4	4770	2.1×10^{-4}
NPC	Ph	NO_2	H	H	370	522	2.0×10^4	7070	6.8×10^{-4}
NC	Me	NO_2	H	H	376	488	4.1×10^3	6100	7.7×10^{-3}
DMC	Me	NMe_2	H	H	422	488	6.8×10^3	3210	3.4×10^{-4}
BC	Ph	NMe_2	H	H	453	533	4.0×10^3	3310	1.1×10^{-3}

Table 4.1 Steady state spectroscopy of GFP-type chromophores in acetonitrile.

4.6.3 Two-Photon Absorption

The two-photon absorption cross-sections of the synthesized chromophores were investigated using excitations around 800 nm. An examination of the TPA characteristics for the synthesized chromophores illuminates the overall significance of different substituent groups on GFP-type chromophores and helps determine which properties make for well-designed two-photon labels for biological studies. For the determination of the best-suited chromophore for application, primary focus was placed on behavior under excitations right around 800 nm as this specifies a material with characteristics most

appropriate for direct examination using typical Ti:sapphire laser sources.

Table 4.2 shows the calculated two-photon cross-sections for the GFP-type chromophores at wavelengths near 800 nm. The single member of the series that exhibited comparatively large response in this region was DMC with a cross-section near 30 GM at 800 nm. This compares favorably to those cross-section values of 6-14 GM obtained in several experimental studies for wild-type GFP that contains a chromophore structurally similar to DMC.[40,59] Rebané et al.[40-42] have published several reports detailing the basic two-photon absorption characteristics of an assortment of other fluorescent protein analogs to GFP which make for good comparisons to our synthetically produced molecules. The authors determined absolute cross-sections over a broad range of excitation wavelengths (500-1300 nm) finding that values were especially small between 700-800 nm for many FPs apart from some red varieties (TagRFP, mRFP) whose cross-sections approach or exceed 100 GM over this range. This would indicate that expanding the extent of conjugation through some means and consequently shifting the absorption to longer wavelengths might have the potential for increased cross-sections. Other studies using DFT calculations have also been performed,[60,61] examining the theoretical two-photon absorption bands in a selection of model FP chromophores predicting two-photon absorption maxima to occur in the 500-700 nm excitation regime with maximum values to be ~175 GM near 600 nm and relative minimums near 800 nm.

Excitation Wavelength (nm)	Chromophore	QY	δ (GM, 10^{-50} $cm^4 s \cdot photon^{-1}$)
780 nm	HC	1.3×10^{-4}	1.69
	MC	2.2×10^{-4}	0.468
	BrC	6.5×10^{-4}	0.0525
	DiBrC	1.5×10^{-2}	0.207
	^{t}BuOC	2.1×10^{-4}	3.19
	NC	7.7×10^{-3}	2.37
	DMC	3.4×10^{-4}	**25.0**
	BC	1.1×10^{-3}	1.32
800 nm	NC	7.7×10^{-3}	1.79
	DMC	3.4×10^{-4}	**29.0**
	BC	3.4×10^{-4}	17.1
820 nm	NC	7.7×10^{-3}	0.432
	DMC	3.4×10^{-4}	**39.4**
	BC	1.1×10^{-3}	13.4

Table 4.2 Two-photon absorption cross-sections of two-photon absorbing chromophores near 800 nm

The effect of conjugation may be evaluated in part with the comparison of BC to DMC. While the additional conjugation produced a red-shifted absorption (Figure 4.7), the overall two-photon absorption response is not as large in magnitude as that found for DMC (Figure 4.9). The implication of this points to a smaller transition dipole moment for BC than is found in its structural analog. Charge-transfer groups were expected to play a critical role in the overall two-photon absorption response of the chromophores as strong donor ($-NMe_2$) and acceptor ($-NO_2$) groups have been shown to significantly affect the two-photon absorption cross-sections of branched and extended conjugation systems.[62,63] Examining the cross-sections measured for the synthesized chromophores, strong dipole character in DMC and BC results in larger cross-sections, but is not reflected in the case of NC. The other synthesized chromophores were excited at wavelengths far from their two-photon absorption maxima thus accordingly had smaller cross-sections (HC, MC, BrC, etc.) or for those excited near twice the one-photon peak,

simply had smaller cross-sections at these wavelengths (NC, BC). By shortening the wavelengths of excitations, improved performance was noted for most systems with BrC and ^{t}BuOC approaching 10 GM cross-sections at 740 nm. This feature is not entirely unexpected as it has been reported both experimentally[40] and theoretically[61] that there is a resonance enhancement effect of the S_1-S_n transition in the range of 550-750 nm which results in an additional strong two-photon absorbing band at these shorter wavelengths.

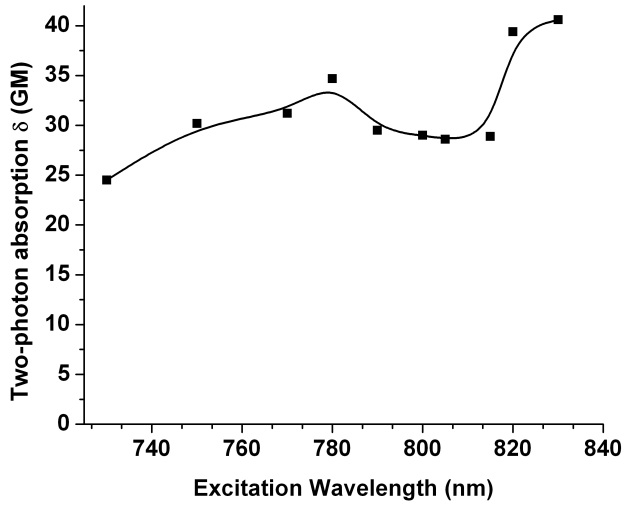

Figure 4.9 Two-photon absorption spectrum of DMC. Fit line provided to guide eye.

4.6.4 Time-Resolved Fluorescence

Lifetime measurements like two-photon absorption cross-sections are important because they are sensitive to changes of the environment of the chromophore and are the foundation of FRET-like studies in biological systems. To fundamentally understand the effect that the various substituent groups have in determining the fluorescence lifetime of GFP-type chromophores, a systematic investigation was undertaken to compare fluorescence lifetimes. Table 4.3 shows the fluorescence lifetimes of the chromophores as observed in acetonitrile. All the chromophores exhibit a two-component lifetime with the shortest component primarily being sub-picosecond except notably for BC (1.11 ps), NC

(4.7 ps), and DiBrC (4.85 ps). There is no clear impact of the substituent group on the duration of this component, however a strong dependence on substitution position of a substituent. These results are consistent with other examinations[50,64] of fluorescence lifetimes with respect to functional group substitution and how it relates to decay behavior. The short components in these chromophores are a result of fast internal conversion and the long components from conformational relaxation from isomerization processes.

Chromophore	τ_1 (ps)	τ_2 (ps)
HC	0.45 ± 0.09 (1)[a]	2.20 ± 0.04 (1)
MC	0.50 ± 0.02 (1)	1.28 ± 0.06 (1)
BrC	0.75 ± 0.04 (1.3)	4.31 ± 0.05 (1)
DiBrC	4.85 ± 0.05 (2)	62.3 ± 0.6 (1)
^{t}BuOC	0.38 ± 0.04 (3)	0.84 ± 0.04 (1)
NPC	0.40 ± 0.05 (2)	1.3 ± 0.2 (1)
NC	4.7 ± 0.3 (1)	53.2 ± 0.6 (1.3)
DMC	0.566 ± 0.001 (1)	3.257 ± 0.001 (1.6)
BC	1.11 ± 0.04 (1)	9.74 ± 0.03 (1.5)

Table 4.3 Fluorescence lifetimes of GFP-type chromophores. [a]Relative amplitude of given lifetime component.

As a baseline for comparison an unsubstituted version of the GFP-type chromophore (HC) was synthesized with a hydrogen at R^2. HC shows a fast initial component (0.45 ps) that is among the quickest components for all the chromophores, and a secondary component that lasts 2.2 ps. For comparison, this roughly equates to the observed behavior for the anionic form of the typical GFP model chromophore, 4'-hydroxybenzylidene-2,3-dimethylimidazolone (HBDI), in acetonitrile whose two-component lifetime was observed[31] to be 0.45 and 1.4 ps. The shortest wavelength absorbing species nearest to that of unsubstituted HC are the *para*-methyl (MC) and *para*-bromo (BrC) substituted versions that both show similar emissive properties as compared to HC in the steady state. As shown in Figure 4.7 & 4.9, these chromophores

have nearly identical absorption and emission maxima, so it leads one to expect similar excited-state fluorescence decay profiles. An examination of the fluorescence decays indicate a two-component lifetime with the shortest lasting less than 1 ps.[47] It should be noted that the minor differences in lifetimes may be related to the withdrawing/donating effect of the group substituted at R^2 with slight donating methyl group causing the shortest lifetime (MC) and the electron-withdrawing bromo group resulting in the longest with the lifetime of BrC nearly four times that of HC. It seems that the excited-state lifetime is strongly related to the substitution of the benzylidene ring and that generally the chromophores with electron-donating substituents will have among the shortest lifetimes, often less than that of unsubstituted, while the presence of electron-withdrawing groups will result in prolonged excited-state lifetimes.

The next two chromophores (DiBrC, ^{t}BuOC) offer several different functional-group characteristics from our set of derivatives. DiBrC represents the lone example of a meta- and di-substituted chromophore and provides an interesting comparison with BrC as to the extent placement of groups effect fluorescence lifetime. The *tert*-butoxy-substituted ^{t}BuOC serves as the closest example to replicating the same inductive properties as the hydroxyl group of the most commonly used GFP-model chromophore HBDI, but also represents the largest physical functionalization at R^2, R^3, or R^4. The different fluorescence behavior of these two is among the starker contrasts of the whole series of chromophores. Despite similar steady-state properties, DiBrC has the longest observed fluorescence lifetime with its secondary component lasting 62.8 ps, while ^{t}BuOC has the shortest lifetimes for both components at 0.38 and 0.84 ps. The long lifetimes for DiBrC are directly related to the meta-substitution of the bromo groups that

has been shown to create a potential barrier for isomerization about the *exo*-cyclic double bond resulting in far longer lifetimes and diminished likelihood of internal conversion.[50] The behavior of ^{t}BuOC is more puzzling as any perceived effects of size should have resulted in shorter and not longer fluorescence lifetimes.

The final comparison of chromophores to consider is that of those possessing the strongest electronic groups and should exhibit certain aspects of charge-transfer. The first two (NC, NPC) both contain *para*-nitro groups and, as was found in the steady state, NPC has a slightly red-shifted fluorescence maximum. The final two shown in Scheme 4.7 (DMC, BC) are both *para*-substituted with dimethylamino groups. Both nitro groups and dimethylamino groups have been shown to be excellent moieties for the synthesis of charge-transfer compounds, but with their incorporation into GFP-type chromophores defining clear explanations for their very different behavior is quite challenging. NC has a tremendously long two-component lifetime that may not be explained under the same considerations as the long lifetime for DiBrC as it cannot be attributed to a substitution effect. However, it would seem as though the strong withdrawing characteristics of the nitro group promotes a large difference between ground and excited state structures that is exhibited by the large Stokes shift observed from steady-state measurements. This reorganization may result in a complicated (slow) relaxation pathway and a barrier to quick internal conversion. Unfortunately, the structural derivative NPC behaves very differently than its less conjugated analog. The fluorescence lifetimes for it are closer to ^{t}BuOC in time-scale which casts doubt about the added effects of replacing the methyl group at R^1 with a phenyl group and would seem to be completely at odds with the expected behavior given the results for NC.

Given the TPA response of DMC (and to some extent BC), the expectation is that there might be longer relative fluorescence lifetimes indicative of the donor-acceptor behavior known to be a general promoter for such characteristics. However, the fluorescence lifetimes are both fairly consistent with those found for minor electronic substituents (BrC). There is a prolonged reorganization time that is consistent with a somewhat complicated relaxation pathway, but does not exhibit long charge-transfer type lifetimes. BC has a two-component decay that agrees favorably with similar GFP-type structures adorned with additional phenyl rings.[64] The added component is presumed to be associated with a pronounced increase in the importance of the axis of rotation about the bond connecting R^1. Figure 4.10 shows a representative time-resolved fluorescence lifetime plot of the synthesized chromophores (DMC). To better elucidate the difference in their fluorescence lifetimes, BC and DMC time-resolved fluorescence decays in acetonitrile (0.38 cP) were compared to those obtained from a very viscous ethanolamine (19.37 cP) solution. The lifetimes of both were found to be relatively unaffected by the dramatic change in solvent viscosity with BC lifetimes being approximately doubled and DMC slowed by more than five times that found in acetonitrile. This result seemingly is the opposite of the expected behavior with the bulkier BC having less of a viscosity dependent lifetime than the smaller DMC. The effect is likely again a result of a twisting component of the added phenyl substituent.

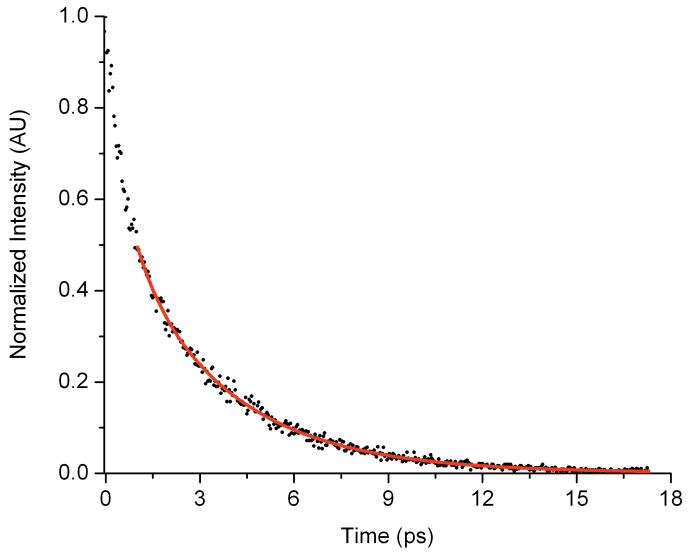

Figure 4.10 Time-resolved fluorescence lifetime decay of DMC in acetonitrile. Best-fit is represented in red.

4.7 Conclusions

Two-photon active green fluorescent protein-type chromophores were synthesized with a diverse set of substituent groups and evaluated for their fundamental steady-state characteristics. A generalized approach for chromophore synthesis was developed allowing for maximum flexibility for the incorporation of functional groups such as donor-acceptor substituents or additional groups to provide extended conjugation. The GFP-type chromophores were found to possess modest two-photon absorption cross-sections near 800 nm with the dimethylamino-substituted DMC clearly having the largest value at nearly 40 GM. This cross-section puts it into a similar regime as other small molecule nonlinear optical absorbers, of which there are a relative few compared to larger multi-chromophore systems. The TPA cross-section of DMC is somewhat smaller compared with those dyes used in our previous peptide studies which had values of 160 and 185 GM respectively[37,38] (Figure 4.11). They are however comparable to the cross-sectional values found for many coumarin-type systems (30 GM)[52] and even larger than

stilbene (8 GM)[65] or 4DMN (~2 GM) that are of similar size. The slight disadvantage presented by DMC is the low "action" cross-section (product of quantum yield and TPA cross-section) and is essentially a reflection of the "brightness" of the material. In this measure, the dye is significantly smaller than these other systems that have order of magnitude or larger TPA "action" cross-section than does DMC. This makes it more difficult to implement for potential imaging applications, however with sensitive detection systems, may still have some utility.

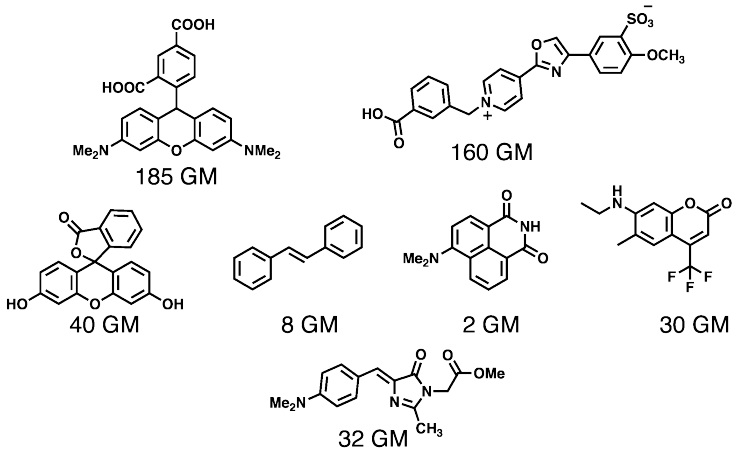

Figure 4.11 Representative small-molecule two-photon absorption cross-sections. (a) TAMRA (b) Cascade Yellow (c) Rhodamine B (d) stilbene (e) 4DMN (f) Coumarin 307 (g) DMC.

Time-resolved fluorescence lifetimes were determined for the synthesized molecules finding that each decayed in a bi-exponential fashion with a sub-picosecond component and a longer picosecond component. The individual effects of substitution position of functional groups and relative bulk size were evaluated and found to be rather significant in changing the fluorescence-decay characteristics in the case of substitution, but ambiguous with respect to relative group bulk. On the whole, these molecules show promise as biological markers, especially DMC given its two-photon absorption response, for application in the study of conformation changes and aggregation of

amyloid peptides, known to play an important role in many neurodegenerative diseases. Investigations are currently in progress using these chromophores as fluorescence dyes in such biological studies of peptides.

4.8 Supporting Information, Preparation of Chromophores: General Procedure & Characterization

Methyl 2-(1-ethoxyethyliden)amino ethanoate (**1**). Previously characterized and prepared in the literature.[8,13]

(*E*)-Methyl 2-((ethoxy(phenyl)methylene)amino)acetate (**2**). Previously characterized and prepared in the literature.[1] ^{1}H NMR (400 MHz, $CDCl_3$) δ: 1.342 (t, 3H, J= 7.0 Hz); 3.691 (s, 3H); 4.074 (s, 2H); 4.311 (q, 2H, J= 7.0 Hz); 7.309 (m, 2H); 7.393 (m, 3H). ^{13}C NMR (100 MHz, $CDCl_3$) δ: 14.141 ($-CH_2CH_3$); 51.763 ($-CH_2-$); 51.999 ($-OCH_3$); 61.848 ($-CH_2CH_3$); 127.638 (Ar); 128.386 (Ar); 129.638 (Ar); 131.633 (Ar); 164.257 (N=C); 171.750 (C=O).

General chromophore synthetic procedure: In a small 4-mL vial equipped with a stirbar, imidate (**1** or **2**) (1.89 mmol) and benzaldehyde (1.89 mmol) were dissolved in a minimum amount of toluene (1 mL). With vigorous stirring, the sealed mixture was heated at 70 ºC overnight in an oil bath. The solvent was removed under reduced pressure and the resulting chromophore purified using column chromatography (silica gel, ethyl acetate/hexanes).

(*Z*)-4-Benzylidene-2-methyl-1-(methoxycarbonylmethyl)imidazol-5-one (HC) Previously characterized and prepared in the literature, ^{1}H NMR (400 MHz, $CDCl_3$) δ: 8.134 (2H, d); 7.409 (3H, m); 7.137 (1H, s); 4.387 (2H, s); 3.776 (3H, s). ^{13}C NMR (100 MHz, $CDCl_3$, δ): 15.493 ($-CH_3$); 41.233 ($-CH_2-$); 52.779 ($-OCH_3$); 128.199 (Ar); 128.687

(Ar); 130.263 (Ar); 132.201 (Ar); 133.940 (Ar-CH=C); 137.980 (C-4); 161.263 (C-2); 167.969 (C=O); 170.014 (C-5).

(*Z*)-4-(4-Methylbenzylidene)-2-methyl-1-(methoxycarbonylmethyl)imidazol-5-one (MC). ^{1}H NMR (400 MHz, $CDCl_3$, δ): 8.035 (2H, d); 7.229 (2H, d); 7.130 (2H, s); 4.394 (2H, s); 3.783 (3H, s); 2.387 (3H, s); 2.333 (3H, s). ^{13}C NMR (100 MHz, $CDCl_3$, δ): 15.501 (-CH_3); 21.677 (Ar-CH_3); 41.272 (-CH_2-); 52.782 (-OCH_3); 128.521 (Ar-CH=C); 129.533 (Ar); 131.303 (C-4); 132.285 (Ar); 137.286 (Ar); 140.943 (Ar); 160.561 (C-2); 168.044 (C=O); 170.085 (C-5).

(*Z*)-4-(4-Bromobenzylidene)-2-methyl-1-(methoxycarbonylmethyl)-1-imidazol-5-one (BrC) ^{1}H NMR (400 MHz, $CDCl_3$, δ): 8.007 (2H, d), 7.542 (2H, d), 7.046 (1H, s), 4.388 (2H, s), 3.786 (3H, s); 2.328 (3H, s). ^{13}C NMR (100 MHz, $CDCl_3$, δ): 15.534 (-CH_3); 41.258 (-CH_2-); 52.827 (-OCH_3); 124.832 (Ar); 126.587 (Ar-CH=C); 131.946 (Ar); 132.887 (C-4); 133.530 (Ar); 138.443 (Ar); 161.761 (C-2); 167.909 (C=O); 169.870 (C-5). HRMS (ES): m/z (M+H) calcd. for $C_{14}H_{13}BrN_2O_3$, 337.0182; found 337.0174.

(*Z*)-4-(4-Dimethylaminobenzylidene)-2-methyl-1-(methoxycarbonylmethyl)imidazol-5-one (DMC). ^{1}H NMR (400 MHz, $CDCl_3$, δ): 8.064 (2H, d); 7.112 (1H, s); 6.702 (2H, d); 4.394 (2H, s); 3.769 (3H, s); 3.053 (6H, s); 2.311 (3H, s). ^{13}C NMR (100 MHz, $CDCl_3$, δ): 15.329 (-CH3); 39.966 (-$N(CH_3)_2$); 41.248 (-CH_2-); 52.596 (-OCH_3); 111.694 (Ar-CH=C); 122.100 (Ar); 129.706 (Ar); 133.948 (C-4); 134.299 (Ar); 151.624 (Ar); 157.536 (C-2); 168.244 (C=O); 169.956 (C-5) HRMS (ES): m/z (M+H) calcd. for $C_{16}H_{19}N_3O_3$, 324.1324; found 324.1322.

(*Z*)-4-(4-Nitrobenzylidene)-2-methyl-1-(methoxycarbonylmethyl)imidazol-5-one (NC). ^{1}H NMR (400 MHz, $CDCl_3$, δ): 8.288 (2H, d); 8.232 (2H, d); 7.083 (1H, s); 4.403 (2H, s); 3.794 (3H, s); 2.366 (3H, s). ^{13}C NMR (100 MHz, $CDCl_3$, δ): 15.646 (-CH_3); 41.286 (-CH_2-); 52.924 (-OCH_3); 123.713 (Ar); 124.188 (Ar); 140.151 (Ar-CH=C-); 140.700 (C-4); 147.839 (Ar); 164.080 (C-2); 167.744 (C-5); 169.645 (C-2). HRMS (ES): m/z (M+H) calcd. for $C_{14}H_{13}N_3O_5$, 303.27; found 304.0923.

(*Z*)-4-(4-*t*-Butoxybenzylidene)-2-methyl-1-(methoxycarbonylmethyl)imidazol-5-one (^{t}BuOC). ^{1}H NMR (400 MHz, $CDCl_3$, δ): 8.067 (2H, d, J_o= 8.4 hz); 7.111 (1H, s); 7.021 (2H, d, J_o= 8.4 hz); 4.384 (2H, s); 3.768 (3H, s); 2.318 (3H, s); 1.387 (9H, s). ^{13}C NMR (100 MHz, $CDCl_3$, δ): 15.455 (-CH_3); 29.991 (-$C(CH_3)_3$); 41.244 (-CH_2-); 52.745 (-OCH_3); 79.450 (-$C(CH_3)_3$); 123.382 (Ar); 128.135 (Ar-CH=C); 128.764 (Ar); 133.402 (Ar); 136.665 (C-4); 157.971 (Ar); 160.317 (C-2); 168.038 (C=O); 170.014 (C-5). HRMS (ES): m/z (M+H) calcd. for $C_{18}H_{22}N_2O_4$, 324.1324; found 324.1322.

(*Z*)-4-(3,5-Dibromobenzylidene)-2-methyl-1-(methoxycarbonylmethyl)imidazol-5-one (DiBrC). ^{1}H NMR (400 MHz, $CDCl_3$, δ): 8.219 (2H, d, J_m= 1.6 hz); 7.635 (1H, s, almost t); 6.892 (1H, s); 4.376 (2H, s); 3.780 (3H, s); 2.347 (3H, s). ^{13}C NMR (100 MHz, $CDCl_3$, δ): 15.546 (-CH3); 41.240 (-CH_2-); 52.859 (-OCH_3); 122.989 (Ar); 124.007 (Ar); 133.192 (Ar); 135.027 (Ar-CH=C); 137.335 (Ar); 139.803 (C-4); 163.178 (C-2); 167.755 (C=O); 169.537 (C-5).

(*Z*)-4-(4-Dimethylaminobenzylidene)-2-phenyl-1-(methoxycarbonylmethyl)imidazol-5-one (BC). ^{1}H NMR (400 MHz, $CDCl_3$, δ): 8.170 (2H, d); 7.741 (2H, dd); 7.503 (3H, m); 7.269 (1H, s); 6.711 (3H, d); 4.514 (2H, s); 3.712 (3H, s); 3.067 (6H, s). ^{13}C NMR (100 MHz, $CDCl_3$, δ): 40.033 (-$N(CH_3)_2$); 43.067 (-

CH_2-); 52.606 (-OCH_3); 111.724 (Ar-CH=C); 122.278; 128.233; 128.900; 130.872; 131.434; 134.208 (C-4); 134.909; 151.857 (C-2); 168.552 (C=O); 170.923 (C-5)

(*Z*)-4-(4-Nitrobenzylidene)-2-phenyl-1-(methoxycarbonylmethyl)imidazol-5-one (NPC). ^{1}H NMR (400 MHz, $CHCl_3$, δ): 3.748 (s, 3H, -OCH_3); 4.558 (s, 2H, -CH_2-); 7.411 (m, 3H, Ar-H); 7.568 (m, 2H, Ar-H); 7.972 (m, 2H, Ar-H)

References

1. Lerestif, J. M.; Bazureau, J. P.; Hamelin, J. *Tetrahedron Lett.* **1993**, *34*, 4639-4642

2. Kerneur G.; Lerestif, J. M.; Bazureau, J. P.; Hamelin, J. *Synthesis* **1997**, 287-289

3. Fülöp, F.; Pihlaja, K.; Neuvonen, K.; Bernáth, G.; Argay, G.; Kálmán, A. *J. Org. Chem.* **1993**, *22*, 1967–1969

4. Pihlaja, K.; Juhász, M.; Kivelä, H.; Fülöp, F. *Rapid Commun. Mass Spectrom.* **2008**, *22*, 1510-1518

5. Kantlehner, W.; Huag, E.; Farkas, M. *Liebigs Ann. Chem.* **1982**, 1582-1587

6. Jain, S.; Jain, R.; Singh, J.; Anand, N. *Tetrahedron Lett*. **1994**, *35*, 2951-2954

7. Roger, R. and Neilson, D.G. *Chem. Rev.* **1961**, *61*, 179-211

8. Lerestif, J. M.; Perrocheau, J.; Tonnard, F.; Bazureau, J. P.; Hamelin, J. *Tetrahedron* **1995**, *51,* 6757-6774

9. Castro, A.; Ramírez, J.; Juárez, J.; Terán, J.L.; Orea, L.; Galindo, A.; Gnecco, D. *Heterocycles* **2007**, *71*, 2699-2708

10. Hu, T. and Panek, J. S. *J. Am. Chem. Soc.* **2002**, *124*, 11368-11378

11. Mrksich, M.; Parks, M. E.; Dervan, P. B., *J. Am. Chem. Soc.* **1994**, *116*, 7983-7988

12. Greene, T. W.; Wuts, P. G.M. *Greene's Protective Groups in Organic Synthesis*, 4th ed.; Wiley-Interscience: Hoboken, 2007; p. 803

13. Cornforth J. and Cornforth, R. *J. Chem. Soc.* **1947**, 96-102

14. Pandit, P.; Chartterjee, N.; Halder, H., Hota, S. K.; Patra, A.; Maiti, D. K. *J. Org. Chem.* **2009**, *74*, 2581-2584

15. Megley, C. M.; Dickson, L. A.; Maddalo, S. L.; Chandler, G. J.; Zimmer, M. *J. Phys. Chem. B* **2009**, *113*, 302.

16. Zimmer, M. *Chem. Rev.* **2002**, *102*, 759.

17. Tsien, R. Y. *Ann. Rev. Biochem.* **1998**, *67*, 509.

18. Matz, M.; Fradkov, A.; Labas, Y.; Savitsky, A.; Zaraisky, A.; Markelov, M.; Lukyanov, S. *Nat. Biotechnol.* **1999**, *17*, 969.

19. Taylor, D.; Woo, E.; Giuliano, K. *Curr. Opin. Biotechnol.* **2001**, *12*, 75.

20. Zipfel, W. R.; Williams, R. M.; Webb, W. W. *Natl. Biotechnol.* **2003**, *21*, 1369.

21. Heim, R.; Prasher, D. C.; Tsien, R. Y. *Proc. Natl. Acad. Sci. U.S.A* **1994**, *91*, 12501.

22. Yang, F.; Moss, L. G.; Phillips, G. N. *Nat. Biotechnol.* **1996**, *14*, 1246.

23. Reid, B. G.; Flynn, G. C. *Biochemistry* **1997**, *36*, 6786.

24. Niwa, H.; Inouye, S.; Hirano, T.; Matsuno, T.; Kojima, S.; Kubota, M.; Ohashi, M.; Tsuji, F. I. *Proc. Natl. Acad. Sci. U.S.A.* **1996**, *93*, 13617.

25. Weber, W.; Helms, V.; McCammon, J.; Langhoff, P. *Proc. Natl. Acad. Sci. U.S.A.* **1999**, *96*, 6177.

26. Chattoraj, M.; King, B. A.; Bublitz, G. U.; Boxer, S. G. *Proc. Natl. Acad. Sci. U.S.A.* **1996**, *93*, 8362.

27. Meech, S. R. *Chem. Soc. Rev.* **2009**, *38*, 2922.

28. Baldridge, A.; Samanta, S.; Jayaraj, N.; Ramamurthy, V.; Tolbert, L. *J. Am. Chem. Soc.* **2010**, *132*, 1498.

29. You, Y.; He, Y.; Borrows, P.; Forrest, S.; Petasis, N.; Thompson, M. *Adv. Mater.* **2000**, *12*, 1678.

30. Stafforst, T.; Diederichsen, U. *Eur. J. Org. Chem.* **2007**, 899.

31. Ivashkin, P.; Yampolsky, I.; Lukyanov, K. *Russ. J. Bioorg. Chem.* **2009**, *35*, 652.

32. Bourotte, M.; Schmitt, M.; Follenius-Wund, A.; Pigault, C.; Haiech, J.; Bourguignon, J. *Tetrahedron Lett.* **2004**, *45*, 6343.

33. Follenius-Wund, A.; Bourotte, M.; Schmitt, M.; Iyice, F.; Lami, H.; Bourguignon, J.-J.; Haiech, J.; Pigault, C. *Biophys. J.* **2008**, *85*, 1839.

34. Munishkina, L.; Fink, A. *BBA-Biomembranes* **2007**, *1768*, 1862.

35. Parthasarathy, A.; Ahn, H.-Y.; Belfield, K. D.; Schanze, K. S. *ACS Applied Materials & Interfaces* **2010**, *2*, 2744.

36. Narayanan, A.; Varnavski, O. P.; Swager, T. M.; Goodson, T. *J. Phys. Chem. C* **2008**, *112*, 881.

37. Wang, Y.; Goodson III, T. *J. Phys. Chem. B* **2007**, *111*, 327.

38. Wang, Y.; Clark, T. B.; Goodson, T. *J. Phys. Chem. B* **2010**, *114*, 7112.

39. Blab, G. A.; Lommerse, P. H. M.; Cognet, L.; Harms, G. S.; Schmidt, T. *Chem. Phys. Lett.* **2001**, *350*, 71.

40. Drobizhev, M.; Makarov, N. S.; Hughes, T.; Rebane, A. *J. Phys. Chem. B* **2007**, *111*, 14051.

41. Drobizhev, M.; Tillo, S.; Makarov, N. S.; Hughes, T. E.; Rebane, A. *J. Phys. Chem. B* **2009**, *113*, 855.

42. Drobizhev, M.; Tillo, S.; Makarov, N.; Hughes, T.; Rebane, A. *J. Phys. Chem. B* **2009**, *113*, 12860.

43. Remington, S. J.; Wachter, R. M.; Yarbrough, D. K.; Branchaud, B.; Anderson, D. C.; Kallio, K.; Lukyanov, K. A. *Biochemistry* **2005**, *44*, 202.

44. Rumi, M.; Ehrlich, J. E.; Heikal, A. A.; Perry, J. W.; Barlow, S.; Hu, Z.; McCord-Maughon, D.; Parker, T. C.; Röckel, H.; Thayumanavan, S.; Marder, S. R.; Beljonne, D.; Brèdas, J.-L. *J. Amer. Chem. Soc.* **2000**, *122*, 9500.

45. Litvinenko, K.; Webber, N.; Meech, S. *J. Phys. Chem. A* **2003**, *107*, 2616.

46. Mandal, D.; Tahara, T.; Meech, S. *J. Phys. Chem. B* **2004**, *108*, 1102.

47. Mandal, D.; Tahara, T.; Webber, N.; Meech, S. *Chem. Phys. Lett.* **2002**, *358*, 495.

48. Webber, N.; Litvinenko, K.; Meech, S. *J. Phys. Chem. B* **2001**, *105*, 8036.

49. Dong, J.; Solntsev, K.; Tolbert, L. *J. Am. Chem. Soc.* **2006**, *128*, 12038.

50. Solntsev, K. M.; Poizat, O.; Dong, J.; Rehault, J.; Lou, Y.; Burda, C.; Tolbert, L. M. *J. Phys. Chem. B* **2008**, *112*, 2700.

51. Usman, A.; Mohammed, O.; Nibbering, E.; Dong, J.; Solntsev, K.; Tolbert, L. *J. Am. Chem. Soc.* **2005**, *127*, 11214.

52. Xu, C.; Webb, W. *J. Opt. Soc. Am. B* **1996**, *13*, 481.

53. Varnavski, O.; Goodson, T. *Chem. Phys. Lett.* **2000**, *320*, 688.

54. Flynn, D. C.; Ramakrishna, G.; Yang, H.-B.; Northrop, B. H.; Stang, P. J.; Goodson, T. *J. Am. Chem. Soc.* **2010**, *132*, 1348.

55. Baldridge, A.; Kowalik, J.; Tolbert, L. M. *Synthesis* **2010**, *2010*, 2424.

56. Jun, E. E. *Justus Liebigs Ann. Chem.* **1893**, *275*, 1.

57. Conway, P. A.; Devine, K.; Paradisi, F. *Tetrahedron* **2009**, *65*, 2935.

58. He, X.; Bell, A.; Tonge, P. *Org. Lett.* **2002**, *4*, 1523.

59. Xu, C.; Zipfel, W.; Shear, J. B.; Williams, R. M.; Webb, W. W. *Proc. Natl. Acad. Sci. U.S.A.* **1996**, *93*, 10763.

60. Nifosì, R.; Luo, Y. *J. Phys. Chem. B* **2007**, *111*, 505.

61. Nifosì, R.; Luo, Y. *J. Phys. Chem. B* **2007**, *111*, 14043.

62. Bhaskar, A.; Ramakrishna, G.; Lu, Z.; Twieg, R.; Hales, J.; Hagan, D.; Van Stryland, E.; Goodson III, T. *J. Am. Chem. Soc.* **2006**, *281*, 1653.

63. Bhaskar, A.; Ramakrishna, G.; Twieg, R.; Goodson, T. *J. Phys. Chem. C* **2007**, *111*, 14607.

64. Petkova, I.; Dobrikov, G.; Banerji, N.; Duvanel, G.; Perez, R.; Dimitrov, V.; Nikolov, P.; Vauthey, E. *J. Phys. Chem. A* **2010**, *114*, 10.

65. Albota, M.; Beljonne, D.; Brédas, J.-L.; Ehrlich, J. E.; Fu, J.-Y.; Heikal, A. A.; Hess, S. E.; Kogej, T.; Levin, M. D.; Marder, S. R.; McCord-Maughon, D.; Perry, J. W.; Röckel, H.; Rumi, M.; Subramaniam, G.; Webb, W. W.; Wu, X.-L.; Xu, C. *Science* **1998**, *281*, 1653.

Chapter 5

Two-Photon Spectroscopy as a New Sensitive Probe for Secondary Structure Determination in Amyloid-β Peptides and Aggregates

5.1 Original Publication Information

The bulk of this chapter was originally submitted to the *Proceedings of the National Academy of Sciences* as the following document:

> "Two-Photon Spectroscopy as a New Sensitive Probe for Secondary Structure Determination in Amyloid-β Peptides and Aggregates" Travis B. Clark and Theodore Goodson III. *Proceedings of the National Academy of Sciences* **2012**, submitted

Modifications to the original document were made solely for adapting the content to this form. References between the original manuscript and supporting information have been unified into a single numbering system.

5.2 Abstract

The development of new sensitive methods for the detailed collection of conformational and morphological information about amyloids is critical to elucidating the critical questions regarding the aggregation processes in neurodegenerative diseases. The solution-based two-photon methodology described in this report interrogates the early conformational dynamics seen in the monomers and soluble oligomers region of

amyloid-β1-42 through the implementation of a nonlinear optical GFP-type chromophore as a covalent label. Concentration-dependent aggregation studies show a strong sensitivity toward conformational changes taking place in the secondary structure of the amyloid peptide. The sensitivity of our two-photon methodology was subsequently compared to circular dichroism spectroscopy performed on similar solutions with results indicating that our two-photon absorption cross-sections trend very similarly to the overall change in ellipticity of the peptides as found using CD, however two-photon absorption exhibits superior sensitivity at the most dilute conditions. This suggests that a two-photon excited methodology could be a sensitive alternative to CD and other commonly used methodologies in this field while avoiding many of the inherent challenges present in particular with CD data collection. The implication of this is significant, as it indicates that a two-photon based technique may be able to reveal answers to the very specific conformational questions about amyloid-β1-42 at dilute, biologically relevant concentrations inaccessible with other techniques.

5.3 Introduction

Conformational changes associated with the aggregation of proteins are vital to understanding the fundamental events involved in the development of neurodegenerative diseases[1,2] such as Alzheimer's disease (AD). The progression from a monomer-state to a complex plaque formation is a complicated process proceeding through a variety of "on" and "off" pathway events each with different conformational and aggregation states that require characterization. At the earliest aggregation stages, transitions from random coil to β-sheet and α-helix as well as from α-helix to β-sheet have been observed using FTIR and NMR spectroscopies.[3] Extensive study by several research groups has indicated that

these non-fibrillar oligomeric Aβ forms are likely significant toxic contributors to Alzheimer's disease (AD).[4] A number of prevailing questions remain regarding the pathways of fibrillogenesis and identifying specific steps that present opportunities for targeted therapeutic intervention.[5] Recent studies have shown that soluble oligomers anywhere from 2 to 24 peptides in size[6] and protofibril structures[7] that contain substantial fractions of β-sheet secondary structure may be critical originators of the cytotoxicity for neurodegenerative peptides such as amyloid-β, but as with formation mechanism, the conformational characteristics at the pre-fibrillar stage remain unclear.[6]

A number of techniques have been utilized (Figure 5.1) to study the various stages of amyloid aggregation from the small monomer[8] to the large fibrils including circular dichroism (CD)[9], quasielastic light scattering (QLS)[10], fluorescence of amyloid-binding dyes[11], mass spectrometry (MS),[12] modeling simulations[13,14], and physical imaging methods like AFM[15] and TEM[16]. Solution-based techniques (CD, MS) are best implemented in the earlier stages of aggregation in which soluble oligomer structures and protofibrils[17] predominate, but have limited capability for the study of larger fibrils due to ionizability and solubility issues respectively. Other techniques such as AFM and fluorescence monitoring of ThT-type fibril binding dyes are somewhat better suited for the larger aggregate structures found towards the latter stages of amyloid fibrillization, however each lacks either the resolution or sensitivity[18] to fully characterize the structures of the early intermediates. Fluorescence-based methodologies utilizing either extrinsic[19] or intrinsic[20] fluorescence labels have been explored as alternative techniques with the capabilities to specifically study oligomeric interactions.

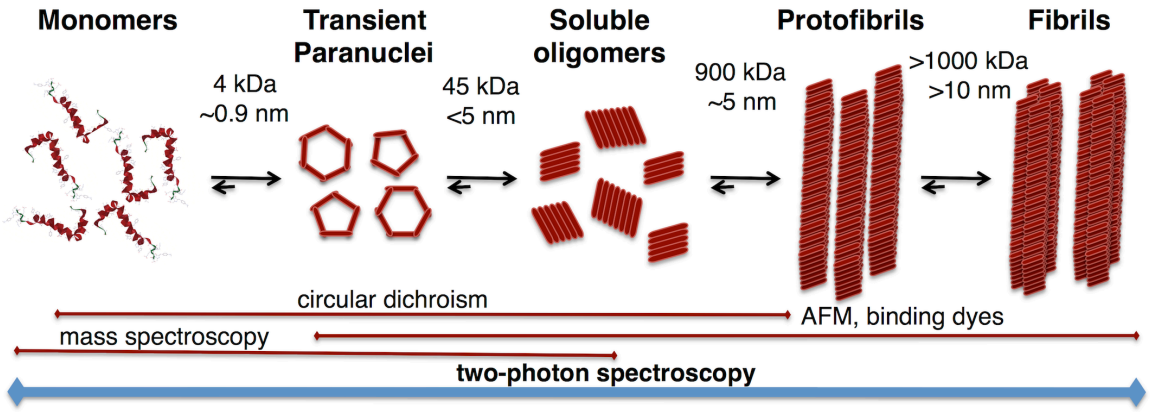

Figure 5.1 Schematic representation of the broad classification of amyloid fibrillization and some commonly associated techniques with their characterization.

For a dye-labeled peptide, a combined approach using nonlinear optical spectroscopy and time-resolved fluorescence studies to examine charge-transfer interactions as a function of conformation should provide a strong avenue for exploring aggregation. Of particular importance is the potential to have higher TPA cross-sections due to cooperative enhancement from interchromophore interactions.[21,22] Two-photon enhancement has been noted in conjugated branched dendrimer systems[21,23,24] with delocalized excitations observed to hop between chromophores. High spatial selectivity afforded from two-photon excitations has further led to an exploration of TPA as a tool for understanding the complex interactions taking place in biological systems. Our group has shown that a two-photon methodology is capable of probing the structural dynamics of a number of fluorophore-labeled systems including the B5 protein associated with herpes simplex virus (HSV),[25] prion peptide ($PrP_{106-126}$),[26] and amyloid-β.[27] Based on these individual studies, TPA techniques are promising for the continued study of conformational changes and aggregation of peptides, however development of better environmentally sensitive TPA chromophores remains important for generating

fundamental data that can be put toward answering the critical questions about amyloid peptides.

In this report, we have implemented a new analog of green fluorescence protein chromophore designed to have strong environmental sensitivity and a TPA cross-section sufficiently large to use as a covalent label in dynamics studies of a N-terminus labeled amyloid-β1-42 peptide utilizing ultrafast spectroscopy. The dimethylamino-substituted chromophore (DMC) was synthesized via a previously published route[28] and covalently attached to the peptide following solid-phase peptide synthesis (Figure 5.2). By labeling at this synthetically accessible position, we are able to introduce the fluorophore into a region of the peptide not centrally involved in the aggregation ensuring that it does not interfere, yet has the flexibility to interrogate nearby changes in the secondary structure of the aggregation prone region of the peptide. The development of the solution-based methodology described here most appropriately interrogates the early conformational dynamics seen in the monomers and soluble oligomers region most commonly studied using CD or MS through the detection of two-photon excited fluorescence. Development of sensitive fluorescence methods for the detailed collection of environmental and conformational information is critical to understanding the various topographies and morphologies that may be adopted by the early oligomers of Aβ, thereby allowing for the development of a targeted therapeutic intervention.

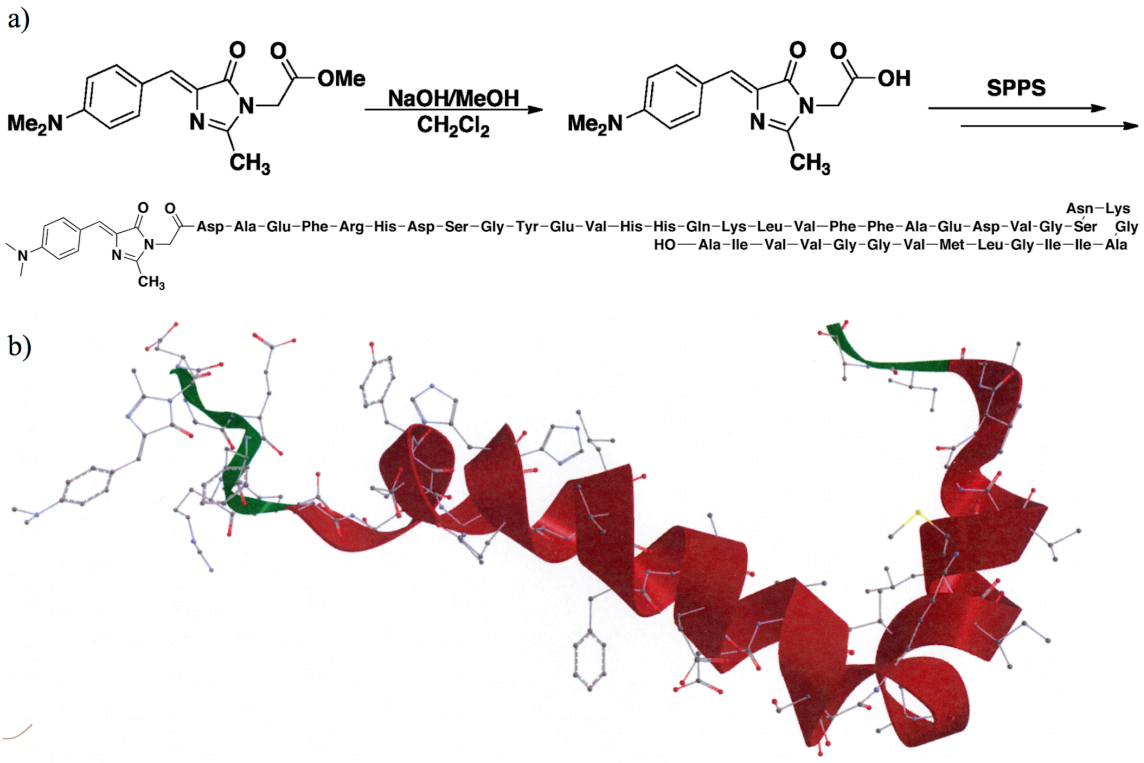

Figure 5.2 (a) Synthetic scheme for generation of DMC-labeled amyloid-β1-42 (b) Model representation of the DMC N-terminus labeled amyloid-β 1-42.

5.4 Results & Discussion

5.4.1 Steady-State Spectroscopy

Prior to a detailed study of the Aβ1-42 aggregation, baseline steady-state studies were performed characterizing the fundamental photophysical properties of the labeled peptide system as compared to that of the isolated chromophore. Different solvent conditions were investigated to examine the changes in absorption and emission spectra (Figure 5.3). The spectral features of DMC were first studied in acetonitrile, showing an absorption near 422 nm and an emission at 488 nm.[28] In the more polar PBS, a significant red-shift to 450 nm and 520 nm was observed for the absorption and emission respectively. HFIP promoted the largest shift in absorption to 475 nm, more than 50 nm longer than in acetonitrile, and had a corresponding emission maximum at 560 nm. These

results indicate a great sensitivity of DMC to environmental conditions especially considering the high and relative polarity of the solvents.

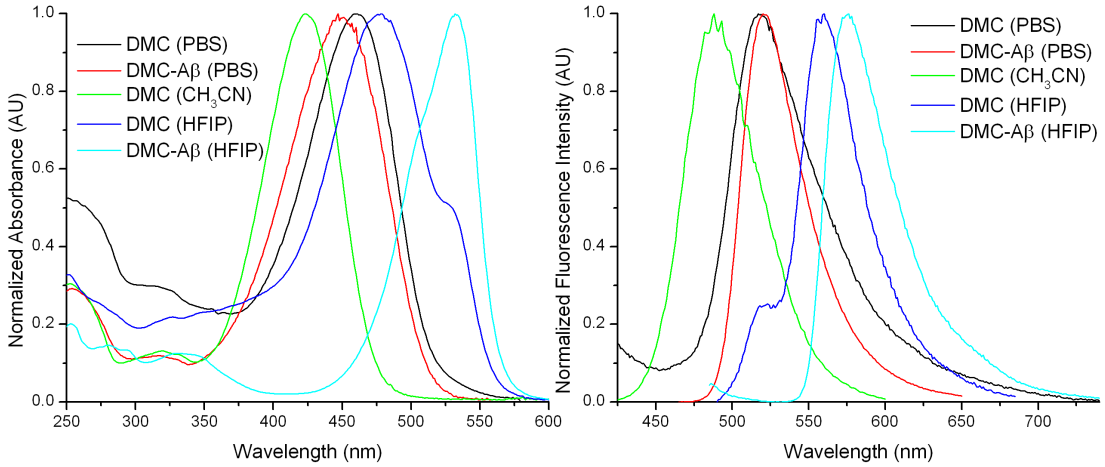

Figure 5.3 Steady-state absorption and emission curves for DMC-Aβ1-42 and DMC in different solvent conditions. The respectively curves are as follows: DMC (PBS), black; DMC-Aβ (PBS), red; DMC (acetonitrile), green; DMC (HFIP), blue; and DMC-Aβ (HFIP), cyan. All peptide solution spectra were taken immediately following preparation. Emission data was collected through excitation at the respective absorption maximums.

Upon attaching DMC to Aβ1-42, further shifts in the linear spectroscopy were noted. A solution of DMC-labeled peptide was prepared in PBS using aliquots taken from the DMC-Aβ stock solution in HFIP. Immediately following preparation, a small absorption shift was noted comparing in comparing with the free-dye spectra. While free DMC showed a maximum absorption at 450 nm, the spectrum for DMC-Aβ1-42 was slightly red-shifted to 460 nm. This effect is attributable to the environmental effects arising from the influence of the microenvironment surrounding the chromophore causing a shift in the ground state absorption. The emission data demonstrates a far less pronounced shift with each having a maximum near 520 nm. Some broadening of the emission spectrum for DMC-Aβ1-42 may be noted but unsurprising given the inhomogeneous nature of the peptide environment. A subsequent examination of DMC-Aβ1-42 in HFIP showed extremely large shifts in both the absorption and emission

spectrums that are significantly larger than found in PBS with maximums found at 532 nm and 575 nm respectively. This effect could be attributable to the lessened capacity for HFIP to hydrogen bond as compared to water thus promoting a greater level of intramolecular interactions that may result in lower energy transitions observed coming from the ground state.

	Abs[a] λ_{max} (nm)	Emiss[a] λ_{max} (nm)	Molar extinction ε ($M^{-1}cm^{-1}$)	Conc. [c] M	QY Φ	TP "action" cross-section $\Phi \cdot \delta$ (GM)	TPA cross-section δ (GM)
DMC-Aβ1-42	460	520	10900[a]	0.5×10^{-6}	3.0×10^{-4}	0.150	540 GM
DMC	450	520	26000[b]	0.5×10^{-6}	9.5×10^{-4}	0.031	32 GM

Table 5.1 Comparison of photophysical characteristics of DMC and DMC-Aβ1-42 in PBS. [a]Phosphate-buffer solution; [b]Determined for DMC-Aβ1-42 in HFIP.

Fluorescence quantum yields were determined in buffer solution for both DMC-Aβ1-42 and DMC. The quantum yield had been previously determined for DMC in acetonitrile (3.4×10^{-4})[28], however the isolated chromophore was found to be slightly more fluorescent in the buffer solution (9.5×10^{-4}). The labeled peptide showed no indications of enhanced fluorescence resulting from the labeling as might have been expected[29] and actually was found to have a quantum yield lower than the isolated chromophore (Table 5.1).

5.4.2 Circular Dichroism Spectroscopy

Circular dichroism spectroscopy (CD) was performed on the aggregating solutions of 0.5, 1, 2.5, 5, 10, and 40 μM immediately following their preparation. Using PBS as a blank, the spectrum for each solution was obtained over the range of 190-240 nm and analyzed. Seen previously in studies externally and from within the group[27,30], as compared with the unlabeled peptide there was no evidence of any effect on the obtained CD spectra for a similarly N-terminus-labeled Aβ peptide. Barrow, et al. have established how changes in secondary structure as the amyloid-β peptide undergoes a conformational

change from α-helical to β-sheet are associated with the spectral changes observed in CD spectrum in composite solutions containing fluorinated alcohols.[9] As was seen in these early studies, our obtained spectra (Figure 5.4) showed negative ellipticities with a bimodal peak centered at 208 nm extending to just beyond 220 nm with their shape and intensity dependent upon the solvent conditions and peptide concentrations. Higher concentrated solutions had a less pronounced signal with the magnitude generally increasing as the concentration of the solution was lowered, behavior consistent with a system with higher β-sheet content. As the mean residue ellipticity of the peptide approaches 0, the predominately α-helical structure of the peptide is changed to increasingly larger percentages of β-sheet structure.[9] Values for the mean residue ellipticity at 222 nm were calculated and are shown in Table 5.2 as a function of concentration and compared to the two-photon data discussed in the subsequent section. Figure 5.4 shows the absolute value of the mean residue ellipticity plotted as a function of concentration so as to facilitate the comparison. At the lowest studied concentrations (0.5 μM and 1 μM) a plateauing of the molar ellipticity is noted. Based on the concentrations of these solutions, a decline in sensitivity for samples at 1 μM given the low optically densities of the fluorophore in solution is not unexpected. The recommended range for sample concentration for circular dichroism measurements is between 1 μM and 1 mM[31], so the limits of accurate detection are clearly being pushed using a sub-μM solution as noted by the 0.5 μM solution breaking the trend established with the other solutions.

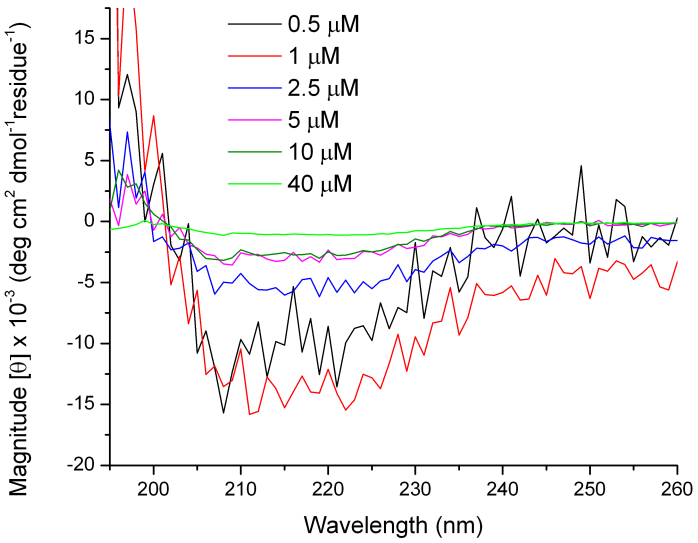

Figure 5.4 Molar ellipticity data of DMC-Aβ1-42 aggregating samples immediately after preparation. A solvent blank was subtracted from each, and an average of three spectra were used to construct the plots.

5.4.3 Two-Photon Spectroscopy

Two-photon absorption spectroscopy was utilized in studying the peptide as a function of concentration and incubation time. Solutions near biologically relevant concentrations (<1 μM)[8] were prepared ranging from 0.5 to 40 μM in PBS by dilution from a HFIP stock solution to have a final HFIP-to-PBS ratio of 20:80. Initial examinations of the aggregating peptide solution were directed toward determining the two-photon absorption cross-section of the labeled peptide system and observing the effect of attaching the chromophore to Aβ1-42. Under excitation at 800 nm, the two-photon excited fluorescence was observed and used to determine the overall two-photon absorption cross-section. The obtained quadratic fluorescence intensity dependence as a function of input power indicated a clear two-photon absorption event (Figure 5.5 inset). A two-photon absorption cross-section was found to be 540 GM for the 0.5 μM solution. Under the same conditions, isolated DMC was found to have a cross-section of 32 GM, almost an order of magnitude smaller than the peptide system (Table 5.1). Given the

relative similarities in quantum yield, such a difference may be attributable to a large change in the transition dipole moments between the free chromophore and the labeled peptide. Effective changes in conjugation and charge separation through the use of donor-acceptor groups[32] often are the largest contributing factors to two-photon absorption enhancement, however in this case the unique electric field and dipole characteristics of a peptide having predominate α-helical structure[33] are likely substantially influencing the TPA properties of the labeled system. Further examination of a wider range of solution concentrations showed a clear trend that peptide concentration and consequently amyloid aggregation made for significant differences in the observed cross-sections. The cross-section results are shown in Table 5.2.

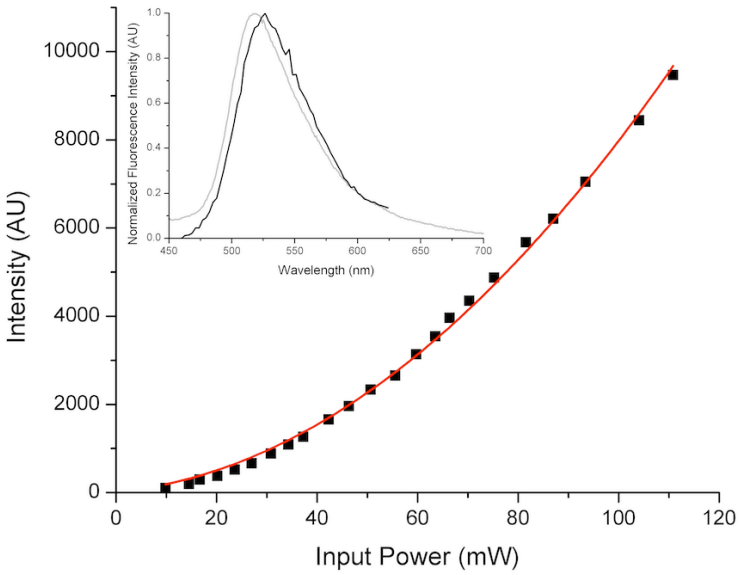

Figure 5.5 Quadratic intensity dependence on input power for DMC-Aβ1-42 40 μM. Inset: Two-photon excited fluorescence (black) compared to one-photon excited fluorescence.

Peptide Conc. (μM)	Ellipticity (deg cm^2 dmol)	TPA cross-section δ (GM)
0.5	9942	540
1	15466	283
2.5	4817	133
5	3027	92
10	2756	108
40	1118	191

Table 5.2 Two-photon absorption cross-section and molar ellipticity data taken over a range of concentrations. All data was collected immediately after preparation of aggregating solution from stock solution. Molar ellipticity values as determined from CD data collected at 222 nm.

Organic molecules typically have cross-section values independent of concentration if prepared in dilute solution, but as shown in Figure 5.6 the values for DMC-Aβ1-42 differ significantly depending upon the concentration. For the highest concentration studied (40 μM), the TPA cross-section was substantially smaller than that observed at the lowest concentration (0.5 μM). Intermediate concentration solutions continued the trend of larger cross-sections being measured at the lowest concentrations. These differences indicate that the critical determining factors in the TPA cross-sections are the conformational changes being undergone in the secondary structure of the amyloid peptide. This is explained suggestively due to the high occurrence of strong dipole moments associated with peptides of predominately α-helical structure versus those with β-sheet or higher order structural content (Figure 5.7). TPA is governed by the changes in polarizability associated with the dipole transitions of the molecules being stimulated from the ground state to the excited state. Peptides with α-helical structure and less ordered secondary structure have larger directional dipoles that favorably interact with the chromophore label ultimately resulting in higher cross-sections. More ordered β-sheet structure results in a loss of strong dipole orientation causing a less pronounced

two-photon absorption for those more highly concentrated solutions with significantly less α-helical structure. Representations of these conformations are shown in Figure 5.7. The distinct ordered dipoles directed through the α-helical structure from the C-terminus toward the N-terminus influence the dipole of the attached chromophore with ~3.5 Debye density per 1.5 Å along the α-helix.[33] The loss of the coiled structure and significant intermolecular interaction greatly disorient the net dipole of the peptide, providing little enhancement for TPA. The great variation in cross-section from the lowest to the highest concentration would indicate that the transition from predominately α-helical structures to ordered β-sheet might be demonstrated over the range of concentrations studied.

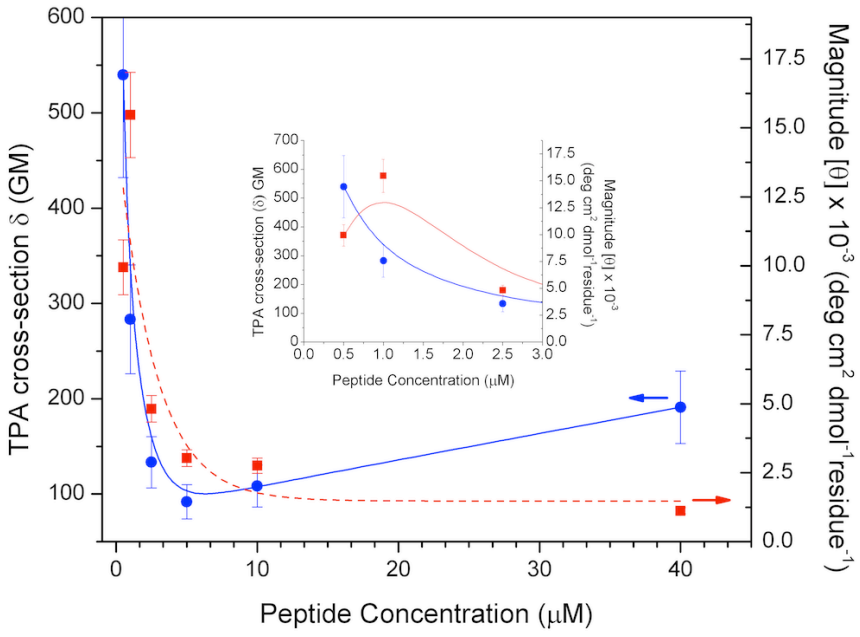

Figure 5.6 Two-photon absorption cross-sections and molar ellipticity as a function of peptide concentration. Blue circles, two-photon absorption cross-sections; red-squares, molar ellipticity values as determined from CD data collected at 222 nm. Inset graph is enlargement of low concentration data. Lines are meant as guides and are not necessarily mathematical fits. Error bars represent standard error associated with multiple TPA measurements and a 10% uncertainty for CD.

The molecular distances associated with the secondary structure of low molecular weight oligomers have been difficult to establish, as amyloid peptides tend to be

noncrystalline making typical crystallography and solution-based NMR methods difficult to utilize for characterization. Consequently, much of the structural analysis in this regime has been left to molecular simulations. Through both experimental[34] and theoretical[35] methods, the earliest oligomeric species have been shown to lack the stable secondary β-sheet structure that may be found at later aggregation stages with geometries that are much more fluid having characteristics of α-helix, β-strand, and random coil and a range of structural forms. Molecular simulations have consistently shown however for later stage amyloid-β fibrils[36-39] or structured oligomers[40] that the inter-strand separation between neighboring β-strands is near 4.8 Å and with the distance between cross-β sheets closer to 9.5 Å (Figure 5.7). This type of structural motif seems to be consistent with the TPA results found at 40 μM. Given the complexity and inhomogeneous nature of the oligomeric structures the kinds of intermolecular or even intramolecular interactions occurring detailed modeling studies would need to be conducted to translate the required dipole moments to structural characteristics. Nevertheless, work done by the Blanchard-Desce group has demonstrated[41] the potential for through-space chromophore interactions to enhance the two-photon absorption cross-sections in the case of some polar arylamine structures designed to dimerize in solution. The interaction distances for these systems are on the order of those inter-strand distances found typically in these amyloid structures, so the possibility exists for some chromophore-chromophore or chromophore-amino acid interactions to also account for the observed two-photon enhancement see in our studies as a function of peptide concentration. Investigations examining such interactions were untaken using time-resolved fluorescence and anisotropy measurements to understand how concentration changes affect the adopted aggregate conformations and

chromophore interactions while also further establishing some boundaries with respect to chromophore distances.

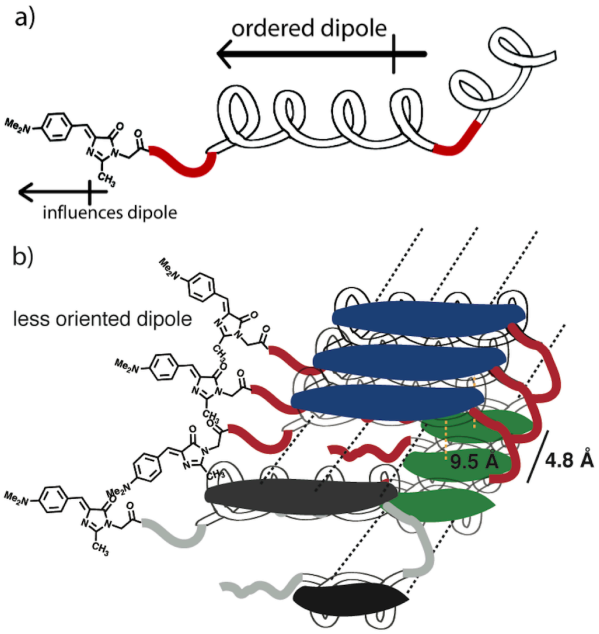

Figure 5.7 Representation of amyloid-β1-42 labeled at the N-terminus with DMC. a) At low concentration, significant quantities of α-helix result in a prominent dipole that increases TPA cross-section. a) At high concentration, significant β-strand/sheet structure results in less oriented peptide dipoles and lessened influence on the TPA cross-section of the attached chromophore. Graphic only shows the basic interaction of several peptide units for clarity, dotted lines indicate further interactions likely occurring.

5.4.4 Comparison of Two-Photon Spectroscopy to Circular Dichroism

A relative comparison between the two techniques shows that the two-photon absorption cross-sections measured as a function of peptide concentration trend very similarly to the relative change in ellipticity of the peptides found using CD over a wide concentration distribution (Figure 5.4). However when the comparison is focused at the lowest concentrations, the trend does not demonstrate the same behavior as an even higher intensity signal is observed using two-photon absorption at 0.5 μM when compared to the previous result at 1 μM. This contrasts from the plateauing seen in the CD data and is an indication that the methodology has better sensitivity to the small

changes in conformation or aggregation at very dilute solution concentrations as well with small relative differences in concentration. As demonstrated, the inherent limitations to the collection of data for quantitative secondary structure determination using peptide concentrations at sub-μM values present large challenges for observation of biologically relevant concentration solutions. A two-photon excited methodology clearly can approach these levels while avoiding some of the other challenges presented in collecting CD data such as background sources of absorption from other solution additives and buffers.[31] The implication of this for our methodology could be significant, as it indicates that a two-photon based technique may be able to reveal answers to the very specific conformational questions about amyloid-β1-42 at dilute, biologically relevant concentrations inaccessible with other techniques.

5.4.5 Fluorescence Lifetimes and Anisotropy

As shown above, the use of two-photon spectroscopy can be a very sensitive probe toward the changes in secondary structure in peptide aggregates and over a broad size and distance dependent range. This approach has been applied to organic macromolecules with specific geometries in the past but not peptide aggregates of this nature. Likewise, it has been shown that fluorescence upconversion measurements may provide compelling evidence of strong intramolecular interactions and coherent energy transfer dynamics in aggregate macromolecular structures.[42] This optical gating experiment is very sensitive to possible quenching and energy transfer mechanisms as a result of conformational changes in the system. The fast time-resolution of the technique allows for a relatively sensitive detection of ultrafast dynamics in organic molecules. Another major advantage of this measurement is the ability to measure the depolarization

contribution of the emission decay by anisotropy measurements which can ultimately lead to analysis of the time-scale and mechanism of energy migration in the system.[43] We have used this methodology extensively for branched macromolecular systems which may follow a Förster energy transfer mechanism.[42] For the case of a "hopping" energy transfer mechanism the anisotropy decay time is related to the donor relaxation time and the angle between the donor and acceptor by,

$$r(t) = \frac{1}{10}\left[1 + 3e^{-\tau/\tau_D}\right], \quad \tau_D = \frac{\tau_{hopping}}{4(1-\cos^2\theta)} \qquad \textbf{Equation 5.1}$$

Initial anisotropy decay times of the order of a few picoseconds to as fast as 50 fs have been analyzed for different branched structures depending on the intramolecular interactions in the system.[23] We have investigated the fast fluorescence dynamics of the prepared aggregate systems. Shown in Figure 5.8 are the fluorescence decay profiles for DMC and three different peptide concentrations spanning from little aggregation to certain aggregates and formation of β-sheet structures. The decay profile for the free dye in water shows the expected single exponential decay of fluorescence on a time scale of ~10 ps (Table 5.3). For the 0.5 and 10 μM peptide concentrations, the decays are similar to that of free DMC, showing a biexponential profile that relaxed to the ground state at ~10 ps. This suggests that any local effects surrounding the functionalized peptide do not inhibit the decay profiles for these two concentrations. However, it is observed for the highest concentration (29 μM) that there is an extended fast component of the decay that is not as strongly pronounced in any of the other systems. The fast component might be attributed to a change in the local environment surrounding the attached dye to the peptide. Previous reports with ultra-fast fluorescence upconversion on organic dipolar chromophores attached to other macromolecular architectures have observed that an

increase in the fast component of the decay might suggest a change in the hydrophilic (or hydrophobicity) region surrounding the chromophore. Indeed, this might be possible here because as the peptide aggregates more strongly, more solvent may be excluded from regions near the chromophore giving the impression of a less solvated local environment. The use of this technique to monitor this process is a powerful approach to monitor chemical and physical changes to the local environment of the peptide as the aggregation process develops.

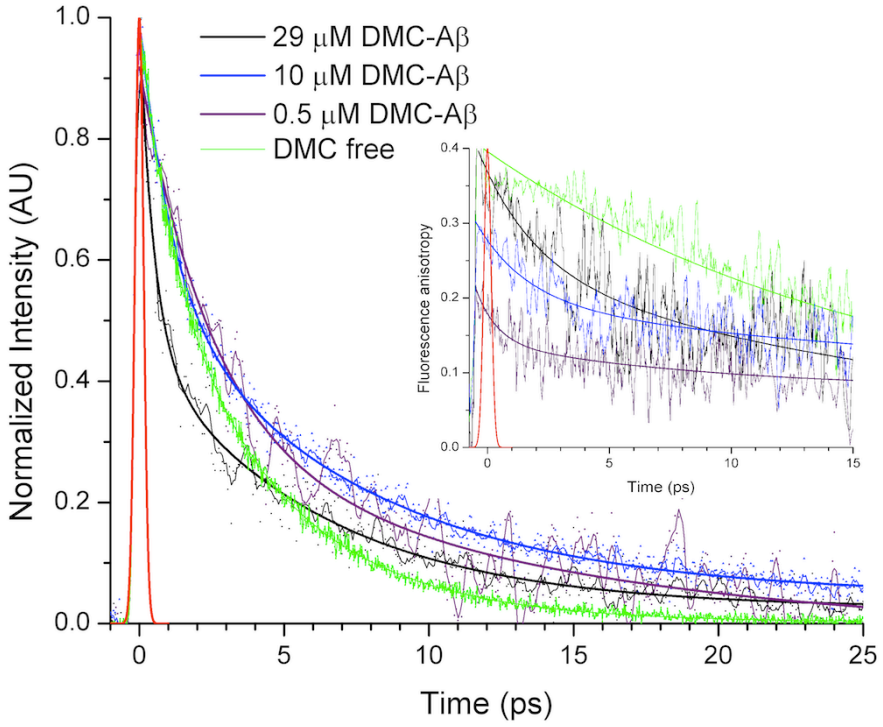

Figure 5.8 Fluorescence decay of various concentrated DMC-Aβ solutions as compared with "free" DMC. Inset: fluorescence anisotropic decay of various DMC-Aβ solutions as compared with "free" DMC. Black, DMC-Aβ 29 μM; Blue, DMC-Aβ 10 μM; Purple, DMC-Aβ 0.5 μM; Green, "free" DMC; Red, instrument response function.

Concentration	Lifetime		Anisotropy		r_0
(μM)	τ_1 (ps)	τ_2 (ps)	τ_1 (ps)	τ_2 (ps)	
29 μM	0.83 ± 0.05	7.1 ± 0.2	2.2 ± 0.9	17 ± 7	0.36
10 μM	1.10 ± 0.07	7.2 ± 0.3	1.9 ± 0.5	16 ± 5	0.25
0.5 μM	2.2 ± 0.8	10 ± 3	0.9 ± 0.5	10 ± 4	0.15
DMC free	1.07 ± 0.07	4.19 ± 0.04	--	16 ± 1	0.36

Table 5.3 Fluorescence lifetimes for DMC-labeled amyloid-β 1-42, compared to "free" DMC. Peptide solutions were prepared to have HFIP:PBS at a 80:20 ratio. Error associated with the uncertainty in the exponential fitting of each decay.

To further understand the energy transfer mechanism in these aggregated peptide systems, the ultra-fast fluorescence anisotropy decay measurements were also carried out. The anisotropy decay dynamics for the same set of aggregating samples (as well as the free DMC sample) are shown in the Figure 5.8 inset. The free chromophore decay is the expected slow (with no fast component) relaxation on this time-scale. This decay (using Equation 5.1) can be fitted with a single exponential component representative of the rotational diffusion of the molecule (Table 5.3). The two lower concentration aggregates show the beginning of a fast component causing them to be fitted with a double exponential decay profile. However, the 29 μM system has an extensive fast component persisting up to 3 ps. The fast component in the two other peptide samples vanishes on a shorter time-scale near 1 ps. The existence of this component in the anisotropy decay is not related to rotational diffusion suggesting that there may be intermolecular energy transfer between two different dye molecules in the aggregate. As noted above, we have already observed an enhancement in the two-photon cross-section for the high concentration aggregated system. Indeed, with fluorescence anisotropy decay measurements the time-scale of the fluorescence depolarization process in the peptide-chromophore system may be a signature of excitonic states with large transition dipoles.[44] This kind of interaction, due to the nature of its relaxation rate, is not commonly observed

in steady state experiments. Indeed, while this fast component, which is indicative of a fast energy transfer, is faster than one would suggest for rotational motion,[45] but it might be analyzed under the context of the Förster model.[46] The coulombic, through-space interaction between chromophores might give insight on the conformational changes occurring in the peptide as it translates through its natural motion seeking lower free energy. Similar findings have been reported with novel conjugated macromolecular systems where the process of energy migration using ultra-fast fluorescence anisotropy decay measurements were found to follow a potential energy dependence governed by the Förster model.[42]

The explanation of the fast kinetics observed in the depolarization process draws new questions concerning the mechanism of the energy redistribution process in aggregated peptide system. To consider this process in terms of the Förster model it is important to consider the interaction radius in regards to the possibility of a fast energy redistribution process. Here, the Förster radius (R_0 = 10.7 Å) and the distance between two chromophores (r) (in the energy migration process) may give an expected energy transfer rate. Using values obtained from the lifetime and r, and calculated (R_0) it is found that for the peptide-chromophore system one would expect under this situation a decay time on the order of hundreds of femtoseconds to a few picoseconds depending upon the exact distances between chromophores, again highlighting the need for modeling of oligomeric conformations. The fluorescence lifetimes observed from our time-resolved studies are within this expected range giving credence to the possibility that such an energy transfer process is being observed.

The initial anisotropy values for the various different solutions showed a significant effect of concentration with the value significantly depressed in the case of the least concentrated 0.5 μM sample. This would indicate some fast depolarizing process occurring very quickly within the time of the instrument response function. Given the large enhancement of the two-photon absorption cross-section that was observed, these results strongly suggest that there is significant chromophore-chromophore interaction occurring, which is somewhat surprising given the very dilute conditions. The suggestion from the CD data that there is significant α-helical structure found in monomeric species provides some support that the peptides may be conformationally ordered in such a way that the interaction strength is high. However, the highest concentrated 29 μM solution lacks the same significant depolarization event seen at the lowest concentration. With significantly lower two-photon absorption cross-sections (at 40 μM) and far slower fluorescence depolarization, this would indicate that chromophore interactions are slightly diminished in this state. The additional order and stability provided by increased β-sheet secondary structure does not bring the more disordered N-terminus region of the peptide into a position favorable for strong interactions with other chromophores evidenced by these results. The intermediate concentrations studied gave rise as expected to data between the two concentration-extremes with anisotropic decay (for the 10 μM sample) similar to that observed for the 29 μM and for a range of samples studied using TPA, cross-sections diminished with the increase in β-sheet content indicated by CD. These results are consistent with the hypothesized complex secondary structure that could lead to a number of different of conformers that accounts for some depolarization and decays consistent with an intermediate oligomer structure between the ordered extremes.

The combined results of time-resolved fluorescence and two-photon absorption spectroscopy demonstrate a high level of sensitivity for changes in amyloid-β conformation as it aggregates from monomers to soluble oligomers.

5.5 Conclusions

The results presented in this report examine the earliest conformational dynamics of amyloid-β peptide covalently labeled with a two-photon absorbing GFP-type chromophore and studied at dilute concentration utilizing a combined approach of two-photon absorption and time-resolved fluorescence spectroscopy. A significant two-photon absorption enhancement was noted comparing the DMC chromophore to the labeled Aβ1-42 segment. Additional concentration-dependent studies indicated that the enhancement was affected to a large extent by the concentration of the peptide solution with its conformational state leading to larger TPA cross-sections due to significant dipole interactions with the attached chromophore. A relative comparison of our TPA studies with circular dichroism spectroscopy showed that the two-photon methodology has greater sensitivity than CD for the conformational changes being undergone at concentrations ~1 μM and lower. The advantages of shifting the excitation source out of the high-energy ultraviolet region where sources of background absorption are much more prevalent coupled with the inherent sensitivity of TPA makes it a viable alternative technique to CD for the characterization of the early conformational changes of aggregating peptides. Fluorescence lifetime and depolarization studies indicated a Förster-type charge-transfer may be observed and the results correlate well with the chromophore interactions explaining the TPA behavior. Additional development of the methodology could result in broadened application outside of solution-phase studies by utilizing two-photon near-field scanning optical microscopy to characterize larger

insoluble aggregates, and thereby yielding a technique that has the capabilities to monitor aggregation over the full fibrillization pathway (Figure 5.1) and the potential to answer some of the prevailing questions that remain about the conformational dynamics for many of the peptides that result in neurodegenerative disease.

5.6 Materials and Methods

5.6.1 Synthesis

(Z)-2-(4-(4-(Dimethylamino)benzylidene)-2-methyl-5-oxo-4,5-dihydro-1H-imidazol-1-yl)acetic acid (DMC-OH). Synthetic method based on that reported in the literature.[47] In a small roundbottom flask, DMC–OMe (260 mg, 0.836 mol) recrystallized from methanol was dissolved in 5 mL 9:1 dichloromethane:methanol creating a reddish solution. NaOH (1 mL, 2 M in MeOH) was added via syringe. After a period of several minutes, the carboxylate salt precipitated as a solid. The solution was suction filtered to collect an orange-ish, fluffy solid. The precipitate was washed with additional portions of dichloromethane to remove any residual starting material. Thin-layer chromatography (eluent: EtOAc) was used to track the full conversion of the starting material. ^{1}H NMR (400 MHz, DMSO, δ): 8.066 (Ar–H, 2H, d); 6.902 (C–CH=C, 1H, s); 6.752 (Ar–H, 2H, d); 4.358 (–CH_2, 2H, s); 3.008 (–$N(CH_3)_2$, 6H, s); 2.259 (–CH_3, 3H, s). ^{13}C NMR (100 MHz, DMSO, δ): 15.079 (–CH_3); ~39 obscured under DMSO peak (–$N(CH_3)_2$; 41.228 (–CH_2); 111.687 (HC=C–); 121.420 (Ar); 127.231 (Ar, 2C); 133.977 (Ar, 2C); 151.447 (Me_2N–C); 159.448 (N=C); 169.328 (O=C); 169.778 (–COOH).

Amyloid-β1-42 was subsequently synthesized via solid-phase peptide synthesis (Anaspec, Inc.) and DMC-OH covalently attached at the N-terminus of the peptide. HRMS (m/z) calcd for DMC-Aβ1-42: 4931.6, found 4931.7 (Figure 5.9).

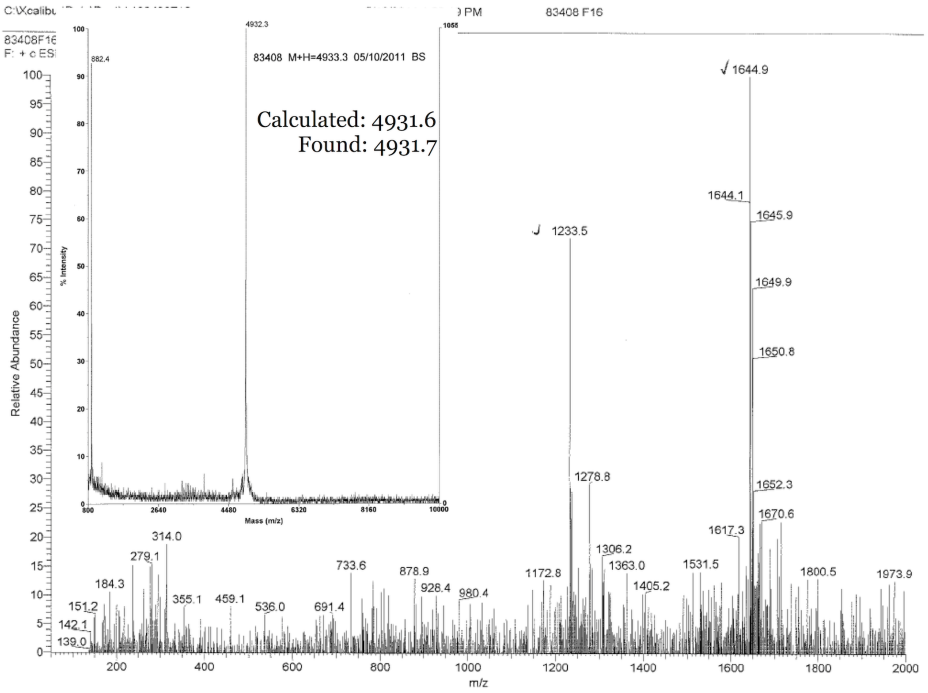

Figure 5.9 Electrospray ionization high-resolution mass spectrum of labeled peptide.

5.6.2 Aβ Sample Preparation

To disaggregate the Aβ and generate monomeric α-helical structures, a stock solution of the DMC-Aβ1-42 was prepared by dissolving 1 mg of the peptide into 1.4 mL hexafluoroisopropanol (HFIP) and subsequently stored in the freezer at -20 °C before use. The concentration of this stock solution (1.44×10^{-4} M) was verified over time using the determined molar extinction coefficient (ε_{475} = 10985 $M^{-1}cm^{-1}$). For concentration dependent aggregation measurements, peptide samples of various concentrations were prepared by dilution from the stock solution and maintained in a cosolvent of HFIP:PBS (20:80). These solutions were then stored in sealed vials in a desiccator. Aggregation solutions were prepared using a phosphate-buffer solution (PBS, without Ca^{2+} and Mg^{2+}). Solutions were observed beginning immediately after preparation.

5.6.3 Steady-State Measurements

Absorption and emission spectra were recorded on an Agilent 8341 spectrophotometer and a Fluoromax-2 fluorimeter, respectively. Quartz cells of path length 0.4 cm were utilized for all measurements unless otherwise noted. Fluorescence quantum yields were performed using fluorescein as the known fluorescence standard and at optical densities below 0.1 near the maximum absorption.

5.6.4 Two-Photon Absorption

Cross-sections were measured using the two-photon excited fluorescence (TPEF) method as described elsewhere.[48] A solution of Coumarin 307 in methanol (< 10-4 M) was used as the TPA reference for studies at 800 nm excitation. A Kapteyn Murnane Laboratories diode-pumped mode-locked Ti:Sapphire laser was utilized for sample excitation. The beam was directed onto the sample cell (quartz cuvette, 0.4 cm path length), and the resultant fluorescence was collected perpendicular to the incident beam. A 1-in. focal length plano-convex lens was used to direct the collected fluorescence into a monochromator whose output was coupled to a photomultiplier tube. The photons were converted into counts by a photon-counting unit. A logarithmic plot of collected fluorescence photons versus input intensity was verified to yield a slope of 2 indicating the quadratic power dependence.

5.6.5 Ultrafast Time-Resolved Fluorescence Upconversion

The fluorescence upconversion system used for time-resolved measurements of the chromophores has been described previously.[49] Briefly, a Tsunami Mode-Locked Ti:Sapphire (Spectra Physics) laser operated at 120 fs with pulses of ~815 nm (gate pulse) having a repetition rate of 82 MHz was used to generate light of 410 nm

(excitation) from second harmonic generation in a β-barium borate crystal. Using a FOG-100 system (CDP Inc.), the gate pulse was channeled through a delay line while the excitation light was up-converted and used to excite the samples. A monochromator detected the second harmonic generation of the gate pulse and emission from the samples, and was amplified on a photomultiplier tube. Fluorescence anisotropy results were collected by changing the polarization of the excitation beam using a Berek compensator to set parallel and perpendicular excitations. The G-factor was determined to be 0.96 using Coumarin 30 as a reference standard.

5.7 Acknowledgements

The authors would like to thank the University of Michigan Peptide Facility and Anaspec, Inc. for the synthesis and purification of DMC-Aβ1-42.

References

1. Ono, K.; Condron, M. M.; Teplow, D. B. *Proc. Natl. Acad. Sci. USA* **2009**, *106*, 14745.

2. Dobson, C. M. *Nature* **2003**, *426*, 884.

3. Maji, S. K.; Amsden, J. J.; Rothschild, K. J.; Condron, M. M.; Teplow, D. B. *Biochemistry* **2005**, *44*, 13365.

4. Walsh, D. M.; Selkoe, D. J. *J. Neurochem.* **2007**, *101*, 1172.

5. Roychaudhuri, R.; Yang, M.; Hoshi, M. M.; Teplow, D. B. *J. Biol. Chem.* **2009**, *284*, 4749.

6. Sakono, M.; Zako, T. *FEBS J.* **2010**, *277*, 1348.

7. Chiti, F.; Dobson, C. M. *Ann. Rev. Biochem.* **2006**, *75*, 333.

8. Nag, S.; Sarkar, B.; Bandyopadhyay, A.; Sahoo, B.; Sreenivasan, V. K. A.; Kombrabail, M.; Muralidharan, C.; Maiti, S. *J. Biol. Chem.* **2011**, *286*, 13827.

9. Barrow, C.; Yasuda, A.; Kenny, P.; Zagorski, M.; Wright, P. *J. Mol. Biol.* **1992**, *225*, 1075.

10. Lomakin, A.; Chung, D. S.; Benedek, G. B.; Kirschner, D. A.; Teplow, D. B. *Proc. Natl. Acad. Sci. USA* **1996**, *93*, 1125.

11. Levine, H. *Protein Sci.* **1993**, *2*, 404.

12. Bartolini, M.; Naldi, M.; Fiori, J.; Valle, F.; Biscarini, F.; Nicolau, D. V.; Andrisano, V. *Anal. Biochem.* **2011**, *414*, 215.

13. Urbanc, B.; Cruz, L.; Yun, S.; Buldyrev, S. V.; Bitan, G.; Teplow, D. B.; Stanley, H. E. *Proc. Natl. Acad. Sci. USA* **2004**, *101*, 17345.

14. Xu, Y. C.; Shen, J. J.; Luo, X. M.; Zhu, W. L.; Chen, K. X.; Ma, J. P.; Jiang, H. L. *Proc. Natl. Acad. Sci. USA* **2005**, *102*, 5403.

15. Mastrangelo, I. A.; Ahmed, M.; Sato, T.; Liu, W.; Wang, C.; Hough, P.; Smith, S. O. *J. Mol. Biol.* **2006**, *358*, 106.

16. Kirkitadze, M. D.; Condron, M. M.; Teplow, D. B. *J. Mol. Biol.* **2001**, *312*, 1103.

17. Walsh, D. M.; Hartley, D. M.; Kusumoto, Y.; Fezoui, Y.; Condron, M. M.; Lomakin, A.; Benedek, G. B.; Selkoe, D. J.; Teplow, D. B. *J. Biol. Chem.* **1999**, *274*, 25945.

18. Losic, D.; Martin, L. L.; Mechler, A.; Aguilar, M.-I.; Small, D. H. *J. Struc. Biol.* **2006**, *155*, 104.

19. Allsop, D. *Biochem. Biophys. Res. Co.* **2001**, *285*, 58.

20. Rolinski, O. J.; Amaro, M.; Birch, D. J. S. *Biosens. Bioelectron.* **2010**, *25*, 2249.

21. Varnavski, O.; Yan, X.; Mongin, O.; Blanchard-Desce, M.; Goodson, T. *J. Phys. Chem. C* **2007**, *111*, 149.

22. Drobizhev, M.; Karotki, A.; Dzenis, Y.; Rebané, A.; Suo, Z.; Spangler, C. W. *J. Phys. Chem. B* **2003**, *107*, 7540.

23. Goodson, T. G. *Acc. Chem. Res.* **2005**, *38*, 99.

24. Bhaskar, A.; Ramakrishna, G.; Lu, Z.; Twieg, R.; Hales, J.; Hagan, D.; Van Stryland, E.; Goodson III, T. *J. Am. Chem. Soc.* **2006**, *281*, 1653.

25. Brown, O.; Lopez, S.; Fuller, A.; Goodson III, T. *Biophys. J.* **2007**, *93*, 1068.

26. Wang, Y.; Goodson III, T. *J. Phys. Chem. B* **2007**, *111*, 327.

27. Wang, Y.; Clark, T. B.; Goodson III, T. *J. Phys. Chem. B* **2010**, *114*, 7112.

28. Clark, T. B.; Orr, M. E.; Flynn, D. C.; Goodson III, T. *J. Phys. Chem. C* **2011**, *115*, 7331.
29. Tolbert, L. M.; Baldridge, A.; Kowalik, J.; Solntsev, K. M. *Acc. Chem. Res.* **2012**, *45*, 171.

30. Bateman, D. A.; Mclaurin, J.; Chakrabartty, A. *BMC Neurosci.* **2007**, *8*, 29.

31. Greenfield, N. J. *Nat. Protocols* **2007**, *1*, 2876.

32. Albota, M.; Beljonne, D.; Brédas, J.-L.; Ehrlich, J. E.; Fu, J.-Y.; Heikal, A. A.; Hess, S. E.; Kogej, T.; Levin, M. D.; Marder, S. R.; McCord-Maughon, D.; Perry, J. W.; Röckel, H.; Rumi, M.; Subramaniam, G.; Webb, W. W.; Wu, X.-L.; Xu, C. *Science* **1998**, *281*, 1653.

33. Hol, W. G. J.; van Duijnen, P. T.; Berendsen, H. J. C. *Nature* **1978**, *273*, 443.

34. Bitan, G.; Kirkitadze, M. D.; Lomakin, A.; Vollers, S. S.; Benedek, G. B.; Teplow, D. B. *Proc. Natl. Acad. Sci. USA* **2003**, *100*, 330.

35. Röhrig, U. F.; Laio, A.; Tantalo, N.; Parrinello, M.; Petronzio, R. *Biophys. J.* **2006**, *91*, 3217.

36. Petkova, A. T.; Ishii, Y.; Balbach, J. J.; Antzutkin, O. N.; Leapman, R. D.; Delaglio, F.; Tycko, R. *Proc. Natl. Acad. Sci. USA* **2002**, *99*, 16742.

37. Li, L.; Darden, T. A.; Bartolotti, L.; Kominos, D.; Pedersen, L. G. *Biophys. J.* **1999**, *76*, 2871.

38. Tjernberg, L. O.; Callaway, D. J. E.; Tjernberg, A.; Hahne, S.; Lilliehöök, C.; Terenius, L.; Thyberg, J.; Nordstedt, C. *J. Biol. Chem.* **1999**, *274*, 12619.

39. Ma, B.; Nussinov, R. *Proc. Natl. Acad. Sci. USA* **2002**, *99*, 14126.

40. Horn, A. H. C.; Sticht, H. *J. Phys. Chem. B* **2010**, *114*, 2219.

41. Terenziani, F.; Parthasarathy, V.; Pla-Quintana, A.; Maishal, T.; Caminade, A.-M.; Majoral, J.-P.; Blanchard-Desce, M. *Angew. Chem. Int. Ed.* **2009**, *121*, 8847.

42. Varnavski, O. P.; Ostrowski, J. C.; Sukhomlinova, L.; Twieg, R. J.; Bazan, G. C.; Goodson, T. *J. Am. Chem. Soc.* **2002**, *124*, 1736.

43. Donehue, J. E.; Varnavski, O. P.; Cemborski, R.; Iyoda, M.; Goodson, T. *J. Am. Chem. Soc.* **2011**, *133*, 4819.

44. Klugkist, J. A.; Malyshev, V. A.; Knoester, J. *Phys. Rev. Lett.* **2008**, *100*, 216403.

45. Bora, R. P.; Prabhakar, R. *J. Chem. Phys.* **2009**, *131*, 155103.

46. Scholes, G. D. *Ann. Rev. Phys. Chem.* **2003**, *54*, 57.

47. Theodorou, V.; Skobridis, K.; Tzakos, A. G.; Ragoussis, V. *Tetrahedron Lett.* **2007**, *48*, 8230.

48. Xu, C.; Williams, R.; Zipfel, W.; Webb, W. *Bioimaging* **1996**, *4*, 198.

49. Varnavski, O.; Goodson, T. *Chem. Phys. Lett.* **2000**, *320*, 688.

Chapter 6

Two-Photon Fluorescence Enhancement of Dye-labeled Calmodulin

6.1 Explanation

The preceding three chapters have firmly established the capabilities of two-photon absorption spectroscopy for the very detailed characterization of the conformational changes of peptide systems utilizing fluorescence probes. Further broadening of the scope and applicability of the technique has been afforded through a collaboration established with Barbara Imperiali's group at the Massachusetts Institute of Technology to characterize the two-photon absorption characteristics of labeled calmodulin systems using custom-designed, fluorescent switching dyes. Following an introductory section explaining the work done previously on the system by the Imperiali group, this chapter will discuss the preliminary findings of our two-photon absorption studies on these systems and reflect upon their pertinence toward the overall objectives of the dissertation work.

6.2 Introduction

The Imperiali lab has investigated extensively over the past decade solvachromatic fluorophores that act as side-chain modifications for amino acids. Over a series[1-3] of several papers, they have described the development of a chromophore based upon dimethylaminophthalimido functionality. These chromophores have been shown to

have very favorable sensitivity to environment changes due to low fluorescence quantum yields in typical water solutions, however strong fluorescence in non-polar media. In a paper published in the *Journal of the American Chemical Society*, they exploited this environmental sensitivity in studying the molecular interactions of calmodulin with another peptide (M13 peptide) that binds with it in a calcium-dependent manner.[1] Calmodulin (CaM) is an important signaling peptide throughout the body that mediates crucial processes such as inflammation, metabolism, intercellular movement, memory, and immune response. This protein is unique because it has four EF-hand motifs that bind calcium ions. Upon binding, CaM undergoes a conformational change in which its N- and C-termini are buried into distinct hydrophobic pockets. A representative schematic illustrates this change in Figure 6.1. The generation of these conformational structures additionally causes an otherwise buried methionine-rich hydrophobic patch to be exposed at the surface thus allowing CaM to activate a variety of other proteins. Through developing fluorescence probes that can detect the binding event associated with CaM and M13, the hope is that such a system will prove useful in creating a generalized tool for monitoring a range of protein-protein interactions in different systems.

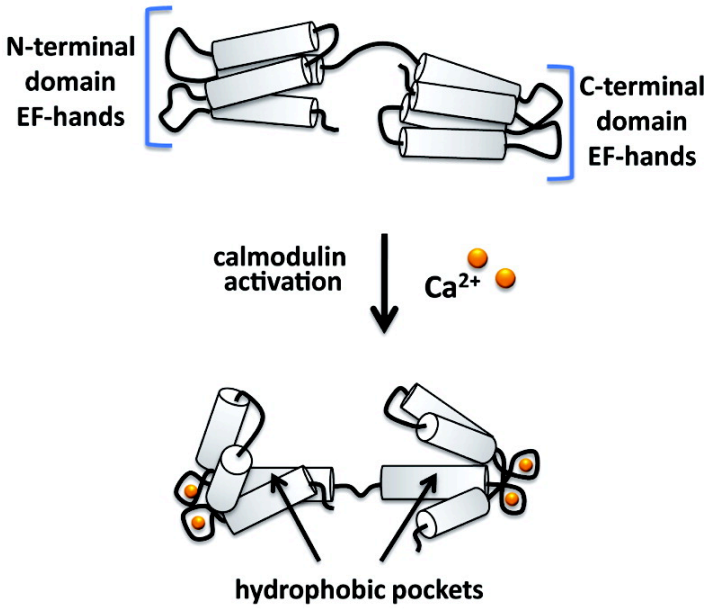

Figure 6.1 Activation of calmodulin through calcium binding. Figure adapted with permission from Loving, G.; Imperiali, B. *Bioconjugate Chem.* **2009**, *20*, 2133. Copyright 2009 American Chemical Society.

To approach identify the protein-binding events within the CaM peptide, the Imperiali lab created a functionalized version of the M13 peptide, incorporating the best version of their chromophore series, 4DMN (Figure 6.2). When the 4DMN-M13 peptide and CaM are combined together in solution without the presence of calcium ions, the system exhibits very low fluorescence emission. However, once calcium is added to the mixture, the system becomes more than several orders of magnitude more fluorescent. They quantified this enhancement through using simple one-photon excited fluorescence spectroscopy, observing ~106 times enhancement between calcium-bound and calcium-unbound states.

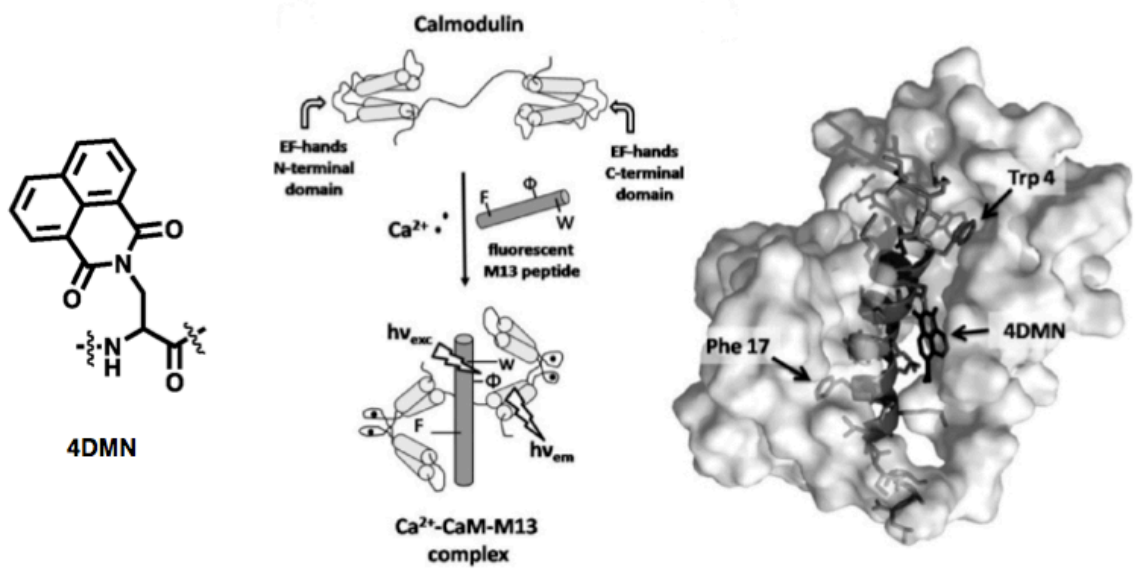

Figure 6.2 (Left) 4DMN fluorophores incorporated into M13. (Middle) Ca^{2+}-Cam-4DMN-M13 complex formation. (Right) Model of the 4DMN-M13 binding pocket. Figure adapted with permission from Loving, G.; Imperiali, B. *J. Am. Chem. Soc.* 2008, *130*, 13630. Copyright 2008 American Chemical Society.

The explained reasoning for such a dramatic increase in fluorescence is associated with changes in the solvent sphere that surrounds the fluorophores as it is influenced by moving from a very hydrophilic to a very hydrophobic environment. This changes the types of interactions both with the solvent and surrounding peptide while simultaneously restricting the movement of the fluorophores, diminishing non-radiative energy loss. An important finding as well was an observed shift in the fluorescence emission spectrum upon binding with a large difference from a 550 nm maximum without Ca^{2+} to 505 nm with calcium. This accentuates the difference in the strict magnitude of fluorescence between the two systems if observed solely at a single wavelength making the overall response more pronounced than if they were more closely matched. Additional studies indicated that they could also quantify the binding of Ca^{2+}.

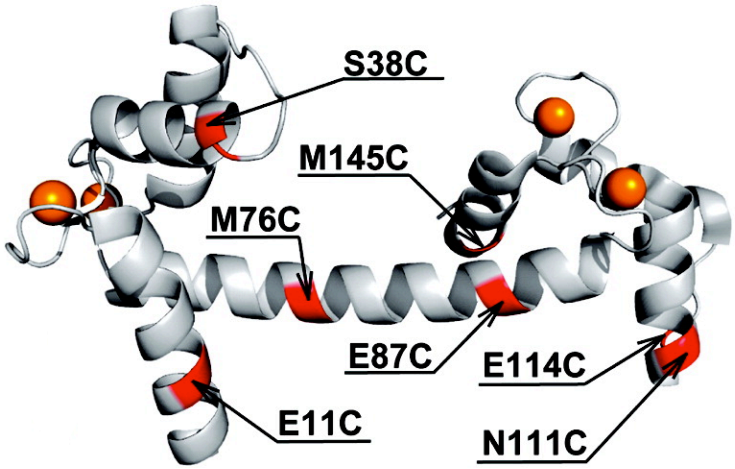

Figure 6.3 Calcium-bound calmodulin peptide with labeled E11C and S38C mutants. Figure adapted with permission from Loving, G.; Imperiali, B. *Bioconjugate Chem.* **2009**, *20*, 2133. Copyright 2009 American Chemical Society.

As an extension of their investigations of the 4DMN chromophore in a subsequent paper published in *Bioconjugate Chemistry*, the Imperiali group examined attaching the fluorophore directly to calmodulin through cysteine mutation. They varied the mutation location all throughout the protein to provide a wide variety of positions with respect to the conformational changes upon calcium binding (Figure 6.3). In an effort to also change the flexibility of the chromophore within its environment, the linker length of the chromophore onto the cysteine residue was also varied (Figure 6.4). Ultimately, seven different locations with four different linker lengths each were considered. Following systematic one-photon excited fluorescence study, the Imperiali group eventually concluded that both the linker length and location play an extraordinary large role in the relative fluorescence increase upon addition of calcium ions and binding peptide. Depending upon the mutation site and subsequent selection of linker length, more than an order of magnitude difference in relative fluorescence response could be observed. This once again highlights the sensitivity of the 4DMN chromophore for the conformational and solvent associated changes that are taking place upon calcium binding. Further tests

against other commonly used, commercially available labels indicated that 4DMN consistently beat the typical systems with respect to overall responsiveness. The overall sensitivity reported with respect to environment makes the 4DMN dye very attractive for any number of fluorescence-based biological applications.

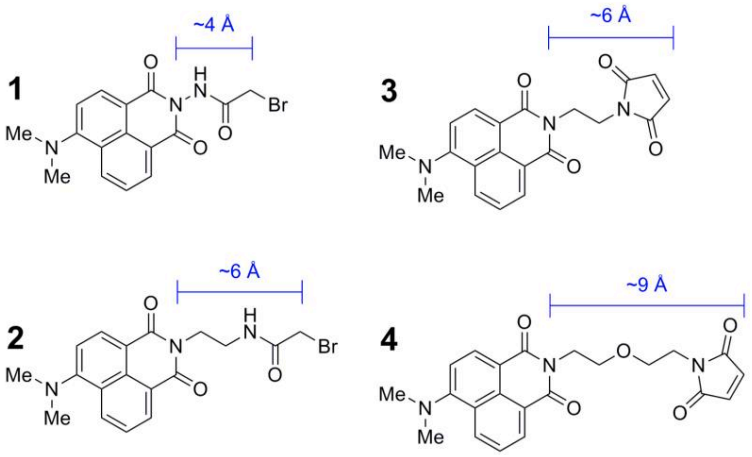

Figure 6.4 4DMN chromophore with linker derivatives. E11C and S38C mutants studied both contain linker 3. Figure adapted with permission from Loving, G.; Imperiali, B. *J. Am. Chem. Soc.* **2008**, *130*, 13630. Copyright 2008 American Chemical Society.

The details and objectives of our collaborative study for this project were very much geared toward the kinds of systems already being studied for my dissertation research. The considerations to be made about these systems presented here are very similar to those directed toward examining the peptide interactions of amyloid-β; an environmentally sensitive probe that has a different response based on interactions with the solvent or surrounding amino acids. An extension of these studies into two-photon spectroscopy has some obvious benefits that have been discussed and demonstrated throughout the course of the work presented in prior chapters. Moving the excitation source out of the visible region and into the near-IR would make imaging applications more attractive as longer wavelength excitations are less damaging than from a high-energy sources. Also, the high spatial selectivity due to the narrow focusing of a two-

photon excitation allows for more directed study of the sample medium. Through studies using two-photon excited fluorescence, we can determine the sensitivity and viability of these chromophore systems as potential two-photon imaging probes. Also from the physical chemistry perspective, interrogating the conformational changes being undergone in the labeled-CaM systems using two-photon spectroscopy and time-resolved fluorescence can illuminate the fundamental details as to fluorescence switching and distinct solvachromatic behavior of 4DMN, perhaps leading to a better understanding of CaM and evaluating the design characteristics for potential improvement.

6.3 Results & Discussion

6.3.1 Calmodulin and 4DMN-M13 System

The one-photon excited fluorescence was observed by exciting near the absorption maximum for each of the two systems studied to verify the observed trends from the Imperiali lab. The initial concentrations of the CaM+4DMN–M13 had been altered from those published to increase the optical density of the absorptions of the two systems. These results are not depicted here, but two solutions with CaM concentrations of 1500 μM, one with EGTA and another with Ca^{2+} in excess were prepared and found to have a far less substantial difference between the respective fluorescence profiles at only a 10-fold difference when the expected value was near 100-fold. The believed cause for this was aggregation-type behavior amongst the proteins due to the solution being so concentrated. Later solutions for this binding peptide system were prepared according to procedures originally outlined by the Imperiali group using a protocol whereby final CaM solutions of 1.5 μM concentration in pH 7.4 TBS-buffer solution where prepared. The solutions for testing Ca^{2+} binding were made with an excess amount of calcium resulting

in a 200 μM final Ca^{2+} concentration. The non-calcium solutions were prepared to have a final EGTA concentration of 50 μM. As shown in Figure 6.5, the one-photon fluorescence showed a substantial difference between the Ca^{2+} bound and unbound with a 108-fold difference. This was consistent with that reported by the Imperiali group.

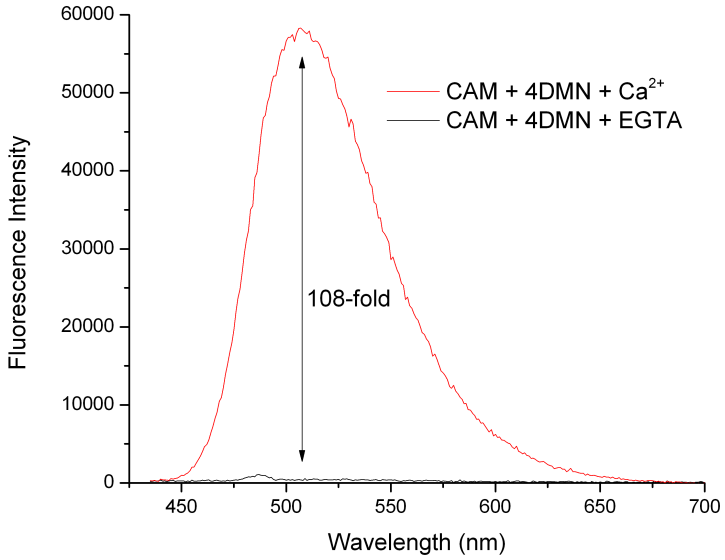

Figure 6.5 CaM+4DMN–M13 one-photon excited fluorescence comparison of Ca^{2+} and EGTA samples.

The same solutions that had been used for one-photon study were used to study the two-photon excited fluorescence characteristics and determine whether a two-photon excitation produced any additional enhancement over the traditional one-photon route. The traditional methodology described in Chapter 2 for our two-photon setup was utilized. As shown in Figure 6.6, the difference in two-photon fluorescence intensities were comparable with those observed under one-photon excitation, if not a little smaller. The relative difference has a larger error than is typically seen in TPEF studies as the EGTA sample had close to no fluorescence above the background making for significant variance for a single wavelength to wavelength intensity comparison. A better way to assess the differences between one-photon and two-photon excitation was thought to be

to a comparison of the two-photon absorption cross-sections. As shown in preceding chapters of this dissertation, these often can be indicative of some fundamental details regarding the conformational changes occurring in the protein system.

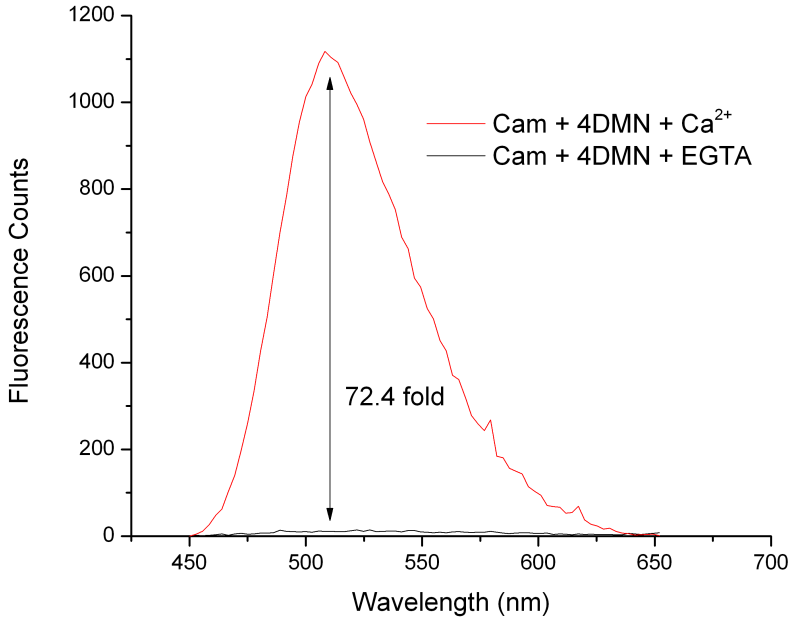

Figure 6.6 CaM+4DMN–M13 two-photon excited fluorescence comparison of Ca^{2+} bound and EGTA samples.

As shown in Figure 6.7, both the calcium bound and non-calcium bound systems responded well to two-photon excitation over a range of powers. Detection of the very nonfluorescent EGTA sample was challenging and longer integration times were necessary to produce the given curve. To determine the actual TPA cross-sections, the fluorescence quantum yields were determined for each system against a known standard that of Coumarin 307. The typical procedure outlined in earlier was used and values of 0.001 for the EGTA system and 0.09 for the Ca^{2+}. Using these values, the TPA cross-sections of 3.9 GM and 2.3 GM were calculated for the EGTA and Ca^{2+} systems respectively. These results represent an average over multiple runs.

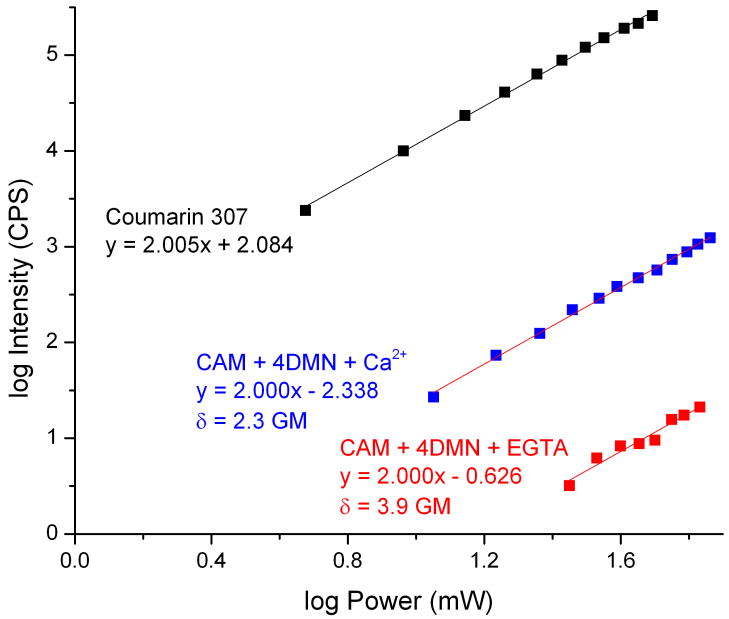

Figure 6.7 CaM+4DMN–M13 two-photon absorption intensity dependence log-log plot comparison. Coumarin 307 was used as the TPA standard and is shown as a reference.

While good two-photon response was noted for the system, the TPA cross-sections determined were small. Surprisingly, there was little to no difference noted between the two samples and the two-photon excited fluorescence showed roughly the same difference, or slightly lower than was observed in using one-photon excitation. From this system alone, it is difficult to understand whether the dynamics of the peptide are being sufficiently probed using two-photon. With the 4DMN label attached directly to the calmodulin protein, it likely would be a better sensor for the conformational changes being undergone. As will been shown in subsequent sections, the two-photon absorption cross-sections certainly appear to be environmentally dependent.

6.3.2 4DMN Cysteine-Mutated Calmodulin

The initial system CaM system with 4DMN interacting via a binding peptide demonstrated the fundamental capability of the chromophore to respond to two-photon excitation. An immediate extension of these studies was to investigate some examples of

the directly labeled CaM to observe whether under a two-photon excitation regime the overall fluorescence response would be heightened as compared to that which the Imperiali group had observed under single photon excitation conditions. A couple different systems were selected for study: one that had a large fluorescence difference (~100 times) between Ca^{2+} bound and unbound, and a second that had a much less pronounced difference (~8 times). These systems will be referred to according to their mutation for the remainder of this chapter. The first system is the S38C system and the second, lower relative fluorescence system is E11C. The spatial locations of these mutations may be viewed in Figure 6.3. Solutions were prepared according to procedures outlined by the Imperiali group using a set protocol whereby final CaM solutions of 1.5 μM concentration in pH 7.4 TBS-buffer solution were prepared. The solutions for testing Ca^{2+} binding were made with an excess amount of calcium resulting in a 200 μM final Ca^{2+} concentration. The non-calcium solutions were prepared to have a final EGTA concentration of 50 μM.

As with the first system studied, initial investigations were performed to verify that the solutions were prepared properly and that the expected fluorescence difference between EGTA and Ca^{2+} was observed. In their published work, the Imperiali group saw a ~8 fold difference in the fluorescence between the Ca^{2+} bound and the EGTA for the E11C system with a linker length of ~6 Å. As depicted in Figure 6.8, there was ~8.4-fold increase in the one-photon fluorescence intensity upon addition of Ca^{2+}, consistent with what had been observed previously. The experiment was repeated multiple times with a high level of reproducibility of the absolute difference.

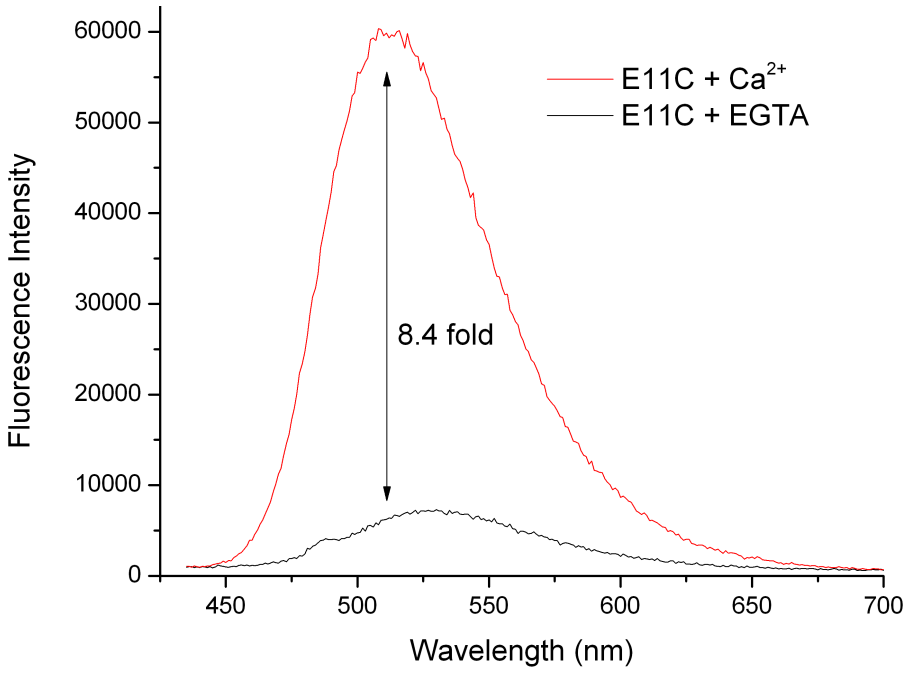

Figure 6.8 E11C one-photon excited fluorescence (λ_{ex} = 420 nm). Comparison of calcium-bound mixture with EGTA control.

With the solutions verified as being properly prepared and behaving as expected, two-photon excited fluorescence studies were next performed. The details of the two-photon absorption experimental setup are the same as previously described in earlier chapters. A change of some significance to the typical procedure was the use of an ultra-small volume cuvette (45 μL), forcing changes to the general setup alignment to properly account for the small window. Two-photon excited fluorescence was measure for each system from an excitation of 800 nm. The results are shown below in Figure 6.9. The relative fluorescence intensity change between the two systems was very consistent with that observed under one-photon excitation.

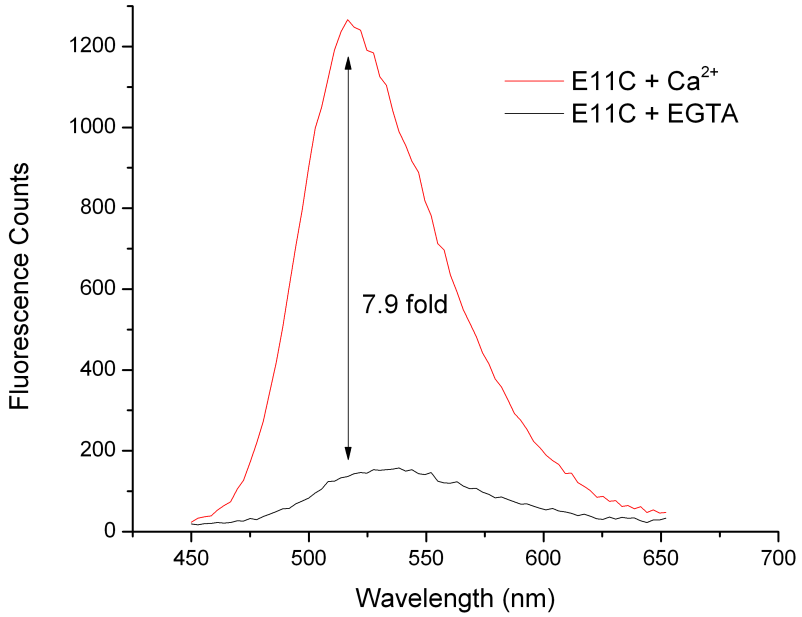

Figure 6.9 E11C two-photon excited fluorescence (λ_{ex} = 800 nm). Comparison of calcium-bound mixture with EGTA control.

The two-photon absorption cross-sections were calculated for both EGTA and calcium-bound E11C samples following the collection of excitation-power dependent fluorescence results. Figure 6.10 shows the log of fluorescence intensity plotted as a function of the log power. Linear fitting indicates good two-photon behavior over a wide power range with a quality slope of 2. A series of three samples were checked for their power dependence and the data averaged to calculate the "action" two-photon absorption cross-section (Table 6.1). There was seen about a 9-fold increase between calcium-bound and EGTA systems in this version of the cross section that does not take into account the fluorescence quantum yield of the respective solutions. The fluorescence quantum yields were eventually determined against Coumarin 307 as a reference dye, finding for the Ca^{2+} sample a quantum yield value of 0.09 and for the EGTA sample a value of 0.01. With those values at hand, the proper two-photon absorption cross-sections were calculated

and are reflected in Figure 6.10. Both samples show nearly identical TPA cross-sections of 3.3 GM.

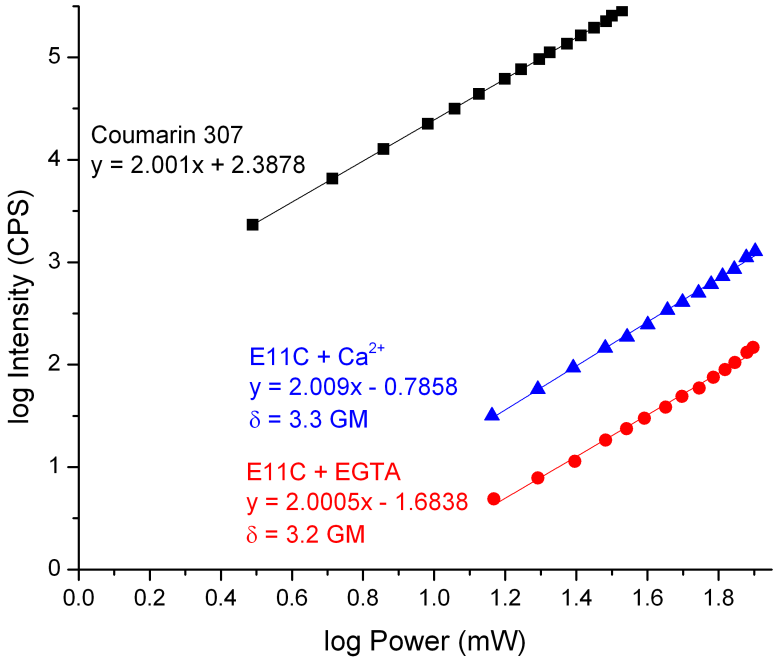

Figure 6.10 E11C linear plots and calculated cross sections for EGTA and calcium-bound mixtures.

The fact that the two TPA cross-sections are the same indicates that the environmental differences around the mutated region resulting from the conformational change of calmodulin from Ca^{2+} binding are not particularly significant. The relative difference in fluorescence is consistent using both one-photon excitation and two-photon excitation. The similarity in cross-sections would seem to preclude major changes in the type or strength of interactions that are occurring with 4DMN.

The same process as was performed for E11C was also done for the S38C sample. Once again all experiments were repeated multiple times, however preparing as consistent of solutions with S38C was more challenging given the large fluorescence difference between the EGTA and Ca^{2+} systems. For the S38C mutant, the one-photon

fluorescence showed a 120-fold increase that matches exactly what had been observed in the Imperiali lab (Figure 6.11).

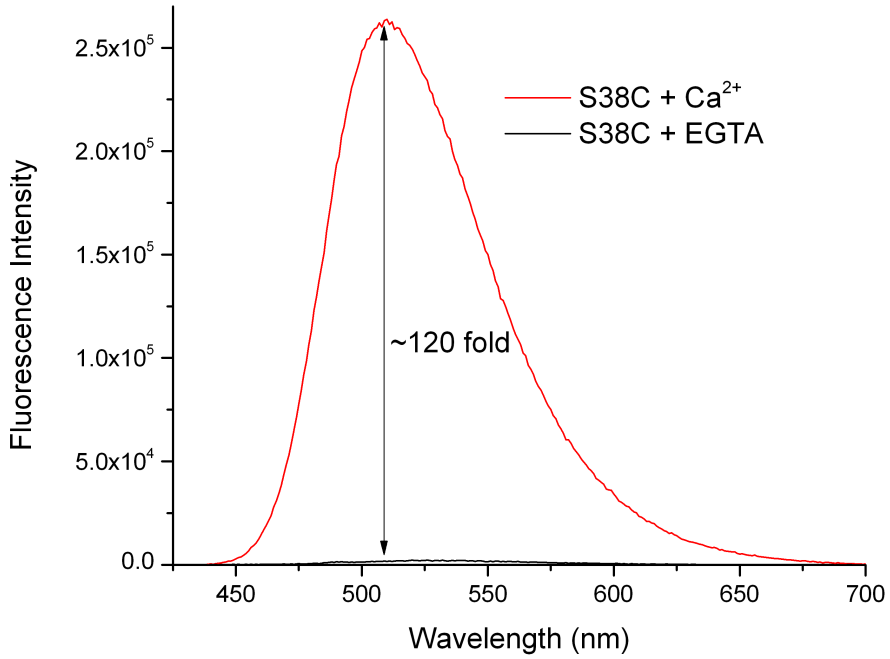

Figure 6.11 S38C one-photon excited fluorescence (λ_{ex} = 395 nm). Comparison of calcium-bound mixture with non-calcium bound mixture.

Subsequent study using the same two-photon methodology as above obtained the two-photon excited fluorescence for S38C (Figure 6.12). The results show once again very consistent results with the one-photon excited route with a 97-fold difference between the Ca^{2+} and EGTA. Given the error in the background, these results essential match the one-photon enhancement. This indicates that there is no conformational preference for these labeled-CaM systems by two-photon excitation as might have been indicated by substantial changes in the relative fluorescence intensities when comparing both one-photon and two-photon routes.

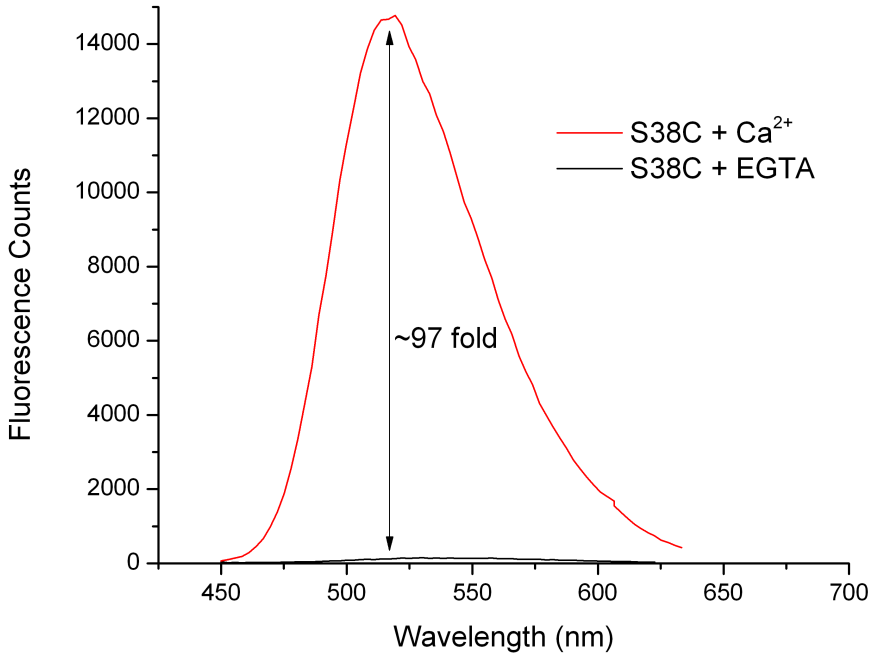

Figure 6.12 S38C two-photon excited fluorescence (λ_{ex} = 800 nm). Comparison of calcium-bound mixture with non-calcium bound mixture.

Determination of the two-photon absorption cross-sections, for each system shown in Figure 6.13 indicates that there is a substantial increase in the overall TPA absorption for 4DMN when placed at this site with this particular linker length. Cross-sections for each system of S38C were found to be 33 GM and 27 GM respectively for EGTA and Ca^{2+} systems. Quantum yields reflected in this cross-section calculation were found to correspond favorably to the relative difference in fluorescence with values of 0.002 and 0.260 determined. These results present the first indication of some level of additional enhancement in signal utilizing two-photon methods, giving clear indication that the relative position of the fluorophore in the calmodulin peptide can show very different responses. The fact that as with the previous systems there is no great difference in the calcium-bound and unbound mixtures would seem to indicate that the conformational changes occurring are not a significant drivers in the overall cross-section measured.

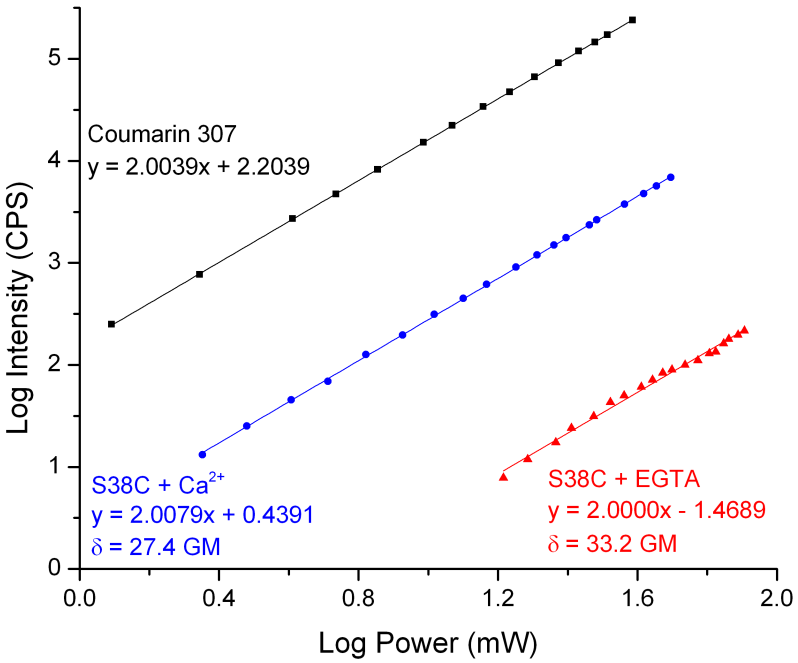

Figure 6.13 S38C two-photon absorption intensity dependence log-log plot comparison. Coumarin 307 was used as the TPA standard and is shown as a reference.

6.3.3 Conclusions

Sample	OPE (Avg Counts)	TPE (Avg Counts)	"action" TPA ηδ (GM)	η	δ (GM)
4DMN-M13 + EGTA	526.5	15	0.0039	0.001	3.9
4DMN-M13 + Ca^{2+}	56942	1049	0.203	0.090	2.3
Ratio	**108**	**72**	**52**	**90**	
E11C + EGTA	6646.7	203.3	0.033	0.010	3.3
E11C + Ca^{2+}	56580.2	1533.4	0.288	0.090	3.2
Ratio	**9.1**	**7**	**9**	**9**	
S38C + EGTA	2200	152	0.080	0.002	33.2
S38C + Ca^{2+}	257447	14666	7.243	0.260	27.4
Ratio	**117**	**97**	**91**	**130**	

Table 6.1 Summary of results for calmodulin 4DMN-M13, E11C, and S38C systems.

In summary, the CaM+4DMN-M13 bimolecular system, S38C, E11C mutant systems have been characterized through the determination of one-photon excited fluorescence, two-photon excited fluorescence, quantum yield, and two-photon absorption cross-sections for each system with and without calcium binding. Table 6.1

summarizes all the findings for the three calmodulin systems. Quantum yield shows universally a significant enhancement upon calcium addition. As described, factors such as solvent exposure, collisional quenching, and local electrostatic fields may quench quantum yield. In the EGTA-bound state, the fluorophore is exposed to a polar, protic solvent in water and thus loses the majority of its emission nonradiatively. Upon calcium binding, conformational changes occur that tucks the fluorophore into hydrophobic pockets minimizing its exposure to the solvent and hindering its movement. These effects prevent unwanted photon-transfer to the bath and permitting a more efficient fluorescence emission.

It was also observed that the two-photon absorption cross-section was not significantly changed upon calcium addition in any of the systems studied. This result is surprising as it indicates that the overall conformation changes of the protein are not materially effecting the microenvironment in these particular regions or are not being detected by this technique. Instead, the only changes manifested are those in emission efficiency. The two-photon absorption cross-section were observed however to vary depending on mutation location and linker length. This indicates that the overall dipole characteristics of the fluorophores are being distinctly effected in different regions of the protein. TPA cross-sections are directly dependent on dipole moment. As the Rebané laboratory has characterized for β-barrel protein structures, local electric fields can influence the magnitude of the dipole moment, translating into a change in the absorption cross-section. **Equation 6.1** shows the relation of the electric field dependence on Δμ as derived by the Rebané, et al.:

$$\Delta\mu = \Delta\mu_{\diamond} + \frac{1}{2}\alpha_{\circ} f_s E \qquad \textbf{(Equation 6.1)}$$

Where Δμ corresponds to change of dipole moment, Δα corresponds to the difference in the corresponding tensor polarizability in vacuum, f_s corresponds to local field factor, and E corresponds to electric field.

Through a similar paradigm, it may be suggested that the local amino acid environment varies at the different fluorophore sites investigated. A cursory examination of surrounding amino acids at E11C and S38C sites support this claim. By looking at the five nearest amino acids on either side of the mutation site, the E11C mutant has a far larger number of charged acidic and basic residues in the local environment. Such a difference may correspond to differences in local electrostatic charge and influence electric field orientation, which will affect the magnitude of the dipole moment and consequently the two-photon absorption characteristics of the fluorophore. Further study of these systems through the use of time-resolved fluorescence studies may provide additional insight into unique environmental changes that occur upon calcium binding and better explain the nature of the two-photon absorption

6.3.4 Preliminary Fluorescence Upconversion

In order to interrogate in greater detail the environmental factors surrounding the conformation changes associated with the initial system of CAM+4DMN–M13 system with and without calcium, the fluorescence lifetimes of the two systems were investigated using time-resolved fluorescence upconversion. The system of solutions was studied at significantly higher concentrations than previously for two-photon absorption studies due to the overall low signal of the 1.5 μM solutions made when placed in 2 mm rotating cell for upconversion. The relevancy of the data needs to be investigated more fully as higher concentration solutions of this system seemed to have inconsistent steady-state one-

photon excited fluorescence results as compared to that observed and published previously. However, the preliminary results should allow for a qualitative comparison of the two systems to be made and an evaluation of how the chromophore environment changes the types of interactions between the two systems.

As shown in Figure 6.14, the fluorescence decay trends for the Ca^{2+} differ from that with the EGTA, especially the short decay component which the calcium bound sample clearly shows faster kinetics than the unbound. A more detailed investigation of the fast component for the EGTA system would be required to make a true comparison, but for the calcium-bound system there is clearly at least one component that is faster than 5 ps which could be indicative of an energy-transfer process occurring due to the new conformational state of the protein.

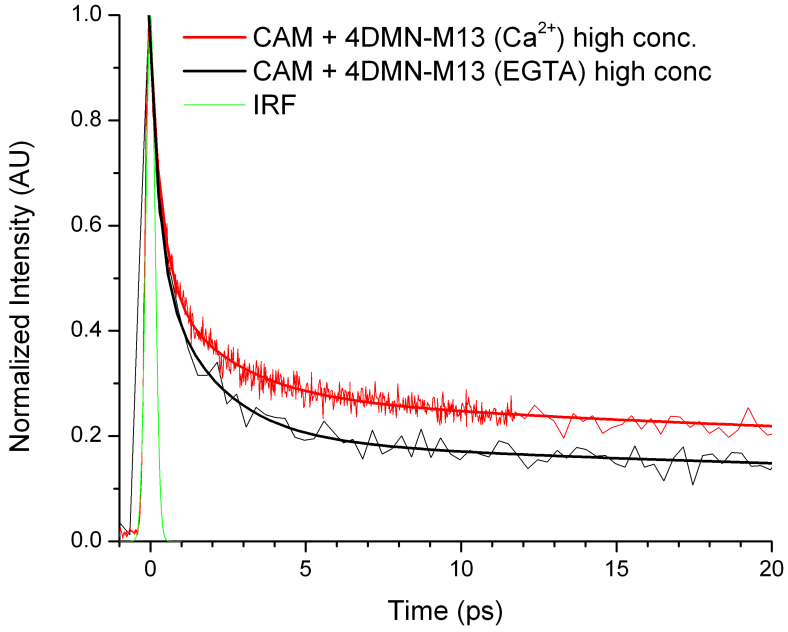

Figure 6.14 Fluorescence lifetimes of CAM+4DMN–M13 with and without Ca^{2+}. Data normalized to peak intensity. The overall fluorescence lifetime is beyond the resolution of the instrumentation.

The preliminary anisotropy data collected from fluorescence upconversion shows fairly divergent behavior for the two systems (Figure 6.15). The depolarization is much more rapid for the EGTA-bound system than the Ca^{2+}-system. If this preliminary data is correct, this presents convincing evidence of the different fluorescence behavior between the two systems. More detailed short time runs would need to be made, but again a significant difference in the fast dynamics of these two systems translates into direct information about the conformation state of the peptide. A closer examination is merited to provide data for reasonable fitting. Additional attempts to run fluorescence upconversion on the calcium and EGTA-bound CAM+4DMN–M13 systems at low concentration proved unsuccessful, so some sacrifice may need to be made between the biological relevancy of the concentrations and achieving sufficient signal for biophysical characterization.

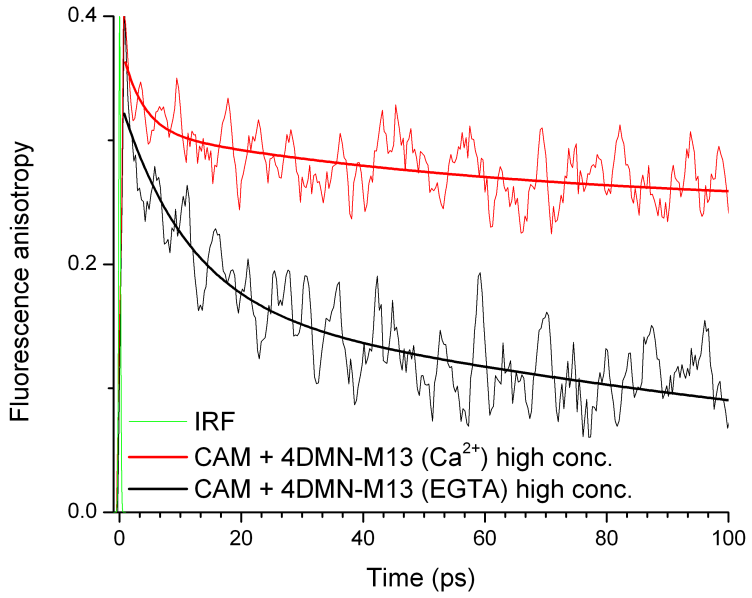

Figure 6.15 Anisotropic decays for CAM+4DMN–M13 systems. Data was averaged via five-nearest-neighbor averaging to obtained smoothed curves.

6.4 Outlook & Future Directions

The collaboration between our lab and the Imperiali lab at MIT has proven to be very fruitful after a small set of very controlled experiments. After some struggles with solution concentrations and preparation, a clear sensitivity for the spatial location of the fluorophore is detected using two-photon absorption methodologies. A more detailed study of the calcium bound and unbound systems may be able to illuminate the conformational differences between these two systems as preliminary results have indicated variations in the fluorescence decay dynamics of the CaM+4DMN–M13 systems. Additionally, widening the scope of study to different linker lengths as well as more mutation sites potentially could elucidate the role that environmental interactions are playing in changing the two-photon absorption cross-sections. Other directions that have been discussed involve using two-photon near-field scanning optical microscopy to develop two-photon imaging systems using 4DMN.

References

1. Loving, G.; Imperiali, B. *J. Am. Chem. Soc.* **2008**, *130*, 13630.

2. Loving, G.; Imperiali, B. *Bioconjugate Chem.* **2009**, *20*, 2133.

3. Loving, G. S.; Sainlos, M.; Imperiali, B. *Trends in Biotech.* **2010**, *28*, 73.

Chapter 7

Summary and Future Work

7.1 Summary & Implications

The overall impact in the work lies with the significant two-photon absorption enhancement observed with labeled Aβ1-42 that corresponds directly to structural features of aggregating peptides. This demonstrates some of the advantages of a two-photon methodology over a traditionally used circular dichroism. This technique has superior low-concentration sensitivity and no limitations due to background sources of absorption. The complete two-photon absorption and time-resolved fluorescence methodology permits detailed conformational and peptide aggregate characterization of the evolution from early oligomer to fibril formation something that could have a huge impact toward therapeutic intervention or fundamental understanding of Alzheimer's disease. Many direct applications for *in vivo* imaging may be envisioned using two-photon-based methodologies including cancer-targeted monitoring as well as peptide aggregation associated with Alzheimer's and Parkinson's disease. Two-photon imaging has the capability to permit detailed tracking of the evolution of disease beginning with some initial misfolded monomer to the formation of toxic oligomers and later fibril structure. This could have a profound impact on the ability to detect and prevent the development of neurodegenerative disease.

This research project has shown the development of a methodology for the study of aggregating peptides from the initial origins of using commercially available dye-

labeled amyloid-β systems to designing, synthesizing, characterizing, and ultimately implementing a new two-photon absorbing chromophore. Throughout the process, it has been demonstrated from a photophysical perspective the advantages of tailoring the chromophore to address the challenges presented for such a system. The environmental sensitivity of DMC as accentuated by the strong two-photon response measured for the labeled amyloid peptide strongly highlighted this effect that was not observed in the studies using the TAMRA label. At the conclusion of this project, a firm foundation for the continued development of nonlinear optical and time-resolved ultrafast spectroscopy for the investigation of peptide systems has been established to perform fundamental investigations of aggregating systems that are otherwise very difficult to study. This fact is further evidenced by our ongoing collaboration with the Imperiali group to implement a two-photon excitation regime to study both the fundamental mechanisms of a dye-labeled protein, but also to use two-photon excited fluorescence in imaging applications. In many ways, the work presented here demonstrates the power of two-photon methodologies and their advantages over traditional techniques for targeting the conformational changes of peptide systems especially in the study of early aggregates of amyloid peptides.

As described in Chapter 3, two-photon methodologies have a distinct sensitivity for aggregating peptides. Our work with TAMRA-labeled Aβ1-42 was able to correlate the secondary structure of the peptide to the fluorescence decay lifetime of the TAMRA label. From this, a model was developed to account for the potential types of interactions that were occurring with the dye as a function of peptide concentration. It was concluded that intra- and intermolecular interactions afford the implementation of two-photon

excited energy-transfer (2PET) based fluorescence studies to the conformational flexibility of the N-terminus in Aβ with residue specific assays. This ability to correlate the peptide conformational state with its fluorescence lifetime at low concentrations opened a new avenue toward the measurement of Aβ conformational fluctuation at the signal molecular level that, as discussed, has provided details unachievable with techniques like CD spectroscopy.

As an extension of this work, in Chapter 4 synthetic organic chemistry was first implemented to design a biologically compatible chromophore structurally similar to that found in green fluorescent protein (GFP), however possessing strong two-photon absorption (TPA) characteristics. This design would serve to provide a system ideally suited for spectroscopic study using excitations from our ultrafast laser systems. Initial synthetic investigations were directed toward a modified version of ZsYellow chromophore, a structural analog to the GFP-chromophore before a generalized approach for the chromophore synthesis was eventually developed to provide flexible substituent incorporation. A library of nine compounds with a variety of different donor−acceptor substituents and functionality providing for extended conjugation was ultimately created via a well-studied cycloaddition reaction combining an iminoglycine methyl ester and a substituted benzaldehyde. Additional synthetic steps yielded label-ready chromophores for application in biological studies.

Spectroscopic characterization of the chromophore library informed and guided the synthetic design of the chromophores as specific considerations were made for the photophysical characteristics including fluorescence quantum yields, lifetimes, and TPA. Steady-state spectroscopy performed on the chromophores determined absorption

maximums in the range of 350-450 nm and moderate fluorescence quantum yields (10^{-4}) from 420-535 nm emissions. Two-photon absorption behavior of the synthesized chromophores was extensively characterized, investigating their absorption cross-sections with the specific goal of ascertaining their viability as biological probes. Cross-sections were found to be good with the best chromophore approaching 40 GM at near 800 nm excitation. Fluorescence lifetimes for the synthesized chromophores were investigated using ultrafast time-resolved fluorescence upconversion and found to be biexponential with generally sub-picosecond and picosecond components. The individual effects of the substitution position and relative size of the functional groups were evaluated and found to be significant in changing the fluorescence-decay characteristics. Of physical characterization data collected, the largest consideration was placed on the TPA cross-section values for the determination of the molecule best suited for biological application.

As described in Chapter 5, large facets of our research efforts were then guided toward the application of our best GFP-type chromophore as a label into folding dynamics studies of amyloid-β1-42. The earliest conformational changes of this aggregating peptide were studied at dilute concentration utilizing two-photon absorption and ultrafast time-resolved fluorescence laser spectroscopies. An unprecedented, significant two-photon absorption enhancement was noted comparing the "free" DMC chromophore (40 GM) to the labeled DMC-Aβ1-42 segment (550 GM). Further concentration-dependent studies in the low micromolar regime indicated that the enhancement was affected to a large extent by the concentration of the peptide solution with its conformational state leading to larger TPA cross-sections due to significant dipole interactions with the attached chromophore. A relative comparison of our TPA

studies with circular dichroism spectroscopy showed that our two-photon methodology may have greater sensitivity than CD for the conformational changes being undergone at concentrations ~1 μM and lower. The advantages of shifting the excitation source out of the high-energy ultraviolet region where sources of unwanted background absorption are much more prevalent, coupled with the inherent sensitivity of TPA, makes advantageous over CD for the characterization of the early conformational changes of aggregating peptides. Investigations into energy-transfer mechanisms using fluorescence upconversion studies allowed for sensitive detection of ultrafast dynamics in the peptide aggregates as a function of concentration. Understanding the depolarization contribution of the emission decay using fluorescence anisotropy measurements led to an explanation of the time-scale and mechanism of energy migration in these early Aβ aggregates. Future development of the methodology outside of solution-phase studies by utilizing two-photon near-field scanning optical microscopy to characterize larger insoluble aggregates could result in broadened application allowing the monitoring of peptide aggregation over the full fibrillization pathway. This approach has the potential to answer some of the prevailing questions that remain about the conformational dynamics for many of the peptides that result in neurodegenerative disease.

7.2 Future Work

As is the nature of scientific research, there is always another question to be answered or a new direction of study to pursue following the completion of a project. From my perspective, there are several clear areas on which to build and improve on the work presented here. These fall under the three broad phases of my research, chromophore design/synthesis, spectroscopic characterization, and biological application.

Chromophore design/synthesis. While the presented library of nine chromophores demonstrated a range of photophysical properties and functionality, the overall collection of fluorescence properties was less than ideal with quantum yields generally $<10^{-3}$. Continuing to refine strategies to improve the quantum yield while at the same time maintaining the favorable two-photon absorption characteristics is something that should be tackled in the future. Derivatives with *ortho*-substitution should be investigated to determine if certain groups might be implemented at these positions to limit the rotation about the benzylidiene group to lessen nonradiative emission pathways and improving fluorescence quantum yields. Similarly, a broader selection of small molecule chromophores should be investigated for even better fluorescence and improved two-photon characteristics. A chromophore such as the 4DMN discussed in Chapter 6 would be an ideal template especially if the fluorescence switching behavior could be manifested in the study of amyloid peptide aggregation.

Spectroscopic characterization. The continued development of the characterization methodology is an important both for the chromophore design and biophysical studies. A primary direction of new spectroscopic implementation should be to pursue using the near-field scanning-optical microscope available in our lab to extend the peptide characterization beyond just solution phase. As touched-on earlier, the ability to precipitate aggregate structures and characterize their morphological features using two-photon excitation would provide the ability to examine amyloid structures from monomer to insoluble fibril, potentially allowing for connections to be made about how the structure evolves. Closely tied to investigating this evolution is an examination of the conformation changes of aggregating peptides as a function of time. In both large studies

that encompass chapters 3 and 5, no systematic methodology was developed that could definitively monitor the changes being undergone as a function of hours or days. The first TAMRA-labeled Aβ systems were studied after 14 days of incubation, while the recent DMC studies were performed immediately following solution preparation. Understanding how these aggregating solutions change over time is fundamental to developing a full picture of the early aggregation process of amyloid peptides.

Biological application. Finally, there remains a great deal of things that could be improved upon for future investigations in areas of study related to the aggregating amyloid peptide systems. The limited scope of our initial investigations precluded any comparisons of multiple different peptide systems. Along with labeled Aβ1-42, additional studies could be performed on Aβ1-40 and compared to the observed spectroscopic characteristics for Aβ1-42, as the two systems tend to aggregate at different rates and have different conformational intermediates. Additionally, there are a host of known familial genetic mutations for amyloid-β that could be part of a larger study and further test the sensitivity of the techniques developed. Similarly, the initial investigations only used N-terminus labeled peptides. Investigating the placement of the chromophore throughout the peptide as side-chain modifications of lysine could substantially increase the conformational details obtained if positioned correctly to not interfere with aggregation. A multiply labeled peptide with chromophores absorbing over different spectral regions could also be envisioned under such an approach. Other systems outside of amyloid-β like α-synuclein (associated with Parkinson's disease) could also be studied to look at the broader applicability of our series of techniques to other aggregating peptides. Lastly, implementation of more rigorous bioanalytical techniques to limit and

understand the diversity of species, especially at early aggregation stages when mass spectroscopy and circular dichroism could be used might substantially improve an understanding of the data collected from two-photon and time-resolved studies.

Chapter 8

General Audience, Non-Specialist Description and Summary

8.1 Explanation

As scientists one of the largest responsibilities we face is the dissemination of our results to each other and to the public at large. With so many great challenges in front of the world today like climate change and the search for renewable energy sources just to name a couple, it is more important than ever for scientists to reach out and present their research in a form that can be understood to those outside of the typical scientific channels. I have personally felt a great burden to convey an understanding of the work I am doing to those closest to me. This last chapter of my dissertation is my best attempt to summarize my years of work in such a manner that someone not very familiar with chemistry may approach understanding at least some fraction of my studies. Some aspects are of course easier to boil down to the basics, while yet other aspects still will undoubtedly require a base of knowledge to which certain readers may not have been exposed. Regardless, for the reader I think there is some utility in persevering through this chapter if only to observe a bit of the thought process that goes into winnowing down a big picture problem to some fundamental questions and then designing a set of experiments to address them. This is at the heart of what chemists do on a daily basis and what I have done over the course of the last five years. What follows will be some

introductory sections that attempt to explain the "big picture" problem that my research sought to address and then some of the experimental techniques that we wanted to implement. Finally, something of the chronology of results from my experiments will be discussed with explanations as to how they approach answering the questions brought up throughout the introductory section.

I should note here before moving on that the impetus for this chapter originates from a talk I heard the current president of the American Chemical Society, Dr. Bassam Shakhashiri, give at the 242nd National Meeting in Denver, CO last summer as part of a symposium about communicating chemistry. During his talk (http://vimeo.com/31914575#t=721), he described an initiative started at the University of Wisconsin (Wisconsin Initiative for Science Literacy, WISL) in 2010 to encourage chemistry graduate students to include a chapter in their thesis directed toward non-specialists. This was a bit of a revelation to me and something I think should be encouraged by all graduate institutions.

8.2 Introduction

Neurological disease affects a large portion of the world's aging population. These diseases include, among others, well-known Alzheimer's and Parkinson's diseases. A great deal of monetary expenditure has been devoted toward research benefiting an understanding of their causes and development of subsequent treatments. A range of researchers in medical fields and many others studying biochemistry and biophysics have devoted extensive time to investigating these diseases as the fundamental questions yet to be answered are manifold. For instance: *what causes someone to develop these diseases? What are the indicators that indicate that the disease has been contracted* and *at what point in the pathology can an individual most effectively be treated?* These are some of

the prominent macroscale questions that anyone would likely consider. But digging deeper, these simple questions lead to a great many scientific concerns that must be addressed prior to even approaching these larger ones. The scientific community in an effort to answer these questions has done a great deal of work to understand, down to the molecular level, how a normal, healthy set of biological structures develop into the toxic species that cause disease.

In order to avoid a lengthy treatise on the finer aspects of the medical end of things that are really beyond the scope of a chemistry PhD, a detailed explanation of the physical mechanisms of how Alzheimer's or any of the other neurological diseases causes memory-loss or its other many deleterious effects will be left for your reading elsewhere. However, so as to understand the origins and motivation of my dissertation work, a brief discussion of the fundamental mechanisms leading down the road to pathogenesis is required and will be made presently.

At the center of these diseases is the concept of protein (or peptide) misfolding. Proteins are important molecules that perform many of the major functions in cells as dictated by information encoded into someone's genes. Proteins are themselves made of a number of smaller molecular building blocks called amino acids that are comprised of carbon, nitrogen, oxygen, and sulfur elements in various arrangements. They are linked together through what are called peptide bonds. Depending upon the structural composition of the protein (i.e. what amino acids are present and in what sequence), the protein can take a multitude of shapes and consequently perform very specific functions depending upon their structure. These shapes are often referred to as conformations. For a particular cellular function, the relevant protein will adapt a conformation for which it

may interact with other proteins or biomolecules. This causes some cellular event to occur. For example, there is a whole class of proteins called enzymes that regulate many of the important cellular functions. The root cause of a range of disease is from proteins that fail to adopt their native conformations and become “misfolded”. Neurodegenerative diseases like Alzheimer’s are the result of a further subset of these types of misfolding events that result in the conversion of typically soluble structures into large organized fibril structures. These misfolded units are due to associations through peptide aggregation that creates extracellular plaques which fall out of solution (and show up on brain scans). The large aggregated species are termed amyloid fibrils, certain forms of which are believed to be associated with toxicity and disease.

Amyloid fibrils form according to a structural pathway beginning with the association of a single protein chain with another to form a two-peptide unit called a dimer. From there, the pathway becomes complex with the growing aggregate structures undergoing conformational and morphological changes as larger and larger organized structures are generated. At some point along this pathway where at any given time many, many different structural forms exist simultaneously, the amyloid structure develops toxicity as a result of increasingly unfavorable interactions among amino acid residues at the aggregate surface with other cellular components. Instead of performing their designed functions, these proteins now cause unintended biological events to occur, inhibiting the typical (and important) functions of the cell, and whose interruption eventually result in cell death. Current research has indicated that this toxicity likely happens far earlier along the fibrillization pathway than the typical diagnostic hallmark of

plaque formation observed by doctors. The large fibril plaques that are easy to find using brain scans fundamentally signals a disease that has progressed to a great extent.

Consequently, there is a need for a methodology that can detect the disease at an earlier time so that therapeutic measures can be targeted and effective. For this reason, research scientists have focused on understanding the conformational states and aggregate structures of amyloid peptides to develop ways to inhibit their continued formation into toxic species. To better facilitate the study of the disease causing fibril formation, a majority of the fundamental experimentation is done synthetically in the lab (*in vitro*), allowing for scientists to control the environment and conditions under which the amyloid peptide aggregates. The techniques and methods that are used to study these smaller, non-plaque structures from the single peptide to the fiber-like latter stages are varied and generally only suited for characterizing a single specific aspect.

Imaging techniques like atomic force microscopy (AFM) or transmission electron microscopy (TEM) are better suited for well-organized, ordered structures that will be found only at advanced stages of aggregation. Other techniques like mass spectrometry (MS), which has the power to determine the exact weight of the aggregate structure, is based upon the way the structure ionizes (breaks apart). It is better suited for very much smaller, soluble structures as these are much more feasible to keep in solution and travel through the instrument. Mass spectrometry cannot really give information about the physical state of the peptide (what shape it has, what it looks like). Another technique commonly used by biochemists however, circular dichroism spectroscopy, is able to give an idea about the larger structural shape of the peptides through differences in how

solutions of amyloid peptide absorb polarized light. (More details about circular dichroism will be offered in the coming sections.)

These are really just a selection of the methodologies being utilized at present to study amyloid peptides and Alzheimer's disease. What is clear from the literature is that there really is no technique that gives all the answers or can illuminate the whole of the fibrillization process. The need is still great for the development of new techniques that can be used to closely interrogate the small changes that are taking place as these peptides misfold. As such, my dissertation research was motivated toward utilizing several laser-based techniques that have been used extensively in our research group for chemical characterization and apply them to this very important biochemical problem.

8.3 Implementation of Techniques and Experimentation

Central to the techniques that we sought to implement to study amyloid peptides are the concepts of absorption and fluorescence. In chemistry, absorption refers to a molecule to taking up energy in the form of electromagnetic radiation (light), most often from the visible spectral region and the near-ultraviolet and infrared regions that lay just beyond what can be detected with our eyes. Absorption is a fairly tangible concept in daily life. Dark, black clothes better absorb the sun's radiation as evidenced by them getting warm on a hot summer day. White clothes however do a poor job. In nature, plants contain a pigment called chlorophyll that is a key component of photosynthesis. Chlorophyll absorbs a wide-range of wavelengths of visible light for conversion into usable energy for the plants. Every molecule or material has different capabilities to absorb light. And as chemists, we can synthesize tailored materials that absorb only the colors of light that are desired.

The concept of fluorescence is more nebulous than that of absorption. Much in the same way that molecules can absorb light energy, certain ones may also release energy in the form of light. This luminescence event is referred to as fluorescence. Fluorescence is often portrayed frequently on any number of CSI-type shows where the forensic investigator shines a black light (an ultraviolet wavelength light source) across a room looking for signs of blood or semen. Either of these materials will absorb the invisible high-energy light of the lamp and give-off light as fluorescence at a longer wavelength, visible to our naked eye. Again, chemists may use knowledge of absorption and its relationship to fluorescence to design molecules that will not only be fluorescent, but also fluoresce with the specific attributes desired. Shown below, Figure 8.1 schematically depicts how the processes of absorption and fluorescence are connected. Together, these related processes in a general sense will be referred to as "photophysics" for simplicity as the discussion becomes increasingly focused on my specific research.

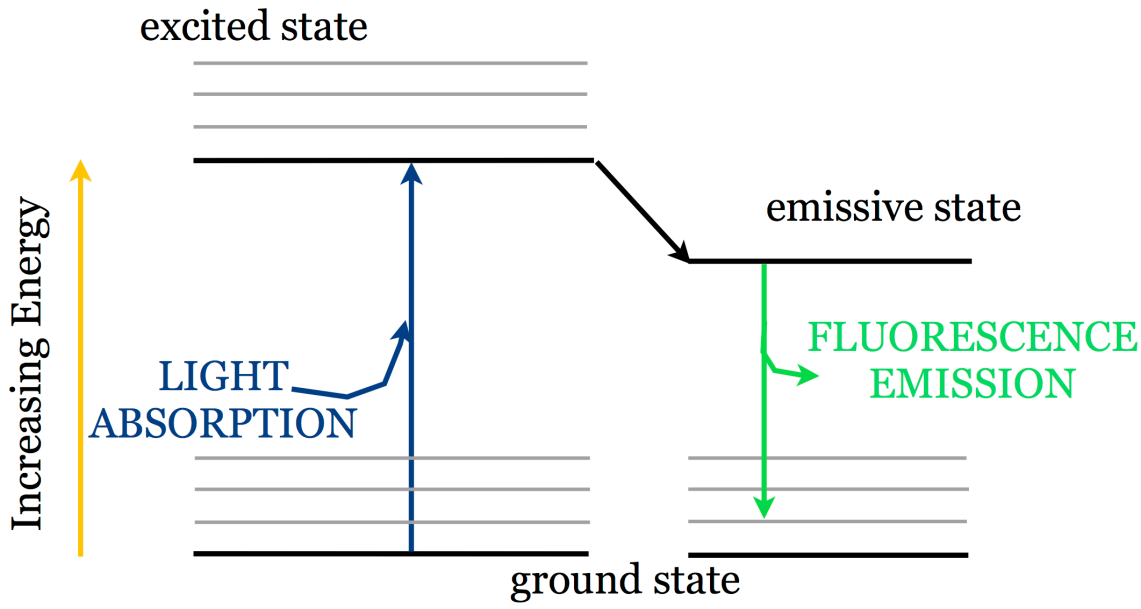

Figure 8.1 Energy level diagrams for absorption and fluorescence. The ground state is the natural resting state for a molecule. Upon being hit light at the appropriate

wavelength, it absorbs energy changing the molecule into its excited state. Eventually, this energy is dissipated (emission) and the molecule returns to the ground state.

As I have only obliquely alluded, the first aspect of my dissertation research was to design and synthesize a molecule for the eventual application of probing those peptide conformational changes being undergone by amyloid-β as it aggregates. The photophysical characteristics of this molecule play a very important role in these studies. It should be mentioned that there are a number of chemical manufacturers that make a wide variety of chemicals, but despite this wide availability of chemicals most are simply starting materials for larger synthetic endeavors. In a way, synthetic chemistry can be thought of a lot like cooking. In much the same way as one would follow a recipe to incorporate the appropriate ingredients and apply the proper heat to generate a desired dish, in performing synthetic chemistry procedures are followed that describe how to combine starting materials that have been purchased (or synthesized independently) and under the best conditions the reaction should be conducted. Unlike most experiences in the kitchen however, synthesized products generated from chemical reactions in the research lab need to be purified to remove undesired any leftover starting material or byproducts that can have undesirable characteristics in the application of newly synthesized product.

When considering the criteria for the molecule to be synthesized a number of things were kept in mind. First, to use this chemical in a biological situation the molecule chosen should not present negative effects like toxicity to the systems we want to study. Secondly, this molecule needs to be fairly proficient at both absorbing visible light (preferably at wavelengths around 400 nm near the blue end of the visible spectrum) and emitting fluorescence. Finally, the molecule in question has to be small so that when

incorporated into the peptide system it does not change the ways in which the amyloid peptides naturally interact with one another. Given these design restrictions, nature was looked to for inspiration and a class of naturally occurring chromophores found in fluorescent proteins of coral and jellyfish were thought to be suitable for our purposes. Scientists have been able to successfully isolate and structurally characterize the important molecular features that give these proteins the strong ability to fluoresce. A selection of these chemical structures is shown below in Scheme 8.1. As can be seen, the constituent units making up these molecules are the same as those that were described for amino acids. This is not coincidental as these molecules (chromophores) are generated from naturally occurring reactions involving various amino acids when placed under the right conditions.

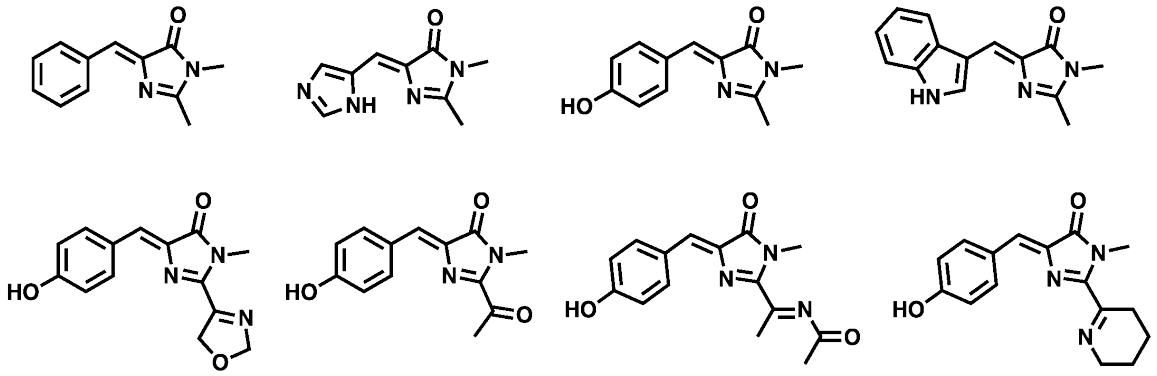

Scheme 8.1 Structure of select fluorescence protein chromophores.

The core ring structure of these chromophores is called an imidazolidinone group (the five membered ring containing two nitrogens and a doubly-bonded oxygen) and provides much of the fundamental photophysical characteristics of the chromophore. Also important structurally is the pendant phenyl ring (the six membered ring with 3 double bonds) and any additional functionality attached to it like the –OH group for some in Scheme 8.1, or in the case of our molecular target, a $–NMe_2$ functional group. Lastly,

in order to be able to physically (covalently) attach the synthesized chromophore to another biomolecule a carboxylic acid group needs to be present somewhere in the structure as that will be the site where the requisite linking chemistry will be able to be performed to add the peptide. Scheme 8.2 shows these groups represented as esters, the doubly-bonded oxygen to the carbon with the –OMe.

From those natural chromophores listed above, a few structural modifications were designed to help improve the absorption characteristics of the molecules and more importantly their ability for two-photon absorption. (A concept that will be explained in-full later.) Synthetically, a variety of different chromophores were made as our strategy shifted from a very complex synthesis to a more simplistic generalized one. Shown below are all the different ones created, many of which had never before been synthesized or reported in the chemical literature. As can be seen, the core structural elements are the same in all of them, however some of the peripheral groups have been modified in an attempt to tailor the photophysical characteristics that each has.

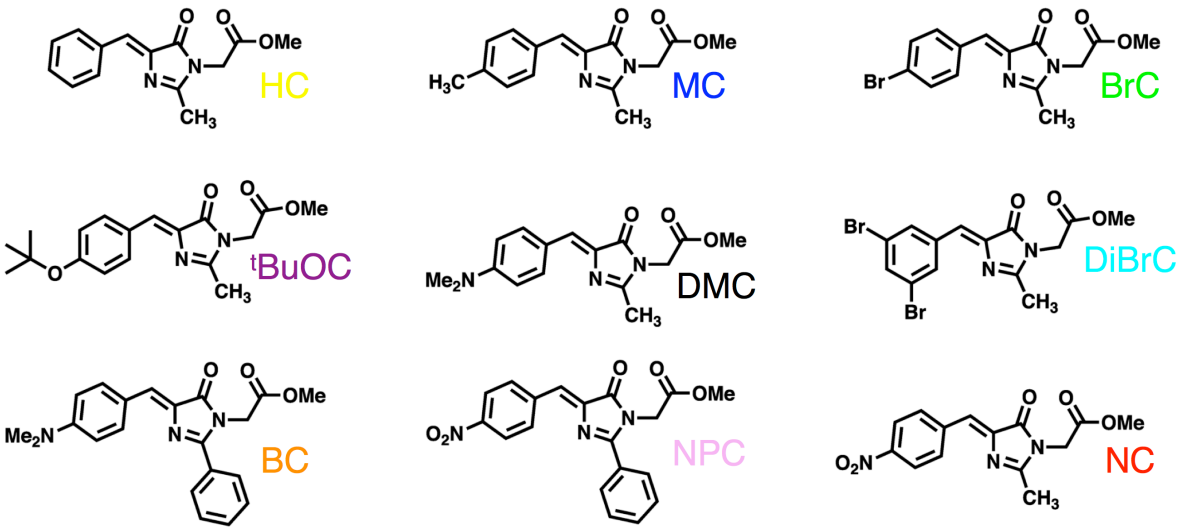

Scheme 8.2 Library of synthesized chromophores.

In conjunction with the synthesis of these chromophores, the characterization of the photophysical properties was completed as each structure was generated. As mentioned previously, our interest in these molecules was directed toward their ability to absorb/emit light. Using what is known as a UV-Vis spectrometer (Figure 8.2a), the chromophore's ability to absorb ultraviolet and visible light was measured. The synthesized molecules were each dissolved in solution and placed in a clear, quartz glass cell through which the light could be passed. The designed chromophores were found to absorb a range of wavelengths whose maxima where anywhere from ~350-450 nm, a fairly significant shift just for swapping a few functional groups. HC showed the lowest absorption maximum at 347 nm and BC had the highest absorption maximum at 453 nm. Importantly, a number of the chromophores were found to have strong absorptions near 400 nm with NC and DMC being particularly well-suited for 400 or 800 nm excitation.

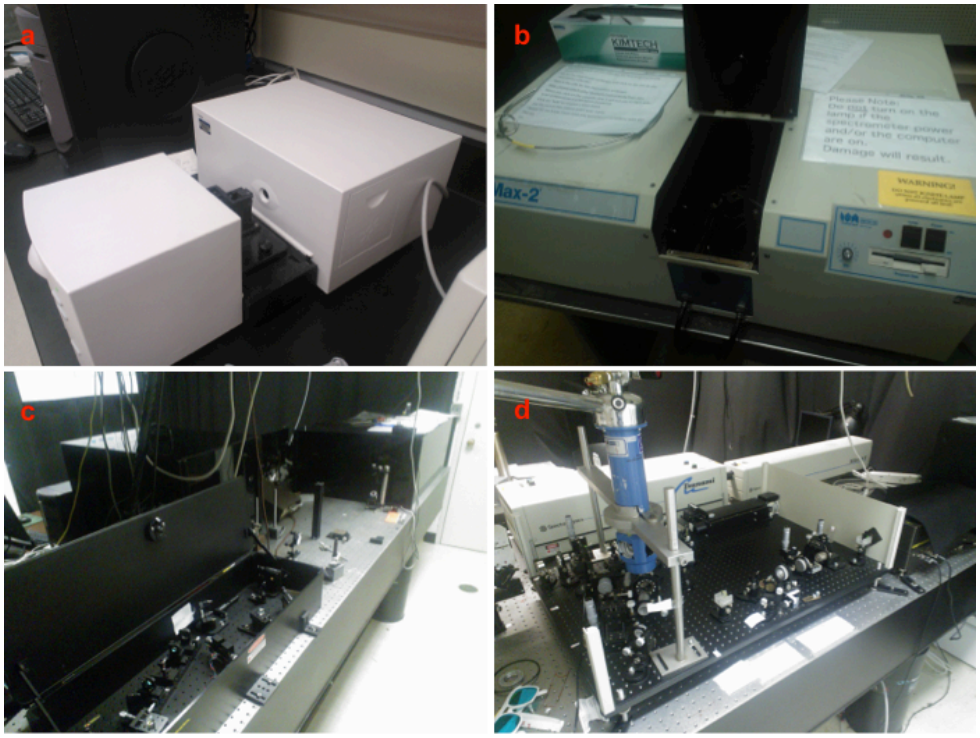

Figure 8.2 Instrumentation used to collect data. (a)UV-vis spectrometer (b) Fluorimeter (c) Two-photon absorption setup (d) Fluorescence upconversion setup.

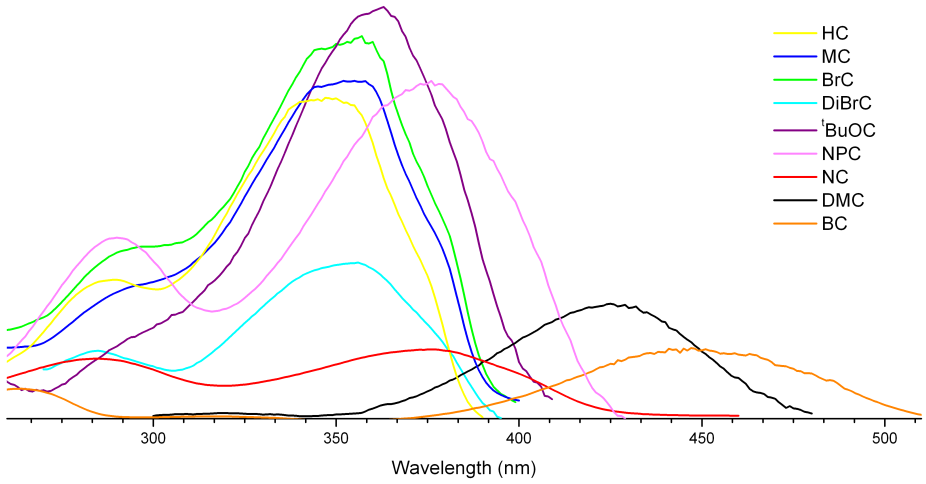

Figure 8.3 UV-vis absorption spectra for synthesize chromophores. Color-coded for each chromophore (not representative of the actual solution colors).

The same chromophore solutions were then used to measure the fluorescence by placing them in a fluorimeter (Figure 8.2b). The fluorescence emission spectra show a broad range of maximum values that were observed depending upon the functional groups that differ in the molecule. All molecules were sufficiently fluorescent to be detected and showed enough promise for continued development toward peptide applications.

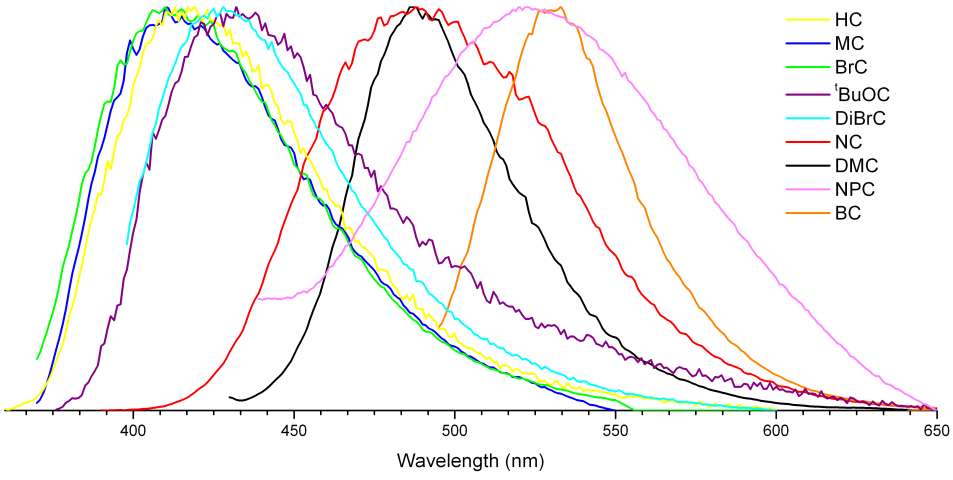

Figure 8.4 Fluorescence emission spectra for library of chromophores. Each was obtained by exciting at the wavelength of maximum absorption. Again, disregard the line colors as they are not representative of the emission color.

While steady-state spectroscopy provides fundamental information about the photophysical properties of the chromophore, a more in depth investigation is required to fully understand the physical chemistry of these molecules to decide which is best suited for biological application. One of the sophisticated techniques that is predominately utilized in our lab is that of two-photon absorption spectroscopy (Figure 8.2c). The notion here is a fairly simple one in principle. Linear, one-photon absorption is the excitation of a molecule by a single photon of light to its excited state, as described in Figure 8.1. Two-photon absorption is different in that to achieve very nearly that same electronic transition from unexcited ground state to some excited state, the molecule absorbs simultaneously two photons of light that are roughly half the energy of the overall transition (Figure 8.5). So, if one thinks about the absorption spectra presented above for the library of chromophores, they all seem to linearly absorb photons of 400 nm light fairly well. Consequently, if one were to probe these same molecules only utilizing two-photon spectroscopy, it would be hypothesized that under the right conditions a light source around 800 nm would be well suited for seeing the maximal two-photon absorption.

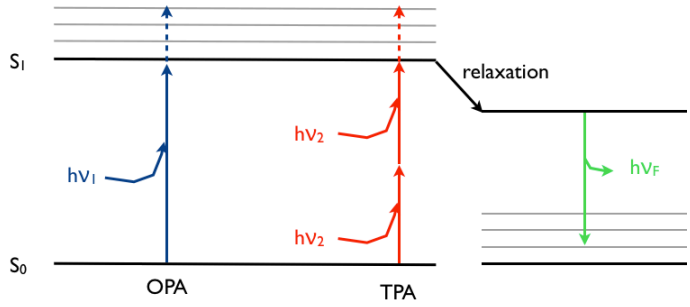

Figure 8.5 Energy diagram for one-photon absorption (OPA) versus two-photon absorption (TPA). Two photons of half the energy of the one photon can make the same transition.

Unlike typical one photon absorption behavior that can be initiated with simple light sources such as the sun or a lamp, two-photon absorption requires special light sources such as those generated from a pulsed laser system. The fundamental processes by which laser light is generated may be read about in detail elsewhere, but femtosecond pulsed laser systems for general scientific use are widely available for purchase from commercial retailers these days. Femtosecond pulses may be generated using a titanium-sapphire laser (Ti:sapphire) that generally tunable over a range of wavelengths depending on the type and configuration but usually centered near 800 nm. Often, these systems are simply referred to as ultrafast laser systems given that a femtosecond is equal to one quadrillionth of a second (1/1,000,000,000,000,000). Ti:sapphire lasers were the primary light sources for the majority of the spectroscopy performed in both chromophore and peptide characterization.

Two-photon absorption is relatively easy to observe given the proper laser system and material to study. The laser beam is focused onto the chromophore solution within the cell and the fluorescence that is generated is collected. Subsequent calculations may then be performed determine the two-photon absorption (TPA) cross-section that essentially relates to the probability of a molecule absorption two-photons of light. The TPA cross-section is a widely recognized value that can be used to compare the overall nonlinear absorption characteristics among many different kinds of materials. The units for TPA cross-section are called Göppert-Mayer (GM) after its discoverer Maria Göppert-Mayer. To provide some perspective as what constitutes a "good" absorption value, the best two-photon absorbing materials can have cross-sections in the hundreds of thousands GM, but these are often large molecules with multiple chromophore units.

Smaller molecules with fewer double bonds like our chromophores will not approach these extraordinary values, but can still be very useful with moderate cross-sections near 100 GM. Table 8.1 below shows the maximum TPA cross-sections that were obtained across a range of excitation wavelengths for each chromophore that was synthesized. The clear maximum belonged to the DMC version of the chromophore. It was admittedly a bit surprising that none of the other chromophores were even comparable in their characteristics given some of the structural similarities.

Chromophore	TPA cross-section (GM)
HC	1.69
MC	0.54
BrC	9.37
^{t}BuOC	8.12
DiBrC	0.85
NC	2.47
DMC	**40.6**
BC	17.1

Table 8.1 Two-photon absorption cross-sections for synthesized chromophores.

The two-photon absorption cross-sections were but one of two major aspects of the chromophore library to be characterized. Based on these results, the molecules were shown to amenable to laser excitation from two-photon type sources, but a full understanding as to their fluorescence characteristics is still missing. To investigate this detail, another ultrafast technique called time-resolved fluorescence upconversion spectroscopy (shown previously in Figure 8.2d) was implemented to determine the fluorescence lifetimes of the chromophore library.

In general, molecules with longer fluorescence lifetimes that are easier to see with the naked eye and detect with instrumentation make better candidates for application in imaging. Fluorescence lifetimes (often interchangeably termed fluorescence decays)

measure of the length of time it takes from the moment the molecule absorbs a photon for the excited molecule to relax back to the ground state. In daily life, the principle of a fluorescence decay is perhaps most widely observed in the limited lifetime of fluorescence in “glow sticks”. Depending on the dyes used in the mixture within, a variety of colors and also luminescence duration may be obtained. The fluorescence lifetimes for these systems are measured in minutes, hours, even days. The chemical reactions set-up in the tubes of these glow sticks are engineered to generate fluorescence constantly over these long periods of time. These contrast with the great majority of fluorescent events observed from individual molecules that occur on timescales far shorter than a second, more commonly in the nanosecond timescale (1,000,000,000 times shorter than 1 second).

For purposes of generalizing this aspect of study, our interest was in the role that changing the structure of the molecule played on lengthening the fluorescence lifetime and thus making the chromophore better suited to act as a fluorescence label. At the same time, a balance was sought with the two-photon absorption characteristics also desired. With this in mind, a relative comparison of the decay times for each chromophore provided the fundamental basis for determining a structure-function relationship. Shown in Table 8.2 is the series of chromophores followed by two columns with lifetime decay components. There are multiple different decay pathways that contribute to the overall decay observed for these molecules, meaning the overall response cannot be fit to a simple single-term exponential function. The data collected for the chromophores was fit to two exponentials, with the second component giving the most information about the overall fluorescence of the molecule.

	Time component 1 (ps)	Time component 2 (ps)
HC	0.45	2.20
MC	0.50	1.28
BrC	0.75	4.31
DiBrC	4.85	62.30
^{t}BuOC	0.38	0.84
NPC	0.40	1.30
NC	4.70	53.20
DMC	0.57	3.26
BC	1.11	9.74

Table 8.2 Fluorescence decays for synthesized chromophores as measured using time-resolved fluorescence upconversion. Time is in picoseconds (ps), longer than a femtosecond, shorter than a nanosecond, 10^{-12} seconds.

From the standpoint of understanding what role the connectivity of the chromophores play, several different attributes were considered including: the physical size of the groups (tBuO is large; H is small), electronic considerations (DMC and NC compared to HC), extending the alternation of double-bonds (BC vs. DMC), and positioning of functional groups (DiBrC has groups in different locations, especially compared to BrC). Figure 8.6 below gives a visual comparison of some of the chromophores lifetimes. The inset shows the full decay of NC as it is significantly longer than the other three examples plotted in the figure. Clearly the $–NO_2$ and the two –Br groups have a significant effect on extending the overall fluorescence lifetime more than any of the other groups attached to the basic chromophore. That said, weighing the overall importance of the molecule's TPA cross-section and fluorescence lifetime together, the difference in tens of picoseconds is not significant enough to overcome the far superior TPA cross-section value that was determined for DMC. With all the spectroscopic characterization considered, steady-state absorption, fluorescence, two-

photon absorption, and time-resolved fluorescence, DMC was deemed the best candidate for pursuing as a label for use in the biological study of amyloid peptides.

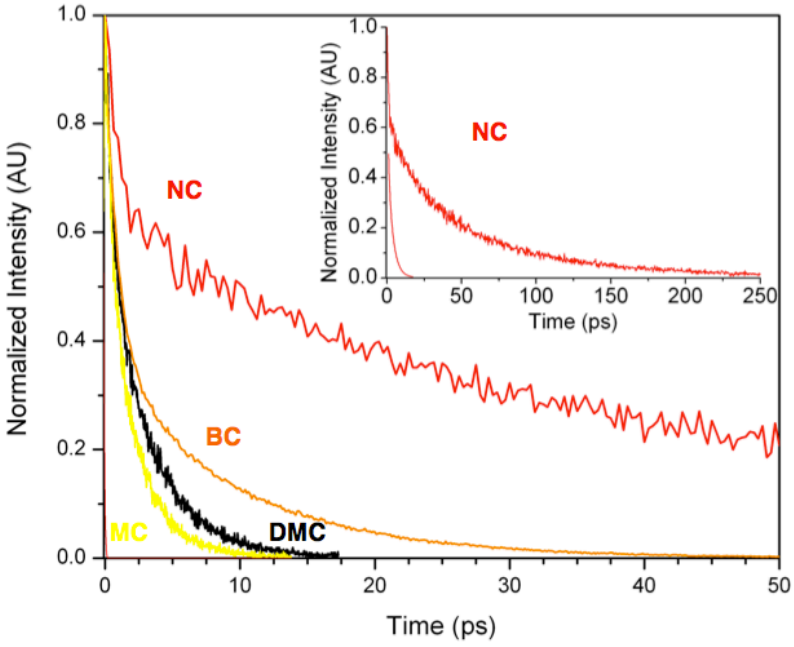

Figure 8.6 Representative examples of the fluorescence decays for library of chromophores. The inset graph shows the full decay of NC that could not be shown on the scale of the main plot.

With the decision made about the molecule to be used for our biological study, the next phase of the project was to begin studying at the peptide responsible for Alzheimer's disease, amyloid-β (Aβ). In the design of the chromophore, great lengths were made to ensure that the appropriate connecting molecules were present to make linking our molecule to our peptide of choice very straightforward. However, the synthesis of amyloid-β is anything but simple. Ideally, one would just buy it off the shelf from one of the commercial providers discussed earlier, but the fact that attaching a custom label was required made this option unviable. The incorporation of the dye in the proper position must be accomplished by generating the peptide one amino acid at a time,

that is, building block by building block. Scheme 8.3 depicts the structural formula for amyloid-β labeled with our synthesized chromophore:

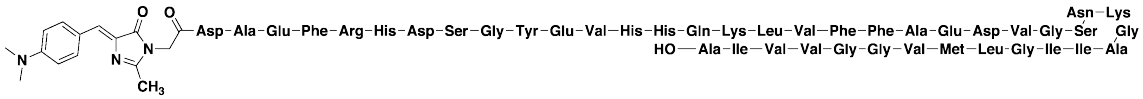

Scheme 8.3 Amyloid-β peptide represented with three letter amino acid abbreviations and DMC chromophore attached at the N-terminus end.

The three-letter codes are abbreviations for the larger chemical structures that are the amino acids making up the peptide. For a number of reasons, the dye was attached at one end of amyloid-β (the N-terminus), one of which being the ease of incorporation. The synthesis of the peptide and attachment of our label was contracted out through the University of Michigan Peptide Synthesis Facility as precisely sequencing and characterizing a chain of 42 amino acids long is not something in which our research group specializes. After some tribulations, ~1 milligram of DMC-labeled peptide was obtained. (For reference, 1 milligram is approximately equal in mass to ~90 grains of sand. Tiny!)

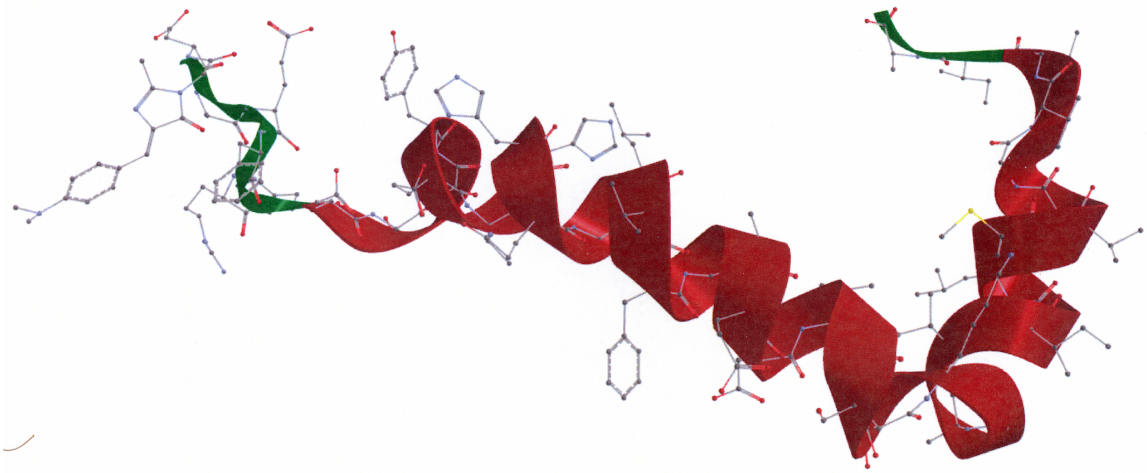

Figure 8.7 Molecular model representation of DMC-Aβ1-42. The red ribbon structure is indicative α-helical structure, green is considered randomly structured. The chromophore can be observed at the far left of the structure.

The research now moves into the final stretch having designed and synthesized the chromophore, characterized it for its photophysical properties, and successfully attached it to amyloid-β peptide. In considering the types of experiments to perform with the labeled peptide there are several things that need to be confirmed about the behavior of this new structure with respect to both the chromophore by itself and the peptide by itself. Most importantly we need to make sure that the manner in which the peptide aggregates has not changed from the labeling because that would call into question the relevance of any of aggregation studies that are performed. Also, the steady-state spectroscopy of the DMC-Aβ needs to be compared to that of DMC to examine how the peptide affects the spectrum of light absorbed. This plays into the ease or difficulty with which successful molecular excitations may be made with our laser systems.

A technique utilized to characterize whether the addition of the chromophore is impacting the structural characteristics of the peptide is circular dichroism spectroscopy. Fundamentally, this is another absorption technique that is typically utilized by biochemists because they can use the data obtained to calculate percentages of secondary structure in the peptide. There are several prominent varieties of secondary structure that are typical in peptides: α-helix, β-sheet, and random coil. Random coil is as the name implies very unstructured with no distinct, random interactions occurring amongst the amino acids. α-Helix is a structural motif that is largely represented by the peptide in Figure 8.7 (above) with segments of the peptide forming helical structures due to the energetic favorability of the interactions. β-Strand or β-sheet is the most ordered structure with significant hydrogen bonding between amino acids in the same chain as well as with neighboring chains. The experimental absorption spectrum that is collected from a

circular dichroism measurement can be compared to spectra of standard peptides with known structural composition to back-calculate the composition of the unknown sample. So for our purposes, the structural characteristics of the labeled peptide need to match that of the unlabeled peptide, an indication that by adding the chromophore nothing fundamental has changed. Based on our experience previously with amyloid-β, it was unlikely that the group we were attaching would play any role at the N-terminus as it is sufficiently far removed from the particularly aggregation prone region of the peptide. Sure enough, no indications of significant behavior changes were noted from our preliminary studies.

An examination of the steady-state absorption and fluorescence emission of the labeled peptide showed that each had been slightly shifted due to the attachment of the peptide (Figure 8.8). While not particularly significant, the relative shift in the absorption does pose some issues as the absorption band is moved farther away from the desired absorption maximum at 400 nm. During the course of these studies several different kinds of solvents with a variety of properties were tried to further examine solvent sensitivity of the overall absorption for the DMC chromophore both attached to the peptide and unattached. This study may be thought of as being similar to the structure-function relationship experiments described earlier. In that work, a number of different structural variants of the chromophore were studied for their effect on the overall photophysical characteristics, but this time the chromophore remains the same and the solvent in which it is dissolved varies. As can be observed from Figure 8.8, there is a great deal of variability depending upon the solvent. This is an important sensitivity for our chromophore to have as it indicates that the environment surrounding the

chromophore changes its behavior, so it can be expected that the changing environment around our chromophore as the peptide aggregates to perhaps manifest itself in the spectroscopy studied.

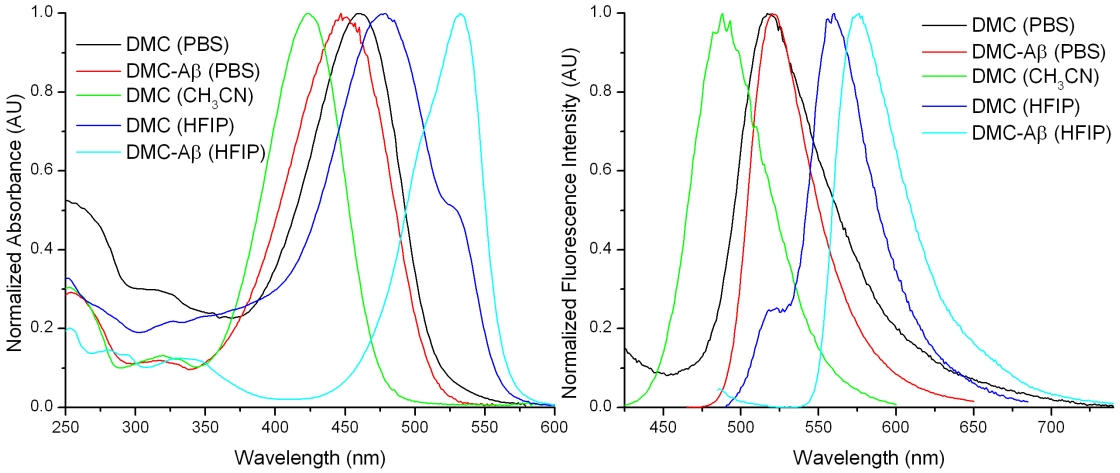

Figure 8.8 Steady-state absorption and emission curves for DMC-Aβ1-42 and DMC in different solvent conditions.

To begin in earnest studying the aggregation of amyloid-β, solutions of the peptide dissolved in water-based solvents needed to be made at biologically relevant concentrations. Obviously natural biological systems are not highly concentrated, with amyloid peptide concentrations typically found at less than 1 μM. (1 μM is one micromolar, or 10^{-6} moles/liter, a very dilute amount for spectroscopy). Approaching these levels of concentration, based on the previous experience with studying the free chromophores appeared initially to be a daunting task, consequently higher concentrations were made at the outset with subsequently more dilute solutions thereafter. Eventually, aggregating solutions of 40, 29, 10, 5, 2.5, 1 and 0.5 μM solutions were made and studied using two-photon absorption, time-resolved fluorescence, and circular dichroism spectroscopies.

Another problem to be considered was how to deal with the changing characteristics of the peptides as they aggregate over time. The objective was to measure the changes in the amyloid-β as they adopt distinct conformations, associating with one another to built larger and larger aggregates. Not having a firm understanding of the rate at which these changes might occur, the simplest maneuver on our part to yield consistently fair results was to prepare all solutions immediately before the spectroscopic studies to be performed. There would just be too much uncertainty as to whether comparisons after several hours or especially several days would be appropriate. Three main experiments were conducted using two-photon absorption, circular dichroism, and time-resolved fluorescence spectroscopies, all examining the role of concentration on amyloid-β aggregation. Each technique will be addressed in turn to conclude the bulk of my dissertation research.

The principles of two-photon absorption spectroscopy were introduced earlier this chapter from a very physical perspective, but they merit revisiting, this time from a practical perspective of the experimentation with respect to our biological studies. Compared to everyday linear absorption, two-photon absorption is particularly sensitive to the interactions of molecular species. For instance, if you have several chromophores fixed such that they are in close proximity (like branches on a tree), the photophysical characteristics observed for the overall system are different than if they were isolated a great distance. So, using our two-photon absorption experiment, we can interrogate the interactions that are occurring between the chromophore-labeled peptide and its neighboring peptides, or as it interacts with itself. Some of the other additional benefits of two-photon excitation also include less photophysical damage from the light source

compared to the higher energy visible light sources and more pinpoint control of the region being illuminated.

A range of peptide concentrations was investigated as explained previously with the basic premise being that at the smallest concentrations there will be less aggregation and at higher concentrations much larger aggregates will be formed. All experiments were performed immediately after the solutions were prepared and were excited with laser light at a wavelength of 800 nm. Shown in the table below are various peptide concentrations studied and the TPA cross-sections determined.

Peptide Conc. (μM)	**TPA cross-section δ (GM)**
0.5	540
1	283
2.5	133
5	92
10	108
40	191

Table 8.3 Two-photon absorption cross-sections determined as a function of peptide concentration.

Immediately it is clear that the values observed for the labeled peptide are substantially higher than that observed earlier for the chromophore alone in solution (~40 GM), in some cases more than 10 times larger. This is a very unexpected result. The peptide really doesn't immediately seem to feature any characteristic features that would add to the cross-section. It is especially surprising when one considers the outlined expectation that chromophore-chromophore type interactions are expected to play prominent roles in increasing the two-photon absorption cross-sections. The general trend revealed by this data indicates that the highest responses occur when the interactions are presumably smallest. (Put a smaller number of molecules in a given space, they will interact far less than if you put many times more in that same space.) While surprising,

this result is promising because it indicates that there is high sensitivity for very dilute peptide solutions and the small conformational differences between solutions with as small of a concentration difference as 0.5 μM versus 1 μM are detectable. In Figure 8.9 below, the general TPA trend as a function of concentration is depicted.

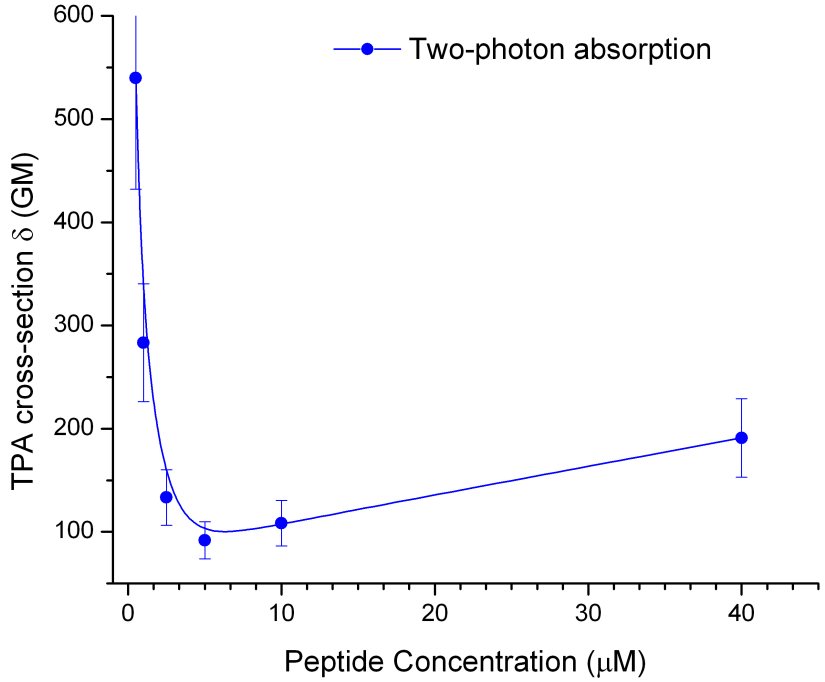

Figure 8.9 Plot showing the general trend of TPA cross-section with respect to peptide concentration.

Alone the two-photon absorption cross-sections do not say very much directly about the actual aggregation state or peptide conformation. Many inferences may be made about the aggregation state of the peptide based on our understanding of two-photon absorption however, benchmarking these results against a standard technique for examining peptide structure like circular dichroism spectroscopy would be beneficial for better characterizing these results. As such, circular dichroism spectra on solutions at the same peptide concentrations were also collected to see how the structural results compared with those hypotheses formed from the TPA. A comparison of the relative

sensitivity of circular dichroism (CD) and two-photon spectroscopy was made with CD representing a technique that is commonly used.

Such analysis returns to a major object of the project outlined earlier to developing new methodologies for studying these peptide systems. As explained before, CD is a common tool used by biochemists to examine the structural characteristics of peptide systems. In the case of our comparison to the two-photon absorption results, our goal was to establish that based on concentration the peptide solutions had differing compositions of structural characteristics. Shown below in Figure 8.10 are the CD absorption curves obtained. Looking at the general trend between the solutions, it is clear that as the solution concentration is decreased from 40 μM to 1 μM the peak at 222 nm becomes more and more prominent. Based on previous work done by others in this field, it is known that this increase corresponds to a higher percentage of α-helical content for amyloid-β.

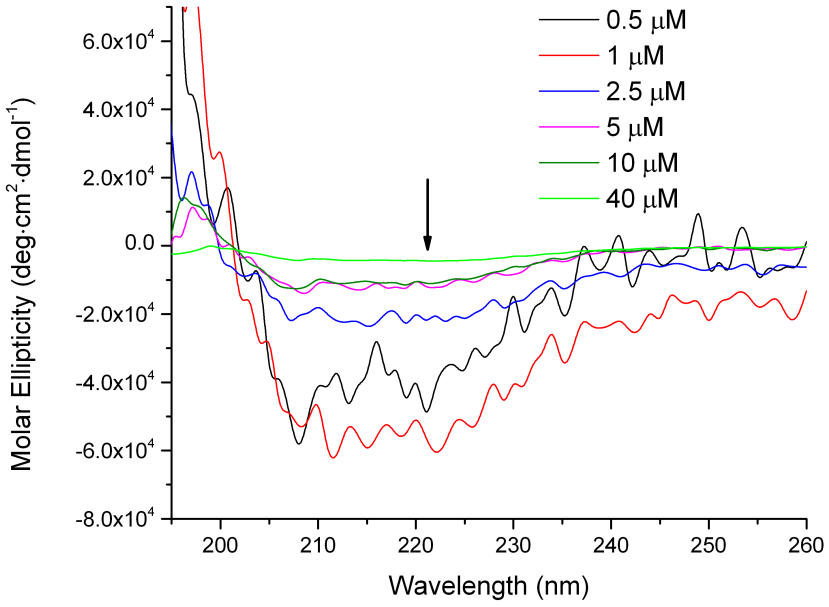

Figure 8.10 Circular dichroism of various peptide solution concentrations. The arrow indicates the direction of the general trend as the concentration is made more dilute.

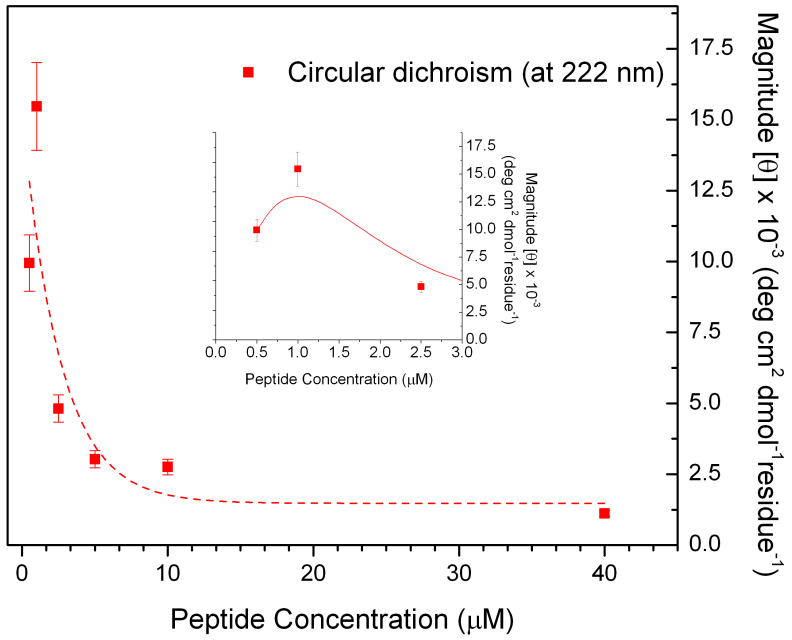

Figure 8.11 The general trends of circular dichroism observed at 222 nm as a function of peptide concentration.

If one simply takes the magnitude of the CD values at 222 nm and plots them as a function of the peptide concentration, Figure 8.11 is yielded. Highlighted in the inset plot is the fact that at the lowest concentrations studied there is a plateauing of the response indicating that the overall sensitivity of the instrumentation is inadequate to detect the small changes made in preparing a solution of 1 μM versus 0.5 μM. (The higher levels of noise in the above plot also evidences this point.) This contrasts from that which was observed using our two-photon methodology; distinctly different cross-sections were noted from the two most dilute samples. If you essentially overlay the two data sets, plotting each as a function of concentration, the results are striking as to how well the trends between the data collected for each technique correlate (Figure 8.12).

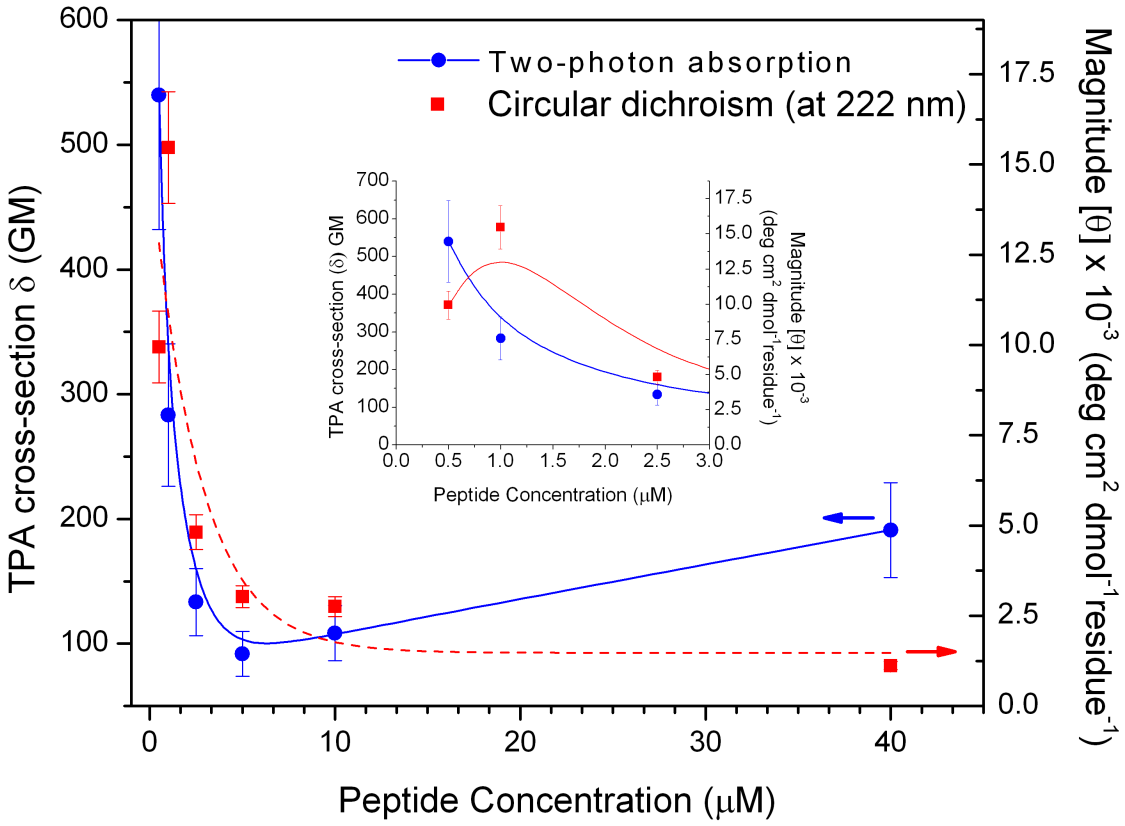

Figure 8.12 Comparison of trends for two-photon absorption and circular dichroism. The inset graph is an expanded view of the low concentration region.

As again emphasized in the inset, at lower concentration two-photon absorption is simply better at detecting the small differences in the structural characteristics of the peptide. However, there is no true set of benchmarks as to our methodology for what a specific two-photon absorption cross-section may indicate as far as peptide conformation or aggregation state, which is still a fundamental goal of the project. Some hypotheses can be generated based on this comparison with CD as to the structural characteristics as well as the role that chromophore interactions play in increasing TPA cross-sections (as discussed earlier), but additional information about what is physically happening with our chromophore on the peptide would be beneficial.

Much the same way as studying two-photon spectroscopy can give information about molecular interactions and peptide conformational changes, time-resolved fluorescence also provides some details as to the types of interactions that are occurring between the chromophore and its surroundings. Putting two (or more chromophores) into the same vicinity can result in changing the electronic characteristics that are observed through spectroscopy. In the case of measuring fluorescence decays, chromophore-chromophore interactions tend to result in the occurrence of multiple decay components that become faster with stronger interactions. Another aspect that may be examined in the context of fluorescence decays is that of how the orientation of the molecules that are excited changes based upon varying the polarization of the laser light. The detailed explanation is rather more nuanced than that, but the basic fact remains that the extent to which these two orientations are related to one another can say a lot about the efficiency of energy transfer between two closely associated molecules. By obtaining this information about the fluorescence decay and anisotropy, more concrete information about the peptide aggregation state could be obtained.

A range of peptide concentrations going from the highly concentrated to the very dilute again was examined, but also that of the free dye without the peptide under the same solvent conditions. The results for both the fluorescence lifetime decay and the anisotropic decay are show below in the table. Once again, the data sets were best-fit with exponential functions to best reflect the nature of the decays (Figure 8.13). The results of these fits can be seen in Table 8.4.

Concentration	Lifetime		Anisotropy	
(μM)	τ_1 (ps)	τ_2 (ps)	τ_1 (ps)	τ_2 (ps)
29	0.83	7.1	2.2	17
10	1.10	7.2	1.9	16
0.5	2.2	10	0.9	10
DMC free	1.07	4.19	--	16

Table 8.4 Fluorescence lifetimes for DMC-labeled amyloid-β 1-42, compared to "free" DMC.

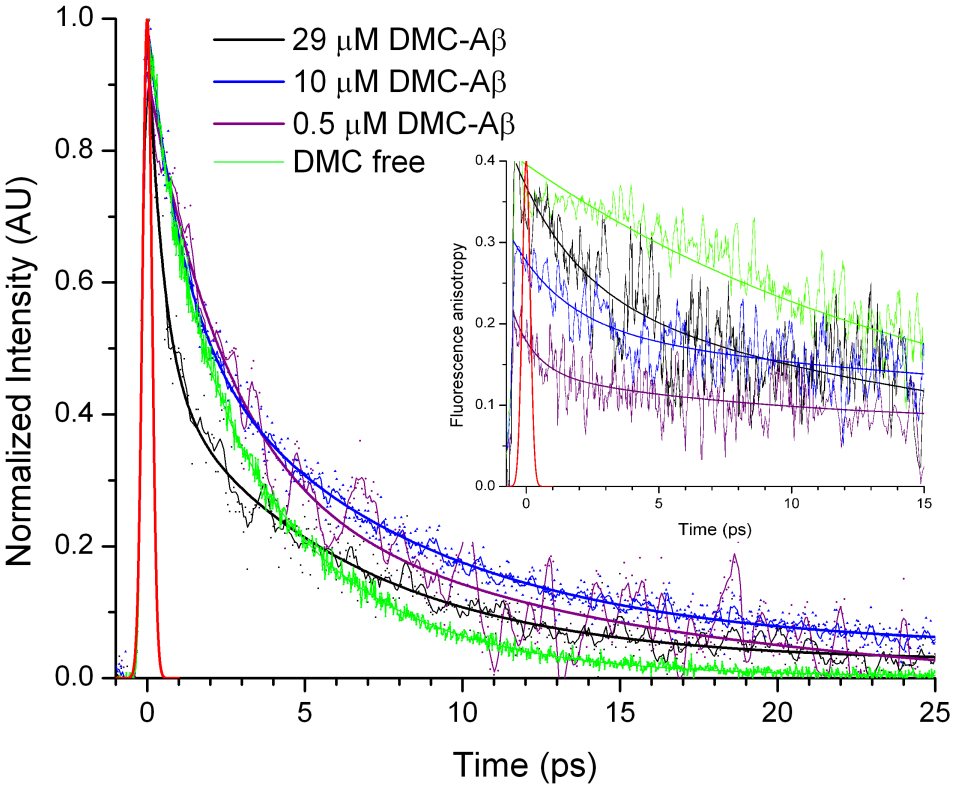

Figure 8.13 Fluorescence decay of various concentrated DMC-Aβ solutions as compared with "free" DMC. Inset: fluorescence anisotropic decay of various DMC-Aβ solutions as compared with "free" DMC. Black, DMC-Aβ 29 μM; Blue, DMC-Aβ 10 μM; Purple, DMC-Aβ 0.5 μM; Green, "free" DMC

Casting aside any of the complex theory for now, a general comparison of the decays for any of the labeled peptide shows a longer decay time than the free dye. This is not unexpected as overall molecular size can have an impact on the decay processes and certainly the peptide with our chromophore attached is far larger than the dye itself. Most molecular motions associated with this chromophore are hindered simply by the

increased bulk of the groups around it. Unlike when the free chromophore was investigated in the context of the chromophore library earlier, the fastest decay component is the more interesting of the two components. From looking at the table, this time gets slower as the concentration is decreased, progressing from 0.83 ps to 2.2 ps. These times are associated with charge-transfer processes associated with molecular interactions between the chromophores. The faster lifetime for the higher concentrated sample indicates that this process proceeds more smoothly when peptide is in the particular conformation that predominates at 29 μM. Fewer interactions that accelerate the decline of fluorescence are occurring at the low concentration. The anisotropy tells a similar story (Figure 8.13), a comparison of the peptide curves with that of the free DMC show extremely different decays. For DMC in green, there is essentially no fast anisotropy component and its signal falls off at a rate consistent with what was seen earlier in our studies. However, a close examination of the peptide curves shows sharp declines immediately after zero time. These declines are directly associated with chromophore-chromophore interactions and provide support for the results observed in the two-photon absorption studies.

8.4 Putting It All Together

And now finally, for the most difficult task of putting together all these results and explaining the overall significance with respect to the fundamental questions that were discussed in the introduction. The range of peptide concentrations that were studied encompasses a variety of different peptide structural regimes. At the lowest, most biologically relevant concentrations, the peptide has undergone relatively small amounts of aggregation. This is evidenced by the lack of strong β-sheet characteristics observed

when studied using circular dichroism spectroscopy. The large two-photon cross-section enhancement indicates that the peptide is in a favorable conformation that would promote increased absorption cross-sections. At high concentration the peptide has more prominent β-sheet characteristics and aggregates into structures such as in Figure 8.14**b**. Though not discussed here, the molecular distances for amyloid-β sheet structures can be estimated based on the fluorescence lifetimes and other techniques as indicated in the figure.

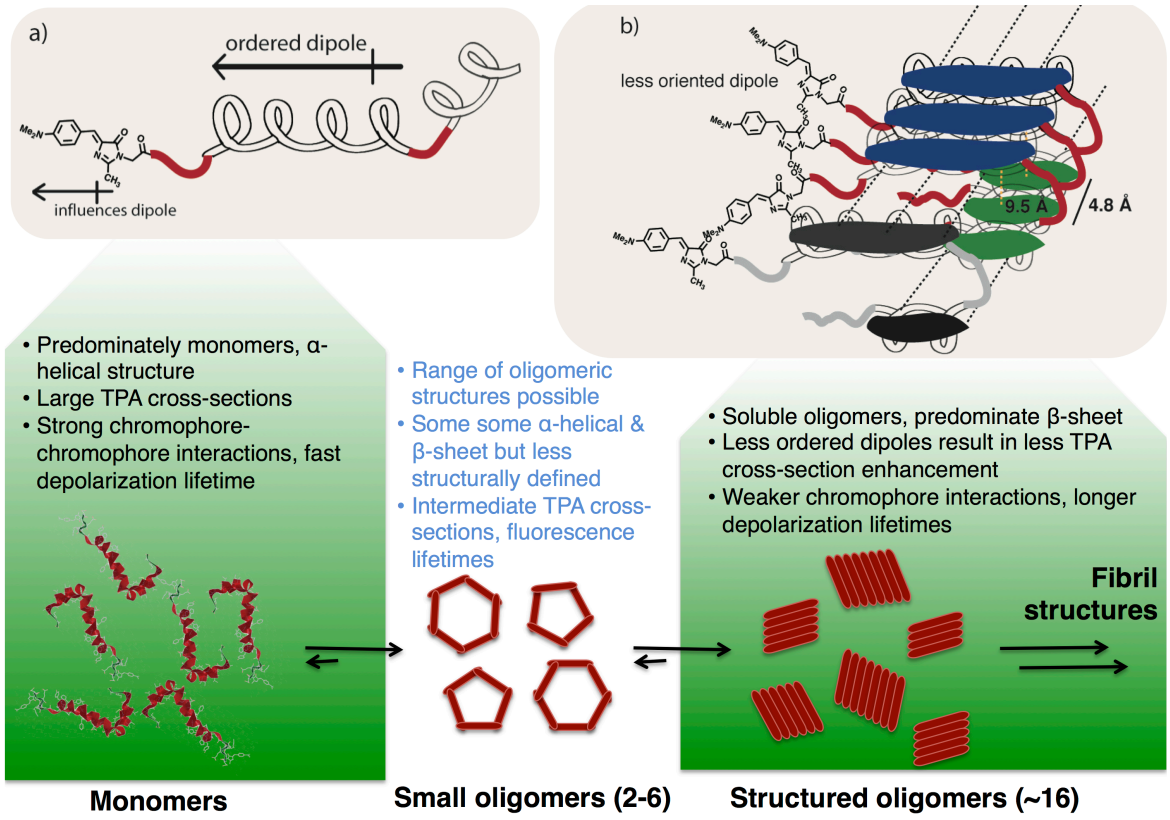

Figure 8.14 Conclusions drawn from experiments with representative structure schematics for each stage.

The overall results demonstrate the capabilities of the techniques that were implemented for looking at the early aggregation of amyloid-β peptide. While none of the results of our experimentation approaches direct answers or provide solutions for

therapeutic intervention for Alzheimer's, the fundamental research performed over the course of the dissertation makes tangible progress toward developing new materials and techniques for answering those big questions. Further research of course needs to be done to fully realize the potential of these new techniques: more sensitive, higher fluorescing peptide labels can be developed; additional attachment positions on the peptide should be considered to examine different aspects of the peptide dynamics; systematic time-domain studies should be done to track the evolution of conformational characteristics. The complete two-photon absorption and time-resolved fluorescence methodology permits however detailed conformational and peptide aggregate characterization of the evolution from early oligomer to fibril formation, something that could have a huge impact toward therapeutic intervention or fundamental understanding of Alzheimer's disease. Many direct applications for *in vivo* imaging may be envisioned using a two-photon-based methodology including cancer-targeted monitoring as well as peptide aggregation associated with Alzheimer's and Parkinson's disease. Two-photon imaging has the capability to permit detailed tracking of the evolution of disease beginning with some initial misfolded monomer to the formation of toxic oligomers and later fibril structure. This could have a profound impact on the ability to detect and prevent the development of neurodegenerative disease.

The nature of scientific research is such that there is always the next question to be answered and the next experiment to be run. My aspect of the project has been completed, but the next person will pick it up and continue to work toward the overarching problems that were outlined at the top. Further details of this work may of

course be found in the preceding chapters of this dissertation with all the details and even more of the scientific jargon left intact.